NAZARBAYEV UNIVERSITY

Quantification of Ambient Insoluble Hexavalent Chromium with Doped Carbon-Dots and Field Measurements

by

Enoch Kwasi Adotey

Submitted in partial fulfilment
of the requirements for the degree of
Doctor of Philosophy in Science, Engineering and Technology

May, 2023

Quantification of Ambient Insoluble Hexavalent Chromium with Doped Carbon-Dots
and Field Measurements

by

Enoch Kwasi Adotey

Submitted in partial fulfilment

of the requirements for the degree of

Doctor of Philosophy in Science, Engineering and Technology

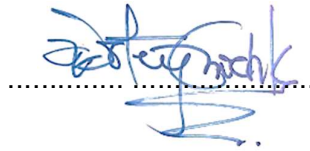School of Engineering and Digital Sciences

Nazarbayev University

Supervised by

Dr. Mannix P. Balanay

Dr. Shah Dhawal

Dr. Mehdi Amouei Torkmahalleh

Prof Philip K. Hopke

May, 2023

Declaration

I declare that the research contained in this thesis, unless otherwise formally indicated within the text, is the original work of the author's original work. The thesis has not been previously submitted to this or any other university for a degree, and does not incorporate any material already submitted for a degree.

Enoch Kwasi Adotey

28th May, 2023

Abstract

Hexavalent chromium Cr(VI) is a known carcinogen and apart from being carcinogenic, its exposure duration has adverse health effects on humans such as perforation of the nasal septum, asthma, bronchitis, pneumonitis, and lung cancer. Insoluble Cr(VI) persists to be more toxic than soluble Cr(VI) since when deposited in the lungs, it acts as a strong oxidizer that can breakdown cell membranes to produce reactive radicals that further causes changes in cell function or mutations. The deliquescence of Cr(VI) under atmospheric conditions (pH ~4), suggested the presence of insoluble/sparingly soluble Cr(VI) species such as $PbCrO_4$, $BaCrO_4$, $CaCrO_4$, and $(NH_4)_2CrO_4$ that can precipitate in solution. Hence, the need to quantify Cr has necessitated the development of advanced materials that can serve as sensors to detect total Cr(VI) (soluble + insoluble) in environmental samples. The main objective of this research was to develop a functionalized method to quantify insoluble atmospheric Cr(VI) concentrations in PM. The method development involved the use of a fluorescent carbon material (N,S-CDs) as a sensor towards Cr(VI) in ambient PM. Laboratory results yielded good recoveries of Cr(VI) with mean (relative standard deviation) values of 106.0% (5.3%), 102.3% (3.6%), 96.4% (1.9%), and 101.7% (2.2%) for $PbCrO_4$, $BaCrO_4$, $CaCrO_4$, and $(NH_4)_2CrO_4$, respectively. The application of the proposed fluorescent method on field PM samples resulted in a method detection limit (MDL) of 0.32 ng/m^3 for total Cr(VI) quantification. This MDL is much lower than the NIOSH 7605 (50 ng/m^3), OSHA ID-215 (3 ng/m^3), and ASTM D 5281-92 (0.2-1.0 ng/m^3) methods. The total Cr(VI) concentrations of ambient PM collected in Aktobe city in the fall and winter seasons had mean (S.D) of 5.30 ± 2.16 ng/m^3 and 2.26 ± 1.80 ng/m^3, respectively. Insoluble Cr(VI) values were 4.80 ± 1.96 and 2.19 ± 1.75 ng/m^3, respectively for the fall and winter seasons. Size-segregated sampling in Astana showed total Cr(VI) in size fraction < 0.25 μm as the highest with a maximum value of 9.77 ng/m^3 in summer. These results showed that total Cr(VI) concentrations on warmer days were significantly higher than on cooler days due to factors including higher temperature, ozone, and NO_2 concentrations on warmer days, and higher VOCs concentration on cooler days. These observations and findings demonstrate that gas-solid reactions of Cr(III) and Cr(VI) can control the speciation of atmospheric Cr, especially below the deliquescence relative humidity (DRH) point (76%).

Acknowledgment

Table of Contents

List of Tables

List of Figures

Do not delete the following section break, otherwise the page numbers will not be converted from Roman to Arabic numerals.

CHAPTER 1.   INTRODUCTION

1.1   The intent of this Thesis

Issues of environmental pollution have been a global concern for decades now. To mitigate environmental pollution, measures are being implemented to develop advanced materials that can be used for sensing and adsorption of toxic materials in humans and the environment, such as chromium.[1-5] Chromium exists primarily in the trivalent (Cr(III)) and hexavalent (Cr(VI)) forms in the environment. Trivalent chromium is nontoxic and used in the human body for the proper functioning of living tissues. The hexavalent form, Cr(VI), however, is a known human carcinogen that can lead to adverse health effects including nasal damage, asthma, bronchitis, and pneumonitis.[6-8] Different analytical techniques have been employed to quantify Cr concentration in the environment including UV-Vis spectrophotometry[9], Ion Chromatography[10-12], Atomic Absorption Spectrophotometry[13], and Electrochemical methods.[14] Even though these conventional methods have been widely used, drawbacks including high cost, extensive professional operation, time consumption, and unsuitable for *in situ* measurements[15-17], have been the major concerns among researchers. Thus, a more robust technique is required for the rapid detection of Cr(VI).

Fluorescence spectroscopy using nanomaterials is gaining much attention due to its characteristics of fast response time, and specific and sensitive detection that can provide real-time monitoring.[18] One such nanomaterial that has gained its application in fluorescent spectroscopy for Cr(VI) detection is carbon dots. Carbon Dots (CDs) are new fluorescent nanomaterials with unique characteristics such as good water solubility, variable fluorescence emission, high biocompatibility, good photostability, and low toxicity.[18-21] CDs are flexible considering that their size can be tailored by altering reaction parameters such as the reactants, temperature, synthesis time, surfactants, additives, etc.[22] Doping CDs with specific elements such as zinc (Zn), nitrogen (N), sulfur (S), or their combinations amongst others[22], plays key roles such as the fluorescence enhancement and shift of emission spectra. Doping CDs with these moieties can also modify the bandgap energy that improves the charge separation efficiency of the materials when used as sensors.[23]

Single or heteroatom doping has improved the quantum yield, water solubility, fluorescent properties, and other physicochemical properties of CDs. Popular among

the doped carbon materials are nitrogen-doped CDs (N-CDs) since nitrogen has a similar electron structure to carbon atoms[24,25] and can share its unpaired electrons (electron donor) to improve the emission properties of the CDs.[26] The fluorescence enhancement of CDs by nitrogen arises from the fact that N-containing functional groups transition easily from the ground state to the lowest excited state of the electrons.[27] Non-metal heteroatom doping of CDs has also improved the properties of CDs.[28] Sulfur (S) is another of the non-metal that can form a heteroatomic structure in CDs (e.g nitrogen sulfur co-doped CDs) and has its electronegativity (2.58) similar to that of carbon (2.55). Since the atomic radius of S (105 pm) is larger than the carbon atom (77 pm), the electron transition of sulfur is faster than for carbon. In heteroatomic CDs, the availability of oxygen and sulfur makes CDs negatively charged, and this enables the nanomaterial to be bonded with positively charged particles.

With these characteristics of doped CDs, there is the possibility to synthesize functional carbon dots that can serve as a chemoselective sensor for Cr(VI) (**Figure 1.1**). Some CDs and doped CDs have already been synthesized for the detection of Cr(VI) in water. Those CDs were, however, only selective towards soluble Cr(VI) and not the insoluble forms of Cr(VI) in water or air. Heteroatom doping has shown its ability to be selective towards Cr(VI) to very low detection limits and thus competitive to the already known conventional methods used for Cr(VI) detection. Thus this thesis focuses mainly on the use of as-synthesized doped CDs as functional carbon material for the selective detection of Cr(VI) from its insoluble species.
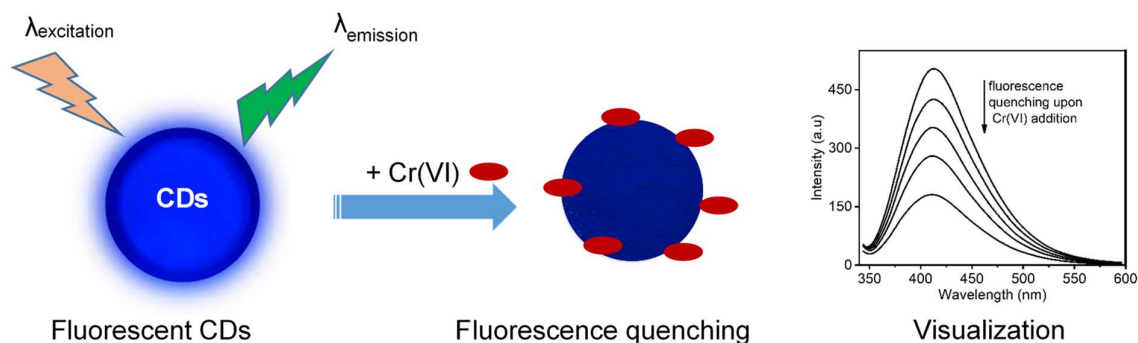
Figure 1.1 Schematic representation of CDs as sensors for Cr(VI) detection.

1.2 Hypotheses:

After conducting literature reviews on Cr(VI) and its relevant atmospheric chemistry, these hypotheses were defined.

1. Functionalized carbon material improves the quantification of insoluble hexavalent Cr in ambient PM
2. The majority of hexavalent Cr in ambient PM of Astana and Aktobe is insoluble Cr(VI)

1.3 Objectives of the Study

1. The primary objective of this thesis is to develop a new functionalized method to quantify insoluble atmospheric Cr(VI) concentrations in PM
2. The secondary objective of this thesis is to measure criteria pollutant concentrations such as O_3, NO_2, SO_2, and PM in Astana and Aktobe to investigate their impact on atmospheric Cr(VI) Chemistry

1.4 Aims of the Study

With the above objectives in mind, this research aims to:

1. Design and use functional carbon material as a sensor to detect Cr(VI) from insoluble Cr salts
2. Quantify insoluble and total Cr(VI) concentrations in the atmosphere emitted from industrial (Aktobe) and urban (Astana) sources in Kazakhstan
3. Investigate seasonal variability of insoluble Cr compounds
4. Present new correlations between the field concentrations of O_3, SO_2, NO_2, and trace metal concentrations with total Cr(VI) concentration

1.5 Scientific Significance and Novelty of Study

The novelty of this thesis is developing an analytical method using functionalized carbon material to quantify insoluble Cr(VI) concentration in PM.

1.6 Research Outputs (Publications)

1. Adotey, Enoch Kwasi, Mehdi Amouei Torkmahalleh, Philip K. Hopke, and Mannix P. Balanay. "N,Zn-Doped Fluorescent Sensor Based on Carbon Dots

for the Subnanomolar Detection of Soluble Cr(VI) Ions" *Sensors* 23, no. 3 (2023) 1632.

2. Adotey, Enoch K., Lyailya Burkutova, Lyazzat Tastanova, Amirbek Bekeshev, Mannix P. Balanay, Sergei Sabanov, Anna M. Rule, Philip K. Hopke, and Mehdi Amouei Torkmahalleh. "Quantification and the sources identification of total and insoluble hexavalent chromium in ambient PM: A case study of Aktobe, Kazakhstan." *Chemosphere* 307 (2022): 136057.

3. Adotey, Enoch K., Mehdi Amouei Torkmahalleh, and Mannix P. Balanay. "Zinc metal–organic framework with 3-pyridinecarboxaldehyde and trimesic acid as co-ligands for selective detection of Cr (VI) ions in aqueous solution." *Methods and Applications in Fluorescence* 8, no. 4 (2020): 045007.

Other related publications

4. Konakbayeva, Dinara, Enoch Kwasi Adotey, Mehdi Amouei Torkmahalleh, Marios M. Fyrillas, Altyngul Zinetullina, Ana M. Rule, and Philip K. Hopke. "A conceptual model to understand the soluble and insoluble Cr species in deliquesced particles." *Air Quality, Atmosphere & Health* 12, no. 9 (2019): 1091-1102.

5. Shah, Dhawal, Mirat Karibayev, Enoch Kwasi Adotey, and Mehdi Amouei Torkmahalleh. "Impact of volatile organic compounds on chromium containing atmospheric particulate: insights from molecular dynamics simulations." *Scientific reports* 10, no. 1 (2020): 1-9.

6. Amouei Torkmahalleh, Mehdi, Zhuldyz Zhigulina, Tomiris Madiyarova, Kamila Turganova, Enoch K. Adotey, and Sergei Sabanov. "Exposure to fine, ultrafine particles and black carbon in two preschools in nur-sultan city of Kazakhstan." *Indoor air* 31, no. 4 (2021): 1178-1186.

7. Torkmahalleh, Mehdi Amouei, Zarina Akhmetvaliyeva, Ali Darvishi Omran, Faezeh Darvish Omran, Mohadeseh Kazemitabar, Mahtab Naseri, Motahareh

Naseri, Enoch Kwasi Adotey, et al. "Global air quality and covid-19 pandemic: Do we breathe cleaner air?." *Aerosol and Air Quality Research* 21, no. 4 (2021): 200567.

8. Torkmahalleh, Mehdi Amouei, Kamila Turganova, Zhuldyz Zhigulina, Tomiris Madiyarova, Enoch Kwasi Adotey, Milad Malekipirbazari, Giorgio Buonanno, and Luca Stabile. "Formation of cluster mode particles (1–3 nm) in pre-schools." *Science of The Total Environment* 818 (2022): 151756.

1.7   Thesis Overview

This thesis is a 2-tier investigation that involves, first, a method development to quantify hexavalent Cr in ambient PM, and second, to quantify ambient Cr and study its atmospheric chemistry. In all, three tasks were investigated. The first stage involved the synthesis of functional materials for the development of an analytical method to quantify total Cr(VI) in ambient air, the second involves the quantification and potential sources identification of ambient soluble and insoluble Cr(VI), and third, the determination of gas-solid (heterogeneous) chemistry of atmospheric Cr. The chapters in this thesis are as follows:

Chapter 1- provides the general intent of this thesis. This chapter also highlights the hypotheses, objectives, aims, and research outputs (publications) involved in this study.

Chapter 2- covers the literature reviews conducted before this research work. This chapter began with understanding Cr chemistry under ambient conditions, some modeling studies conducted, and finally the use of functional carbon materials as sensors for Cr(VI) detection. Literature work on the use of functional materials for Cr(VI) detection was only performed for soluble Cr(VI) in water and, no study was conducted on detecting either soluble or total/insoluble Cr(VI) in ambient air samples.

Chapter 3- describes the synthesis of functional carbon materials for the detection of Cr(VI). This chapter also elaborates on the method development for the detection of insoluble Cr(VI) using doped carbon dots.

Chapter 4- reports on the quantification of soluble and insoluble Cr(VI) in ambient PM samples collected in Astana and Aktobe sampling stations. Characterization of potential sources was also performed during these field campaigns.

Chapter 5- summarizes the entire research work with concluding remarks and recommendations for future works.

CHAPTER 2. LITERATURE REVIEW

Chromium is the 21st most abundant chemical element available on the Earth's crust at, about 100 ppm. Almost all naturally occurring chromium species are found in the trivalent state and in combination with iron or other metal oxides.[29] Chromium with varying oxidation states exists in some synthetic organic compounds such as bipyridine, carbonyl nitrosyl, organometallic complexes, and chromium carbonyls.[30] The oxidation states Cr(III) and Cr(VI) are the only known stable valence states found in the environment. Other states such as Cr(IV) and Cr(V) are unstable and formed as intermediates during the reaction of Cr(III) and Cr(VI) with oxidizing and reducing agents.[31]

2.1 Sources of Ambient Chromium

Chromium exists in the atmosphere in two forms; the solid and liquid phases. Anthropogenic sources (man-made) of atmospheric chromium account for about 60-70%, while the remaining 30-40% emanates from natural sources. The average atmospheric concentrations of chromium in rural and polluted urban areas ranged from 0.01 to 1.0 $\mu g/m^3$, respectively.[32]

2.1.1 Natural Sources of Chromium

Chromium in atmospheric particles is usually coated with water or dissolved in liquid phases, such as fog droplets. With a negligible vapor pressure of chromium at atmospheric temperatures, no gaseous form of chromium ever existed.[32] The major natural sources of atmospheric chromium are volcanic eruptions and erosion from soils and rocks.[33,34] Naturally occurring crocoite, a finely divided lead chromate ($PbCrO_4$) was found on the eastern slopes of the Ural Mountains as an orange-red mineral.[29,30] There is inadequate information about chromium emission from volcanic eruptions, however an average of 65 ng/m^3 concentrations was reported in the Mount St. Helens volcanic eruption that occurred on September 22, 1980.[33] In soil compositions, insoluble chromium is available as chromite, $FeCr_2O_4$ (also known as Cr-Fe spinel).[30,35] An average concentration of chromium in the soil was reported in a range of 1.04 - 3016 $\mu g/g$.[35] Other natural sources like airborne sea salt particles and smoke from forest wildfires are minimally accounted for as sources of Cr.[34]

2.1.2 Anthropogenic Sources of Chromium

The quantity of Cr available at a given time and location depends on numerous factors viz. the intensity of industrial processes, closeness to the emission sources, the quantity released, and the influence of meteorological conditions.[31] Major human activities leading to an increase of ambient chromium include those from metallurgical industries, refractory production, electroplating, and fuel combustion. Production of Cr-containing chemicals, especially chromates and dichromates, pigments, Cr trioxide, and Cr salts also contribute to the amount of Cr released into the atmosphere.[31] Mining of chromium ore exists in over 20 countries with 81% of the production concentrated in four (4) major countries. About 49% of the world's total comes from South Africa and 32% from Kazakhstan, India, and a lesser portion from Turkey.[30] South Africa and Kazakhstan are categorized as major chromium ore producers since they produce consistently over about 1 Mt Cr Ore/y[36] and they possess the world's largest geological chromium resources amounting to about 95%.[37] The summary of the world's mine production and reserves is shown in Table 2.1.

Table 2.1 World Mine and Production Reserve[37,38]

Countries	Mine production (1000 metric tons)					Reserves
	2017	2018	2019	2020	2021	
United States	-	-	-	-	-	620
Finland		2,210	2,200	2,290	2,300	13,000
India	3,500	4,300	4,100	2,500	3,000	100,000
Kazakhstan	4,580	6,690	6,700	7,000	7,000	230,000
South Africa	16,500	17,600	17,000	13,200	18,000	200,000
Turkey	6,500	8,000	10,000	8,000	7,000	26,000
Other countries	4,580	4,250	4,000	3,980	4,100	n/a
World total	35,700	43,100	44,000	37,000	41,000	570,000

The Republic of South Africa is known to be the largest supplier of chromite ore worldwide and its resources are estimated to be 72% - 80% of the world's total chromite ore reserve.[39-41] A large tonnage of chromite ore from the country is still exported to meet the demands for the world's production of chromium chemicals and refractories.[29,39,40] Statistical data indicate that the ferrochrome smelting industry in South Africa produced about 46% of the world's production volume of ferrochrome (Fe-Cr), typically consisting of 48%–54% Cr.[39] Industrialization activities have in-

creased in recent years with a total number of fourteen Fe-Cr smelter plants available in the Republic of South Africa.[39,42] Currently, these plants are contributing to a huge production capacity of about 4.7 million tons/year.[42]

Among the Commonwealth of Independent States (CIS) countries, Kazakhstan has about 90% of the total share of chromite ore. The industrial sectors found in Kazakhstan include fuel production, mining, smelting, and chemical industries. These industries are of much concern to regulatory authorities due to hazardous emissions emanating from their daily activities. Among the sources of atmospheric pollution, the mining and metallurgical plants were considered to have significantly contributed about 20% of the republic; of which Cr is a part.[43,44] Significant hotspots of anthropogenic emissions have been identified mainly in the industrial regions of Kazakhstan.

Temirtau, located close to the Karaganda region is known for its heavy coal mines, steel complexes, and metallurgy enterprises which are sources of chromium emission into the atmosphere. Another industrial hub is the Pavlodar region, which houses the production of bauxite, alumina, and aluminum, heat and power, oil refining, and mechanical engineering. Industrial activities in this region also contribute to the emission of chromium into the atmosphere.[44]

Aktobe, another industrial area, is located in the western part of Kazakhstan. The environmental rating of the International Academy of Ecology labeled Aktobe as one of the seven polluted cities of Kazakhstan because of its numerous industrial activities. The level of atmospheric pollution of about 42% was attributed to activities of 5 main industries: JSC "CNPC-Aktobe", LLP "Kazakhoil Aktobe" UMG "Aktobe", JSC "INTERGAS Central Asia", branches of JSC "TNC "Kazchrome", Aktobe Ferroalloy Plant (AFP) and Donskoy GOK (GGOK).[45] Aktyubinsk Chromium Compounds Plant in Aktobe is the main producer of chromic compounds in Kazakhstan with a capacity of 103.27 thousand tons. The product range in this plant includes chromic anhydride, chrome oxide, sodium bichromate, chromium sulfate, and potassium bichromate.[46]

 "Kazchrome" represents the main ferroalloys division and consists of different mining sites and metallurgic plants located in Kazakhstan. **Table 2.2** shows a summary of the asset of "Kazchrome".

Table 2.2 List of Kazchrome assets

Asset Type	Activities
Donskoy Mining and Processing Combine	Two underground and one open pit mine, Two processing plants
Aksu ferroalloy plan	Ferroalloys smelting plant
Aktobe ferroalloy plant	Ferroalloys smelting plant
Aktobe Power Generation	Turbines and thermal power plant
Kazmarganets	Manganese mine and processing plant

Source[47]

Donskoy Mining Plant: The chromite mining activities of Donskoy are located near the town of Khromtau situated in northwest Kazakhstan, approximately 90 km east of the capital, Aktobe. Currently, mining activities consist of two producing underground mines, an operating open pit mine, two beneficiation plants, two pelletizer plants, and a fine tailings treatment plant.[47] Chrome ore, for the past 14 years, has been in existence and extracted mainly from the KazaMolodezhnaya and Yuzhny mines.[47,48] Chromite mining and production were 6.0 and 4.4 million tonnes, and 5.6 and 3.7 million tonnes, respectively for 2019 and 2020.[47,49,50]

Aktobe Smelter: The Aktobe ferroalloy plant is located near Aktobe City, occupying a large industrial estate on the outskirts of the City. The three current smelting complexes were built from the 1940s to the 1970s. In 2017, the plant produced about 524 kt of ferroalloy products including high-carbon ferrochrome ("HCFeCr"), medium-carbon ferrochrome ("MCFeCr"), and low-carbon ferrochrome ("LCFeCr").[47] Chrome ore production was 0.65 and 0.67 million tonnes, respectively for 2019 and 2020.[49,50]

Aksu Smelter: The Aksu ferroalloy plant is situated about 6km north of the town of Aksu and 25 km south of Pavlodar. The smelting facility comprises four (4) smelting stations and a steady increase in production has been observed over the past 20 years. Aksu is considered one of the world's largest ferroalloy plants and produced about 1,088 kt of ferroalloy products in 2017. Products produced by the smelting plant include high-carbon ferrochrome ("HCFeCr") and ferrosilicochrome ("FeSiCr") grades.[47] Chrome ore production was 1.16 and 1.12 million tonnes, respectively for 2019 and 2020.[49,50]

2.2 Health Impacts of Hexavalent Chromium

According to International Agency for Research on Cancer (IARC) and USEPA, Cr(VI) has been identified as a Group A human carcinogen. The trivalent chromium, Cr(III), however, is an essential part of micronutrients and plays a crucial role in the metabolism of lipids and proteins in the human body.[31] Three possible routes have been identified as a means by which an individual gets exposure to Cr. These routes are through inhalation, ingestion, and dermal, for which 14 days or less are considered acute, 15 to 364 days as intermediate, and 365 days and above are considered chronic.[51]

Currently, quantification of environmental exposure specifically to Cr(VI) compounds is gaining more attention. Earlier studies focus on total chromium exposure and emphasis was not laid on the valence states of chromium during exposure. Hence, this thesis focuses more on the +6 valence state of atmospheric chromium and its quantification. Exposure to Cr(VI) through inhalation could cause lung cancer as well as other exposure routes lead to different non-cancerous effects. In biological systems, chromium particles accumulate in the bifurcations of the bronchi and about 15.8 mg/g of tissue was reported as the Cr concentration within the lung.[52] Agency for Toxic Substances and Disease Registry (ATSDR) revealed that the human lungs are capable of clearing about 53% - 85% of the Cr(VI) by absorption into the blood or by mucous in the pharynx, however, the remaining 15% - 47% is deposited in the lung. This accumulated Cr(VI) contributes to the toxicity of chromium.[53] Studies conducted on animals revealed that slightly soluble and highly insoluble Cr(VI) particles in the forms of chromates of zinc, lead, strontium, barium, and sintered calcium usually induced a tumor response, though with variable efficacy.[54] Workers and inhabitants near Cr(VI) industrial facilities as well as those near Cr waste disposal sites have the highest potential for exposure to Cr(VI) with the extent of exposure to specific Cr compounds largely depending on the type of industry.[53]

2.2.1 Chromate Pigment Industry:

Workers in chromate pigment industries would be exposed to chromates as well as soluble Cr(VI) compounds used in pigment production. Exposure to Cr in the chromium pigment industry showed shreds of evidence for an increase in the risk of lung

cancer. For example, an earlier study reported that elevated lung cancer rates were found in chromium industrial workers as well as the occurrence of increased lung cancer rates concerning their job type and employment duration.[53]

2.2.2 Chrome Plating and Welding:

Persons found in chrome plating sectors can be exposed to soluble Cr(VI) compounds.[55] The impact of chromic acid mist containing Cr(VI) in the air on the nostril and kidney was studied on chrome platers and their exposure was reported to have concentrations above $1\mu g/m^3$. Some of the symptoms associated with this exposure included the reddening of the nasal mucosa, nasal irritation, and changes in pulmonary function.[56] Long-term exposure to Cr(VI) can lead to other effects such as perforations and ulcerations of the septum, bronchitis, reduction in pulmonary function, pneumonia, asthmatic conditions, and nasal itching. For an 8-hour time-weighted average (TWA), exposure to chromic acid mists and dissolved hexavalent chromium aerosols of more than $2 \mu g/m^3$ can cause nasal septum ulceration or perforations.[56]

2.2.3 Ferrochromium Alloy Industry:

Workers in the ferrochromium alloy industry are more prone to Cr(III) compounds and Cr(VI) compounds as well as other toxic chemicals that could lead to cancer. Studies conducted on 1,876 workers in a ferrochromium plant in Sweden reported that workers were exposed to metallic chromium, Cr(III), as well as Cr(VI). The levels of exposure were 0-2.5 mg/m^3 and 0-0.25 mg/m^3 for Cr(III) and Cr(VI) respectively.[53] An occurrence of lung cancer was found in an investigation conducted in Norway among workers in a ferrochromium industry and furnace operators were exposed to total chromium within values of 0.04-0.29 mg/m^3, whereby 11–33% of this constituted chromium (VI).[53] Another study reported the distribution of lung cancer in Slovak Republic within a ferrochromium production facility. Ferrochromium workers exhibited higher lung cancer rates compared to nearby residents with concentrations in the smelter being 0.03-0.19 mg/m^3 and 0.018-0.03 mg/m^3 for total chromium and chromium(VI) respectively.[53]

Table 2.3 Guidelines to Chromium (VI) in Air

Type of Guideline	Chromium Species	Specification	References
INTERNATIONAL			
World Health Organization (WHO)	Chromium (VI)	1 µg/m^3 for lifetime risk of 4×10^{-2}	[57]
NATIONAL			
American Conference of Governmental Industrial Hygienists (ACGIH)	Calcium chromate, as Cr	0.001 mg/m^3	[58]
	Water-soluble chromium (VI) compounds	0.05 mg/m^3	
	Metal and chromium(III) compounds	0.5 mg/m^3	
	Insoluble chromium (VI) compounds	0.01 mg/m^3	
	Lead chromate, as Pb	0.05 mg/m^3	
	Lead chromate, as Cr	0.012 mg/m^3	
	Strontium chromate, as Cr	0.0005 mg/m^3	
	Zinc chromate, as Cr	0.01 mg/m^3	
National Institute for Occupational Safety and Health (NIOSH)	REL (8-hour TWA): Chromium, metal, chromium (II), and chromium (III) compounds	0.5 mg/m3	[59]
	REL (10-hour TWA): Chromium (VI) trioxide, as Cr	0.001 mg/m^3	
	IDLH, Chromium metal, as Cr	250 mg/m^3	
	IDLH, Chromium(VI) trioxide, as Cr (VI)	15 mg/m^3	
Occupational Safety and Health Administration (OSHA)	Chromium(II) compounds, as Cr	0.5 mg/m^3	[60]
	Chromium (III) compounds, as Cr	0.5 mg/m^3	
	Chromium metal and insoluble salt, as Cr	1.0 mg/m^3	
PEL (8-hour TWA)	Chromium (VI) compounds	0.5 µg/m^3	[61]

Table 2.3 summarizes the types of guidelines for various chromium species. The World Health Organization (WHO) reported its chromium (VI) exposure limit of 1 µg/m^3 for lifetime risk of 4×10^{-2}.[57] The Occupational Safety and Health Administration

(OSHA) has established its permissible exposure limit (PEL) of Cr(VI) as 0.5 µg/m^3.[55,60] The National Institute for Occupational Safety and Health (NIOSH) determined the recommended exposure limit (REL) (time-weighted average workday-10h TWA) of Cr(VI) as 1 µg/m^3, while the immediately dangerous to life and health (IDLH) limit of Cr(VI) as chromic acid and chromates was determined to be 15000 µg/m^3.[55,59] The threshold limit value-time weighed average (TLV-TWA) established by the American Conference of Governmental Industrial Hygienists (ACGIH) was 10 µg/m^3 (confirmed carcinogen; allergen) and 50 µg/m^3 (confirmed carcinogen) for insoluble and water soluble Cr(VI) compounds, respectively.[55] ACGIH also recommended the TLV (8 hours-TWA) values for calcium chromate, Cr metal and Cr(III) compounds, lead chromate, strontium chromate, and zinc chromate to be 1 µg/m^3 (a suspected carcinogen), 500 µg/m^3 (allergen; no known carcinogenicity), 12 µg/m^3 (a suspected carcinogen), 0.5 µg/m^3 (a suspected carcinogen) and 10 µg/m^3 (confirmed carcinogen), respectively.[58]

Several previous works and standards have exemplified the fact that Cr(VI) is toxic and many environmental factors influence its oxidation state; however, care must be taken during sampling to accurately measure atmospheric Cr(VI). In line with this, Torkmahalleh et al[62] developed a sampler that collected Cr(VI), and prevented chromium interconversion during the sampling interval and subsequent field storage period (the post-sample collection). Earlier available methods to quantify ambient soluble and insoluble Cr(VI) concentrations are discussed in subsequent sections.

2.3   Measurement Methods for Airborne Hexavalent Chromium

In the quest to protect public health and the environment, few methods have been adopted to quantify different species of Cr in ambient air particulate matter. The already developed methods to measure airborne Cr(VI) was performed through a 3-stage procedure; sampling, extraction of Cr(VI), and analysis of the extract. The sections below discuss the methods employed for the determination of airborne Cr(VI).

2.3.1   Measurement of Hexavalent Chromium in Ambient Air

2.3.1.1   ASTM D 5281-92 Method

The standard method known for the determination of Cr(VI) in ambient air is the ASTM Method D 5281-92.[63,64] This method is used to quantify total Cr(VI) in ambient

particulate matter (PM). A set of three 500 mL Greenberg-Smith impingers were filled with $NaHCO_3$ buffer (pH~8) and used to sample ambient particulate matter. A solution consisting of 2% NaOH-3% Na_2CO_3 was heated at 95 ºC to extract the samples and then followed by 1,5-diphenylcarbazide colorimetry at 540 nm for the detection of Cr(VI).[64] The method detection limit (MDL) was reported as 0.2-1.0 ng/m^3. One major limitation of the impinger technique is that the procedure is cumbersome, as such the method is not feasible for large-scale ambient air monitoring campaigns.[65-67]

2.3.1.2 ERG Method

A sensitive method was developed by the Eastern Research Group Inc. (ERG) for the measurement of soluble Cr(VI) in ambient air.[68] The ERG method involves sampling on a $NaHCO_3$-pretreated cellulose filter and ultrasonic extraction of the particles with 20 mM $NaHCO_3$ solution. The final stage is followed by the speciation and detection of the soluble Cr(VI) with IC-UV. The method detection limit (MDL) was reported as 0.013 ng/m^3. A limitation of this process is that the IC-UV analysis was incapable of quantifying both the recovery and conversion of soluble Cr(VI) and soluble Cr(III) in the extract.

2.3.1.3 Method developed by Meng, et al. [69]

In order to have a more thorough understanding of the exposure of humans to ambient air Cr (VI), Meng, et al. [69] developed a sensitive and more reliable filter-based method for Cr(VI) detection. This method was developed to quantify soluble Cr(VI) in ambient air by using $NaHCO_3$-pretreated mixed cellulose ester (MCE) filters for sampling and extracting ultrasonically with 60 ºC, pH=4, HNO_3 solution. Finally, speciation was conducted with IC (IonPac CG5A, Dionex, IL) and detection with ICP-MS.[69] Isotope spikes, ^{50}Cr(III) and ^{53}Cr(VI) were used to monitor inter-conversion between Cr(III) and Cr(VI) oxidation states. The MDL was found to be 0.16 ng/m^3, which depicts the method's suitability for the measurement of soluble Cr(VI) in ambient air. The percent difference was <25% for the collocated field samples.[69] The method had a 90.9 ± 8.8% (N = 11) recovery of the Cr(VI) spiked on NIST 1648 Urban PM, which was pre-coated on the MCE filters.[69] A limitation of this method was that the extraction efficiency, as well as stability of Cr species during sampling, storage, and extrac-

tion, were not thoroughly investigated. Further optimization was thus conducted by Huang, et al. [70] to this effect, as discussed below.

2.3.1.4 Microwave Digestion Method

A microwave-assisted digestion method has been developed by Huang, et al. [70] to measure insoluble Cr(VI) in ambient particulate matter. In their method, Teflon filters were employed in the sampling campaign to collect ambient particulate matter. The samples were then placed in 10-20 mL VWR microwave digestion vials and a solution consisting of a mixture of 2% NaOH - 3% Na_2CO_3, volume 1:1, at pH ~11.7, was added to the vial. Microwave digestion is followed by ramping for 15 min to 95 °C and holding it for 1 hour over a pressure < 220 psi at 300W. At the end of the digestion, the solution was sampled with a 10ml BD syringe, filtered with a 0.45 μm filter, and then sent for analyses using the IC-UV.[70] The method detection limit obtained was 0.33 ng/m^3. The method was tested in the laboratory with Cr(VI)-certified reference materials and field samples collected from 4 different sites in New Jersey. The total Cr(VI) recoveries for the Cr(VI)-certified reference materials, SQC 012 and SRM 2700 were 119.5 ± 10.4% and 106.3 ± 16.7% respectively. Total Cr(VI) in the reference urban PM (NIST 1648a) was also determined by this method and found to be 26.0 ± 3.1 mg/kg (CV=11.9%). The insoluble Cr(VI) concentrations obtained by this method were based on the difference between the total Cr(VI) and soluble Cr(VI) concentrations.

A limitation of the method was that other insoluble forms of Cr(VI) under atmospheric conditions, such as $CaCrO_4(s)$, $SrCrO_4(s)$, and even $(NH_4)_2CrO_4(s)$ (under sufficiently high concentrations of NH_4^+ and CrO_4^{2-} in the solution), were excluded in that study.

2.3.2 Measurement of Hexavalent Chromium in Occupational Facilities

The standard methods available for the measurement of airborne Cr(VI) in occupational facilities include NIOSH 7600, NIOSH 7605 (modified from NIOSH 7600), NIOSH 7703, and OSHA ID-215.[71-74]

In NIOSH 7605, a 37-mm PVC filter was used to sample airborne PM, and the filter samples were either extracted with 2% NaOH-3% Na_2CO_3 solution at 95 ºC for total Cr(VI) or extracted with 0.05 M $(NH_4)_2SO_4$-0.05M NH_4OH at room temperature

for soluble Cr(VI). This was followed by Cr speciation using Ion Chromatography (IC) and Cr(VI) detection with 1,5-diphenylcarbazide colorimetry. The limit of detection (LOD) of NIOSH 7605 was reported as 20 ng/m^3,[75] quite lower than the 500 ng/m^3 LOD of NIOSH 7600.[63,64] NIOSH 7703 was developed for in-situ measurement of soluble airborne Cr(VI) in occupational environments.[71] In the NIOSH 7703 method, samples were ultrasonically extracted with 0.05M $(NH_4)_2SO_4$-0.05M $NH_3 \cdot H_2O$, and the sample extracts were subjected to strong anion solid phase extraction using 0.5M $(NH_4)_2SO_4$-0.1M $NH_3 \cdot H_2O$ before Cr(VI) detection with 1,5-diphenylcarbazide color-imetry. The LOD of NIOSH 7703 was reported as 90 ng/m^3.[75] In OSHA ID-215, parti-cle collection was done with a PVC filter, and the filter extraction with 10% Na_2CO_3-2% $NaHCO_3$ mixed with phosphate buffer and magnesium sulfate at a temperature of 95 ºC for the quantification of total Cr(VI). Detection of Cr(VI) was done using 1,5-diphenylcarbazide colorimetry with LOD of 10.8 ng/m^3.[75]

2.4 Chemistry and Speciation of Chromium

Although chromium oxidation states range from -2 to +6, +3 and +6 are the most sta-ble valence states available in the environment. Elemental Cr and Cr(II) are easily oxidized to Cr(III) whereas the Cr(IV) and Cr(V) states are formed as unstable inter-mediates during the reaction of Cr(III) and Cr(VI) with oxidizing and reducing agents, respectively. Redox reaction plays a significant role while studying the solution chem-istry of Cr. Most of the atmospheric Cr chemistry is known to occur either in atmos-pheric droplets (e.g fog and cloud) at pH ~5 or in atmospheric liquid-coated particles having a pH ~1.[32] Because of that, this thesis focuses on the most stable chromium species, Cr(III) and Cr(VI), available in the atmosphere.

2.4.1 Aqueous Chemistry of Cr(III)

Under atmospheric conditions, Cr(III) can undergo reversible aqueous reactions such as those of hydrolysis, hydration, polymerization, and even with anions. Table 2.4 shows the possible reactions of Cr(III). Trivalent Cr in the aqueous phase can exist in varying forms such as Cr^{3+}, $Cr(OH)_2^+$, $Cr(OH)^{2+}$, and $Cr(OH)_4^-$.[30] The Cr^{3+} species are mostly found at pH <4 (Figure 2.1), and with increasing pH, it hydrolyses leading to the formation of $Cr(OH)_2^+$, $Cr(OH)^{2+}$, $Cr(OH)_4^-$, and $Cr(OH)_3$.[76] Cr^{3+} also reacts with certain ions including sulfate, chloride, bromide, fluoride, and cyanide.[76] Since at-

mospheric particles and droplets have acidic pH values, Cr^{3+} and $Cr(OH)^{2+}$ are pre-dominant compared to other Cr(III) hydroxides. Three equilibria have been identified as very important when studying the solution chemistry of Cr(III) under typical atmospheric pH and low concentrations of ions; the precipitation of chromium hydroxides, the precipitation of chromium sulfates, and the complexation by fluoride ions.[32]

Table 2.4 The equilibrium chemistry of Cr(III)[32]

Reaction	Equilibrium Reaction	Equilibrium Constant at 25°C
1	$Cr(OH)_3(s) + 3H^+ \leftrightharpoons Cr^{3+} + 3H_2O$	$< 2 \times 10^9$ M^{-2}
2	$Cr(OH)_3(s) + 2H^+ \leftrightharpoons Cr(OH)^{2+} + 2H_2O$	6.3×10^5 M^{-1}
3	$Cr(OH)_3(s) + H^+ \leftrightharpoons Cr(OH)_2^+ + H_2O$	0.3
4	$Cr(OH)_3(s) \leftrightharpoons Cr(OH)_3(aq)$	1.5×10^{-7}
5	$Cr(OH)_3(s) + H_2O \leftrightharpoons Cr(OH)^{4-} + H^+$	5×10^{-19}
6	$2Cr(OH)_3(s) + 4H^+ \leftrightharpoons Cr_2(OH)_2^{4+} + 4H_2O$	5×10^{-13}
7	$3Cr(OH)_3(s) + 5H^+ \leftrightharpoons Cr_3(OH)_4^{5+} + 5H_2O$	2×10^{17}
8	$4Cr(OH)_3(s) + 6H^+ \leftrightharpoons Cr_4(OH)_6^{6+} + 6H_2O$	6.3×10^{20}
9	$2Cr(OH)^{2+} \leftrightharpoons Cr_2(OH)_2^{4+}$	10^4 M^{-1}
10	$Cr(NO_3)_3(s) \leftrightharpoons Cr^{3+} + 3NO_3$	≤ 0.39 M
11	$Cr^{3+} + SO_4^{2-} \leftrightharpoons CrSO_4^+$	1.38 M^{-1}
12	$Cr_2(SO_4)_3(s) \leftrightharpoons 2Cr^{3+} + 3SO_4^{2-}$	1.3×10^{-7} M^5
13	$Cr^{3+} + Cl^- \leftrightharpoons CrCl^{2+}$	2.2×10^{-1} M^{-1}
14	$CrCl^{2+} + Cl^- \leftrightharpoons CrCl_2^+$	2.9×10^{-2} M^{-1}
15	$CrCl_3(s) \leftrightharpoons CrCl_2^+ + Cl^-$	$\leq 1.53 \times 10^{-3}$ M^2
16	$2CrClOH^+ \leftrightharpoons CrCl_2^+ + Cr(OH)_2^+$	0.4
17	$CrCl_2OH + H^+ \leftrightharpoons CrCl_2^+ + H_2O$	10^6 M^{-1}
18	$Cr^{3+} + Br^- \leftrightharpoons CrBr^{2+}$	0.95×10^{-3} M^{-1}
19	$Cr^{3+} + F^- \leftrightharpoons CrF^{2+}$	2.6×10^4 M^{-1}
20	$CrF^{2+} + F^- \leftrightharpoons CrF_2^+$	2.5×10^3 M^{-1}
21	$CrF^{2+} + F^- \leftrightharpoons CrF_3$	3.0×10^2 M^{-1}

2.4.2 Aqueous Chemistry of Cr(VI)

In the aqueous phase, Cr(VI) ions are available as chromate or dichromate ions. Three chromate species commonly found are CrO_4^{2-}, $HCrO_4^-$, and H_2CrO_4.[77] At considerably low pH ~1, the predominate Cr(VI) is H_2CrO_4 whereas pH > 6 has only CrO_4^{2-} as the existing specie (Figure 2.1).[78] In-between pH 1 and 6, the predominant species is $HCrO_4^-$ with a comparatively low Cr(VI) concentration. However, with an increase in Cr(VI) concentration, the dichromate $Cr_2O_7^{2-}$ becomes more profound.[77] Considering the pH range of atmospheric particles and droplets, $HCrO_4^-$ has been identified as the dominant specie. The reactions of CrO_4^{2-} are known to form precipitates with Pb^{2+}, Cu^{2+}, K^+, Na^+, and Zn^{2+}. The dichromate ion, $Cr_2O_7^{2-}$, also forms precipitates with $Na_2Cr_2O_7$ and $K_2Cr_2O_7$. In the presence of Cl^- ions under acidic conditions, $HCrO_4^-$ could react to form CrO_3Cl^-.[32] Table 2.5 highlights the Cr(VI) reactions under typical atmospheric conditions.
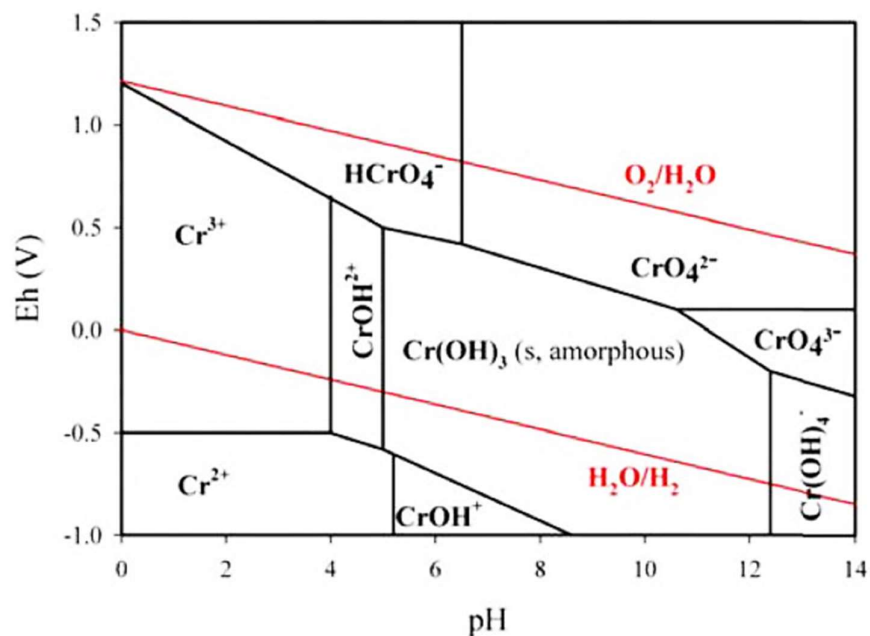
Figure 2.1 Eh-pH diagram of Chromium[70]

2.5 Interaction between Cr (III) and Cr (VI)

Under conditions of chemical equilibrium, chromium in the environment undergoes changes in its oxidation state when the redox conditions available in the environment are altered or if migrating chromium encounters varying redox conditions. Chromium

(VI) is known to be strongly oxidizing as depicted by its stability under high redox potentials. Likewise, it reacts with other reducing agents available in the environment.[79] The Eh and pH (Figure 2.1) of the solution are the two variables essential to identifying the valence states of Cr species and the concentrations of any Cr-containing ions available for any reactions that will ensure stability with solids containing Cr.[70] Hence, the physical and chemical states of Cr species in an aqueous layer of ambient particles and solution could be determined by the Eh and pH. The Eh constitutes the distribution of Cr between Cr(VI) and Cr(III), while the pH determines the distribution of Cr(III) as Cr^{3+} and $Cr(OH)_3$. For instance, under alkaline conditions (pH ~12) which is typically used in the extraction of Cr(VI), Cr^{3+} that is present in ambient PM would precipitate as $Cr(OH)_3$. Thus sufficient $Cr(OH)_3$ solids available in an aqueous media could lead to the dissociation of Cr^{3+} with amorphous $Cr(OH)_3$.[70,80]

Table 2.5 Cr(VI) reactions under atmospheric conditions[32]

Reaction	Equilibrium Reaction	Equilibrium Constant at 25 °C
1	$H^+ + CrO_4^{2-} \leftrightharpoons HCrO_4^-$	1.04×10^6 M^{-1}
2	$H^+ + HCrO_4^- \leftrightharpoons H_2CrO_4$	0.21 M^{-1}
3	$H^+ + Cr_2O_7^{2-} \leftrightharpoons HCr_2O_7$	< 0.03 M^{-1}
4	$HCrO_4^- + HCrO_4^- \leftrightharpoons Cr_2O_7^{2-} + H_2O$	98 M^{-1}
5	$HSO_4^- + HCrO_4^- \leftrightharpoons CrSO_7^{2-} + H_2O$	4.1 M^{-1}
6	$HSO_3^- + HCrO_4^- \leftrightharpoons CrSO_6^{2-} + H_2O$	36 M^{-1}
7	$H^+ + Cl^- + HCrO_4^- \leftrightharpoons CrO_3Cl^- + H_2O$	11 M^{-2}
8	$HCrO_4^- + H_2PO_4^- \leftrightharpoons HCrPO_7^{2-} + H_2O$	2.9 M^{-1}
9	$HCrO_4^- + H_3PO_4 \leftrightharpoons H_2CrPO_7^- + H_2O$	9.4 M^{-1}
10	$CeCrO_4^{2+} \leftrightharpoons CrO_4^{2-} + Ce^{4+}$	10^{-10} M
11	$KCrO_4^- \leftrightharpoons CrO_4^{2-} + K^+$	0.27 M
12	$K_2CrO_{4(S)} \leftrightharpoons CrO_4^{2-} + 2K^+$	0.23 M^3
13	$PbCrO_{4(S)} \leftrightharpoons CrO_4^{2-} + Pb^{2+}$	2.8×10^{-13} M^2
14	$CuCrO_{4(S)} \leftrightharpoons CrO_4^{2-} + Cu^{2+}$	3.6×10^{-6} M^2
15	$ZnCrO_{4(S)} \leftrightharpoons CrO_4^{2-} + Zn^{2+}$	1.1×10^{-5} M^2
16	$Na_2CrO_{4(S)} \leftrightharpoons CrO_4^{2-} + 2Na^+$	3.65 M^3
17	$K_2Cr_2O_{7(S)} \leftrightharpoons Cr_2O_7^{2-} + 2K^+$	$\leq 4.9 \times 10^{-3}$ M^3
18	$Na_2Cr_2O_{7(S)} \leftrightharpoons Cr_2O_7^{2-} + 2Na^+$	$\leq 5.1 \times 10^2$ M^3
19	$(NH_4)_2CrO_{4(S)} \leftrightharpoons 2NH_4^+ + CrO_4^{2-}$	≤ 20 M^3
20	$(NH_4)_2 Cr_2O_{7(S)} \leftrightharpoons 2NH_4^+ + Cr_2O_7^{2-}$	≤ 4.0 M^3
21	$CaCrO_{4(S)} \leftrightharpoons Ca^{2+} + CrO_4^{2-}$	2.5×10^{-4} M^2
22	$CrO_{3(S)} \leftrightharpoons CrO_{3(aq)}$	6.2 M

2.5.1 Oxidation of Cr(III) to Cr(VI)

Schroeder and Lee [81], first reported on the oxidation of Cr(III) to Cr(VI) by the action of Mn(IV) to Mn(II) as illustrated in the reaction (1.1). Their studies showed that the reaction was rapid initially but it slowed down significantly after some time. The reactions were heterogonous and the oxidation rate was controlled by the available surface area of MnO_2. Further studies conducted by Seigneur and Constantinou [32] on the chemical kinetics of atmospheric Cr also emphasized that the oxidation of Cr(III) by manganese seems slower and occurs only under extreme conditions.[32]

$$2Cr(III) + 3MnO_2 \rightleftharpoons 2Cr(VI) + 3Mn(II) \tag{1.1}$$
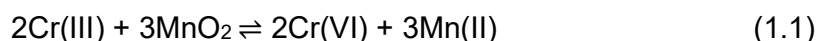
With a decrease in pH, the rate of reaction was observed to have increased according to Guertin, et al. [82]. Work conducted by Nico and Zasoski [83] also reported that Mn(III) in the manganese oxides has the potential to react with Cr(III) which could impact the oxidation of Cr(III) to Cr(VI).

Table 2.6 Reduction of Cr(VI) to Cr(III)[32]

Number Reaction	Number Reaction
1	$Cr^{6+} + 3V^{2+} \rightarrow Cr^{3+} + 3V^{3+}$
2	$HCrO_4^- + 3V^{3+} + H^+ \rightarrow Cr^{3+} + 3VO^{2+} + H_2O$
3	$Cr^{6+} + 3VO^{2+} \rightarrow Cr^{3+} + 3VO_2^+$
4	$Cr^{6+} + 3Fe^{2+} \rightarrow Cr^{3+} + 3Fe^{3+}$
5	$2 HCrO_4^- + 3HNO_2 + 5H^+ \rightarrow 2Cr^{3+} + 3NO_3^- + 5H_2O$
6	$2 HCrO_4^- + 3H_2S + 8H^+ \rightarrow 2Cr^{3+} + 3S + 8H_2O$
7	$2 HCrO_4^- + 9I^- + 14H^+ + 4H_2O \rightarrow 2Cr(H_2O)_6^{3+} + 3I_3^-$
8	$2 HCrO_4^- + 4HSO_3^- + 6H^+ \rightarrow 2Cr^{3+} + 2SO_4^{2-} + S_2O_6^{2-} + 6H_2O$
9	$2Cr^{6+} + 3HCOOH \rightarrow 2Cr^{3+} + 3CO_2$
10	$3Cr^{6+} + 2C_2H_5OH \rightarrow 3Cr^{3+} + 2CH_3COOH$
11	$2H_2AsO_3^- + 3Cr^{6+} \rightarrow 3Cr^{3+} + 2H_2AsO_4^-$
12	$2HCrO_4^- + 3H_2O_2 + 8H^+ \rightarrow 2Cr^{3+} + 3O_2 + 8H_2O$

2.5.2 Reduction of Cr(VI) to Cr(III)

Under favorable conditions Cr(VI) is reduced to Cr(III) with its reactions listed in **Error! Reference source not found.**

Work conducted on organic compounds reveals they contribute immensely to the reduction of ambient Cr(VI). Organic compounds like humic acids and fulvic acids were identified as reducing Cr(VI) to Cr(III) in soils. With increasing pH, the rate of the reduction decreases however, this rate increases with increasing initial chromium concentration, as well as an increase in the concentration of soil humic substances.[77] At very low pH, the half-life for Cr(VI) reduction with humic acids was determined to be approximately 3 days, but this time increases over a pH range of 4-7.[84] Thus, in the context of airborne particulates, humic-like substances could reduce Cr(VI) to Cr(III) in a similar manner.

Iron (II) interaction with chromium revealed that it reduces Cr(VI) to Cr(III). In sodium chloride solution, the rate of the reduction of Cr(VI) by Fe (II) decreases over the pH of 1.5-4.5, but increases within pH 5.0-8.7. It however remained fairly constant over pH 4.5-5.0.[85] Temperature ranges of 5-40°C showed varying trends for the reduction of Cr(VI) by Fe(II) over at pH 4 to 6. At pH 4, the rate of reduction remained approximately constant over the aforementioned temperature range. The reduction rate however increases with increasing temperature at pH 6.[85] Tests conducted in the laboratory showed that the reduction of Cr(VI) by Fe(II) was achieved within 5 minutes.[86] Under alkaline conditions, Pettine, et al. [85] revealed that Fe(II) controls the reduction of Cr (VI) in aqueous anoxic.

Reduced sulfur in the forms of S, S^{2-}, H_2S, and S_2O_3 reduces Cr(VI) to Cr(III). Laboratory work reveals that in the presence of sulfide, the reduction of Cr(VI) initially is rapid, later slows down in a few minutes, and reaches completion at the end of 1 day.[81] In the presence of other metal ions, Pettine, et al. [85] investigated the rate of the reduction of Cr(VI) using H_2S in NaCl media. They reported that all the metals except Ca^{2+} and Zn^{2+} showed an increase in the rate of reduction of Cr(VI). A phenomenon was observed wherein there was a linear increase in the rates for Pb^{2+}, Cu^{2+}, Cd^{2+}, and Ni^{2+} as a result of the formation of metal chromates that reacted faster than free chromates. The half-life of Cr(VI) ranges from a few hours (4-6 hours at 1mM H_2S) to many days (160-250 days at 1μM H_2S) in anoxic water.[87] Reduction of Cr(VI) with S(IV) in NaCl media plays a role in strong acidic matrices, pH <3, as in particles and

fog droplets [88]. Earlier work conducted by Pettine, et al. [88] showed that at pH=3 and a temperature of 10 °C, the half-life was 24 minutes; comparable to the value of 23-30 minutes as reported by Seigneur and Constantinou [32]. Increasing pH values from 2 to 5, however, showed a decrease in the rate of the reduction of Cr(VI) by S(IV).[88]

The reduction of Cr(VI) by phosphoric acid (H_3PO_3) in the presence of H_2SO_4 and $HClO_4$ was investigated by Khan, et al. [89]. They reported that with increasing H_2SO_4 and $HClO_4$ concentrations, the rate of the reaction equally increased. The presence of Cu(I) at low pH, similar to that of atmospheric aqueous media also reduces Cr(VI) to Cr(III).[90] Similarly, at lower pH, the reduction of Cr(VI) with H_2O_2 is feasible in atmospheric media.[91] Goshu, et al. [92] also investigated the reduction of Cr(VI) in the presence of additives of $Cu(NO_3)_2$, $Fe(NO_3)_3$, and $Ni(NO_3)_2$.[92] The extent of Cr(VI) reduction to Cr(III) in the systems decreased by the order of $Cu^{2+} > Fe^{3+} > Ni^{2+}$. Likewise, the effect of anions on the degree of Cr(VI) reduction was reported in the order of $NO_3^- > Cl^- > SO_4^{2-}$.[92]

2.6   Models to Simulate Atmospheric Cr Chemistry

The study of the atmospheric chemistry of chromium has been on the rise, particularly about other reactive species in varying environments (airborne, water, and soil). Under atmospheric conditions, Cr speciation and quantification are challenging due to interconversion between Cr(III) and Cr(VI) in the presence of oxidants and reductants. Additionally, the valence state of Cr in the atmosphere is dependent on the solution equilibrium between Cr(III) and Cr(VI). The interconversion between these two species occurs in solution as well as via a solid-gas reaction. [62,93] Because of the uncertainties in quantifying ambient Cr(VI) due to these challenges, researchers conducted various studies to predict the chemistry of Cr under atmospheric conditions.

Seigneur and Constantinou [32] performed a computer-based simulation on atmospheric chromium chemistry using different equilibria and kinetic reactions at pH ~1 (liquid-coated particle) and pH~4 (liquid droplet). Their simulation outputs illustrated overall reactions of Cr(VI) to be speedy after reacting with various reactants at pH~4. The oxidation of Cr(III) by Mn was relatively slower and the overall reaction was the reduction of Cr(VI) to Cr(III) with half-lives ranging from a few seconds to several minutes.[32] Their work however excluded the interactions between Cr(III) and other gases such as VOCs, ozone, and reactive oxygen species.

Grohse [94] also studied the conversion rate of Cr(VI) in the presence of reactants; HNO_3, HCHO, O_3, NO_2, SO_2, m-xylene, benzene, Fe^{2+}, and V^{2+} in a laboratory chamber using typical atmospheric conditions. Their results revealed that after 24 hours, the conversion rate ranged from less than 5 to 99%. The variation in this conversion attributed to the different concentrations of the reacting species with Cr(VI) as well as the systems' relative humidity.[94] The reaction of Cr(III) VOCs was however not investigated in their work.

Amouei Torkmahalleh, et al. [95] further developed a computer model by utilizing the earlier concept of Seigneur and Constantinou [32] whereby they used field data collected from New Jersey, US, to understand the chemistry and speciation of soluble, and insoluble chromium in pH~9.[95] Simulation results revealed that Cr(VI) was dominant as CrO_4^{2-} in the soluble form whereas $(NH_4)_2CrO_4$, $CaCrO_4$, $BaCrO_4$, and $PbCrO_4$ precipitated. The reduction of Cr(VI) to Cr(III) was higher than the oxidation of Cr(III) to Cr(VI) according to their findings. A basic pH solution retarded the conversion of Cr(VI) in the presence of Fe(II) and As(III) though it facilitated the precipitation of Cr(III).[95] Aerosolized gases such as O_3, O_2, HO_2, and HO_3 were employed in their model, however, the reaction of VOCs was excluded to ascertain the Cr chemistry under atmospheric conditions.

Konakbayeva, et al. [96] developed a modeled Cr speciation in deliquesced particles (pH~4) to provide more insight into the soluble and insoluble forms of atmospheric Cr particles. Equilibrium reactions, including redox reactions, dissolution, precipitation, and kinetic reactions represented the aqueous chemistry of atmospheric Cr in their model. Air containing small amounts of gaseous species such as SO_2, NH_3, O_2, and O_3, whose concentrations were constant with time, were used in the model. Results showed that the insoluble Cr(III) compound, $Cr_2(SO_4)_{3(s)}$, was the dominant form of Cr(III) at pH~4. Interaction of VOCs with Cr(III) and/or Cr(VI) was however not reported in the work. The overall conversion direction was identified as from Cr(VI) to Cr(III).[96]

Recently, Shah, et al. [97] used molecular dynamics simulation to study the impact of VOCs on chromium-containing atmospheric particulate. Interaction energies and diffusivity for different VOCs in atmospheric particles that contained Cr(III) via classical molecular dynamics simulations. VOCs such as xylene, toluene, ascorbic acid, carbon tetrachloride, styrene, methyl ethyl ketone, naphthalene, and anthra-

cene in Cr(III) solutions, with and without air were used to study their impact on Cr solution chemistry. They observed changes in the interaction energy between Cr(III) and water within the range of 48% to 180% for the different VOCs, with the highest change being anthracene and the lowest change being naphthalene. No direct interactions however were observed between Cr(III) particles and the VOCs, except ascorbic acid. Their simulation thus gave more insight into the chromium chemistry and reaction rates in the atmospheric particles in the presence of VOCs.

2.7   Challenges With Ambient Cr(VI) Quantification

2.7.1 Efficiency of Extraction

The extraction efficiency is of paramount importance to the measurement of Cr(VI) in ambient air. Weak acidic (HNO_3, pH = 4), neutral (deionized water), and weak basic ($NaHCO_3$, pH ~ 8.5) solutions have been employed but could not dissolve insoluble chromates.[98] Strong acidic solutions can dissolve insoluble chromates at high temperatures and pressure however, interconversion of Cr(VI) to Cr(III) emerges during the extraction process.[99] In this regard, the use of alkaline solutions is a possible remedy. The reaction of alkaline buffers with CO_3^{2-} heated with a hotplate was first used to extract the insoluble fractions of Cr(VI) from soil and airborne PM collected from occupational facilities.[72,75,100,101] The dissolution of the insoluble fractions of Cr(VI) was explained with the following equations[98] ;

$$BaCrO_4 + CO_3^{2-} \rightarrow BaCO_3 \downarrow + CrO_4^{2-} \tag{1.2}$$

$$PbCrO_4 + OH^- \rightarrow Pb(OH)_2 \downarrow + CrO_4^{2-} \tag{1.3}$$
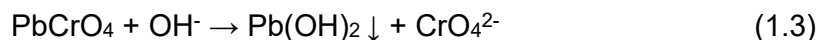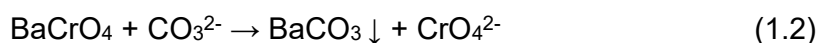
Generally, a hotplate is used to heat the alkaline solution during extraction.[72,100] A new way of extraction using a microwave has been identified due to its numerous advantages including easy operation, and automation.[102] Using a microwave extraction technique improved the extraction efficiency as well as being an alternative to the conventional hotplate digestion method.

2.7.2 Sensitivity

The trace levels of Cr(VI) depend on the environment in which trace levels are being monitored. For instance, trace levels of Cr(VI) in ambient air are in the range of 0.1 - 8.4 ng/m^3.[103-105] In occupational facilities, on the other hand, levels of Cr(VI) in the air are relatively higher than in the ambient air.[106,107] In the metal welding industry, concentrations of total Cr(VI) in the welding fumes were reported as 20 mg/m^3.[106] Measurements conducted in the aircraft painting industry revealed total Cr(VI) levels within the range of 4.0 - 400 $\mu g/m^3$.[107] Having identified the possible levels of Cr(VI) in ambient air, the already standard methods developed for the measurement of total Cr(VI) in workplace air samples (NIOSH 7605 and 7703) may not be sensitive enough to detect trace levels in ambient air.[75,101,108] The development of a new method for the measurement of total Cr(VI) and/or insoluble Cr(VI) is thus essential such that the MDL would be much lower than the already standard methods.

2.7.3 Interconversion between Cr(III) and Cr(VI)

An environmental challenge that affects the accuracy of measurement of ambient Cr(VI) concentrations is the reduction of Cr(VI) to Cr(III) and vice versa during sampling. Seigneur and Constantinou [32] initially modeled the atmospheric reactions of Cr on liquid-coated particles and droplets and identified that the half-life of Cr(VI) ranged from 6s to 7 hr, depending on the reactant concentrations. Grohse [94] also investigated the reactions of Cr(VI) in the presence of gases and reactants (HNO_3, HCHO, O_3, NO_2, SO_2, m-xylene, benzene, Fe^{2+}, and V^{2+}) using a reaction chamber with varying Cr(VI) concentrations and relative humidity. The authors reported that after 24 hrs, Cr(VI) conversion to Cr(III) was in the range of <5% to 99%. This large variation accounted for a result of different concentrations of the species that reacted with Cr(VI). An average half-life of 16 hrs for Cr(VI) in the atmosphere was reported during their investigation.

Meanwhile, other pathways were reported for the reduction of Cr(VI) to Cr(III) such as with Iron(II)[85], reduced sulfur species such as S, S^{2-}, H_2S, and S_2O_3,[81] humic and fulvic acids[77], and Cu(I) at low pH.[90] Goshu, et al. [92] further reported the efficiency of cations and anions on the conversion of Cr(VI) to Cr(III) to be in the order of Cu^{2+} > Fe^{3+} > Ni^{2+} and NO_3^- > Cl^- > SO_4^{2-} respectively.[92] Werner, et al. [109] and Nico, et al. [110] reported that gaseous reactants (ROS and O_3) play a significant role in the

solution chemistry of atmospheric chromium, in which the reaction of the gaseous species with Cr(VI) leads to its reduction to Cr(III).

Chamber and field study of atmospheric Cr(VI) conducted by Huang, et al. [111] also exemplified the fact that SO_2, PM matrix, ROS, and RH could influence the valence state of soluble Cr during sampling. While incorporating basic filter media, the authors reported that diesel particulate matter (DPM) and secondary organic aerosols (SOA) matrix induced Cr(VI) reduction after exposure to clean air, whereas ROS in SOA enhanced Cr(III) oxidation. Meanwhile increasing deliquescence relative humidity (DRH) from 40% to 70% led to the oxidation of Cr(III) in SOA, and the presence of organics in DPM and SOA facilitated Cr(VI)-Cr(III) inter-conversion.[111] Amouei Torkmahalleh, et al. [112] also showed that oxidants such as ozone and ROS could convert Cr(III) to Cr(VI) at low RH. The authors however indicated that on PM-laden filters, the oxidation of Cr(III) by O_3 could be slowed by a decrease in temperature; thus sampling Cr(VI) in a cool environment could give a less biased result when oxidation of Cr(III) occurs in the presence of atmospheric oxidants.[112]

In view of controlling the interconversion between Cr(VI) and Cr(III), Amouei Torkmahalleh, et al. [62] postulated that keeping filters dry during and after sampling below its deliquescence relative humidity (76%) of ambient particles is a prominent way to improve the sampling of Cr(VI). They designed and constructed a new Clarkson Cr(VI) sampler such that deliquescence during sampling would not lead to aqueous phase reactions since the relative humidity of the sampled air was reduced below the deliquescence relative humidity (DRH) of the ambient particulates.

After 24-hour sampling intervals, the average recovery values of Cr(VI) spikes for summer and winter sampling were 57% and 72% respectively, whereas the corresponding average values for NATTS Cr(VI) samplers were reported as 46% for both summer and winter sampling, respectively. Thus preventing the ambient particles on the filters from deliquescing is very essential to improving the sampling of Cr(VI).[62]

2.8 Carbon-based Materials

Carbon-based materials are gaining more popularity in research since they play important roles in the aspect of material science. These materials stretch from conventional industrial carbon (such as carbon black, and activated carbon) to modern in-

dustrial carbons (carbon fibers, graphite) and carbon nanomaterials (graphene and carbon nanotubes). Carbon-based materials serve as the fundamental platform for most research and its applications in the area of chemistry, materials, and other disciplines owing to their environmental friendliness. Additionally, the outstanding physical, chemical, thermal, and electrical properties of carbon-based materials enable them to be used in various fields. The carbon-based materials are grouped into families of carbon nanotubes[113], carbon nanofibers[114], graphene nanosheets[115], graphene quantum dots[116], graphene nanoribbons[117], and graphene nanoparticles.[118] These various derivatives serve as essential materials that acts as a compatible scaffold onto which other structural materials can be built. Extensive studies in the past decade revealed that these carbon-based materials possess superior properties like chemical stability, biocompatibility, low toxicity, and flexibility for surface functionalization.[119] Additionally, their nanosize allows them direct interaction with the pathways of other molecules and living systems.[120]

2.8.1 Carbon Dots (CDs):

Limitations such as the unavailability of an appropriate band gap prevent normal carbon from being an efficient luminescent material. Carbon dots (CDs) are gaining popularity due to characteristics of excellent and tunable photoluminescence (PL), high quantum yield (QY), low toxicity, small size, appreciable biocompatibility, and low cost.[119,121] This carbon family has found applications in various fields including biomedicine, catalysis, optoelectronic devices, and anticounterfeiting.[119,121] CDs are generally defined as quasi-0D carbon-based material with a size of less than 10 nm, and fluorescence is their intrinsic property.[121] Carbon nanoparticles with fluorescence ability were first reported by Xu, et al. [122] who accidentally obtained the particles from the purification of single-walled CNTs. Later in 2006, Sun, et al. [123] named this type of carbon particle as CDs, after synthesizing with laser ablation but with a quantum yield (QY) of about 10%. Initial development of the CDs was limited due to issues of low QY and extensive preparation procedures.[121] The breakthrough came in 2013 when Zhu, et al. [124] used citric acid (CA) and ethylenediamine as precursors to synthesize polymer-like CDs having a QY of ~80% via the one-step hydrothermal method. Currently, this QY is the highest value achievable for carbon-based fluorescent materials and is used in printing inks as well as in functional nanocomposites.[121,124]

Characteristics such as high QY, low toxicity, facile synthesis approach, and high resistance to photobleaching of CDs led to a vibrant interest in this research area. Different strategies and technologies for CDs were further developed by researchers with significant breakthroughs including multicolor/deep red/near-infrared (NIR) emission[125-127], narrow full-width at half maximum (FWHM)[125,128], photoluminescence[125,127], chirality[129,130], and room temperature phosphorescence[131,132] among other applications. CDs are classified mainly as graphene quantum dots (GQDs), carbon quantum dots (CQDs), and carbonized polymer dots (CPDs), with respect to their mechanism of formation, micro-/nanostructures, and properties.[121]

GQDs comprise one- or multiple-layer graphite structures with chemical groups attached on the surface/edge or within the interlayer defect of the nano-material.[133,134] The optical properties of this nanomaterial are dominated by surface structures as well as the size of π-conjugated domains. GQDs are anisotropic having their lateral dimensions usually larger than their height. CQDs and CPDs are usually spherical, and often obtained from small molecules, polymers, or biomass by assembling, polymerization, crosslinking, and carbonization.[125,127,128] CQDs usually constitute multiple-layered graphitic structures connected to surface groups. CPDs were first mentioned in 2013 and these CDs are aggregated and made up of carbonized polymer hybrid nanostructures.[135,136] The structural arrangement of CPDs shows they have unique "core−shell" nanostructures that comprise carbon cores <20 nm, dehydrated crosslinking polymer frames, and functional groups joining the shells.[125,137] These properties of CPDs lend credence to their higher stability, better compatibility, easier modification, and functionalization.

2.8.2 Synthesis Classifications of CDs

Two types of techniques are available for the synthesis of CDs; the Top-down method and the Bottom-Up method. Techniques such as Laser ablation, arc discharge, electrochemical oxidation, ultrasonic treatment, and chemical oxidation are under the top-down methods. Other methods such as the pyrolytic process, template method, hydrothermal/solvothermal methods, and microwave-assisted synthesis are generally grouped under the bottom-up method.

2.8.2.1   Top-Down Method

In this method, carbon macromolecules are divided into smaller sizes via physical forces, and then surface modification is conducted to the resulting material to enhance their properties (e.g fluorescence). Some of the top-down approaches include laser-ablation, arc-discharge, chemical oxidation, and electrochemical methods. For example, laser ablation as a top-down method employs a high-energy laser pulse that irradiates the surface of the target to a thermo-dynamic mode that generates high temperatures and pressures, while the heat content increases and later evaporates into a plasma mood. In the end, the vapor crystallizes into nanoparticles[119,138]. Sun, et al. [123] synthesized CDs via laser ablation into a carbon target using water vapor and Argon as the carrier gas at a high temperature of 900 °C and 75 kPa. After applying nitric acid reflux for 12 hours, the surface was immobilized using attachment of the organic samples like amine-terminated poly-ethylene glycol and poly(-propionyl ethylene eimine-coethyleneimine) to produce acidified CQDs having luminescence properties.[123] The main advantage of the laser ablation technique is the simplicity of operation, which leads to the production of different nanostructures. In contrast, a high amount of carbon material is required for the carbon targets, which makes it expensive.[119] The arc-discharge method was used during the synthesis of single-walled nanotubes (SWNTs) where the first fluorescent CDs were discovered as a byproduct at the end of the reaction.[122] Chemical oxidation is used wherein acids with strong oxidization potentials are added to carbon atoms to break them into small organic molecules. This treatment converts smaller molecules into carbonaceous materials, which are cut into smaller sheets by the oxidation process [139]. Electrochemical oxidation is one of the easy methods used to produce nanomaterial and is regarded as one of the suitable methods for synthesizing CQDs. This method is mostly preferred since it can regulate particle sizes, and achieve high purity, high yield, and good PL of synthesized CQDs.[140]

2.8.2.2   Bottom-Up Method

This method synthesizes CDs from small carbon molecules using starting materials such as citrates, carbohydrates, and other known green materials. The functional states and sizes of the CDs produced under this method are easily altered.[141,142] The synthesis of CDs under this process is initiated by the carbonization of available car-

bon precursors and dehydration through heat treatment via hydrothermal, micro-wave, or pyrolysis processes.[142-144] Processes such as thermal decomposition, hydrothermal treatment, and microwave techniques fall under this category.

Thermal decomposition, a pyrolytic process, is a well-known method for the production of CDs at high temperatures. Advantages of this method span from the simplicity of operations, solvent-free usage, ranges of precursors that can be incorporated, short synthesis duration, large-scale production, and low cost.[145]

Hydrothermal carbonization (HTC) or solvothermal carbonization is considered an inexpensive and eco-friendly method for the production of carbonaceous materials. Usually, an organic solution reacts with precursor(s) that are sealed in a hydrothermal reactor amidst increased temperatures. CQDs can be produced by this method using various raw materials such as protein, glucose, citric acid, etc.[146]

Microwave techniques are considered electromagnetic waves with a wavelength in the range of 1 mm and 1 m, which provides massive energies to decompose the chemical bonds available in substrates.[119] The main advantages of this technique are being quick and affordable, a short reaction time, and gives homogeneous heating that enables the user to obtain smooth size distribution of the CDs.[144,147] The microwave-assisted hydrothermal method is also common and used to synthesize CDs from a variety of organic substrates (sucrose, glucose, saccharides, amino acids, and proteins) that serve as building blocks for the CDs.[144,148]

2.8.3 Characterization of CDs

Different procedures have been exploited for the characterization of the CDs, such as Transmission electron microscopy, X-ray diffraction, Fourier transform infrared spectroscopy (FTIR), Photoluminescence, Ultraviolet spectroscopy, and Raman spectroscopy.

2.8.3.1 Transmission Electron Microscopy (TEM)

TEM uses very high resolution typically, in the range of 0.1-0.2 nm, to identify the ultrastructure of samples and CDs for that matter. This analytical procedure also serves as a means to study the morphological structure of nanomaterials concerning their shapes, sizes, and even dispersion.[149] TEM thus plays a crucial role in describing the nature of CQDs and GQDs since their structures are very distinct. For exam-

ple, Sun, et al. [123] who first worked on CQDs described them as having a quasi-spherical shape with sizes <10 nm in diameter when observed with TEM. Fluorescent GQDs were synthesized by Pan, et al. [150] and described as having a crystalline structure with a single or a few graphene layers. More so, synthesized GQDs are mostly elliptical or circular.

2.8.3.2 Fourier Transform Infrared Spectroscopy (FTIR)

The frequencies of the radiation at which the materials are absorbed are detected due to the vibrational motions of molecules in the materials. FTIR spectroscopy proves to be a fast technique for the identification and characterization of chemical structures in a given material.[151] Generally, CQDs can be obtained by the oxidation of the carbon precursor(s), and as such the surfaces of CDs are generally endowed with functional groups such as hydroxyl, epoxy, ether, carboxylic acid, or carboxyl.[119] The use of FTIR has been identified as a renowned method to analyze the aforementioned oxygen-containing groups. FTIR plays a significant role in CDs where they can identify available functional groups before and after transformations such as stabilizing the energy surface, improving the fluorescence quantum yield, and reducing the toxicity of the CDs.[152]

2.8.3.3 Ultraviolet Spectroscopy (UV)

Different applications of GQDs and CDs have seen the accumulation of photons over shortwave lengths due to the presence of π-π* transition of the C=C bonds. CQDs are known to exhibit strong optical adsorption in the UV region of 260 nm to 320 nm and comparatively absorb even better over longer wavelengths than GQDs. The presence of a sharp peak over the range of 270 nm to 390 nm usually indicates a contribution to the n-π* transition of the C=O bonds present.[153] Modifications such as surface passivation and varying functional groups can alter the adsorption characteristics in nanomaterials. For example, Cao, et al. [154] who synthesized N-CDs with excellent water solubility with bright cyan fluorescence identified two absorbance bands at 260 nm and 340 nm, which were attributed to the π-π* transition of the C=C sp^2 bonds in the carbon core and the n-π* transition of the C=O/C–N moieties present on the surface of the N-CDs, respectively.[154]

2.8.3.4   Photoluminescence (PL)

One of the prominent features of CDs has been their ability to undergo PL which originates from quantum confinement. Due to the emissive traps available on the surface of CDs, their PL quantum yield has seen a decline. The quantum yield however can be enhanced through the process of surface passivation or modification. The presence of structural layers and good crystallinity in GQDs are contributing factors to their greater quantum yield as compared to bare CDs [119]. Various CDs and GQDs have been synthesized via diverse methods to yield different PL colors within the UV and visible light range, and sometimes closer to the infrared region. Jiang, et al. [155] used a facile approach to prepare photoluminescent carbon dots that resulted in the emission of three bright and stable red, green, and blue colors of luminescence when observed under UV light. The emissions of these colors of PL were attributed to different sizes and nitrogen content varied in the CDs.[155] Zhao, et al. [156] equally synthesized a high photoluminescence quantum yield of multi-colored CDs via a one-pot solvothermal process, and when observed under UV light the CDs emitted a red, green, and blue color.

2.8.3.5   X-Ray Diffraction (XRD)

XRD technique is used to characterize CQDs as well as to obtain information on particle size, phase purity, crystallinity, as well as the crystalline stages of CDs.[152] For example, Chen, et al. [20] synthesized GQDs using starch precursors via a hydrothermal reaction, and the XRD patterns showed a broad peak of 2.4 nm similar to the characteristic pick of carbon (002). Ming, et al. [157] also synthesized a low-cost nitrogen-doped carbon dots (N-CDs) fluorescent sensor for sensitive detection of Cr via a one-step hydrothermal method. The XRD pattern of the N-CDs showed a strong diffraction peak at 21.6°, which was attributed to the highly disordered carbon present in the CDs.

2.8.3.6   Raman Spectroscopy

Raman spectroscopy is one of the fast and non-destructive techniques that use high-resolution features to characterize the lattice structure, electronic, and optical properties of carbon materials (diamond and graphite, 2D graphene, 1D carbon nanotubes, 0D fullerenes, and CQDs).[158] A Raman spectroscopy investigation on GQDs was

conducted by Dervishi, et al. [159] which revealed the D and G bands in the CDs. The D and G band frequencies and intensity increased as the size of GQD increased. The authors further indicated that as the size of the GQDs increased, the integrated intensity ratios of D and G bands (ID/IG) also increased as it approaches 2 nm and then decreased again when the graphene structures got larger.[159]

2.8.4 Application of CDs in Cr(VI) detection

Measures to mitigate environmental pollution have necessitated the development of advanced materials that can be used for sensing and adsorption of toxic substances in humans and the environment. Various methods such as UV-Vis spectrophotometry, ion chromatography[10-12], atomic absorption spectrophotometry[13], and electrochemical methods[14] have been used to measure Cr pollution in the environment. Even though these methods have been used, drawbacks such as high cost, extensive professional operation, time-consuming operation, and unsuitable for real-time monitoring[15-17] have been a concern among researchers. Thus there is a growing need to have a robust method for the rapid detection of Cr(VI) ions.

2.8.4.1   Colorimetric Sensing of Cr(VI) ions

Colorimetric sensing of analytes is vital in analytical chemistry since a color change enables quick detection of analytes with the human eye.[160] Since CDs are capable of absorbing light in the visible region, they can be suitable agents for colorimetric sensing of many metallic ions including Cr(VI).[18]

Babazadeh, et al. [161] used a one-pot oxidative technique to synthesize a stable suspension of N-doped carbon dots in water–THF solutions (N-CDs-W-THF). Colorimetric detection of hexavalent chromium in water was performed by the N-CDs-W-THF which showed selective variations of optical absorbance for Cr(VI) ions in water.[161] A distinct absorption band peak at 550 nm was seen and this increased linearly, with the Cr(VI) ion in the range of 1-100 μM. This enabled the visual and ratiometric determination of Cr(VI) with a LOD of 300 nM.[161] Studies conducted by Daniel [162] showed the fabrication of a novel molecular probe using a smart carbon dot and a Schiff's base viz 4-amino -N-[(2-hydroxyphenyl)methylidene] benzoic acid. The CDs composite served as a useful colorimetric molecular probe for sensing Cr(VI) in aqueous solutions. Their study indicated that the colorimetric sensor was

able to effectively sense Cr (VI) in the aqueous solutions even into the picomolar concentration range.[162] Goswami, et al. [163] produced CDs from biomass and later fabricated them into g-C_3N_4 to get a metal-free enzyme. The CDs retained some peroxidase activities, as exemplified by the catalyzed oxidation of 3,3',5,5', -tetramethyl benzidine (TMB) in the presence of H_2O_2, as well as showing a color change from transparent to blue.[163] In an acidic solution, the presence of Cr (VI) accelerated the breakdown of H_2O_2 to -OH radicals and thus causing an increase in the rate of TMB oxidation. The CD/g-C_3N_4 served as a visual colorimetric sensor for the detection of Cr(VI) that yielded a LOD of 0.31 µM, due to the probable electron transfer between TMB and H_2O_2.[163] Xu, et al. [164] reported the synthesis of amphibious yellow luminescent carbon dots (Y-CDs) via a rapid and low-cost microwave method. The Y-CDs demonstrated good solubility and strong yellow fluorescent color both in water and organic solvents. Hexavalent Cr ions were detected by the fluorescence color changes when Y-CDs were present in the aqueous solutions, and the LOD obtained was 0.02 µM.[164] In addition, the team developed Cr(VI)-test paper system for visual on-site sensing of Cr(VI). Considering the unique features of Y-CDS, not only can it be used as a visual on-site sensor for Cr(VI) but can also be used in other applications such as bio-imaging and optical devices.[164]

2.8.4.2   Fluorimetric Sensing of Cr(VI) ions

Fluorescence spectroscopy using nanomaterials has been on the rise as a result of its unique features such as fast response time, and specific and sensitive detection of analytes.[18] The fluorescence feature of CDs can either be quenched or enhanced upon its interaction with metal ions in solution. This unique characteristic enables CDs to be used in fluorimetric metal ion sensing. Although enhancement of fluorescence is possible, the most widely observed phenomenon is quenching when metal ions interact with CDs. Fluorimetric chemosensor development has been on the rise and investigations have been conducted in view of using these sensors to detect Cr(VI) in aqueous solutions.

Shen, et al. [165] synthesized N,S co-doped carbon dots using biomass via a hydrothermal treatment, and passivating with ammonium persulfate. The NS-CDs showed excellent fluorescent properties including high quantum yield (18.7%) and good stability. The fluorescence of NS-CDs was effectively quenched by Cr (VI),

within the concentration range of 1 to 40 µM, due to the antioxidation of NS-CDs.[165] Dual emissive carbon dots (DECDs) were synthesized by Ma, et al. [166] via hydrothermal treatment using m-aminophenol and oxalic acid. The DECDs exhibited a dual emission fluorescence peak at 430 nm and 510 nm when initially excited at 380 nm, as well as good water solubility and stable fluorescence. The DECDs served as an excellent probe for the determination of Cr(VI) with a LOD of 0.4 µM over a linear range of 2 to 300 µM.[166] Zheng and his coworkers used a thermal pyrolysis method to prepare an "on-off-on" fluorescent CDs with a high quantum yield (88.6%) using citric acid and diethylenetriamine as a surface passivation agent.[167] The CDs served as a fluorescent chemosensor for the determination of Cr(VI) that showed a "turn-on" fluorescent emission in the linear range of 0.01−50 µmol/L.[167] Laddha, et al. [168] used a microwave-assisted technique to synthesize blue emissive multifunctional NSP co-doped CDs that were used as a probe for the detection of Cr(VI). In the synthetic process, simple precursors like glutathione, polyethylene glycol, and o-phosphoric acid were used to achieve a good quantum yield of the CDs. The blue fluorescence emission exhibited by the NSP-CDs was quenched upon the addition of Cr(VI) in the presence of other interfering ions within a linear range of 0.1–100 µM. A limit of detection of 4 nM was reported for Cr(VI) detection.[168]

2.8.5 Doping CDs for Cr(VI) Detection

Generally, the size of CDs can be controlled by altering reaction parameters such as the concentration of reactants, reaction temperature, synthesis duration, surfactants, additives, etc.[22] Highly fluorescent CDs synthesized from precursors such as orange juice, glucose, banana juice, citric acid, etc., mostly show blue-emitting fluorescence. However, the emission spectra of CDs can be altered by doping with specific elements (Figure 2.2) such as cobalt (Co), copper (Cu), zinc (Zn), nitrogen (N), sulfur (S), phosphorus (P), boron (B), etc., or their combinations.[22] The doping of CDs plays key roles such as the enhancement of fluorescence and shift of emission spectra. Additionally, doping CDs with other elements modifies the bandgap energy with resultant improvements in the charge separation efficiency when in use as chemosensors.[23]
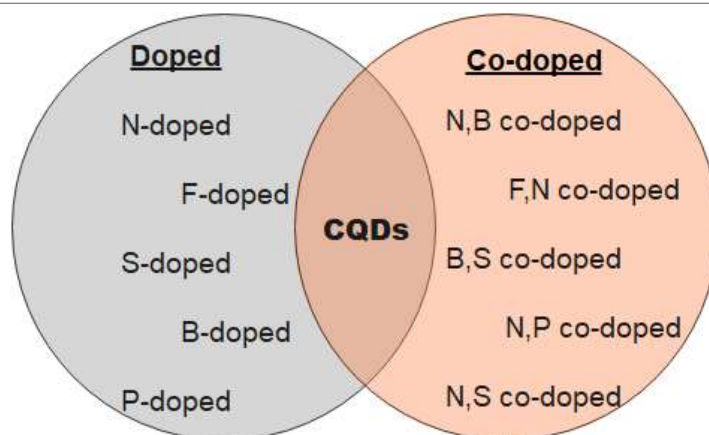
Figure 2.2 Varieties of doped and co-doped CDs.

2.8.5.1 Metal Doped-CDs for Cr(VI) ions Detection

There is an increasing concern for the development of less-toxic sensing probes that can prevent re-contaminating during their operation and CDs however have already demonstrated their abilities in this regard.[169] Hence researchers have developed a few metal-based CDs chemosensors that have high sensitivity and selectivity toward Cr(VI) ions. These CDs possessed distinctive optical properties and extra sensing capability due to their metal-coordination platforms that are present after doping with different metal impurities.[169]

Zhang, et al. [169] reported novel cobalt(II)-doped CDs (CCDs) that showed rapid selectivity and sensitivity for Cr(VI) ions, with a LOD of 1.17 µM in the linear range of 5 µM to 125 µM. The CCDs were synthesized via a solvothermal process using 1-(2-Pyridylazo)-2-naphthol (PAN) and cobalt chloride as the precursors. The authors identified that the surface groups of CCDs interacted with Cr(VI) ions that formed non-radiative complexes that weakened the surface emissive strength of CCDs.[169] Qing, et al. [170] used a hydrothermal-carbonization treatment to dope Cu^{2+} onto carbon dot surfaces thereby fabricating Cu^{2+}-CDs. Waste tea extract, ethylenediamine, and copper acetate were the precursors used in the synthesis. The sensing ability of Cu^{2+}-CDs for Cr(VI) showed a bright blue fluorescence upon the addition of Cr(VI) to the solution matrix. The LOD of CrO_4^{2-} and $Cr_2O_7^{2-}$ were 2.044 µM and 1.418 µM, respectively.[170]

Adotey, et al. [171] also used 4-pyridinecarboxaldehyde and zinc nitrate hexahydrate co-ligands approach to successfully synthesize a mixed-ligand luminescent

carbon material (N,Zn-CDs) as a sensitive probe for the detection of Cr(VI) anions. The fluorescent intensity of the microwave-synthesized material decreased with an increase in Cr(VI) concentration anions due to the inner filter effect. Anti-interference study of the sensor in the presence of other metal ions indicated the sensitivity and selectivity of the probe toward chromium ions. A detection limit of 0.47 nM towards soluble Cr(VI) species was achieved using the fluorescent method.[171]

2.8.5.2 Non-Metal Doped-CDs For Cr(VI) ions Detection

Apart from surface functionalization, single or heteroatom doping has also improved the quantum yield, water solubility, fluorescent properties, and other physicochemical properties of CDs. Typical non-metals used in doping CDs for Cr(VI) detection include nitrogen, sulfur, phosphorus, or their combinations to form heteroatoms. The inclusion of these non-metals can affect the overall electrical distribution, electronic energy level as well as fluorescent properties of CDs.

Nitrogen-doped CDs (N-CDs) are the most widely studied and easily investigated type of doping since nitrogen has a similar electron structure to carbon atoms.[24,25] Nitrogen can share its unpaired electrons (electron donor) and improve the emission properties.[26] This impact on CDs arises from the fact that N-containing functional groups transition easily from the ground state to the lowest excited state of the electrons.[27] The first ever N-CDs were reported by Liu, et al.[172] wherein a hydrothermal treatment was used on plant grass which served as an N-rich source. Following that report, researchers began synthesizing a large number of N-CDs for many applications including sensing of Cr(VI). Bleibtreu, et al.[19] synthesized a low-cost N-CDs fluorescent sensor for sensitive detection of Cr(VI) via one-step hydrothermal treatment using thymidine as a carbon source. The interaction between N-CDs and the concentration of Cr (VI) showed a LOD of 1.26 nM ranging from 0.1 µM to 430 µM. Chen, et al.[20] also reported the synthesis of highly luminescent N-doped carbon dots (CG-CDs) using citric acid and glycine. The fluorescent sensor showed a high quantum yield of 78% as well as rapid response, high selectivity, and sensitivity towards Cr(VI). A good linear relationship between the concentration of Cr(VI) ions and fluorescence intensity was obtained with a LOD of 4.16 mM.[20] Pyrolysis of citric acid with glutamic acid also resulted in the formation of fluorescent N-CDs.[21] The fluorescence intensity of N-CDs was quenched by Cr(VI), and the quenching mechanism

was attributed to the inner filter effect (IFE) and static quenching effect. The linear range for Cr(VI) detection was 0.01 µM to 250 µM with a LOD of 5 nM.[21] Other researchers used different methods, precursors, and altered reaction parameters to synthesize N-CDs that were selective towards Cr(VI): microwave synthesis of N-CDs by Cao, et al. [154] and Bu, et al. [173], detected Cr(VI) with LODs of 0.12 µM, 0.24 µM respectively; hydrothermal treatment of precursor to yield N-CDs according to Li, et al. [174], and Wang, et al. [175] exhibited LODs of 2.60 nM, 2.10 µM, 20 nM for Cr(VI) detection, respectively.

Developments of CDs with non-metal heteroatoms doping have also been reported to improve the properties of CDs.[28] Sulfur (S) is one of the non-metal that can form a heteroatomic structure in CDs and has an electronegativity (2.58) similar to that of carbon (2.55). The atomic radius of S (105 pm) is much larger than carbon atom (77 pm), as such electron transition of sulfur is easier than for carbon. In heteroatomic CDs, the presence of oxygen and sulfur makes CDs negatively charged, and this enables the nanomaterial to be bonded with positively charged particles e.g Cr(VI) cations. For example, Wang, et al. [176] synthesized multifunctional nitrogen and sulfur-doped fluorescence carbon dots (NS-CDs) with citric acid monohydrate (carbon source) and thiosemicarbazide (nitrogen and sulfur source) as precursors. The fluorescence quenching mechanism of NS-CDs with Cr(VI) was attributed to the inner filter effect and a low detection limit of 0.33 nM for Cr (VI) detection.[175] An acid-base neutralization and exothermic carbonization technique were conducted by Song, et al. [177] to produce fluorescent sulfur and nitrogen dual-doped carbon dots (SN-CDs) by mixing glucose, 1,2-ethylenediamine, and concentrated sulfuric acid. Fluorescence quenching of SN-CDs was based on the inner filter effect and the LOD of Cr(VI) was 0.56 nM.[177] Work conducted by Yang, et al. [178] revealed the synthesis of fluorescent NS-CDs by microwave-assisted pyrolysis with ammonium citrate and cysteamine hydrochloride as raw materials. The NS-CDs demonstrated excellent fluorescent "turn-off" with Cr(VI) in a linear quantification range of 0.35 to 126.0 µM and LOD of 0.11 µM.[178] Liu, et al. [179] also used microwave-assisted pyrolysis to prepare NS-CDs from citric acid and N-acetyl-L-cysteine as the carbon source and N,S dopant, respectively. The NS-CDs served as a probe for chromium (VI) sensing in the linear range of 0.5 to 125 mM, and a detection limit of 20 nM.[179]

CHAPTER 3.   APPLICATION OF FUNCTIONAL CARBON MATERIALS FOR

Cr(VI) DETECTION

The development of advanced materials is becoming popular since they serve as sensors for toxic substances, especially for Cr detection.[1-5] Although different methods have been employed to quantify the level of Cr pollution in the environment,[10-12] concerns such as high cost, requirement for well-qualified professional operation, time-consuming among others[15-17] necessitate the development of a more robust method to quickly detect Cr(VI) ions.

Fluorescence spectroscopy using nanomaterials is gaining popularity due to its distinct advantages such as fast response time, and specific and sensitive detection to provide real-time monitoring.[18] Carbon Dots (CDs), a family of fluorescent nanomaterials, are playing significant roles in research due to characteristics such as hydrophilicity, tunable photoluminescence, good biocompatibility, excellent photostability, and low toxicity.[18-21] All these unique properties as well as chemical inertness have found CDs applications as photo-catalysts, energy conversion, sensors, and bio-imaging.[1,180-183] Several methods have been used to synthesize fluorescent CDs such as arc discharge[184], electrochemical etching[185], laser ablation[186], hydrothermal processes[19], and ultrasonic synthesis.[187] The use of these conventional methods often yielded low quantum yield (QY), high cost of equipment, and complicated professional handling.[21] Microwave-assisted synthesis of CDs is becoming popular due to factors such as its ease of operation, fast synthesis duration, simplicity, and low cost.[188]

Properties including the electron transfer ability of the CDs improve their fluorescence characteristics compared to other carbon-based materials such as carbon nanotubes, carbon nanofibers, and graphene.[18,23] Doping CDs with certain elements play an important role in changing the material's bandgap energy which results in the enhancement of the charge separation efficiency of sensors.[23] Non-metals such as nitrogen have been doped into carbon dots (N-CDs) and serve as an important component in the design of composite sensors. Doping carbon dot sensors involve adding guest molecules into the host carbon material, and the guest binds with the host molecules to give preference to specific elements to be detected.[15,16,189] Immobilized Lewis base pyridyl nitrogen sites found on the organic structure were also identified

to have fluorescent properties that show selective sensing towards metal ions.[189,190] Developments of CDs with non-metal heteroatoms doping have also been reported to improve the properties of CDs.[28] Sulfur (S) is one of the non-metal that can form a heteroatomic structure in CDs and has an electronegativity (2.58) similar to that of carbon (2.55). The atomic radius of S (105 pm) is much larger than carbon atom (77 pm), thus electron transition of sulfur is easier than for carbon. In heteroatomic CDs, the presence of oxygen and sulfur makes CDs negatively charged, and this enables the nanomaterial to be bonded with positively charged particles e.g Cr(VI) cations. Hence this chapter reports the synthesis of nitrogen-sulfur co-doped functional carbon material (N,S-CDs) as a sensor for Cr(VI) from insoluble Cr salts, and its applicability to quantifying insoluble Cr(VI) in ambient PM.

3.1   Materials, Reagents, and Instrumentations

Citric acid monohydrate ($C_6H_8O_7 \cdot H_2O$, purity $\geq 98\%$), 4-pyridinecarboxaldehyde (purity $\geq 98\%$), thiourea (purity $\geq 98\%$), potassium chromate (purity $\geq .99\%$), potassium dichromate (purity $\geq 99\%$), hydrochloric acid (purity $\geq 37\%$), nitric acid ($\geq 70\%$). Ethanol and isopropyl alcohol were all purchased from Sigma-Aldrich Company, and used without any further purification. Ultrapure water was prepared through a Milli-Q water purification system with an electric resistance of 18.25 MΩ cm.

CEM Focused Microwave™ Synthesis System, Discover® SP, helped to perform the materials synthesis under controlled conditions. An infrared spectroscopy analysis was conducted on the Nicolet iS10 FT-IR spectrometer. Fluorescence experiments were done on a Cary Eclipse Fluorescence spectrophotometer (Agilent Technologies). Excitation and emission slit widths on the fluorescent spectrometer were each set to 20.0 nm. X-ray diffraction patterns (XRD) were identified using a Rigaku SmartLab® X-ray diffraction system at an angular range of 5-80° and a scanning rate of 5° min^{-1}. Scanning Electron Microscopy (SEM) images were observed under a Scanning Electron Microscope FeSEM Auriga (Crossbeam 540). The microscope configuration on the FeSEM allowed for performing Energy Dispersive Spectroscopy (EDS) analysis, imaging, and analytical performance of the GEMINI column linked for particles. Nitrogen Porosimeter (automated gas sorption analyzer) determined the porosity and surface area of the synthesized particles. Simultaneous Thermal Analyzer (STA) 6000 was used to conduct thermogravimetric analyses

(TGA) with the following conditions: air heating rate of 5°/min, flowing air pressure of 20 ml/min, and temperature range of 30-600 °C. Zeta potential was measured on ZN3600 Zetasizer (Malvern Panalytical Ltd.) at room temperature. Nexsa X-Ray Photoelectron Spectrometer (XPS) (Thermo Scientific) was used to study the surface chemistry, elemental composition, chemical state, and electronic state of the elements within the nanomaterial. Transmission Electron Microscope JEOL JEM-1400 Plus was used to collect high-quality images of the size and crystallography of the synthesized nanomaterial. Fluorescence decay time was performed using the Edinburgh Instruments FLS1000 Photoluminescence Spectrometer (Edinburgh Instruments Ltd.). Where applicable, Ion Chromatography/Ultraviolet Spectrometry (IC-UV) was used for the detection of Cr(VI) in an aqueous solution. The IC-UV uses Dionex IonPac AG7 guard (2 × 50 mm) and Dionex IonPac AS7 analytical columns (2 × 250 mm). An eluent of 250 mM ammonium sulfate/100 mM ammonium hydroxide at a flow rate of 0.36 mL/min, a 1000 µL injection volume, and a post-column reaction with 2 mM 1,5-diphenylcarbazide/10% methanol/1 N sulfuric acid (using a 125 µL reaction coil) followed by visible absorbance detection at 530 nm.[191]

3.2 Synthesis of Functional Carbon Materials for the Detection of Cr(VI)

A functionalized carbon material was synthesized under controlled conditions in the lab and their selectivity toward Cr(VI) detection was tested. The experimental conditions are summarized in Table 3.1.

Table 3.1 Conditions used for the synthesis of the functional carbon materials.

Functional material	Precursors	Synthesis type	Solvent	Conditions
N,S-CDs	Citric acid monohydrate, 4-pyridinecarboxaldehyde, thiourea	Microwave	5mL H_2O	5 min ramping to 190 °C, holding at 30 min, pressure < 200 psi, constant stirring

3.2.1 Synthesis of a Luminescent Functional Carbon Material (N,S-CDs)

The N,S-doped carbon particles were produced via a microwave method using citric acid monohydrate (C-source) and 4-pyridinecarboxaldehyde (N-source), and thiourea

(N,S-source). The optimal synthesis condition used for the luminescent particles involved reacting 420 mg of citric monohydrate, 1mL of 4-pyridinecarboxaldehyde, and 50 mg thiourea in 5 mL of double distilled water. The mixture was pre-stirred for 5 min at room temperature in a 35 ml microwave vessel. Thereafter, the vessel was transferred into the microwave system, and synthesis was conducted under the following conditions: ramping within 5 min to 190 °C with constant stirring, holding at 30 min at a pressure < 200 psi. Just after the reaction, 350 µL $NH_4OH_{(aq)}$ solution was drop into the sample and stirred for 5 minutes, to stabilize the particles in solution. The particles were purified in a centrifuge by washing with ethanol and DI in succession. The brownish carbon particles were dried overnight under a vacuum at 70 °C. A control sample was also synthesized similarly without the addition of thiourea for comparisons. Additionally, other variations in the ratios of the precursors incorporated in the synthesis were studied (Table 3.2).

3.3 Characterization of the Synthesized Particles

3.3.1 UV-VIS Absorption

Fine suspensions of the synthesized particles and about 5µL of 10 µg/L Cr(VI) standard solution were transferred into a quartz cuvette, mixed and the absorption spectra were recorded in a UV-Vis spectrometer.

3.3.2 Zeta Potential Titration

Dispersed as-synthesized particles (2 mg/1.5 mL_{DI}) and Cr(VI) standard solution were used to investigate the electrostatic interaction between the particles and Cr(VI). The zeta potential was done by using different concentrations of Cr(VI) standard solution in the aqueous suspension. These investigations were conducted three times to get an average value.

3.3.3 ImageJ Analysis

Initial images from the SEM and TEM were used for the analyses in ImageJ software (http://imagej.nih.gov/ij/docs/guide). The diameter of each particle in images was measured, and where applicable the length, height, or breadth of each particle was measured to get an average value for the construction of size distributions.

3.3.4 Fluorescence Detection of Cr(VI)

Known masses of the particles were dispersed in double distilled water and sonicated. Thereafter, a 10 µg/L Cr(VI) solution was prepared from a Cr(VI) standard solution (TraceCERT®, 1000 mg/L Cr(VI) in H_2O). Spectroscopic experiments with a fluorescent spectrometer were conducted by the incremental addition of Cr(VI) concentrations to the aqueous solution in a quartz cuvette and its intensity was recorded.

3.3.5 Limit of Detection (LOD) and the Analytical Detection Limit (ADL)

Varying concentrations of K_2CrO_4 were added to the suspension of particles in solution and the emission spectra were recorded. The area under the curve was calculated for each spectrum. Eight (8) replicates of the particles were analyzed and the added Cr(VI) concentrations were plotted against the area of each fluorescence intensity. The slope of the regression line was determined by statistical analyses and the LOD was calculated as; (3 × standard deviation/slope). The ADL was calculated as 3 times the standard deviation (SD) of low concentration of spiked Cr(VI). In this experiment, 8 blank filters were spiked with Cr(VI). The proposed fluorescent method of detecting Cr(VI) was used on all these samples.

3.3.6 Anti-Interferences Study

Known masses of different salts were added to 5 mL water to prepare a 1.0 mM ionic solution. The ionic solutions comprise m-Cl_X (m = Sn^{2+}, Ca^{2+}, Na^+, Li^+, Co^{2+}, NH_4^+, K^+, Zn^{2+}, Fe^{3+} and Cu^{2+}), $MgSO_4$, $Pb(NO_3)_2$, $Ni(NO_3)_2 \cdot 6H_2O$, $CrCl_3 \cdot 6H_2O$, $FeSO_4 \cdot 6H_2O$, $CsNO_3$, $RbNO_3$ as cations, and Na_x-k (k= NO_2^-, CO_3^{2-}, HCO_3^-, SO_4^{2-}, OH^-, PO_4^{3-}) and K_x-n (n= Br^-, I, IO_3^-, NO_3^-, MnO_4^-) as the anions. A volume of 10µL ionic solution each was added to the 1500 µL aqueous suspension and the fluorescence intensity was conducted. Thereafter, 100 µL of 10 µg/L Cr(VI) was also added, mixed and the fluorescence intensity was measured.

3.3.7 pH Stability Test

About 2 mL volume of the fine suspensions of particles was measured into centrifuge tubes containing DI-water pH range of 1.5 to 13.0. Meanwhile, the pH adjustments in the centrifuge tubes were done by adding 0.1M HCl and/or NaOH. The mixture was

equilibrated at room temperature for 5 min in a quartz cuvette and thereafter the fluorescence spectra were measured.

3.4 Development and Measurement Method For Insoluble Cr(VI) in Ambient Air; using Functionalized Carbon Materials

Exploratory research was employed to develop an analytical method for the detection of total Cr(VI) (soluble Cr(VI) + insoluble Cr(VI)) in ambient air using carbon-based materials. The study design is explained in the following section.

3.4.1 Method Development

The method development for the quantification of total Cr(VI) in ambient air was conducted via the following steps: synthesizing functional carbon material, ambient air sampling on filter and extraction of total Cr(VI) into aqueous form, and detection of Cr(VI) in the samples using the luminescent functional material. Primarily, the research is based on the synthesis of functionalized carbon materials and the detection of both soluble and insoluble forms of Cr(VI) with the functionalized materials using a fluorescence spectrophotometer. The criteria for the optimal conditions were: **a)** more than 90% efficiency of dissolving Cr(VI) in insoluble/sparingly soluble chromates ($PbCrO_4$, $BaCrO_4$, $CaCrO_4$, and $(NH_4)_2CrO_4$), **b)** minimum interferences from other competing ions in the solution matrix, and **c)** ~5% RSD of Cr(VI) detection in the analytical method. The experimental works are explained below.

3.4.2 Digestion of insoluble Cr(VI) salts/ total Cr(VI) in PM$_{10}$ field samples

The microwave-assisted method[70] was employed in the extraction of the total Cr(VI) available in the insoluble Cr(VI) and/or the field PM samples collected on Teflon filters. Briefly, the Cr(VI) samples were extracted in a microwave under these conditions; 3% Na_2CO_3 - 2% NaOH (pH ~ 13), ramping within 15 minutes to 95 °C and holding for 60 min. For the IC-UV analyses, portions of the extract were taken using a 10 ml BD syringe and filtered via a 0.45 μm filter (Thermo Scientific 25 mm Nalgene Syringe filter SFCA) to remove large particles before analyses.[70] A portion of these solutions were also analyzed on the fluorescence spectrophotometer using the NS-CDs as a sensor to detect total Cr(VI). The microwave-digested insoluble/sparingly soluble Cr(VI) salts were diluted to about 5×10^3 times. A 10 μL

portion of the diluted fraction was then spiked into a 1500 µL volume of the NS-CDs solution, and the fluorescence response was recorded.

3.4.3 Extraction of Soluble Cr(VI) from field samples (Cellulose filter samples)

The pretreatment of the cellulose filters and the extraction of soluble Cr(VI) was conducted as described by ERG [68]. Pretreatment involves leaching the cellulose filters overnight in a 10% HNO_3 acid solution to remove any residual Cr contaminant, washing in ultrapure H_2O until the pH was between 5 and 6, and drying overnight in a clean fume hood. The filters were then impregnated with 500 mL of 0.12M $NaHCO_3$ solution to obtain a basic cellulose filter. The basic filters, with pH between 9 and 10, were further dried in the fumehood. Extraction of soluble Cr(VI) was conducted by transferring the filters into a 15 mL centrifuge tube, adding 10 mL of 20 mM $NaHCO_3$ solution, and shaking the samples on a laboratory shaker for 45 minutes. Samples were then filtered and analyses were conducted using the fluorescent method and IC-UV (as verification).

3.4.4 Fluorescence Detection of Cr(VI)

About 1mg N,S-CDs was added to 20 mL phosphate buffer saline solution (PBS, pH ~7.4) and used in the fluorescent experiment as a sensor to detect Cr(VI). The resultant CDs-PBS solution matrix had a pH of ~7.2. Varying concentrations of K_2CrO_4 were added to the suspension of particles in PBS solution and the emission spectra were recorded.

<u>Reagent grade insoluble Cr(VI) salts</u>**:** The reagent grade insoluble Cr(VI) salts were digested using the metheod described in section 3.4.4. In addition, 20 mg of K_2CrO_4 was equally digested with the samples and later used for the construction of the calibration curve. Portions of the K_2CrO_4 extract was serially diluted to obtain various concentrations for the construction of the calibration curve. Thereafter, 10 µL volume of the digested insoluble Cr(VI) was spiked into a 1500 µL volume of the N,S-CDs solution, and the fluorescence intensities was recorded.

<u>Total Cr(VI) in the PM samples</u>**:** The same calibration curve employed for the reagent grade insoluble Cr(VI) detection was used for the total Cr(VI)-containing PM samples. Then 10 µL portions of the digested PM solution was added to 1500 µL volume of the NS-CDs solution, and the fluorescence responses was noted.

Soluble Cr(VI) in the field samples: The same suspension (1mg NS-CDs/20 mL PBS) was prepared and soluble Cr(VI) collected on basic-cellulose filters was determined with this solution matrix. The calibration curve construction involved preparing varying concentrations of Cr(V)/K_2CrO_4 in 10 mL of 20 mM $NaHCO_3$ solution and recording their fluorescence responses. After the extraction of soluble Cr(VI) from the cellulose filters (section 3.4.3), 10 μL portions of the sample were spiked into a 1500 μL volume of the NS-CDs solution, and the fluorescence responses were recorded.

3.4.5 Limit of Detection

For all the fluorescent experiments, the emission spectra of the NS-CDs suspension was recorded. The area under the curve for each spectrum was calculated from the titration. Eight (8) replicates of the synthesized CDs were analyzed and the added Cr(VI) concentrations plotted against the area of each fluorescence intensity. The slope of the regression line was determined by statistical analyses and the LOD calculated as; (3 × standard deviation/slope).

3.4.6 Results and Discussions
3.4.6.1   Characterization

The FTIR spectrum in Figure 3.1(a) shows weakly developed peaks at 3104.9 and 3054 cm^{-1} that can be attributed to the vibrational bands of =CH and –CH, respectively.[19,177,192] The -CN peaks[177,184,193] at 2354.3, and 1408.8 cm^{-1} show the stretching vibration of the pyridyl nitrogen, indicating that 4-pyridinecarboxyaldehyde participated in the synthesis of the carbon material.[189] The peak at 1700.5 cm^{-1} is assigned to the C=O stretching vibrations of the aromatic rings in 4-pyridinecarboxaldehye and carboxylic group in citric acid.[189] The peak at 1328.3 cm^{-1} is associated with –CHO deformation out of the plane as well as the C-N stretching in 4-pyridinecarboxyaldehyde.[189,194] The vibration band at 1615.6 cm^{-1} is attributed to the asymmetric stretching vibration on the carboxylic functional group (-COOH) in citric acid.[20,194,195] The in-plane and out-plane stretching of the aromatic C-H groups of the benzene rings could be assigned to the peak present around 759 cm^{-1}.[194,195] The incorporation of thiourea introduced symmetrical deformation in C=S peaks at 758.4 cm^{-1}, an asymmetric C=S vibration at 1472.9 cm^{-1}, and the S=O stretching at 1142.7

cm^{-1}.[196] This shows that thiourea was incorporated in the formation of the as-synthesis particles.

The powder XRD pattern of the carbon material was characterized to show its crystalline nature. Figure 3.1(b) shows distinct diffraction peaks in the pattern around 16.7°, 26.2°, 28.1°, 37.6°, and 40.5° respectively. The corresponding interlayer spacing (d) was calculated via Bragg's law (the wavelength of Cu-Kα (λ) is 0.154 nm). The distinguishable (002) peak of graphite[197] at 26.2° has an interplanar distance, d_{002}, of 0.340 nm, which is the same as the interlayer spacing of crystalline graphite (d=0.34 nm).[198] This shows the graphitic nature of the as-synthesized carbon material. A high diffraction peak around 16.7° (d_{001} = 0.531 nm), 28.1° (d_{200} = 0.318 nm), and 40.5° (d_{430} = 0.223 nm) perhaps was due to sp^3 layers spacing in sulphur[199,200] during synthesis originating from the intercalation of sulfur groups which resulted in a decrease in interlayer spacing. Generally, the slight difference from the original graphitic peaks in the as-synthesized material may be due to the synthesis process wherein functional groups such as aldehyde, hydroxyl, carbonyl groups, and sulfur groups were incorporated into the material and bonded to the edges of basal planes of the crystal structure.[201]

TGA indicates the amount and rate of change of the weight of the as-synthesized particles (weight loss) for temperature under controlled conditions. TGA of the N,S-doped particles (Figure 3.1(c)) showed a 98.89 wt% overall total weight loss in a single step on heating to 600 °C. The analysis further suggests that the particles were stable at 165 °C and weight loss occurred afterward from this temperature. About 0.75 wt% weight remained at about 290 °C due to the combustion of the carbon content in the N,S-doped carbon particles.
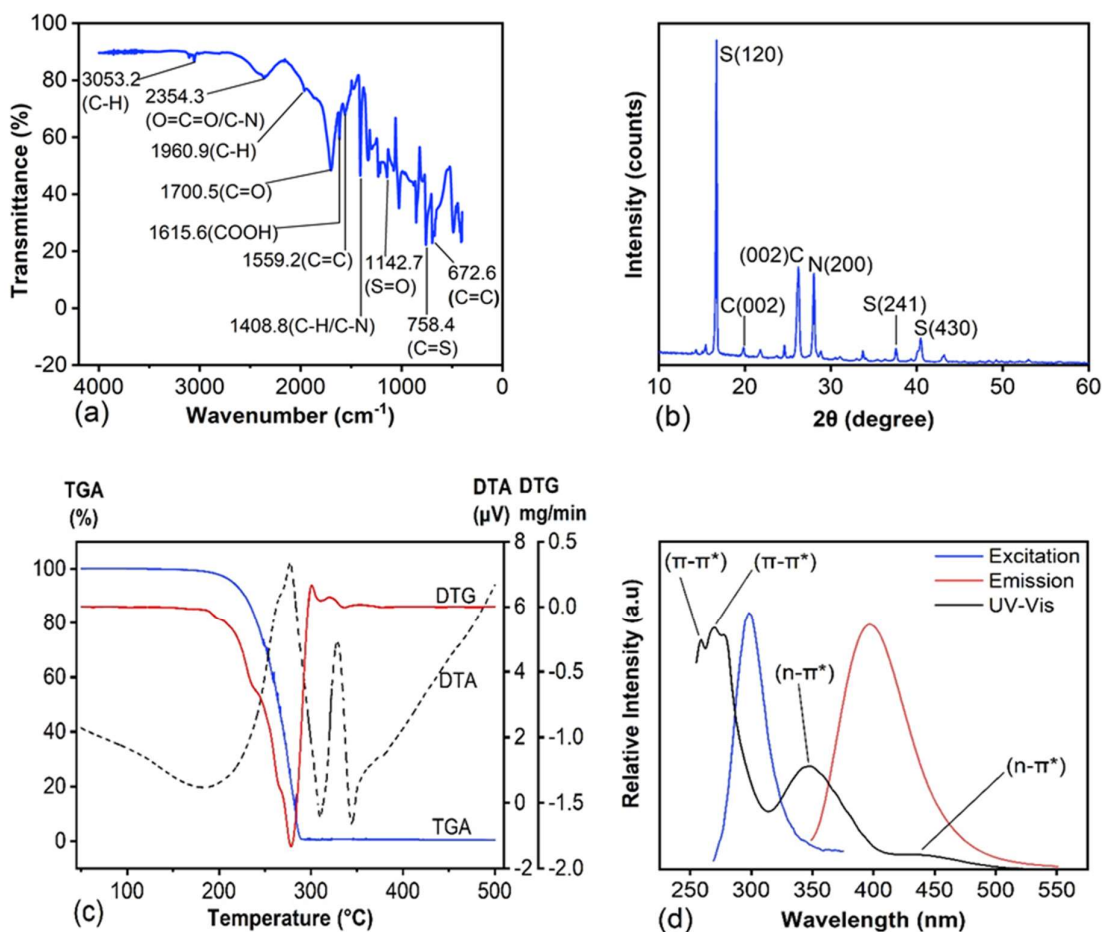
Figure 3.1 (a) FTIR, (b) XRD, (c) TGA, and (d) UV-Vis, excitation, and emission of the as-synthesized particles.

The optical properties of the N,S co-doped CDs were determined using UV-Vis and fluorescence spectroscopy (Figure 3.1(d)). The wavelength response of the spectra is in the range of 200 nm to 600 nm and the strongest visible light absorption of the particles is seen as a peak at 350 nm. These absorption characteristics suggested that the doped carbon particles could be activated by visible light. The UV-Vis spectrum shows two distinct absorptions at about 259 and 270 nm, which can be attributed to π-π* electron transition of aromatic sp^2 domains of C=C and C=N bonds present in the CDs.[202] The stronger shoulder of the peak appeared at 350 nm due to the n-π* electron transition from C=O bonds as well as a peak at 428 nm due to C=S bonds. Typically, broad absorption bands between 300 and 400 nm are associated with the trapping of excited state energy by the surface state that yields strong fluorescent properties. Fluorescence emissions are dependent on the excitation wave-

length of CDs. The excitation at 250 nm to 600 nm of the N,S-CDs yielded a maximum peak at 330 nm. Upon excitation, an emission peak with a maximum of 400 nm was observed

The fluorescence properties of CDs largely depend on the carbon material and the available functional groups present in the precursors. Functional groups such as N and S-containing CDs are known to show higher QY compared to undoped CDs. Typically, N-doped CDs show strong fluorescence effects in blue shift, while N,S-doped CDs usually exhibit a wide range of excitation wavelengths with the highest QY values. This is evident in the 75.8 % QY (Table 3.2) value measured for the as-synthesized N,S-CDs, compared to the 65.6 % QY value of N-CDs (control sample, ID: M_1). Varying the ratios of the precursors showed QY values of 74.4, 52.0, 11.5, 22.1, 45.1, 65.6, and 29.0 % for T_1, T_2, T_3, N_2, N_3, M_1, and M_3 respectively. The trend in the values indicates the functional role of sulfur, where it enhanced the QY of the carbon materials. Table 3.2 shows that a few amounts of thiourea (25-50 mg) were enough to achieve high QY (~76 %), compared to its exclusion (ID: M_1) or when in larger quantities (ID: T_2, T_3). In addition, decreasing the amount of 4-pyridinecarboxaldehyde showed lower QY, and higher volumes also did not significantly improve the QY compared to the QY obtained by N,S-CDs.

Table 3.2 Variations in the ratios of the starting materials, their LODs, and QY for soluble Cr(VI) detection in ambient PM.

Sample ID	CA (mg)	4-Py (µL)	TU (mg)	Comment	LOD (nmol/L)	QY %
T_1			25	Varying concentrations of S	0.019	74.4
N,S-CDs	420	1000	50		**0.008**	**75.8**
T_2			75		0.035	52.0
T_3			100		0.013	11.5
N_1		250		Varying concentrations of N	-	-
N_2	420	500	50		0.024	22.1
N_3		1500			0.011	45.1
M_1		1000	-	no TU	0.020	65.6
M_2	420	-	50	no 4-Py	-	-
M_3		1000	50	No NH_4OH	0.013	29.0

Note: CA: citric acid monohydrate; 4-Py: 4-pyridinecarboxyaldehyde; TU: Thiourea, QY=quantum yield

The TEM image is shown in Figure 3.2(a), while the size distribution of the N,S-doped particles is in the range of 4 to 27 nm (Figure 3.2b). The dispersibility of the particles in water was quite good however, the TEM images were seen as aggregates indicating that particles were not fully protected by the functional groups present and may be polydispersed. From the TEM images (Figure 3.2a insert), the particles had a spherical shape when in solution, and the crystal lattice of 0.34 nm typical of graphite [198] was observed. Analysis of the particles' sizes using *ImageJ* software measured the mean particle diameter as 10 nm after measuring more than 100 particles from the TEM images.

Element	Line	Mass%	Atom%
C	K	65.64	76.03
N	K	16.09	15.94
O	K	8.43	7.31
S	K	0.04	0.02
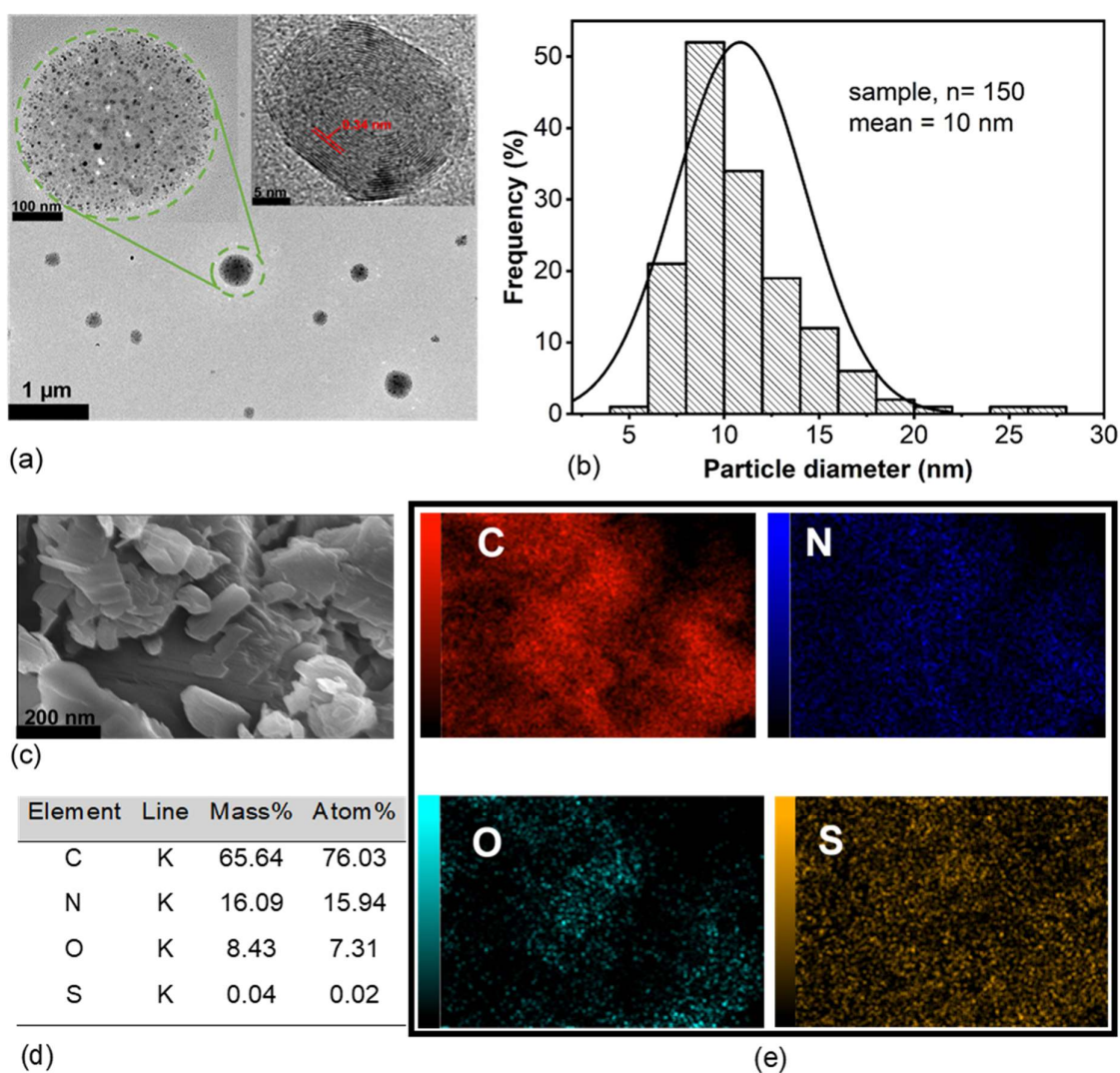
Figure 3.2 (a) TEM, (b) TEM size distribution, (c) SEM, (d) EDS, and (e) elemental mapping of the N.S co-doped carbon material.

The SEM image (Figure 3.2c) of the dried particles reveals the morphology of the particles as irregularly shaped. The elemental composition of the particles in Figure 3.2(d) from the EDS spectrum shows compositions of carbon (C), oxygen (O), nitrogen (N), and sulfur (S) as 65.64%, 8.43%, 16.09%, and 0.04% respectively. The elemental mapping (Figure 3.2e)) estimated the spatial distribution of available elements in the carbon materials. The images showed uniform distribution of elements and the successful doping of nitrogen and sulfur atoms into the structure of the carbon materials. This EDS quantitative analysis, therefore, confirmed the incorporation of nitrogen, sulfur, and carbon into the material.

3.4.6.2   XPS study of Cr(VI)-CDs attachment

To investigate the surface chemical compositions and the valence states of N,S-CDs, XPS (Figure 3.3(a)) analyses showed the existence of C, N, O, and S peaks in the as-synthesized doped carbon dot. The XPS reveals the N,S-CDs had a composition of 68.8% C, 7.1 % N, 22.7% O, and 1.4% S. The interaction of the available valence states was studied after the addition of Cr(VI) standard solution to the solution matrix. The deconvoluted C1s peaks consist of three types as seen in Figure 3.3 (b). The peaks at 286.1, 287.4, and 289.5 eV are assigned to the C$\equiv$N, C=O, and O-C=O groups, respectively. Among these carbon variations, C$\equiv$N was dominant in the C1s peak which showed that N was incorporated in the doped material and was more than the content of oxygen-containing functional groups available in C1s. In the O1s spectra, (Figure 3.3 (c)), the peaks at 532.7 and 533.5 eV were ascribed to C-OH, while the peak at 532.2 eV was assigned to C-O. The deconvoluted N1s spectra in Figure 3.3 (d) show four binding energies namely; the graphitic N-C due to the substitution of carbon by nitrogen atoms, located at 399.1 eV; and N-H located at 400.1 eV. The binding energies between N-O and N$\equiv$C were distinguishable at 400.1 and 402.4 eV, respectively. The overall intensity of the N1s peaks indicated that N from the pyridyl and thiourea were incorporated in the doped carbon material. The S2p deconvoluted peak in Figure 3.3 (e) identifies four distinct peaks at a binding energy of 164.2-164.5, 164.9, 165.1, and 167.1 eV, corresponding to the S-C, S-O, S=O, and O-S=O respectively. Of these, the S=O functional group was dominant indicating that the oxygen-containing sulfur group likely played a more functional role than the carbon-sulfur-containing group present. Figure 3.3 (f) shows the deconvoluted XPS

spectra of Cr2p after Cr was added to the N,S-CDs. The Cr2p3/2 peak revealed two peaks at 572.7 eV and 575.2 eV, respectively as elemental Cr (Cr-Cr)[203,204] and Cr-N/Cr-O. A broad peak appeared at 580.6 eV which was assigned to Cr(VI) species, including those of CrO_3, CrO_4^{2-} and $Cr_2O_7^{2-}$.[203] The binding energies of the Cr2p1/2 peak were revealed at 584.7 eV, which was ascribed to Cr-N/Cr-O states present in the matrix.[204] Among the variable Cr peaks, Cr-N was dominant in the deconvoluted peaks. This further suggests that Cr was bonded to the nitrogen moieties in the N,S doped carbon dot which participated in the effective quenching of the fluorescent intensity of the nanomaterial. Thus, it is further proof that Cr successfully binds with N in the N,S-CDs when in solution.
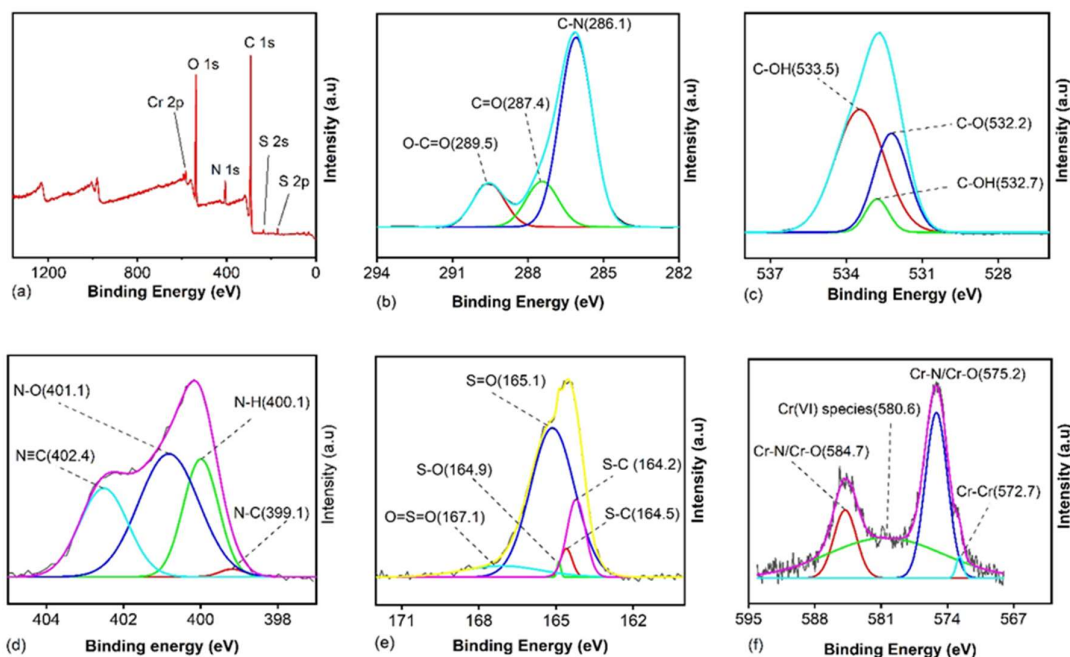
Figure 3.3 XPS spectra of N,S-CDs + Cr(VI) system (a) Survey spectrum, (b) Carbon deconvoluted peaks (C 1s), (c) Oxygen deconvoluted peaks (O 1s), (d) Nitrogen deconvoluted peaks (N 1s), (e) Sulfur deconvoluted peaks (S 2p), and (f) Chromium deconvoluted peaks.

Speciation of Cr(VI) depends on pH and concentrations as shown in the pH/Eh diagram of chromium (Figure 2.1).[30,70] The carbon material in the water had a pH~7.2, and so we would expect more of CrO_4^{2-}/$Cr_2O_7^{2-}$ to be the Cr species present in the solution during the investigation. The Cr(VI) standard used was in the form of

$NH_4(CrO_4)$, and the reversible reaction with CrO_4^{2-} anions and H^+ would ionize to form $Cr_2O_7^{2-}$ anions in the solution according to the Equation 3.1[30,205];

$$2CrO_4^{2-} + 2H^+ \leftrightarrow Cr_2O_7^{2-} + H_2O \qquad (3.1)$$
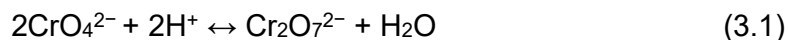
Thus Cr(VI) ions in the solution would interact with the N,S-CDs using the available pyridyl nitrogen (-NH), hydroxyl (-OH) and aldehyde groups (-CHO).[205] Similar to the study conducted by Bandara, et al. [205], the pyridyl nitrogen present in the carbon material in our study (pH~7.2) will follow the relation in Equation 3.2:

$$R-NH + OH^- \rightarrow R-NH^- + H_2O \qquad (3.2)$$
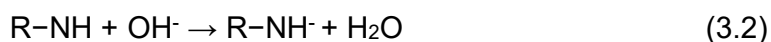
Equation 3.2 denotes that the pyridyl functional groups in the carbon material remained negatively charged. Thus, we can theorize that available nitrogen groups in the as-synthesized carbon material were responsible for the coordination of Cr(VI) species from the aqueous solution through an electron transfer with the positively charged Cr(VI) ions, which resulted in the quenching phenomenon of the luminescent N,S-CDs. This phenomenon was exemplified in the attachment of Cr to N as presented Figure 3.3 (f). Similarly, the schematic diagram in Figure 3.4 depicts the mechanism behind the Cr(VI) coordination.
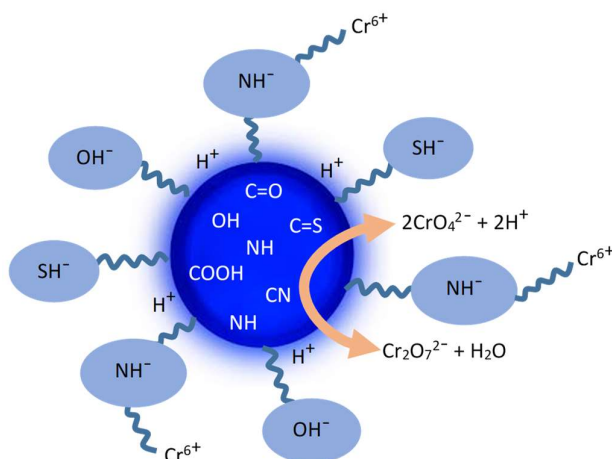
Figure 3.4 Schematic diagram to depicts the mechanism behind the Cr(VI) coordination.

3.4.6.3 Anti-Interference Effect

The interferences from cations and anions play a significant role in the stability and quality of the luminescence of the doped carbon particles. Figure 3.5(a) shows that the metal cations solutions did not significantly affect the luminescence intensity upon their addition to the aqueous solution matrix, a characteristic that shows the selectivity of the material towards Cr(VI).[189] This implies that upon the addition of cations, the free nitrogen and sulfur atoms in the solution retained their strong binding to the ions and were unable to reduce the efficiency of the linkers to coordinate with the carbon materials. This resulted in a less quenching of the luminescence intensity.
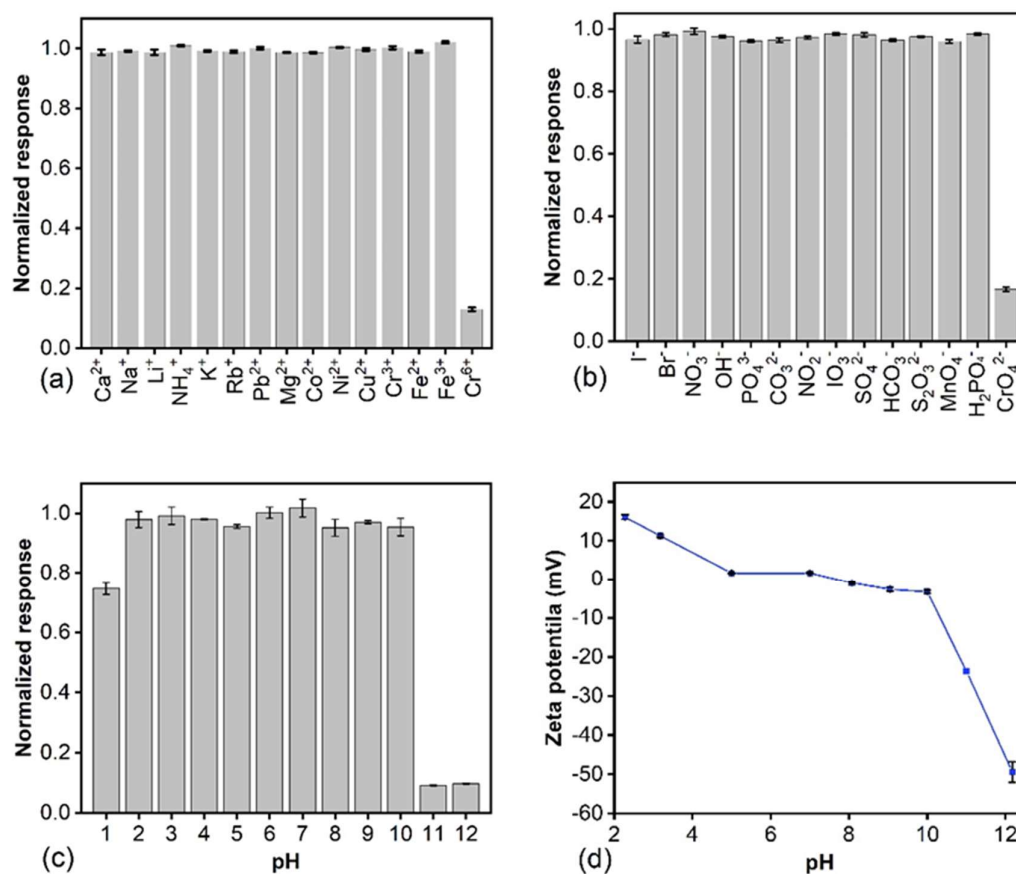
Figure 3.5 The effect of (a) cations, (b) anions, and (c) solution pH on the N,S-doped CDs, and (d) the zeta potential of the particles in different pH solutions.

Hydroxyl groups and free carboxyl oxygen atoms present in the aqueous matrix could also influence the interactions between the carbon particles and anions [206].

Hence, an evaluation of the potential interference of anions with the as-synthesized material was investigated. The result in Figure 3.5(b) shows that the anions also had a negligible impact on the fluorescence intensity of the carbon materials in the aqueous form. These tests show the high degree of the carbon materials to detect Cr(VI) ions with fewer interferences from other ions, suggesting that the ions were weakly bound to the active sites of the particles in the solution.

3.4.6.4   The Effect of pH on the Solution Chemistry of the N,S-CDs

The solution pH is known to affect the surface chemistry of the adsorbent and the adsorbate.[207] The luminescence intensity in Figure 3.5(c) however did not significantly change in the ranges of pH 2 to 10, which indicates that the particles were stable within this range. An initial decrease in the fluorescence intensity was observed at pH ~1. A sharp quenching of the luminescent intensity was however observed at pHs 11 and 12. Thus the results identify good stability of the particles in the pH range of 2-10. The particles' zeta potential charges with varying pHs in Figure 3.5(d) also showed the phenomenon where at lower pH, the surface zeta potential on the particles was positively charged, and higher pHs increased the negative surface zeta potential charges on the particles. Higher pHs contain more anions that enable an exchange of ions through displacement reaction with OH^-.[208]

3.4.6.5   Luminescence Experiment of N,S-CDs on Cr(VI) Detection

An aqueous solution of the N,S-CDs was prepared and K_2CrO_4 was added to the suspension. Figure 3.6(b) illustrates the quenching effect of the fluorescent intensity after adding varying concentrations of Cr(VI) to the N,S-CDs suspension. The quenching phenomenon could be due to the interaction of the chromium ions with the pyridyl nitrogen binding sites in the N,S-CDs solution matrix.[16] Thus, upon the addition of higher concentrations of Cr(VI), weak atomic interactions between the nitrogen moieties and Cr(VI) ions occurred which results in a decrease in the intra-ligand fluorescence efficiency of the N,S-CDs.[16,189,190] For total Cr(VI), the area under the curve against the concentrations was plotted (Figure 3.6(a)), with the equation of the line y = 1846.39x + 881.95 and a regression coefficient of R^2=0.9945. The calculated detection limit of 5.32 ng/L (0.1 nM) Cr(VI) ions was obtained based on a 3δ/k relationship (δ represents the standard deviation of 8 replicates, k is the slope of

the calibration curve). The calibration curve for the quantification of soluble Cr(VI) in ambient PM (Figure 3.6(b)) shows the equation of the line as $y = 40837x + 486.33$ and a regression coefficient of $R^2=0.9987$. The calculated limit of detection of 0.44 ng/L (0.01 nM) Cr(VI) ions was obtained based on the use of 8 replicates. The performance of the N,S-CDs is highly competitive with known CDs used for the detection of Cr(VI) ions in the aqueous phase.
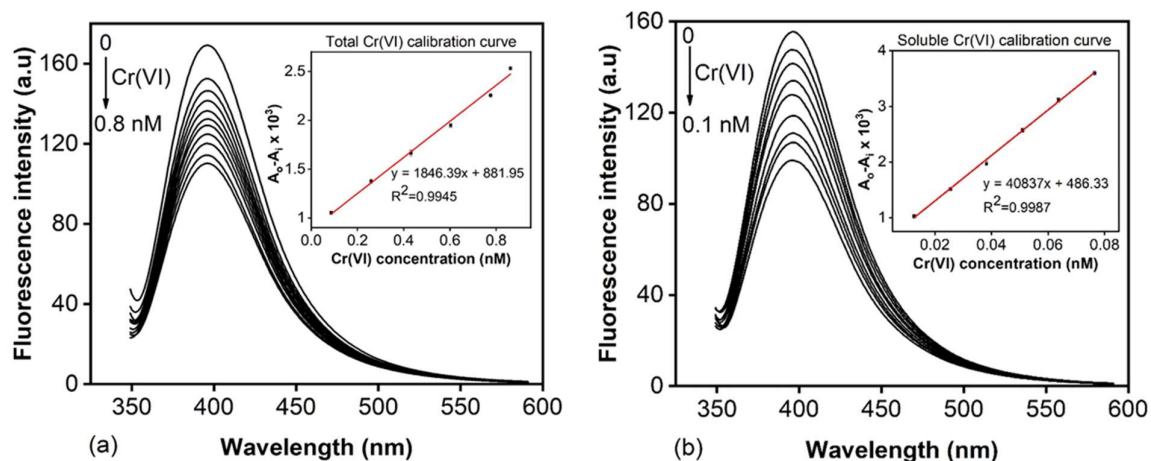
Figure 3.6 Quenching of the fluorescent intensity of the aqueous N,S-CDs using variable concentrations of Cr(VI) (insert: the calibration curve for Cr(VI) versus the area under the curve) for (a) total Cr(VI) and (b) soluble Cr(VI).

3.4.7 Application of N,S-CDs to detect Cr(VI) in insoluble/sparingly soluble salts

The recovery of Cr(VI) in the insoluble/sparingly soluble salts using our proposed fluorescent method showed average values (Table 3.4) of 106%, 102%, 96%, and 102%, respectively, for $PbCrO_4$, $BaCrO_4$, $CaCrO_4$, and $(NH_4)_2CrO_4$. The relative standard deviation (RSD) of the Cr(VI) recoveries was close to 5% (N=7) and this good precision suggested the suitability of the method to recover total Cr(VI)/insoluble in the ambient PM. The calibration curve in Figure 3.6 was used for the analyses of the samples. Comparatively, the IC-UV method was also used to evaluate the fluorescent method (Table 3.4). Results obtained from the IC-UV were similar to those obtained from our proposed method and thus show the proposed method could be an alternative approach to be used in the future.

Table 3.3 The Limit of Detection (LOD) and Analytical Detection Limit (ADL) for total and soluble Cr(VI) detection

Parameters (n=8)		LOD (µg/L)	RSD (%)	LOD (nM)
Calibration curve, Total Cr(VI)		0.0053	5.2	0.1024
Calibration curve, Soluble Cr(VI)		0.0004	6.7	0.0085

Parameters (n=7)	Spiked Conc. (µg/L)	Recovery (µg/L)	RSD (%)	ADL (ng/m$^3_{air}$)
Spiked samples, Soluble Cr(VI)	0.3	0.291	8.4	0.031

Parameters (n=7)	Avg Conc. (µg/L)	Avg. Conc. (nM)	Std. Dev	MDL (ng/m$^3_{air}$)
Field Blank, Total Cr(VI)	0.366	7.036	0.13	0.324

3.4.8 Application of the N,S-CDs on Cellulose Filter samples (soluble Cr(VI))

A good reproducibility of the calibration curve of the NS-doped carbon material was confirmed by using eight (8) independently prepared particles in the same way. These values were used to construct the calibration curve as presented in Figure 3.6(b). The repeatability was checked with one NS-doped carbon in successive Cr(VI) ion sensing. The estimated LOD of the soluble Cr(VI) concentration based on Figure 3.6(b) was 0.0085 nM, with an RSD of 6.7% (n=8).

3.4.9 Method Detection Limit (MDL) and Analytical Detection Limit (ADL)

Seven (7) field blanks were collected each for total and soluble Cr(VI) for the determination of the MDL. For total Cr(VI) the MDL, calculated according to the USEPA method, was 0.32 ng/m^3 (n=7). For the cellulose field blanks, our proposed fluorescent method could not distinguish peaks for soluble Cr(VI) due to probable low concentrations. Hence, we spiked 0.3 µg/L of Cr(VI) standard solution, according to USEPA[209], and the recovery determined using our proposed method. The ADL for soluble Cr(VI) using our proposed method was 0.031 ng/m^3, with an average Cr(VI) recovery of 0.29 µg/L (n=7, RSD=8.4%). The current MDL for the determination of total Cr(VI) using our proposed fluorescent method (0.32 ng/m^3), is similar to the 0.33 ng/m^3 value reported by Huang, et al. [70], but much lower than the 50 ng/m^3, 3

ng/m^3, and the 0.2-1.0 ng/m^3 values reported by the methods used by NIOSH 7605, OSHA ID-215 method, and ASTM D 5281-92 respectively.

Table 3.4 Cr(VI) recovery from insoluble and sparingly soluble Cr(VI) salts using our fluorescent method and the IC-UV method.

	Proposed Fluorescent Method (N=7)				
Parameters	PbCrO$_4$	BaCrO$_4$	CaCrO$_4$	(NH$_4$)$_2$CrO$_4$	SQC(012)
Average	106.0%	102.3%	96.4%	101.7%	103.5%
St. Deviation	5.6%	3.7%	1.8%	2.3%	6.4%
CV (RSD)	5.3%	3.6%	1.9%	2.2%	6.2%
Minimum	99.7%	97.9%	94.2%	98.5%	94.6%
Maximum	114.2%	108.3%	99.0%	105.2%	111.4%

	IC-UV Method (N=7)				
Parameters	PbCrO$_4$	BaCrO$_4$	CaCrO$_4$	(NH$_4$)$_2$CrO$_4$	SQC(012)
Average	97.5%	86.0%	91.5%	99.8%	105.4%
St. Deviation	4.5%	5.7%	2.7%	6.4%	9.4%
CV (RSD)	4.5%	6.6%	2.9%	6.5%	8.9%
Minimum	94.2%	80.6%	89.2%	92.8%	92.2%
Maximum	106.7%	94.2%	95.7%	109.9%	115.0%

3.4.10 Quantification of insoluble Cr(VI) in the ambient PM samples

Table 3.5 shows the results of using our proposed fluorescent N,S-CDs as a sensor to quantify total, soluble, and insoluble Cr(VI) concentrations in the field samples. Table 3.6 also shows the results obtained using the conventional IC-UV as a verification method to quantify total, soluble, and insoluble Cr(VI) concentrations in the field samples. As a pilot study, the N,S-CDs as a sensor were applied on 15 field samples collected from the sampling station at Aktobe (section 5.2.1). After creating a good reproducibility of the calibration curve of the NS-CDs (n=8), the various Cr(VI) forms were quantified in the samples. The repeatability of results was checked with 8 replicate analyses and the mean values of total Cr(VI) in ambient PM are reported in Table 3.5. The concentrations of total Cr(VI) in the samples were in the range of 7.5 to 58.1 ng/m$^3_{air}$, indicating the ability of the fluorescent N,S-CDs to detect Cr(VI) at high concentrations. Likewise, the soluble Cr(VI) in the sample was determined using the calibration curve obtained in Figure 3.6(b). Repetitive measurements (n=8) of soluble Cr(VI) on the basic-cellulose filters were conducted and the average soluble Cr(VI) concentrations were determined. The concentrations of soluble Cr(VI) recorded in the PM samples was in the range of 0.04 to 0.27 ng/m$^3_{air}$, with a mean of 0.11 ng/m$^3_{air}$. In

this study, the insoluble Cr(VI) fraction in the PM samples is given as the difference between the total Cr(VI) and the soluble Cr(VI). Table 3.5 and 3.9 show the results of the insoluble Cr(VI) concentrations in the PM samples. Both methods show that the insoluble Cr(VI) concentrations were statistically significantly higher ($p < 0.001$) than the soluble Cr(VI) concentrations, which agrees with the modeling results in the literature.[95,96] This implies that both soluble and insoluble Cr(VI) species were present in ambient PM. The statistical analyses further show that the insoluble Cr(VI) fraction accounted for a statistically significant larger portion of the total Cr(VI) in ambient PM, compared to the soluble Cr(VI).

Table 3.5 Determination of total and insoluble Cr(VI) concentrations in the ambient PM samples using our proposed fluorescence method

Samples	Total Cr(VI) ng/m^3_{air}	Soluble Cr(VI) ng/m^3_{air}	Insoluble Cr(VI) ng/m^3_{air}
S#1	41.59 (8.2)	0.08 (6.1)	41.52
S#2	9.98 (9.2)	0.27 (1.5)	9.71
S#3	9.51 (8.7)	0.24 (1.6)	9.28
S#4	20.96 (4.9)	0.08 (2.9)	20.88
S#5	8.59 (9.5)	0.04 (9.2)	8.55
S#6	10.95 (7.9)	0.12 (4.2)	10.82
S#7	27.37 (3.2)	0.06 (5.5)	27.30
S#8	13.83 (9.7)	0.11 (3.1)	13.73
S#9	17.57 (6.6)	0.13 (2.7)	17.44
S#10	9.86 (8.1)	0.10 (2.6)	9.76
S#11	12.66 (7.6)	0.11 (4.3)	12.54
S#12	58.14 (1.8)	0.10 (3.5)	58.04
S#13	7.53 (9.7)	0.05 (3.5)	7.48
S#14	10.03 (9.3)	0.07 (7.2)	9.96
S#15	13.22 (9.7)	0.06 (5.6)	13.16

Note: values reported as mean (%RSD), n=8

The IC-UV results in Table 3.6 were used to evaluate the fluorescent method and the results were identical to those obtained via the proposed N,S-CDs fluorescent method (Table 3.5). The soluble Cr(VI) value in the sample with ID S#12 was not reported due to contamination before its analysis in the IC-UV. Despite the slight fluctuations in the concentrations of Cr(VI) in some samples, our proposed method using fluorescent N,S-CDs still shows its promising ability to be used for the quantification of insoluble Cr(VI) in ambient PM. The concentrations of Cr(VI) determined in this short period (13th to 30th September) however showed higher concentrations,

compared to the earlier studies (section 5.2) we conducted in winter and fall at Aktobe city[210].

Table 3.6 Determination of total and insoluble Cr(VI) concentrations in the ambient PM samples via IC-UV method

Samples	Total Cr(VI) ng/m$^3_{air}$	*Soluble Cr(VI) ng/m$^3_{air}$	Insoluble Cr(VI) ng/m$^3_{air}$
S#1	41.26 (2.7)	1.64	39.62
S#2	9.22 (7.2)	0.34	8.89
S#3	9.02 (3.3)	0.35	8.67
S#4	17.00 (3.9)	0.11	16.89
S#5	9.99 (9.9)	0.07	9.92
S#6	10.34 (2.8)	0.13	10.21
S#7	25.21 (3.7)	0.08	25.13
S#8	12.38 (4.3)	0.12	12.26
S#9	15.60 (0.3)	0.12	15.49
S#10	11.94 (1.0)	0.10	11.83
S#11	10.24 (1.9)	0.15	10.09
S#12	57.24 (1.8)	-	-
S#13	8.11 (2.0)	0.60	7.52
S#14	10.49 (2.2)	0.06	10.43
S#15	10.21 (8.7)	0.04	10.17

Note: values reported as mean (%RSD). *No values of %RSD is reported for the soluble Cr(VI). The IC-UV instrument broke down after analyzing the first set of soluble Cr(VI) samples and we could not perform replicate analyses of the samples. This is because after 3 hours interconversion of Cr(VI) is known to occur when samples are already prepared, so the result would be biased after waiting for 2 days until the instrument was repaired.

3.4.11 The Mechanism of Fluorescence Quenching Ability with Cr(VI)

Phenomena such as the conversion of fluorescent materials to non-fluorescent forms, inner filter effect (IFE), and fluorescence resonance energy transfer (FRET) [211] were thought of as the plausible reason for the fluorescent quenching of carbon dots. However dues to the good chemical stability in the range of pH 2-10 achieved for the N,S-CDs, the possible loss of fluorescence ability to a non-fluorescent state could not be certain. The impact of IFE and FRET was investigated by analyzing the overlap of UV-Vis spectra of N,S-CDs. The overlap of UV-Vis adsorption spectra with the excitation and emission spectra of the N,S-CDs system is evident in Figure 3.1(d). The IFE is associated with the overlap of these spectra and thus could be responsible for the fluorescence quenching of Cr(VI), whereby the chromium ions competed with the ligand for the absorption of light energy.[206] Hence, the decrease in light absorbed by

the ligand led to a decrease in the electron transfer from the ligand to the metal ions present. Further verification of the concept of IFE was conducted via the time-resolved fluorescence decay measurements. To this effect, varying concentrations (0, 0.24, 0.69, 1.30 µg/L) of Cr(VI) were added to 2mg/1.5mL N,S-CDs solution to study the fluorescence decay spectra of N,S-CDs in the absence and presence of Cr(VI). The fluorescence decay in Figure 3.7(b), a system fitted with a three-exponential function, resulted in a mean lifetime of ~1.4 ns. Given the unchanged time-resolved decay in this experiment, it is evident that the fluorescence quenching ability of N,S-CDs was dominated by the IFE of Cr(VI); via a static quenching mechanism. Hence we can postulate that the UV-Vis absorption spectra, of available Cr(VI) ions in the PM samples, overlapped with the excitation and emission spectra of the N,S-CDs leading to the quenching of the fluorescent spectra.
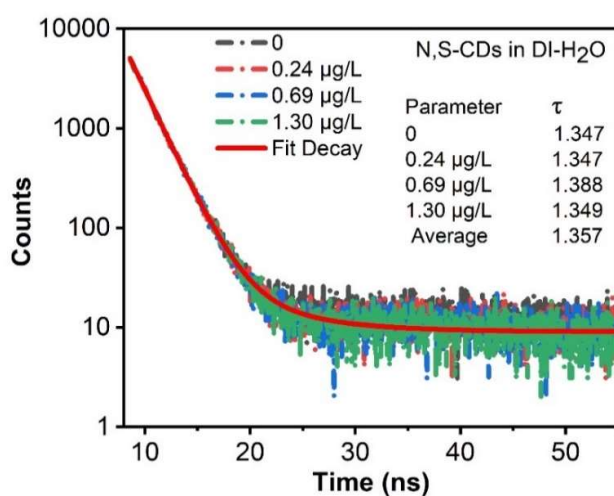
Figure 3.7 Fluorescence lifetime decay of the N,S-CDs system at different Cr(VI) concentrations.

3.4.12 Conclusion

This study successfully synthesized CDs that were sensitive to detect Cr(VI) from reagent grade insoluble Cr(VI). Passivation of the surface with 4-pyridincecarboxyaldehyde and thiourea resulted in the formation of NS-CDs with excellent QY of ~76%. The fluorescence experiment detected Cr(VI) ion at very low concentrations with a LOD of 0.01 nM and 0.1 nM, respectively for the quantification of soluble Cr(VI) and total (soluble + insoluble) Cr(VI) species. The fluorescence

probe was applicable, for the first time, to real-time PM samples collected from the ambient air to detect both soluble and total Cr(VI). The ADL for soluble Cr(VI) in ambient PM via the proposed fluorescence method was 0.031 ng/m^3 (RSD=8.4%), while the MDL for the determination of total Cr(VI) using the method was 0.32 ng/m^3.

Important characteristics to ascertain an IFE mechanism requires that no chemically interaction occur with species present (i.e. no newly formed absorption peak must be present) and the quencher must not change the fluorescence lifetime of the fluorescence material. Given the unchanged time-resolved decay in the NS-CDs, it is evident that the fluorescence quenching of NS-CDs was dominated by the IFE of Cr(VI); via a static quenching state.

Considering characteristics such as high water solubility and tunable photoluminescent, as well as the advantages of the fluorescence technique (Table 3.7), the as-synthesized NS-CDs can serve as a promising alternative in sensing Cr(VI) in ambient air particulates. This study therefore promotes the development of carbon-based functional materials, which can serve as sensors for the detection of airborne pollutants, such as metal ions.

Table 3.7 Advantages of the proposed method to other conventional methods.

Proposed fluorescent method	Conventional Methods
Low cost to acquiring instrument	High cost to purchase instruments
Time saving during analyses	Time consuming
Easy to operate	Requires highly qualified operators
Real-time measurement possible	Non-real time measurement
In-situ monitoring of samples possible (especially soluble Cr(VI) detection)	Restricted to offsite analyses

CHAPTER 4.   MEASUREMENT OF ATMOSPHERIC TOTAL AND INSOLU-BLE Cr(VI) IN KAZAKHSTAN

The acceleration in urbanization, industrialization, and population in Kazakhstan, has impacted the quality of air in the country over the past decades. In urban and highly industrialized regions, exposure to poor air quality has resulted in harmful health and environmental outcomes.[212,213] Astana, Kazakhstan's capital, has doubled its population in the last 15 years and is currently the fastest-growing city in the country [214]. The increase in population has been linked to high energy consumption and the rise in vehicular traffic in many megacities [214,215], and these changes would equally impact the air quality in Astana. Studies conducted by Kerimray, et al. [214] showed that Astana's air pollution levels have reached unhealthy conditions. The authors [214] cited that levels of PM_{10}, NO_2, SO_2, and Total Suspended Particles (TSP) were elevated in Astana, and exceeded both the annual limit values of WHO and EU and also the air quality standards in Kazakhstan. No systematic study on selected pollutants has been presented in recent times for Astana, and thus the quantification of atmospheric Cr(VI) will be a unique case study for the international air pollution research community.

Astana, situated in the dry grass steppe zone, can be classified as a coal-powered megacity having more than 600 operating industrial organizations [216]. Previous studies[217,218] indicated that vehicular traffic accounts for up to 55% of the total air pollution in the city. The existing coal power plants namely "Astana-energy JSC CHP-1 (22 MW)" and "Astana-energy JSC CHP-1 (360 MW)," are suspected to have contributed about 24 % to the total air pollution.[217,218] Stationary sources including boiler houses, private organizations, and state agencies are also suspected to have contributed more than 20% to the pollution menace.[217,218] Concerns from some residents of Astana have been raised given the poor air quality and the frequent formation of smog in the city.[217] In general, there has been inadequate information or existing data relating to ambient concentrations of air pollutants (e.g Cr(VI)) in the Central Asian region, especially in, Kazakhstan. This scarcity of such vital information may retard the development of regulations to control Cr(VI) pollution in the country and especially in a fast-growing city like Astana. A few studies also commented on the environmental consequences of aerosol pollution in the region of Astana.[219,220]

The main aim of this study was to measure size-segregated Cr(VI) concentrations in the ambient PM of Astana city. Currently, no studies have been conducted on the size-segregated total Cr(VI) in the literature. The second aim of this study investigates the gas-solid interaction of atmospheric Cr.

4.1 Sampling Campaign at Astana Air Quality Station

4.1.1 Data Sources and Handling

Astana (51.1605N, 71.4704E), the capital city of Kazakhstan, covers an area of 722 square kilometers and 347 meters above sea level a has a population of about 1.25 million. PM samples were collected from an Air Quality station located on Nazarbayev University (NU) campus, in Astana, Kazakhstan. The station is situated ~300 m from two major highways (I-490; East and I-590; West) and forms part of the representative citywide air quality. The station is also about 13.5 km away from the two main coal-fired heat and power plants "Astana-energy JSC CHP-1" and "Astana-energy JSC CHP-2".[221]

A 24-hour sampling was done using a 5-stage personal-size Sioutas cascade impactor to measure total Cr(VI) concentrations from July 2020 to November 2020. Hourly volatile organic compound (VOC; sensor sensitive to various VOCs, including benzene and toluene, but not propane, formaldehyde, or low molecular weight alcohols)[222], NO_2, SO_2, O_3, $PM_{2.5}$, and PM_{10} concentrations were obtained from an automatic Air Quality Monitoring System (AQM65, Aeroqual Ltd., New Zealand) at the station. Meteorological data such as temperature, relative humidity, wind speed, and wind direction were also retrieved from the AQM65 for the qualitative interpretation of the pollution trend. The calibration of ozone gas is discussed in the next section.

Table 4.1 List of potential pollutant sources near the sampling station.

ID	Activity	Distance from sampling site (km)
1	Coal and Heat Powered Plant (CHP-1)	~12.5
2	Coal and Heat Powered Plant (CHP-2)	~13.5
4	Astana International Airport	~8.3
5	Astana Railway Station	~11.6
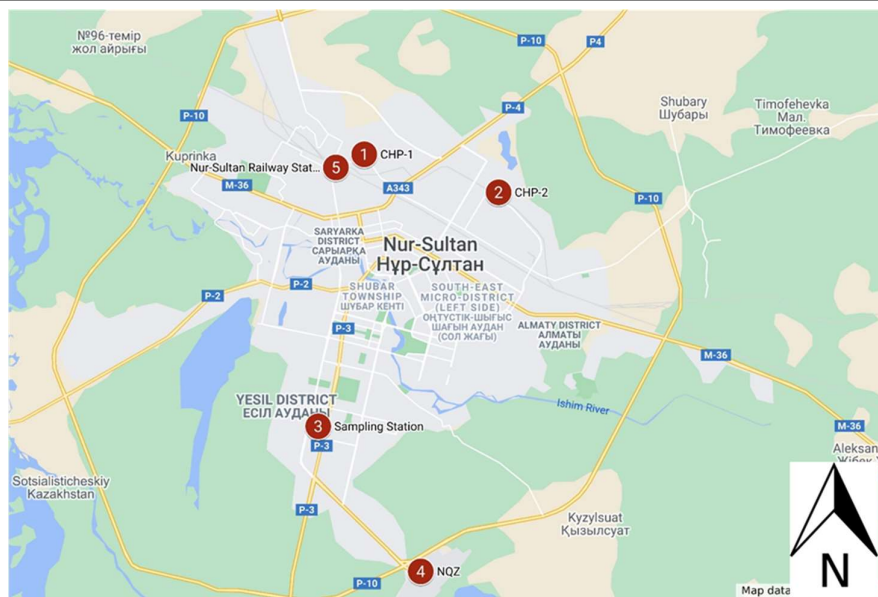
Figure 4.1 Map showing the two main coal-fired heat and power plants Astana-energy; (1) JSC CHP-1" and (2) "Astana-energy JSC CHP-2, and the monitoring station site (3). The monitoring site is also located about 7.8 km from the Astana International Airport (NQZ) (4) and ~11.6 km from the Astana Railway Station (NRS) (5). The scale map is ~2.0 km. Credit: ©OpenStreetMap contributors.

4.1.2 Calibration of The Ozone Gas Module

The ozone analyzer module in AQM65 is typically Aeroqual's proprietary gas-sensitive semiconductor (GSS) sensor and requires field calibration using standard calibration equipment and gases.[223] Since the ozone monitors in Aeroqual slightly deviate from the performance standards, Masiol, et al. [224] conducted post-processing of the Aeroqual raw data to suit scientific interpretation. The authors [224] use their 24-hour averaged ozone concentrations that showed a good fit with a Federal Equivalent Method (FEM) O_3 analyzer. The calibration equation, Equation 4.1,[224] was used in this study to calibrate AQM65 ozone measurements with the assumption that the Aeroqual ozone sensors used in our study and by Masiol, et al. [224] show similar performance.

$$y = 0.65x + 13.98, \text{ with } r^2 = 0.74 \tag{4.1}$$

where y is the Aeroqual O_3 concentration (ppb), x is the Teledyne API T400 photometric analyzer (FEM O_3 analyzer), and r^2 = the coefficient of determination.

4.1.3 Sampling With 5-Stage Sioutas Impactor

Teflon filters (25 mm in diameter, 0.5μm PTFE filter with laminated PTFE support, SKC) were used to collect PM samples with size fractions; > 2.5 μm, 1.0 to 2.5 μm, 0.50 to 1.0 μm, 0.25 to 0.50 μm. Particles above each cut-point were collected onto the filter in each stage when the Sioutas Impactor was operated with a 9 L/min pump. The last stage consists of Teflon filters with a size of 37 mm (2.0 μm PTFE filter with PMP support ring, SKC), to collect samples with < 0.25 μm cut-point.

4.1.4 Determination of Soluble And Insoluble Cr(VI) in Ambient Air

Analytical techniques for the determination of soluble Cr(VI) and insoluble Cr(VI) are discussed below.

4.1.4.1   Analytical Method For Soluble Cr(VI) Determination

Cellulose filters were pretreated by leaching overnight in a 10% HNO_3 acid solution to remove any residual Cr contaminations.[68] Filters were later washed in ultrapure H_2O until the pH was between 5 and 6, and dried overnight in a clean fume hood. The filters were impregnated with 500 mL of 0.12M $NaHCO_3$ solution to obtain a basic cellulose filter. The basic filters, with pH between 9 and 10, were further dried in the fumehood. To avoid contamination, all filters were handled with plastic or PTFE forceps.[62]

Quantification of soluble Cr(VI) concentrations was conducted using the method developed by ERG [68]. Briefly, filter samples were transferred into a 15 mL conical centrifuge tube, and 10 mL of 20 mM sodium bicarbonate ($NaHCO_3$) solution was added. The centrifuge tubes with the samples were transferred onto a shaker (MaxQ™ 4000 Benchtop Orbital Shakers, Thermo Scientific™) and shaken for 45 minutes. About 10 mL of the extract was later fetched with a BD syringe and filtered via a 0.45 μm filter (Thermo Scientific 25mm Nalgene Syringe filter SFCA) to remove particles before the analyses. The samples were then analyzed on IC-UV (530 nm wavelength) within ~3 hours to avoid any inter-conversion between Cr(VI) and Cr(III) in the extract. Laboratory and Field blank samples were analyzed in the same manner as field samples.

4.1.4.2   Analytical Method For Total Cr(VI) Determination

The microwave-assisted extraction method developed by Huang, et al. [70] was used for the extraction of total Cr(VI) in this study. The filter samples were extracted in a microwave system with 3% Na_2CO_3 - 2% NaOH (pH ~ 11.8) solution by ramping within 15 minutes to 95 °C and holding it for another 60 minutes. The extracts are then sampled with a 10 ml BD syringe and filtered via a 0.45 µm filter (Thermo Scientific 25 mm Nalgene Syringe filter SFCA) before analyzing on the IC-UV.[70] This extraction method used alkaline buffers containing CO_3^{2-} as the extraction solution for total Cr(VI) because heated alkaline buffer solutions with CO_3^{2-} or OH^- can dissolve insoluble Cr(VI) as indicated by Huang, et al. [70]. Insoluble Cr(VI) was expressed as the difference between the total and soluble Cr(VI) components.

For the quantification of trace amounts of Cr, Pb, Fe, and Mn, the filter samples were digested in an acid mixture (2.5 mL HNO_3; 0.7 mL HCl) by ramping over 30 minutes to 175 °C in a microwave (Milestone Ethos UP Microwave Digestion Oven, Milestone Inc.), and holding it further at this temperature for extra 30 minutes.[225] The selected trace elements in the PM_{10} samples were measured on an inductively coupled plasma mass spectrometer (ICP-MS, iCAP™ RQ Thermo Fisher Scientific).[226]

4.1.5 Quality Control/Quality Assurance (QC/QA)

For the microwave digestion method, a Cr(VI) certified reference material, SQC 012 was employed to assess the method's accuracy. Approximately, ~20 mg SQC 012 was coated on the Teflon filters and microwave extracted using conditions the same as for the collected samples, and the extracts were later analyzed on IC-UV. The ~20 mg weight was used to have a sufficient amount of the Cr (VI) certified reference materials that would give homogeneity in the certified material.[70]

The extraction method for soluble Cr(VI) quantification was evaluated by calculating the relative standard deviation (RSD) for the results of replicate analyses of the Cr(VI) standard solutions. The method detection limit (MDL) and recovery efficiency were obtained by spiking the pre-treated cellulose filters with 0.1 ng/mL Cr(VI) standard solutions. The filters were then extracted and analyzed using the same method employed for the cellulose PM samples collected from the field.

4.1.6 Statistical Analyses

Comparisons between groups of samples were conducted using the Wilcoxon rank sum test.[227] For the Astana field samples, statistical analyses were performed on the concentrations of the different PM sizes of > 2.5 μm, 1.0 to 2.5 μm, 0.50 to 1.0 μm, 0.25 to 0.50 μm, and < 0.25 μm. The coefficient of determination (r^2) was calculated to examine any relationship among the concentrations of each size fraction and gases, as well as for some meteorological variables.

In the Aktobe sampling campaign, statistical analyses were conducted on the concentrations of soluble Cr(VI), total Cr(VI), and their ratios. Insoluble Cr(VI) concentrations were determined as the difference between total Cr(VI) and soluble Cr(VI) concentrations, concerning the amount of volume of air sampled. For each filter sample where both total Cr(VI) and total Cr were available, Cr(III) was calculated by subtracting the total Cr(VI) from total Cr according to equation 4.2.

$$Cr(III) = total\ Cr - total\ Cr(VI) \tag{4.2}$$

The coefficient of determination (r^2) was equally calculated to investigate any relationship among Cr(VI) and some trace elements (Cr, Pb, Fe & Mn), and for meteorological variables. The Shapiro-Wilk normality test[228] indicated that the data were not normally distributed so the non-parametric two-sample Wilcoxon rank test[229] was performed on the datasets.

4.1.7 Conditional Bivariate Probability Function (CBPF)

CBPF is described in detail by Uria-Tellaetxe and Carslaw [230] and has been widely used to relate pollutant concentrations to wind speed and direction. The CBPF incorporates the conventional conditional probability function (CPF)[231] with wind speed as a third variable.[230] This function assigns the observed pollutant concentrations to particular cells that are defined by ranges of wind direction and wind speed[230], in contrast to CPF[231] which only allocates concentrations to wind direction sectors. CBPF can be defined as:

$$\text{CBPF}_{\Delta\theta,\Delta v} = \frac{m_{\Delta\theta,\Delta v}\ |[C] \geq x}{n_{\Delta\theta,\Delta v}} \tag{4.3}$$

where mΔθ, Δv is the number of samples in the wind sector Δθ with wind speed interval Δv with concentration [C] greater than a threshold value x, nΔθ, Δv being the total number of samples in that wind direction-speed interval.[230] Thus, CBPF is more appropriate in localities characterized by complex sources and can identify different pollutants' sources as compared to other techniques in use e.g. CPF. The open-source R programming package "OpenAir" was utilized to implement the CBPF. The fractional contribution (%) of Cr species per a given wind direction was determined by initially calculating the contribution of exposure from the directional wind average values.

4.1.8 Samples Handling And Storage

At the end of each sampling period, sampled filters were picked up from the chromium sampler and stored in a freezer at approximately -20 °C until analysis. Chromium speciation during frozen storage has been investigated by researchers and frozen storage of sampled filters is known to prevent Cr(VI) conversion.[68] The work of ERG [68] indicated that frozen cellulose filters spiked with Cr(VI) solutions showed an insignificant loss for up to 11 days at -18 °C (due to its stability, >80% recovery was achieved for Cr(VI).

4.1.9 Field Blank (FB) and Lab Blank (LB)

Blank Teflon and Cellulose filters were used for LB and stored in the freezer (- 20 ºC) until analyses. Another set of blank Teflon and Cellulose filters was used as the FB. For the FB, the designated filters were taken to the field, loaded in the cartridge holder but no air sampling was conducted, then returned to the lab after 24 hr exposure, and stored in the freezer at -20 ºC until analyses. The difference in Cr concentrations between FB and LB suggested the influence of field trips on the original filters.

4.1.10 Results and Discussions on the Heterogeneous (Gas-Solid) Chemistry of Atmospheric Cr-Astana Study

Table 4.2 displays the size-segregated Cr(VI) concentrations, gas concentrations, and meteorological measurements obtained in this study. **Figure 4.2** shows the sta-

tistical distribution of the size-segregated Cr(VI) concentrations. The overall Cr(VI) concentrations for all size ranges: > 2.5 μm, 1.0-2.5 μm, 0.50-1.0 μm, 0.25-0.50 μm, and < 0.25 μm were mean (SD) [range]; 1.12 (0.76) [0.007-2.88], 1.56 (1.52) [0.12-6.37], 1.47 (1.82) [0.005-9.71], 1.013 (1.07) [0.005-4.32], 4.84 (2.17) [1.044-9.77] ng/m^3, respectively (**Table 4.2**). The combined fractions (> 2.5 μm to < 0.25 μm) is presented as the total suspended particles (TSP) with their overall Cr(VI) concentrations as 10.0 (4.98) [1.94-23.47] ng/m^3. Cr(VI) concentrations were detected in all of the field samples (*N*=185).

4.1.10.1   Seasonal Variations of Cr(VI) Concentrations (Summer And Fall)

The mean (SD) for ambient Cr(VI) concentrations for the size fraction > 2.5 μm were 1.15 (0.77) ng/m^3 and 1.09 (0.77) ng/m^3, respectively, during summer and fall. The seasonal concentrations of the remaining size fractions are also shown in **Table 4.2** and **Figure 4.2**. From **Table 4.2**, the size 1.0-2.5 μm had mean Cr(VI) concentrations of 1.99 (1.85) ng/m^3 and 1.05 (0.78) ng/m^3, respectively, in summer and fall. The remaining segregated fractions with their seasonal comparison are as follows; 0.25-0.50 μm (summer; 1.09 (1.08) ng/m^3, fall; 0.92 (1.08) ng/m^3), and < 0.25 μm (summer; 5.84 (2.08) ng/m^3, fall; 3.67 (1.65) ng/m^3). The sum of all the fractions (TSP) yielded 11.73 (5.30) ng/m^3 and 7.97 (3.77) ng/m^3 as the total Cr(VI) concentrations for the summer and fall seasons, respectively. Generally, the comparative analyses of the seasonal variations of the size fractions from > 2.5 μm to < 0.25 μm showed higher concentrations of Cr(VI) in summer than in fall (**Table 4.2**), which show consistency with earlier modeling studies.[95,96] The seasonal trend for the size fraction < 0.25 μm however showed a statistically significant difference with a magnitude of 1.6 times higher level in summer (p<0.01) than in the fall. Total Cr(VI) in TSP also showed a statistically significant difference over the seasons (p<0.05).
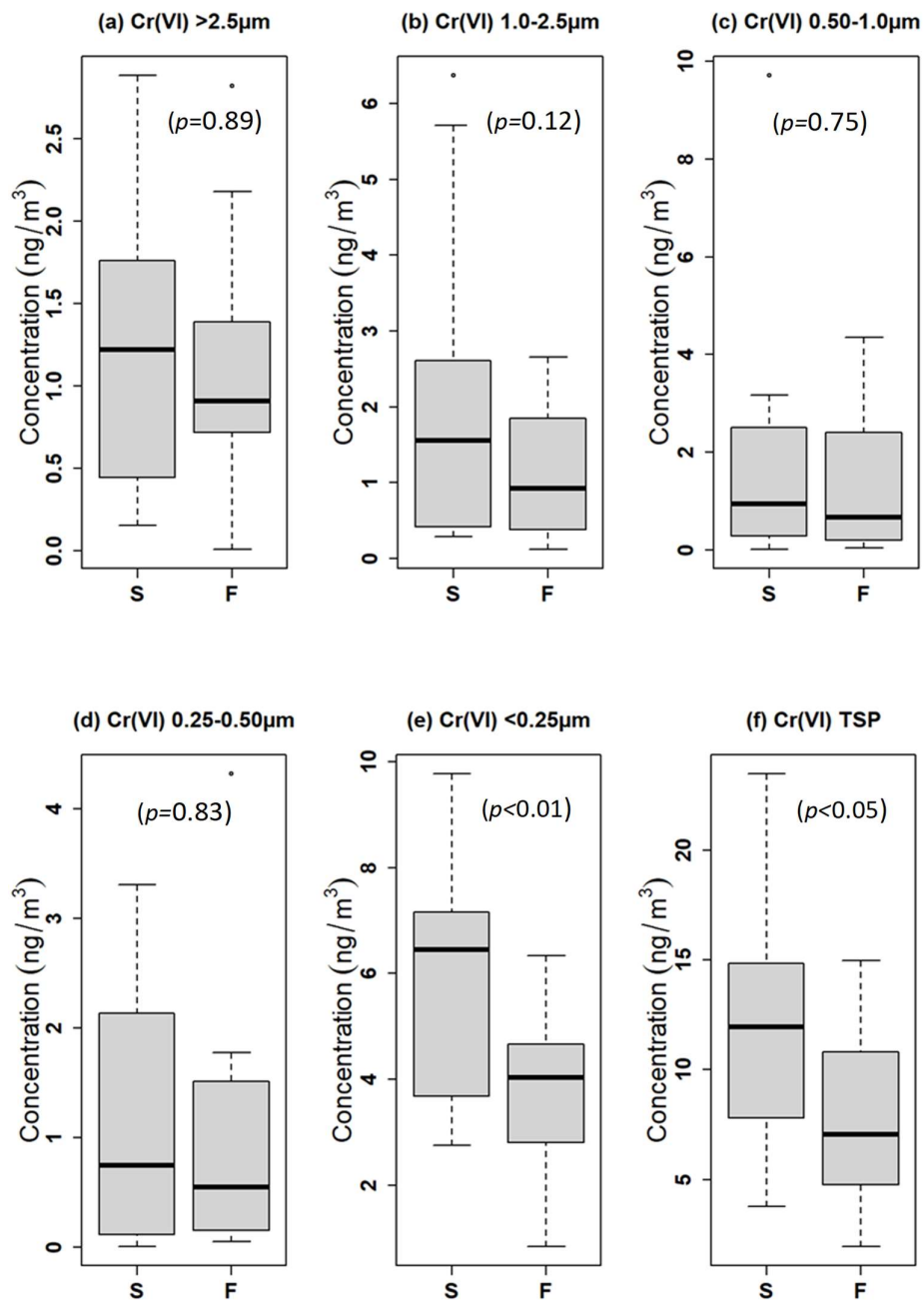
Figure 4.2 Seasonal variations for the size segregated fractions of total Cr(VI), where S=summer and F= fall seaon.

Table 4.2 Descriptive statistics of parameters over the sampling period

Parameters	Summer season (N=20)	Fall season (N=17)	Statistically significant
>2.5 µm (ng/m^3)	1.15 (0.77) [0.15-2.88]	1.09 (0.77) [0.007-2.82]	No, p=0.89
1.0-2.5 µm (ng/m^3)	1.99 (1.85) [0.28-6.37]	1.05 (0.78) [0.12-2.66]	No, p=0.12
0.50-1.0 µm (ng/m^3)	1.66 (2.21) [0.005-9.71]	1.24 (1.25) [0.05-4.35]	No, p=0.75
0.25-0.50 µm (ng/m^3)	1.09 (1.08) [0.005-3.31]	0.92 (1.08) [0.05-4.32]	No, p=0.83
< 0.25 µm (ng/m^3)	5.84 (2.08) [2.75-9.77]	3.67 (1.65) [0.85-6.33]	Yes, p<0.01
TSP (>2.5 to <0.25 µm) (ng/m3)	11.73 (5.30) [3.77-23.47]	7.97 (3.77) [1.94-14.96]	Yes, p<0.05
Temperature, °C	23.47 (3.72) [16.83-29.33]	4.21 (3.48) [-1.44 – 9.87]	Yes, p<0.001
Relative Humidity (%)	52.30 (12.0) [31.20-82.10]	64.44 (13.92) [38.10-83.80]	Yes, p<0.05
Pressure, hPa	967.31 (5.02) [954-975.9]	977.98 (10.13) [957.9-989.5]	Yes, p<0.01
Wind Speed, m/s	1.67 (0.55) [0.69-3.09]	1.96 (1.08) [0.10-4.14]	No, p=0.60
Wind Direction, °	171.98(120.39) [26.0-350.0]	225.29 (58.88) [46.80-315.90]	No, p=0.18
PM$_{2.5}$, µg/m^3	8.42 (4.39) [0.87-16.56]	8.08 (4.92) [1.16-15.96]	No, p=0.66
PM$_{10}$, µg/m^3	7.11 (3.50) [1.62-14.89]	7.74 (4.61) [0.88-15.86]	No, p=0.75
O$_3$, ppb	35.88 (5.37) [25.95-44.26]	31.14 (4.20) [22.13-37.92]	Yes, p<0.01
NO$_2$, ppb	5.83 (2.16) [1.40-10.19]	0.43 (0.47) [0.001-1.40]	Yes, p<0.001
SO$_2$, ppb	1.44 (1.18) [0.37-5.33]	1.54 (1.026) [0.57-4.31]	No, p=0.68
VOC, ppb	0.48 (1.10) [0-4.75]	6.91 (1.25) [5.37-9.74]	Yes, p<0.001

NB: result presented as mean (S.D) [Range]

Table 4.3 Overall descriptive statistics of the Cr(VI) (ng/m^3) concentrations collected over the 5-stages

Statistics	>2.5 µm	1.0-2.5 µm	0.5-1.0µm	0.25-0.5µm	< 0.25 µm	TSP
Average	1.12	1.56	1.47	1.01	4.84	10.00
Min.	0.0068	0.12	0.005	0.0053	0.84	1.93
Max.	2.88	6.37	9.71	4.32	9.77	23.47
Median	1.07	1.24	0.73	0.55	4.55	9.61
St. Dev.	0.76	1.51	1.82	1.07	2.17	4.98
Count(n)	37	37	37	37	37	37

NB: TSP is the sum up of > 2.5 µm to < 0.25 µm stages

The descriptive statistics for $PM_{2.5}$ and PM_{10} are presented in **Table 4.2**. The overall $PM_{2.5}$ concentrations had a mean of 8.26 µg/m^3 in the range of 0.87-16.56 µg/m^3. The summer mean (SD) value of 8.42 (4.39) µg/m^3 was higher than the fall mean value of 8.08 (4.92) µg/m^3, although not statistically significantly different (p=0.66). PM_{10} concentrations in summer were 7.11 (3.50) µg/m^3, while a mean of 7.73 (4.61) µg/m^3 was recorded in fall; about 0.92 times higher than the summer values but not statistically significant.
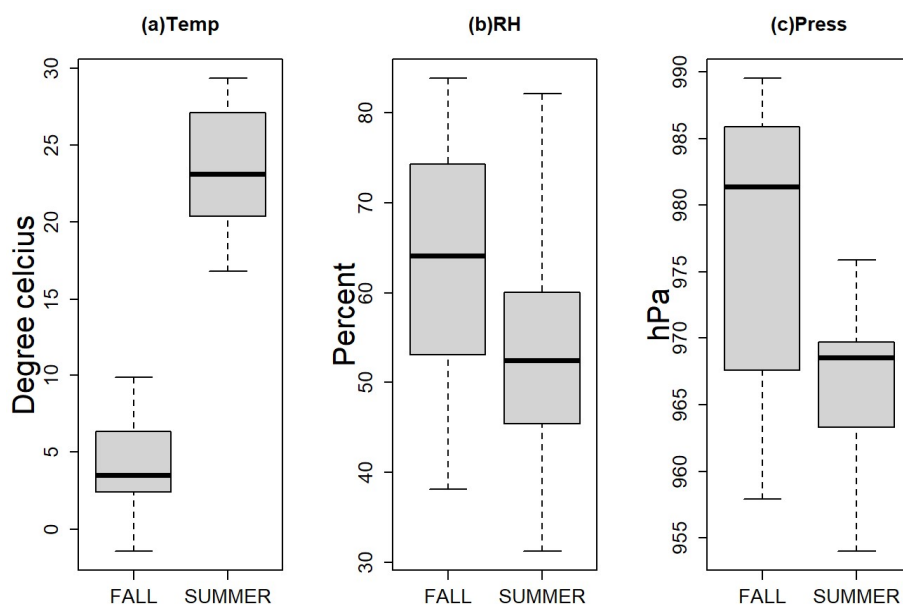
Figure 4.3 Distribution of meteorological conditions during the sampling period
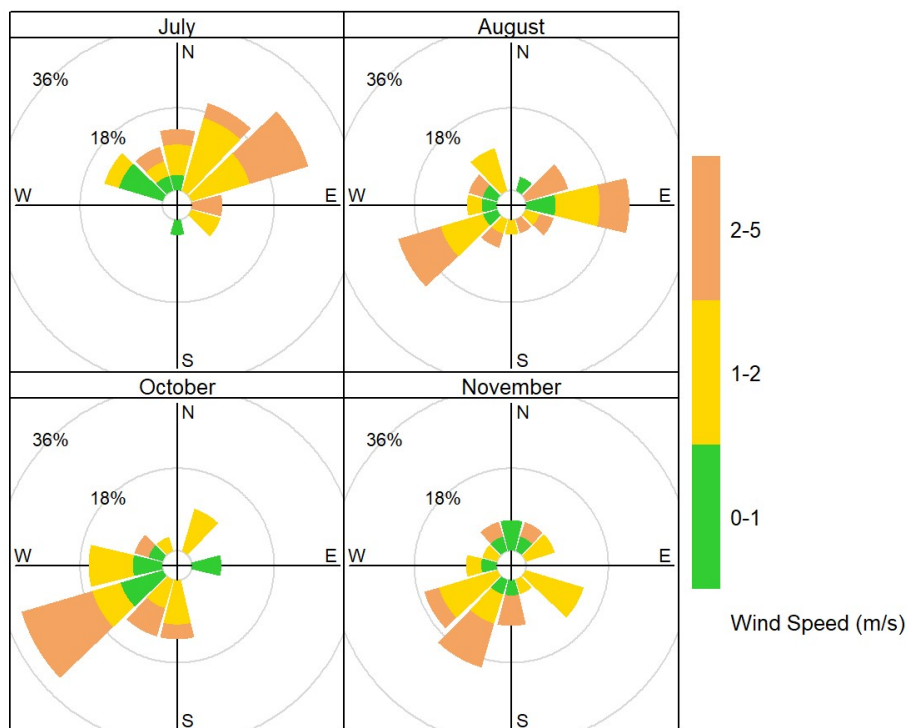
Figure 4.4 Windrose over the sampling periods

The statistical distribution of the meteorological conditions during the study period can be found in **Table 4.2**, Figures 4.3, and 4.4. The temperature distribution in summer was in the range of 16.83-29.33 °C, while a mean temperature of 4.21 (3.48) °C in the range of -1.44 to 9.87 °C was recorded for fall. The mean value of 23.47 °C in summer was about 5.6 times statistically significantly (p<0.001) higher compared to the fall mean value. Relative humidity of 52.30 (12.0) % was recorded in the summer, while 64.44 (13.92) % was recorded in the fall. The fall RH values were about 0.8 times statistically significantly (p<0.05) higher than in the summer season. No statistically significant changes occurred in the wind speed during the summer and fall periods (p=0.658). The wind rose diagram (**Figure 4.4**) revealed that in July, northeasterly winds were prevalent, with wind speeds of 2-5 m/s being dominant. The latter part of summer (August) revealed more easterly and southwesterly winds. In fall, about 30% of southwesterly winds occurred in October and about 20% in November in that same direction. No significant changes in pressure were recorded during the two seasons. The mean concentration of NO_2 was statistically significant in summer (mean: 5.83 ppb), compared to fall (mean: 0.44 ppb) (p<0.001). Similarly, there was a change in the VOC concentrations when summer (mean: 0.48 ppb) was

compared to the fall (mean: 6.91 ppb). The VOC concentrations showed a statistically significant change (p < 0.001) such that fall concentrations were about 14.5 times higher than the summer concentrations. The concentrations of O_3 were statistically significant (p < 0.01) when the summer concentrations with a mean of 35.88 ppb were compared to fall (31.14 ppb). Sulfur dioxide however did not show any statistically significant changes (p=0.68) when summer was compared to fall.

4.1.11 Correlation of Cr(VI) Concentrations with Other Parameters

The coefficient of determination (r^2) in Table 4.4 showed that O_3 could explain only about 6% variation in the Cr(VI) concentrations in all 5 size fractions. However, NO_2 and SO_2 explained about 15.4% and 14.5% variability, respectively, in the Cr(VI) concentrations measured for 1.0-2.5 µm size fraction. A relatively higher variability in the Cr(VI) concentration in the smallest size fraction, i.e., Cr(VI) < 0.25 µm, was accounted for by NO_2 (r^2 = 0.19), VOC (r^2 = 0.22), and temperature (r^2 = 0.23). As noted earlier in Table 4.2, the mean temperature in summer (23.47 °C) was about 1.06 times (in Kelvin unit) statistically significantly higher than in fall (p< 0.001). Table 4.4 further shows the potential effect of temperature on Cr chemistry where about 83%, 40%, and 84% variabilities could be explained by NO_2, O_3, and VOC, respectively.

Generally, the Cr(VI) concentrations were higher in the size fraction < 0.25 µm (Figure 4.2(e)) than in other sizes, and it also had the maximum Cr(VI) concentrations of 9.77 ng/m^3. These high concentrations in the size fraction < 0.25 µm than other coarse sizes suggest the potential contribution of airborne Cr(VI) particles from combustion sources (power plants, biomass burning, fuel oils, and vehicle exhaust)[232] since these sources are known markers that are linked to anthropogenic emissions in urban areas, especially from industrial and traffic origins.[232] Hence, a source apportionment (e.g., Chemical Mass Balance model) in the future is necessary to determine the extent of the contribution of airborne Cr(VI) particles from the coal power plants into ambient PM. Meanwhile, the higher concentration of Cr(VI) found in size fractions < 0.25 µm could be linked to the surface area (filter size at this stage is 37 mm), since surface area creates how particles interact with their surroundings, through gas, liquid, or solid interactions. Since the particles are ultrafine (< 0.25 µm), the surface area per unit volume also increases as it interacts with available gaseous pollutants. This is evident in the 22% variation in the Cr(VI) < 0.25 µm

size that was explained by VOC (Table 4.4), suggesting that higher gas-solid reactions may have led to the formation of Cr(VI) in ultrafine particle fractions. The high concentrations of Cr(VI) in size fraction < 0.25 μm may pose greater risks since smaller airborne particles are known to penetrate deeper into lower lung airways.[233]

Table 4.4 The coefficient of determination (r^2) of size fractions with gases and temperature.

Variables	A	B	C	D	E	TSP	NO_2	O_3	VOC	SO_2
NO_2	2.0E-04	0.15	0.04	4.0E-05	0.19	0.15				
O_3	0.058	0.026	3.0E-06	0.002	0.001	1.0E-04	0.26			
VOC	2.0E-07	0.087	0.019	0.014	0.22	0.14	0.61	0.32		
SO_2	0.009	0.15	0.01	0.05	0.051	6.0E-05	0.031	0.008	0.022	
TEMP	0.003	0.099	0.015	0.004	0.23	0.13	0.83	0.40	0.84	0.001

NB: Size fraction A: > 2.5 μm, B: 1.0-2.5 μm, C: 0.50-1.0 μm, D: 0.25-0.50 μm, and E: < 0.25 μm.

Table 4.5 The coefficient of determination (r^2) for size fractions with $PM_{2.5}$, $PM_{10,}$ and some meteorological conditions.

Variables	A	B	C	D	E	TSP	$PM_{2.5}$	PM_{10}	WS
$PM_{2.5}$	0.046	0.005	0.01	0.03	0.014	0.006			
PM_{10}	0.04	0.047	0.019	0.035	0.01	0.021			
WS	2.9E-04	0.009	0.001	0.11	0.033	1.7E-04	0.10		
RH	0.11	0.005	0.002	0.021	0.014	0.001	0.30	0.15	0.02

4.1.12 Comparison of Cr(VI) Levels in This Study to Other Studies

Cr(VI) concentrations found in this study were compared to other scholarly work as shown in Table 4.6. The overall mean Cr(VI) concentrations (Table 4.3) of 1.12, 1.56, 1.47, 1.01, and 4.84 ng/m³ for the 5-cascades as expected were higher than the soluble Cr(VI) values reported in the literature (Table 4.6). Results from the very few studies on total Cr(VI) concentrations in the literature (Table 4.6) show that our current results were comparable to theirs. For instance, the measurement of total Cr(VI) concentrations in PM_{10} with mixed Cr emission sources in New Jersey [70] reported the

mean concentrations of 1.05-1.41 ng/m^3 and 0.99-1.56 ng/m^3 for total Cr(VI), respectively for winter and summer, and these values were lower than the TSP concentrations in our study. The authors indicated that the source of Cr(VI) in the New Jersey study was due to the nearness of the highway to the sampling station, while our present study was conducted a little further away from the highways (I-490 and I-590) in Astana. A study similar study conducted by other researchers[234] on the size-segregated analyses of Cr(VI) showed that generally, size fraction 1.0-5.6µm (the 6th lower fraction out of 8 stages) had the highest Cr(VI) concentrations. Although their measurement was only based on soluble Cr(VI), in contrast to total Cr(VI) in our investigation, a similar phenomenon was observed where Cr(VI) concentrations were highest in the smallest particle size fractions (< 0.25 µm). The authors [234] also reported higher Cr(VI) concentrations in summer than in winter, a similar situation observed in the seasonal trend in our study, implying that atmospheric reactions such as photo-oxidation occurred in summer that promoted Cr(III) to Cr(VI). The overall averages of total Cr (VI) concentration (1.121, 1.557, 1.470, 1.01, and 4.84 ng/m^3) in this investigation did not exceed the Inhalation Reference Concentration (RfC) of 8 ng/m^3.[235] The RfC for upper respiratory effects is based on nasal mucosal irritation, shrinking, and perforation due to occupational exposures to chromic acid mists and dissolved hexavalent chromium aerosols.[235] However, there were many exceedances for the TSP size fraction. For individual values for the TSP sample in this study, the total concentration of Cr(VI) exceeded the RfC value 22 times (15 times in summer and 7 times in fall) with an overall average of 10.0 ng/m^3.
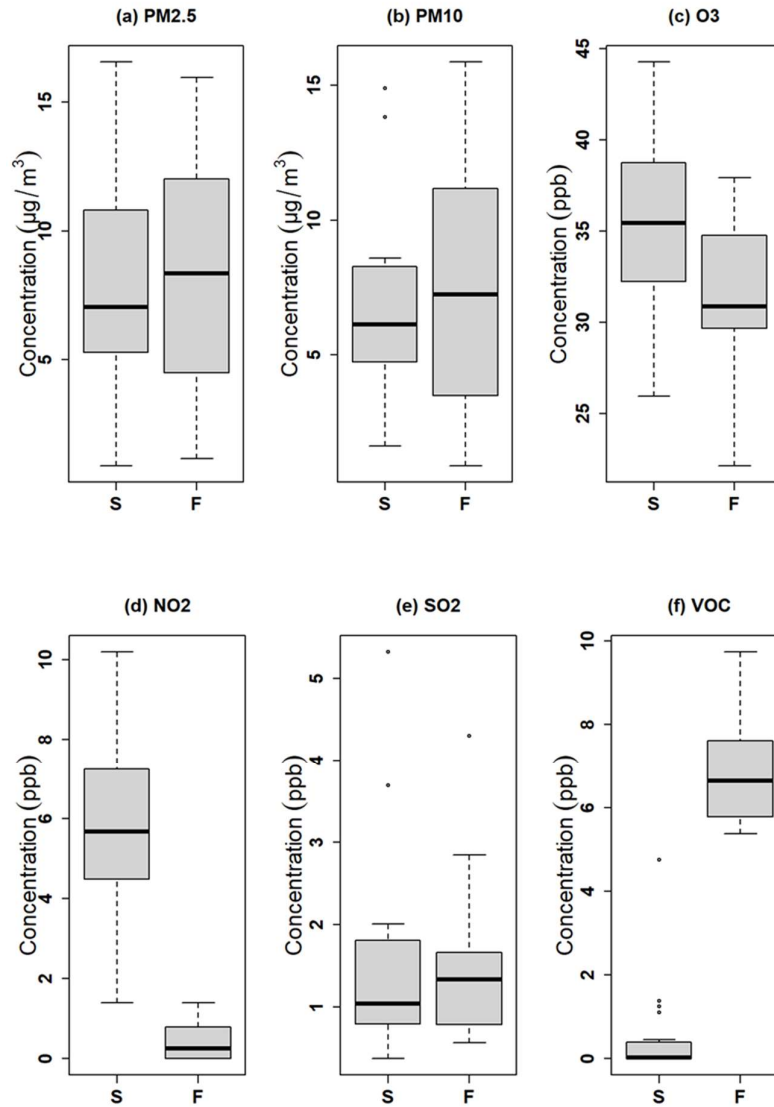
Figure 4.5 Seasonal variations of other pollutants at the sampling site.

Table 4.6 Comparison of Cr(VI) concentrations in this study with earlier studies in Literature

City/Country	Total Cr (ng/m^3)	Soluble Cr(VI) (ng/m^3)	Total Cr(VI) (ng/m^3)	Location	Reference
Hamilton, Canada		0.55		Industrial	[236]
Vienna, Austria		0.04-0.23			[237]
Regensburg, Germany		1.0		Urban	[238]
Industrial complexes, Korea		0.09-1.40		Industrial	[239]
Sydney, Australia		0.14		Residential	[240]
Frankfurt, Germany		16.3		Rural	[241]
Isfahan, Iran	27	5.4-8.2		Industrial	[242]
Elizabeth, NJ, USA		0.03		Traffic	[62]
Wilmington, USA		0.5		Urban	[243]
Radom, Poland	25		6	Urban	[244]
western Bushveld Complex, South Africa			4.6 (median)	Regional background	[245]
Santiago, Chile		5.0		Urban	[246]
Flemish, Belgium	34-96	0.9		Industrial	[247]
New Jersey, USA		0.13 (site I) & 0.08 (site II); summer, 0.02 (site I) & 0.03 (site II); winter		Traffic/ Urban	[234]
New Jersey, USA		0.001-2.97		Mixed	[68]
New Jersey, USA		0.03-0.19 (winter) 0.12-0.37 (summer)	1.05-1.41 (winter) 0.99-1.56 (summer)	Urban & Suburban	[70]
Aktobe city, Kazakhstan	46.39	0.01-1.36 (winter) 0.01-1.27 (fall)	0.11-5.33 (winter) 0.70-9.44 (fall)	Urban/Industrial	[210]

4.1.13 Potential Sources of Pollutants in Astana Field Study

In July, about a 25% probability of the prevailing wind blowing from the NE direction with a speed from 1 to 5 m/s, while in August (the latter part of summer) prevailing winds occurred from the E and SW directions with about 20% probability each (**Figure 4.4**). Low pollution levels are known to occur usually under high windy conditions via advection and increased turbulence. As such the relatively high wind speed from the SW directions (~4.5 m/s, **Figure 4.6**) showed lower concentrations of the criteria pollutants which could be due to non-significant available source(s) and/or fewer urban structures in that direction. Low wind episodes on the other hand usually result in decreased pollutant dilution, and this could be a reason for the low concentrations of PM_{10}, $PM_{2.5}$, O_3, and SO_2 in the ESE-SE directions at ~2.5 m/s speed (**Figure 4.6**). Probabilities of VOC and NO_2 emanating from the ESE-SE directions at this same wind speed (~2.5 m/s) were however low, <10% (**Figure 4.6**). The plots also identified potential sources with S to W winds with probabilities of approximately 20% for PM_{10} (**Figure 4.6**(b)), 50% for SO_2 (**Figure 4.6**(d)), and 25% for VOC (**Figure 4.6**(e)). The potential source for these pollutants appears to be a local source with a speed of ~ 2.3 m/s.

(a)   CPF at the 75th percentile (=12)

(b)   CPF at the 75th percentile (=9)

(c)   CPF at the 75th percentile (=37)

(d)   CPF at the 75th percentile (=1.8)

(e)   CPF at the 75th percentile (=6.5)

(f)   CPF at the 75th percentile (=5.7)
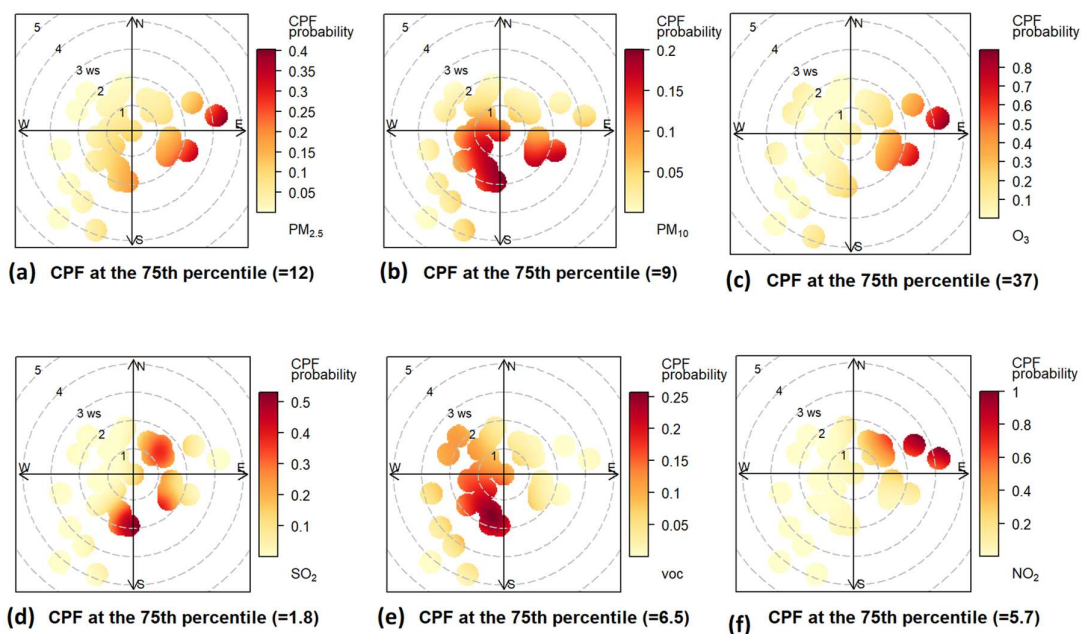
Figure 4.6 CBPF plots for different pollutants; (a) PM_{10}, (b) $PM_{2.5}$, (c) O_3, (d) SO_2, (e) VOC, and (f) NO_2

The fractional contributions of the pollutants in **Table 4.7** shows that the contribution for PM_{10}, O_3, and VOC emanated from the S-SW wind direction, with 21.34%, 21.26 %, and 39.03%, respectively. The influence of S wind was also identified with SO_2 with a fractional contribution of 23 % (**Table 4.7**), emphasizing that the local source in the S to W direction is a potential contributor to the surrounding air quality in this study. Another source in the NE direction for SO_2 appears to be a local source (~1.5 m/s) with ~ 40% probability (**Figure 4.6**(d)) and its fractional contribution was 21.31% (**Table 4.7**) in the NE-E direction. The coal and heat-powered power plants (CHP-1 and CHP-2, Figure 4.1 and **Error! Reference source not found.**) are located in the N-NE direction and could be a potential source if the prevailing wind during summer (from NE and E) is blown towards the sampling site. Low wind episodes (~ 3 m/s) in the NE direction however yielded probabilities of 40 %, 90%, and ~100% for $PM_{2.5}$, O_3, and NO_2 respectively. The adjoining highways near the sampling site; Turan Avenue (West), Uly-Dala Avenue (North), and Kabanbay Batyr Avenue (East) are approximately 500 m away from the site. Hence the relatively high probabilities identified for $PM_{2.5}$, O_3, and NO_2 in NE indicated probable local diffusion from vehicular traffics, and other source (s) nearby in that direction, assuming the wind episodes occurred downwind with respect to the location of our sampling station (Figure 4.1). The CBPF plots for the size segregated fractions showed source contributions from the S-SW wind direction for > 2.5 µm and 0.5-1 µm with approximately 18% probability for both. The source appears to be a distance source at ~4 m/s and the fractional contributions (Table 2.13) were 39.72% and 38.68%, respectively in the S-W direction. Another source is visible in NW for > 2.5 µm (**Figure 4.7**) with a fractional contribution of 27.93% covering the NE-N direction. A low wind speed of 2 m/s in **Figure 4.7** shows a 60 % probability of W, N, and E winds impacting the concentrations of the size 1.0-2.5 µm. Two prominent sources were identified in the ENE (45% probability) and SSE (40% probability) directions for 0.25-0.50 µm (**Figure 4.7**). For the ultrafine size fraction, < 0.25 µm, the potential source is visible in the NE direction with ~35% probability of its occurrence (**Figure 4.7**(e)).
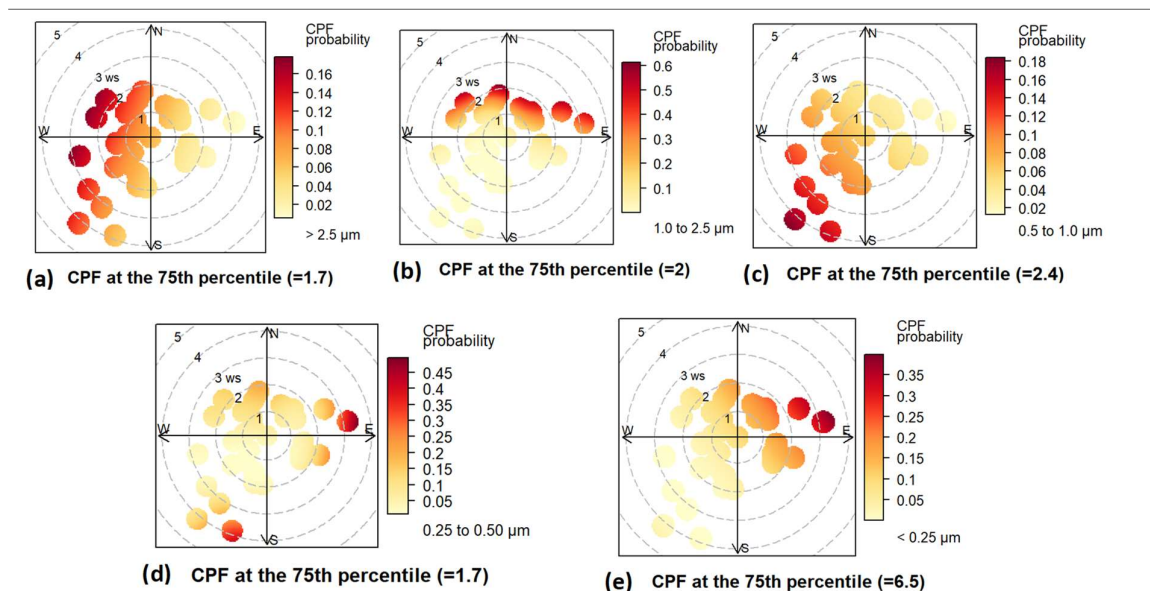
Figure 4.7 CBPF plots for the size segregated fractions of total Cr(VI) in this study.

Table 4.7 The fractional contribution of pollutants per wind direction

Parameters	N-NE	NE-E	E-SE	SE-S	S-SW	SW-W	W-NW	NW-N
>2.5 µm	9.69%	11.41%	11.25%	0.00%	20.22%	19.50%	16.89%	11.05%
1.0-2.5 µm	18.42%	20.54%	10.41%	0.00%	13.26%	14.26%	15.11%	7.98%
0.5-1.0µm	25.37%	9.16%	7.66%	0.00%	17.31%	21.37%	12.01%	7.12%
0.25-0.5µm	11.92%	9.57%	12.21%	0.00%	25.09%	13.86%	15.27%	12.07%
< 0.25 µm	10.92%	10.64%	17.92%	0.00%	16.61%	9.86%	16.41%	17.64%
TSP	14.17%	11.94%	13.92%	0.00%	17.45%	13.72%	15.50%	13.29%
$PM_{2.5}$	7.65%	14.37%	18.02%	0.00%	19.84%	15.02%	12.97%	12.12%
PM_{10}	6.80%	12.14%	17.98%	0.00%	21.34%	15.54%	12.53%	13.67%
RH	5.85%	9.89%	13.03%	0.00%	22.39%	19.18%	15.50%	14.16%
NO_2	21.13%	17.68%	27.55%	0.00%	7.87%	2.49%	6.80%	16.46%
O_3	8.51%	11.37%	19.28%	0.00%	21.26%	14.88%	11.61%	13.09%
VOC	1.96%	6.07%	0.49%	0.00%	39.03%	32.73%	18.74%	0.99%
SO_2	13.68%	21.31%	13.33%	0.00%	23.00%	11.88%	9.31%	7.48%
TEMP	14.97%	15.04%	27.49%	0.00%	10.08%	3.98%	9.82%	18.62%

4.1.14 Condensed Gas-Solid Chemistry of Cr

Aqueous reactions and gas-solid reactions are the two main reactions known to facilitate the interconversion of Cr in ambient PM. Earlier works showed that Cr(VI) and

Cr(III) interconversion can occur in the solution upon the deliquescence[93] and also via the gas-solid reactions in the presence of the O_3, reactive oxygen species (ROS), and volatile organic carbons (VOCs).[112] The total Cr(VI) concentrations in the size fractions in this study (except < 0.25 µm and TSP) in summer and fall (**Table 4.2**) were not statistically significantly different. Earlier studies identified that insoluble Cr(VI)[70,210] and insoluble Cr(III)[95,96] were the dominant forms of Cr(VI) and Cr(III), respectively, in ambient PM. Furthermore, we recently demonstrated that the Cr(III) concentration is considerably higher than the Cr(VI) in the ambient PM[210], which is consistent with the literature.[70] Hence the gas-solid reactions of the Cr(VI) with VOCs and of Cr(III) with O_3 and other atmospheric oxidants could drive the atmospheric chemistry of the chromium particularly when we observed the average RH to be below the deliquescence point in this study (Table 4.2).

The results of our study (Tables 4.2 and 5.4) provide new insight into the gas-solid chemistry of atmospheric Cr, and help us to propose a new mechanism for such reactions. Table 4.4 shows that about 13% and 15% variability of Cr(VI) in TSP fraction could be explained by the changes in temperature and NO_2, respectively, and about 14% with VOCs. Relatively high variations in the concentrations of NO_2 (r^2=0.83), VOCs (r^2=0.84), and O_3 (r^2=0.40) could be explained by the temperature changes that occurred over the two seasons (Table 4.4). Previous laboratory studies showed that Cr(III) and Cr(VI) reach equilibrium in the presence of the Ozone and VOCs through a gas-solid reversible reaction.[112] The r^2 value of ~40% for the variation in Cr(VI) that can be accounted for by O_3 in this study is consistent with laboratory observations, and indicate that increased O_3 concentrations increased the rate of reaction of O_3 with Cr(III) and resulted in increased Cr(VI) concentrations. Similarly, the ~14% variation in Cr(VI) concentration that is explainable by changes in VOC supports previous laboratory observations showing the conversion of Cr(VI) to Cr(III) can occurs in the presence of VOCs.[112] Additionally, the 15% r-squared value between Cr(VI) and NO_2 concentrations suggests that NO_2 can oxidize Cr(III) to Cr(VI), such that elevated NO_2 concentrations would result in higher Cr(VI) concentrations.[111] The products of this reversible reaction could be NO and Cr(VI). However, since the Cr(III) and NO_2 concentrations are expected to be higher compared to Cr(VI) and NO in ambient air, the overall direction of this reaction could be in favor of the conversion of the Cr(III) to Cr(VI). Amouei Torkmahalleh, et al. [112] report-

ed an increase in the rate of the gas-solid reaction at a higher temperature which is well supported by the observed positive correlation between temperature and Cr(VI) in this study (Table 4.4). The observed seasonal differences in total Cr(VI) concentration in the present study supports our proposed gas-solid reaction mechanisms. We recorded statistically higher total Cr(VI) concentration in summer compared to fall for the particles smaller than 0.25 μm which is the size at which we recorded the highest concentration. This observation is in agreement with our recent study in Aktobe city[210] where the total Cr(VI) concentration was higher in the fall compared to the winter suggesting that the total Cr(VI) concentration increases with temperature (Table 4.2). The difference in total Cr(VI) concentration between the two seasons could be due to the differences in the emission rate, meteorological conditions, and the rate of the gas-solid reactions between the summer and fall seasons. However, meteorological factors (except temperature) including wind speed and wind direction did not statistically significantly change between the two seasons. As for the source emission rate, although we do not have any data about Cr emission rates, the $PM_{2.5}$ and PM_{10} concentrations did not statistically significantly change between summer and fall. This observation could suggest that the Cr emissions potentially remained unchanged between the two seasons, and thus, the difference between the two seasons could be mainly driven by the difference in the chemistry of the atmospheric Cr. Considering the condensed gas-solid reaction of the Cr represented by reaction 4.4, four factors could lead to the increased total Cr(VI) concentrations in summer compared to the fall.

$$Cr(III)(s) + O_3 + NO_2 + A \leftrightarrow Cr(VI)(s) + VOCs + SO_2 + B \qquad (4.4)$$
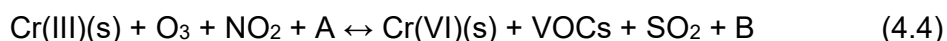
where A and B are any products of the oxidation and reductions of the reactive gases.

Firstly, the higher temperature in summer compared to the fall resulted in a higher overall reaction rate in summer compared to the fall. The overall reaction rate is defined as the difference in the reaction rates of the forward reaction and backward reaction in reaction 4.4 which is in favor of the oxidation of the Cr(III). Earlier studies [62,70,234] amongst others (**Table 4.6**) reported higher levels of Cr(VI) concentrations in summer than in winter due to higher temperatures during their study period. The second factor is the ozone concentration. Since the change in the ozone concentra-

tions between summer and fall was statistically significant (p< 0.01), the higher ozone concentrations in summer due to the higher rates of the photo-oxidation reactions could increase the rate of the overall reaction in summer greater than the fall season.[112] Exemplified is the work of Yu, et al. [234] who reported higher Cr(VI) in summer than in winter and implied that at higher temperatures in summer, stronger photochemical reactions led to the oxidation of Cr(III) to Cr(VI) to give higher Cr(VI) concentrations in ambient air Thirdly, **Table 4.2** shows statistically significant higher NO_2 concentration (p <0.001), in summer compared to fall. This increase in the NO_2 concentration promoted the conversion of Cr(III) to Cr(VI) at a higher rate in summer compared to the fall resulting in higher Cr(VI) concentrations. Finally, VOC (p<0.001) concentration underwent statistically significant increases in fall compared to the summer suggesting a higher rate of Cr(VI) conversion in fall compared to the summer. An overall schematic diagram is shown in **Figure 4.8** to depict the potential reaction of gases pollutants with available Cr species in ambient air.
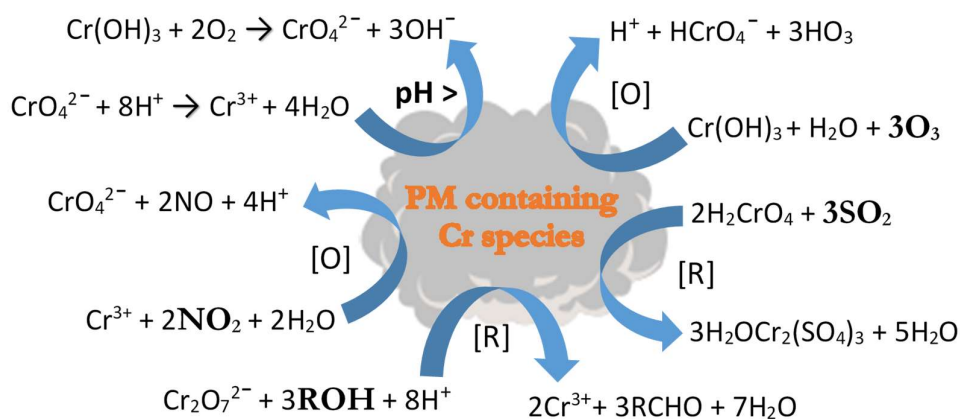
Figure 4.8 Schematic diagram to show the possible reactions of gaseous pollutants with ambient Cr species

This study demonstrated that total Cr(VI) including soluble and insoluble Cr(VI) dominated the smaller size particles (<0.25μm) in the ambient PM and a higher temperature is in favor of Cr(VI) in this size range. Unlike previous studies in the literature that demonstrated that higher temperature promoted the conversion of Cr(VI) to Cr(III), we have sufficient field evidence[210] that temperature and total Cr(VI) are positively correlated. The reason for such a considerable discrepancy in understanding the chemistry of atmospheric Cr is that previous studies in the literature implemented

analytical methods that were able to quantify only soluble forms of Cr(VI) rather than insoluble forms. However, with the development of an analytical method that enables us to measure total Cr(VI) (insoluble + soluble) and employing this method in the present study, we have concluded that gas-solid chemistry could be more influential than aqueous chemistry in driving the chemistry of atmospheric Cr. This conclusion is supported by the recent modeling[96] and field studies[210] as well as the observations made in the current study that demonstrated insoluble Cr(III) and insoluble Cr(VI) dominated atmospheric Cr(III) and Cr(VI). The observed seasonal variabilities in the gas concentrations, total Cr(VI) concentrations, and the temperature as well as the presented correlations between the gas concentrations and total Cr(VI) concentrations helped us to conclude the reaction in equation 4.4.

The present study is subject to some limitations. We studied the Cr chemistry over two seasons to completely evaluate this chemistry a longer sampling campaign is required. Our observations were made when the average RH was below deliquescence suggesting the absence of the major aqueous chemistry of atmospheric Cr. The relative importance of the homogeneous (aqueous) and heterogeneous (gas-solid) chemistry of atmospheric Cr needs to be investigated in the future. The total Cr(VI) was presented for only the summer and fall seasons in this study. To understand the seasonal variations of total Cr(VI), sampling during winter and spring is required which is the aim of our future study. This study investigated size-segregated Cr(VI) concentrations and possible Cr chemistry with some selected gases. There is however the need to assess the kinetics of such reactions at varying RH, temperature, and concentrations in the laboratory.

4.2 Sampling Campaign at Aktobe Air Quality Station

Concerns about airborne particulate matter (PM) have been raised globally due to its impact on atmospheric processes, harmful health effects, and global climate change.[248-251] Hexavalent chromium, a known oxidizer, can break down cell membranes due to the production of reactive radicals that alters functionality in cells.[53] The soluble form of Cr(VI) is less toxic than insoluble Cr(VI) since when the soluble form can be reduced to Cr(III) in the bloodstream. However, inhaled insoluble Cr(VI) is deposited in the lung and it can lead to chronic health issues.[53] Earlier studies[30] indicated that 53-85% of inhaled Cr(VI) can be cleared by the lungs while 15-47% of

the remainder is not absorbed into the bloodstream and this can be linked to Cr(VI)'s toxicity. Only a few data are available on the ambient concentration for soluble and insoluble Cr(VI) in the Central Asian region, especially in Kazakhstan, where several multiple trace element mines and mineral processing facilities are located. The absence of information can hinder the development of control remedies that would be required to combat Cr(VI) pollution in the country, such as in industrial cities like Aktobe. Previous investigations in the literature raised concerns about the regional environmental impacts of air pollution, including Cr(VI), in the region of Aktobe.[219,220] The fast rise in industrialization and energy consumption has seen a rise in the concentrations of environmental pollutants, part of which was Cr, have been identified in the city of Aktobe.[219]

The main aim of this study was to measure total atmospheric Cr(VI) (soluble and insoluble) and identify potential sources of Cr(VI) in this urban area upwind of a Cr industrial zone through collocated monitoring of both forms of Cr(VI). Additionally, this field monitoring investigated the relationship between Cr(VI) and other trace element concentrations that were investigated through collocated samplings.
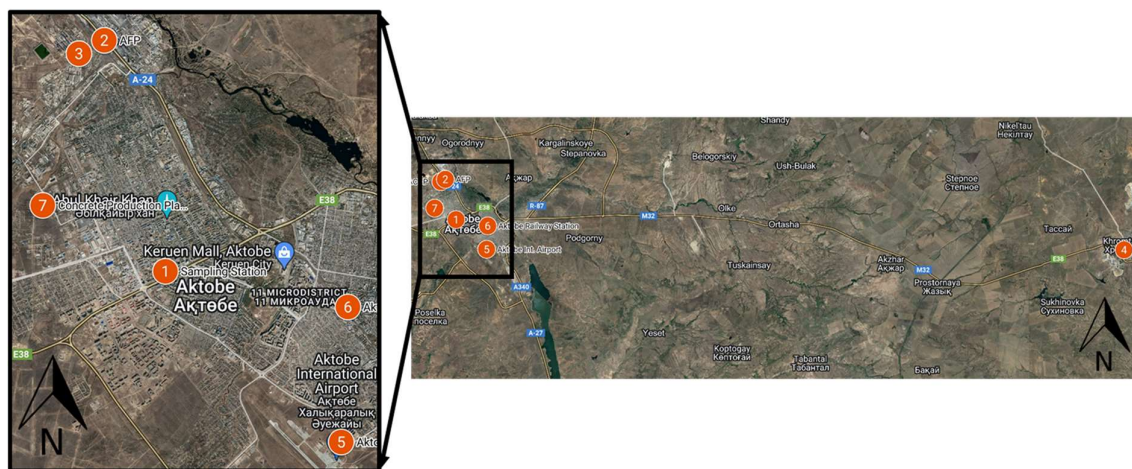
Figure 4.9 Map showing the monitoring site (1) and chromium emission sources; (2) Aktobe Ferroalloys Plant (AFP), (3) Aktobe Chromium Compounds Plant (ACCP), (4) Donskoi Chromium Ore Enriching Plant (DCOEP),(5) Aktobe International Airport, (6) Aktobe Railway Station (ARS) and (7) mixed Concrete production plants. The scale map is 1 km for the top figure and 10 km for the lower map. ©OpenStreetMap contributors.

Table 4.8 List of potential sources near the sampling site.

ID	Activity	Distance (km)
1	Aktobe Ferroalloys Plant (AFP)	7.6
2	Aktobe Chromium Compounds Plant (ACCP)	6.1
3	Donskoi Chromium Ore Enriching Plant (DCOEP)	113
4	Aktobe International Airport (AIA)	6
5	Aktobe Railway Station (ARS)	4.4
6	Concrete Production Plants (CPP)*	3.5

*Includes: "Ecotone-Batys", "Photon Aktobe", "Aktobe Story Concrete", "Reinforced Concrete", and Vibro Master Kazakhstan Plants: These facilities are involved in the production of paving slabs and autoclaved aerated concrete for construction purposes, and are very close to each other, and are located WNW of our sampling site.

4.2.1 Sampling Location

Sampling was conducted on the rooftop of an administrative building (~8.5 m high) on the campus of Aktobe Regional University (ARU), Aktobe (Latitude 50.289052N, Longitude 57.153522E). The ARU campus (Figure 4.9) is situated at the center of Aktobe, at the intersection of two major roads (Zhubanov Brothers 263 and Aliya Moldagulova Avenue 34) with high traffic flows. Apart from the known Cr industrial facilities, other possible air pollution sources are listed in Table 4.8 The meteorological conditions for the study area were retrieved from the Iowa Environmental Mesonet website [252].

4.2.2 Sampling Handling

An outdoor sampling of PM_{10} was conducted from September 2019 to March 2020 with two FRM PM_{10} samplers (Rupprecht and Patashnick Model 2000H) running side by side for 24 hours with a 16.7 LPM flow rate. These samplers, also known as Clarkson Cr(VI) samplers were designed and constructed by Amouei Torkmahalleh, et al. [62] for improved Cr(VI) sampling. Briefly, the samplers were able to reduce the relative humidity of the ambient air below the deliquescence relative humidity (DRH) of the PM matrix which will minimize the interconversion of Cr oxidation states by preventing deliquescence.[62] One sampler measured total Cr(VI) while the other sam-

pled soluble Cr(VI) in ambient PM. Each filter sample after sampling was received in a petri dish and stored in a freezer at -20 °C for analysis.

Collocated trace elements were also collected using a PM_{10} single-stage Harvard Impactor that operated at a flow rate of 20 LPM for 24 hours. The impactor was mounted at a height of ~1.5 meters. The inlet of the impactor was inverted (inlet down, impactor base up) to avoid condensation on the filter material during sampling, especially in the winter season.[253]

A Microwave System (Multiwave PRO, Anton Paar with HP 500 plus vessels) was employed for extraction purposes. Detection of Cr(VI) was conducted on IC-UV with its analytical conditions as described in the materials and reagent section.[191] The trace elements (Cr, Fe, Pb, and Mn) in PM_{10} samples were collected on a Teflon and analyzed on ICP-MS.

4.2.3 Materials and Reagents

Total Cr(VI) in the PM samples were collected on Teflon filters (PTFE, hydrophobic, 2.0 μm, 47 mm, white, plain, polypropylene ring, PM2547050, Millipore). Soluble Cr(VI) fractions were collected on Cellulose filters (Whatman® quantitative filter paper, ashless, Grade 41, diam. 47 mm) due to their low chromium background concentrations.[68] Trace elements were sampled on Teflon filter membranes (PTFE filter, no support pad, 2.0 μm, w PMP ring 37mm, SKC Inc.). Reagent grade of an insoluble Cr(VI) compounds; $PbCrO_4$, $BaCrO_4$, $CaCrO_4$, $(NH_4)_2CrO_4$ (purum p.a., ACS reagent, ≥ 98.0%), was employed for the verification of the total Cr(VI) digestion method. Other reagents used included NaOH (ACS reagent, ≥ 97.0%, pellets), HNO_3 (67-69% trace grade, Fisher Chemical), and Na_2CO_3 (anhydrous, for analysis EMSURE® ACS, ISO, Reag. Ph Eur). The accuracy of the extraction method was done using SQC 012 with certified Cr(VI) concentrations of 143 ± 2.54 mg/kg.[254] QA/QC experiments were done using Cr(VI) standard solution (*Trace*CERT®, 1000 mg/L Cr(VI) in H_2O).

4.2.4 Clarkson Cr(VI) Sampler and its Concept of Operation

The Clarkson Cr(VI) sampler was designed and constructed by Amouei Torkmahalleh, et al. [62] to keep the sampling filters dry (RH < 76%) during the sampling and post-sampling periods. The RH of the air passing over the filter was maintained below 76% (the deliquescence relative humidity (DRH) of the ambient parti-

cles) to keep the filter dry.[62,93] The dry filter slows down the reduction reactions of Cr(VI) with ambient particles by inhibiting aqueous Cr(VI) chemistry.[112] The Clarkson sampler (Figure 4.10(a)) consists of an FRM sampler (Rupprecht and Patashnick Model 2000H) equipped with PM_{10} cut-point inlet, which allows both clean and dried air to be sampled into the device. In summer the clean air was cooled to about 10 °C to slow down Cr(VI) reactions on the filter due to the decreased temperature of the sampled air. However, in winter the clean air was warmed to 10 °C to decrease the RH. The sampler's pump draws air through two paths; the clean air and the ambient air paths (inlet). The sampling flow rate was set to 16.7 LPM, and clean air was introduced into the FRM at ~5 LPM. The Clarkson sampler operated from 10:00 AM to 10:00 AM. HEPA-filtered air was forced through a mechanical dryer (Model No: D18IN, Ingersoll Rand, USA) to remove air moisture to provide dry air across the filter samples. Four paths were available for the air stream leaving the dryer, where each path entered the drier enclosure (DE) of the Clarkson sampler. The mechanical dryer was connected to one Clarkson sampler to remove enough water/moisture from the air in hot and humid seasons during the sampling campaign.

4.2.5 Components of the Drying Enclosure

The drying enclosure (Figure 4.10(b)) comprises two 47 mm cellulose filters, two HEPA filter capsules, a membrane dryer (Thermo Fisher Scientific, USA), a chiller/heater (TE Technology; model CP-065), two needle valves, a vacuum pump, and a vacuum pressure gauge. The chiller unit cools the air during summer, while the heater unit heats the incoming inflowing air in the winter. The original set point of the chiller/heater was recommended as 10 °C which would result in an actual working temperature of 10 ± 0.5°C.[62] Needle valves were available to adjust the flow rate of the clean airflow, while a membrane dryer enabled the removal of moisture from the airflow. A counterflow purge air driven by 24 ± 1 in Hg pressure drop was applied across the dryer unit to prevent any form of water saturation. The vacuum pump provided purge airflow, which passed through a cellulose filter and a HEPA filter before entering the dryer. A needle valve installed on this unit was used to adjust the flow rate of the purge air to ~0.5 LPM. To ensure good insulation on the clean air tubing, an abrasion-resistant gum rubber tubing (1/4″ ID, 1/2″ OD, 1/8″ WT) was used to cover the semi-flexible polyethylene foam rubber (McMaster Carr). The insulation

was very important to minimize any temperature drop along the line entering the Clarkson sampler [62].

(a) (b)
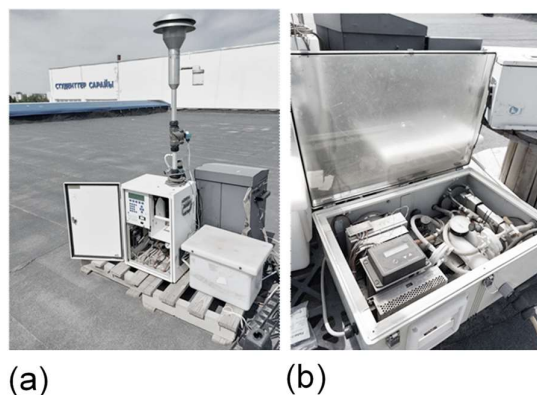
Figure 4.10 (a)The Clarkson sampler (modified Rupprecht and Patashnick Model 2000H) equipped with PM10 inlet, and (b) the drying unit connected to the sampler.

4.2.6 Results and Discussions

4.2.6.1   QA/QC

The MDL (99% confidence level) was estimated according to the USEPA method 40 CFR 136 Appendix B.[209] For the cellulose filter, seven replicate measurements were used to determine the recovery efficiency and MDL values (**Table 4.9**) after spiking with the 0.1µg/L Cr(VI) standard solution. The ratio of measured Cr(VI) to reference Cr(VI) concentrations constitutes the recovery of Cr(VI) from the extraction methods. Recoveries of Cr(VI) were close to 100% for the spiked Cr(VI) standard solutions on the cellulose filters. The Cr(VI) standard solution is in the form of soluble NH_4CrO_2.[255] The good Cr(VI) recoveries for the cellulose spiked filters indicated that the extraction method was effective to recover the soluble Cr(VI) species on the cellulose filters via the ERG [68] method. Evaluation of the total Cr(VI) concentrations in the samples was done using SQC 012 and $PbCrO_4$. SQC 012 comprises mainly soluble Cr(VI) compounds[254] while reagent grade $PbCrO_4$ is an insoluble Cr(VI) compound. The estimated Cr(VI) recoveries for SQC 012 and $PbCrO_4$ indicate that the microwave method can effectively recover total Cr(VI) in the PM collected on the Teflon filters. Good precisions, with CV% of 15.0 (n = 3) and 8.0 (n = 4) were, respectively, for the SQC 012 and $PbCrO_4$ (**Table 4.9**).

Table 4.9 QA/QC

Filter	Species	n	CV (%)	Recovery (%)	MDL (µg/L)
Cellulose	Soluble Cr(VI)	7	5.9	97.0 (5.7) [87.2-104.7]	0.0179
Teflon	Total Cr(VI)	3	15.0	120.7 (18.2) [99.9-132.9]	-
Extraction efficiency for $PbCrO_4$ as insoluble Cr(VI)		4	8.0	95.5 (7.7) [90.4-106.7]	-

Recoveries reported as mean (SD) [range]

4.2.6.2   Seasonal Variation of Cr(VI) Concentrations and Total Cr.

The results for total Cr(VI), soluble Cr(VI) concentrations, and the ratio of soluble/total Cr(VI) are summarized in Table 4.10. The statistical distribution of the Cr(VI) samples collected over the fall and winter seasons is shown in Figure 4.11. The overall total Cr(VI) concentrations had a mean (SD) value of 3.73 (2.45) ng/m^3 in the range of 0.11-9.44 ng/m^3. The soluble Cr(VI) concentrations were in the range of 0.01-1.36 ng/m^3 with a mean of 0.15 (0.33) ng/m^3. Cr(VI) was detected in all the PM samples; total Cr(VI) (n=30) and soluble Cr(VI) (n = 40).

   The total ambient Cr(VI) and soluble Cr(VI) concentrations in fall (mean (SD) [range]) were 5.30 (2.16) [0.70-9.44] ng/m^3 and 0.23 (0.38) [0.01-1.27] ng/m^3, respectively. The winter concentrations were 2.26 (1.80) [0.11-5.33] ng/m^3 and 0.10 (0.28) [0.01-1.36] ng/m^3, respectively, for total Cr(VI) and soluble Cr(VI). The seasonal variations of total Cr(VI) and soluble Cr(VI) are shown in Figures 4.10(a) and 5.10(b), respectively. The measured total Cr(VI) concentrations in the fall were about 2.3 times higher than in the winter season ($p < 0.001$). The soluble Cr(VI) concentrations were also higher in fall ($p < 0.05$) about 2.3 times than in winter (Figure 4.11 (b)). The overall ratios of soluble Cr(VI)/total Cr(VI) and insoluble Cr(VI)/total Cr(VI) are shown in Figures 4.10 (c) and 4.10 (d).
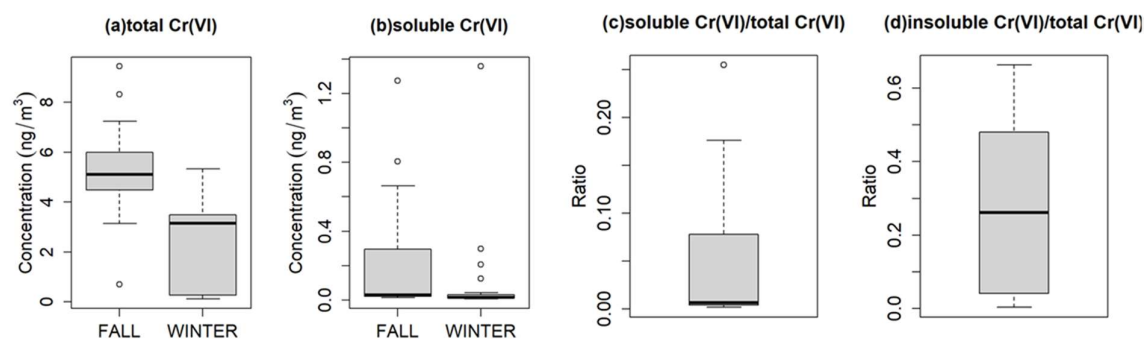
Figure 4.11 (a) Distribution of total Cr(VI), (b) soluble Cr(VI), (c) overall ratio of soluble Cr(VI)/total Cr(VI), and (d) overall ratio of insoluble Cr(VI)/total Cr(VI) concentrations in ambient PM_{10}.

The insoluble Cr(VI) concentrations (Table 4.10) were statistically significantly higher ($p < 0.001$) than the soluble Cr(VI) concentrations in both seasons, which agrees with the modeling results in the literature.[95,96] This indicates that both soluble and insoluble Cr(VI) fractions were present in ambient PM. Furthermore, the statistical analyses indicated that the insoluble Cr(VI) fraction accounted for a statistically significant ($p < 0.01$) larger portion of the total Cr(VI) in ambient PM than the soluble Cr(VI). Seasonal differences ($p < 0.001$) in the ambient insoluble Cr(VI) concentrations were present. In fall, the Cr(III) concentration had a mean of 54.69 (79.20) [2.08-223.62] ng/m^3,　while an average of 28.20 (73.38) [0.13-258.58] ng/m^3 was found in winter. The seasonal trend showed that Cr(III) concentrations in fall were higher than in winter, although not statistically significant ($p = 0.106$). The distribution of total Cr (Figure 4.12(d)) showed that overall, its mean concentration was 39.61 ng/m^3 in the range of 0.35-261.60 ng/m^3. The mean ambient total Cr concentration in fall was 50.67 (81.6) ng/m^3 with a range of [0.35-244.18] ng/m^3, and the winter season had a mean of 26.19 (68.58) ng/m^3 in the range of 0.35-261.60 ng/m^3. This seasonal difference was however not statistically significant ($p = 0.226$).

Table 4.10 Descriptive statistics and seasonal variations of parameters. Values in the table are reported as; mean (SD) [range].

Parameters	Fall season (N=19)	Winter season (N=25)	Statistically significant
Total Cr (VI), ng/m^3	5.30 (2.16) [0.70-9.44] (n=14)	2.26 (1.80) [0.11-5.33] (n=16)	Yes (p < 0.001)
Soluble Cr(VI) , ng/m^3	0.23 (0.38) [0.01-1.27] (n=16)	0.10 (0.28) [0.01-1.36](n=24)	Yes (p < 0.05)
Insoluble Cr(VI), ng/m^3	4.80 (1.96) [0.15-8.63] (n=13)	2.19 (1.75) [0.09-4.15] (n=15)	Yes (p <0.001)
Soluble Cr(VI) /Total Cr(VI), %	9.56 (21.34) [0.40-77.75] (n=13)	5.30 (17.89) [0.18-25.48] (n=15)	No (p = 0.554)
Total Cr(VI)/Total Cr, %	34.07 (25.86) [0.31-71.01] (n=10)	34.83 (23.55) [0.97-66.33] (n=12)	No (p = 0.974)
Total Cr(III), ng/m^3	54.69 (79.20) [2.08-223.62] (n=10)	28.20 (73.38) [0.13-258.58] (n=12)	No (p =0.106)
Total Cr, ng/m^3	50.67 (81.60) [0.35-244.18] (n=17)	26.19 (68.58) [0.35-261.60] (n=14)	No (p = 0.226)
Total Mn, ng/m^3	36.16 (24.77) [0.13-98.40] (n=17)	6.26 (6.95) [0.13-28.32] (n=14)	Yes (p < 0.001)
Total Pb, ng/m^3	6.99 (7.40) [0.26-31.02] (n=17)	2.58 (1.95) [0.27-6.67] (n=14)	No (p = 0.045)
Total Fe, ng/m^3	1204.37 (799.12) [7.19-3409.93] (n=17)	192.90 (129.66) [7.07-475.10] (n=14)	Yes (p < 0.001)
Temperature, °C	7.39 (5.69) [-2.31-17.08] (n=19)	-6.60 (5.82)[-17.92-(-0.35)] (n=25)	Yes (p < 0.001)

The simultaneous measurements of total Cr(VI) and total Cr provide useful information regarding the concentration of total Cr(III). The overall soluble Cr(VI)/total Cr(VI) ratios (Table 4.10) were in the range of 0.18 - 77.75%, with a mean of 9.83%. During fall, the mean soluble Cr(VI)/total Cr(VI) ratio was 9.56 % within the range of 0.40 - 77.75%, while in winter a mean of 5.30% with a range of 0.18-25.48% was calculated. Previous studies in the literature only investigated seasonal trends of soluble Cr(VI) in total Cr concentration collected in PM samples [239,242]. Our study however investigated both the soluble and insoluble Cr(VI) fractions present in ambient total Cr. The overall ratios of total Cr(VI)/total Cr (Table 4.10) had a mean of 34.49% in the range of 0.31-71.01%. The mean total Cr(VI)/total Cr ratio of 34.07 (25.86)% and 34.83 (23.55)% were obtained, respectively, in the fall and winter seasons. The seasonal comparison indicated that the total Cr(VI)/total Cr ratios were not statistically significantly different (p =0.974) for the two seasons.

In summary, seasonal variations were observed for the Cr(VI) concentrations whereas not for Cr(III) and total Cr concentrations. These differences could be due to the dominance of Cr(III) concentration in total Cr compared to Cr(VI)[236,244], which is consistent with our observations for Cr(III) concentrations in this study. Although Cr(III) concentrations were high, slight changes in emission rates from fall to winter may not significantly change its concentration but could change Cr(VI) concentrations. However, since no Cr emission rates were measured in this study, an absolute conclusion cannot be deduced. Additionally, there is a lesser possibility for the ambient conversion of Cr(III) to Cr(VI) in transit due to the lower oxidant concentrations and low ambient temperature (slower rates). The potential sources of Cr(VI) and the impact of trace metals (Pb, Fe, and Mn) are discussed in subsequent sections.
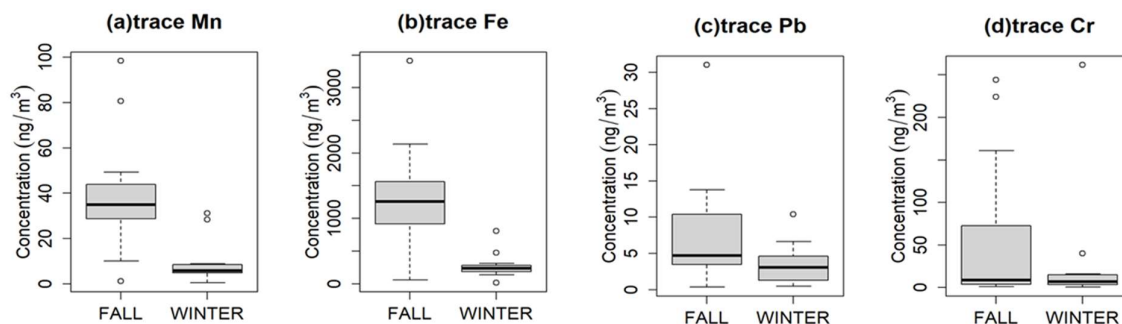
Figure 4.12 Distribution of trace levels of Cr, Mn, Pb, and Fe content in PM_{10} during the sampling period

4.2.6.3   Exploration Of Potential Sources of Cr(VI)

CBPF has gained much attention for source identification of air pollutants since it can show probabilities of high concentrations that are observed at a given location by wind direction/speed and identify the potential directions of local emission sources [230,256]. Figures 4.12(a) to 4.12(c) identified potential sources with SSW-S winds with probabilities of ~25% for total Cr(VI), 12% for soluble Cr(VI), and 16% for insoluble Cr(VI). The source in the S direction appears to be a far distant source that occurred within the speed of 8-10 m/s. The fractional contributions of species per wind direction (Table 4.11) indicated that the highest contributions from total Cr(VI) (44.9%), insoluble Cr(VI) (45.5%), total Cr (36.2%), and total Cr(III) (52.7%) originated from the S. The contribution of S wind on these Cr(VI) species indicates that this source could immensely impact the surrounding air pollution. A distinct difference between

the Cr(VI) species due to S, with Cr(III) in the SE, was identified (Figure 4.13(d)). Cr(III) source in the SE direction spread from 2-4 m/s, indicating local diffusion from vehicular traffics, while the probable distant source(s) could be due to emissions due to the use of diesel-powered locomotives at the railway station (Figure 4.9 and Table 4.8, ID = 5).
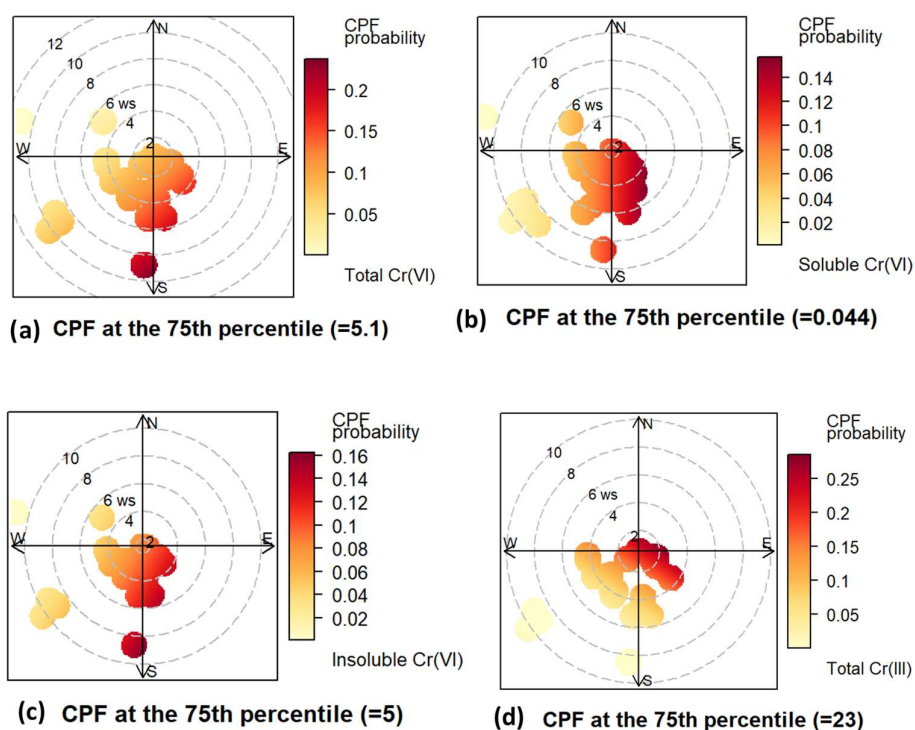
Figure 4.13 CBPF plots highlighting potential source(s) of (a) Total Cr(VI) ng/m^3, (b) Soluble Cr(VI) ng/m^3, (c) Insoluble Cr(VI) ng/m^3, and (d) Total Cr(III) ng/m^3.

Table 4.11 Fractional contributions of chromium oxidation states per wind direction.

Direction	Total Cr(VI)	Soluble Cr(VI)	Insoluble Cr(VI)	Total Cr	Total Cr(III)
North	2.7%	N/A	N/A	22.0%	21.9%
East	28.2%	55.9%	28.9%	16.4%	16.5%
South	44.9%	15.5%	45.5%	36.2%	52.7%
West	24.2%	28.6%	25.6%	25.4%	8.9%

Results also identified local sources at low wind speeds (< 2 m/s), which could be due to diffuse emissions of chromium from the Aktobe urban conurbation, typically

originating from ground-level road traffic and possible domestic heating emissions from coal stoves in winter. This deduction can be attributed to the fact that the wind directions where these sources are dominant correspond to the Aktobe urban area and secondly, the Cr concentrations under low wind speeds are indicative of probable surface emissions.

Potential source contributions were also seen in the SSE and SE wind directions. In the SSE direction at 4-6 m/s wind speed (Figure 4.13(a) to 4.13(c)), total Cr(VI), soluble Cr(VI), and insoluble Cr(VI) had approximately 15% probabilities for each specie emanating from that direction. A possible source in the SSE wind direction is the Aktobe International Airport (Figure 4.9 and Table 4.8, ID = 4) which is at a distance of ~6 km from the sampling station. The work of Abegglen, et al. [257] reported that engine lubrication oil and abrasion from engine-wearing parts in aircraft [258] are the major sources of Cr emission. A source in the SE was seen for soluble Cr(VI) (Figure 4.13(b)) and total Cr(III) (Figure 4.13(d)) with probabilities of 16% and 20%, respectively. Likely source contribution in the SE direction could be emissions originating from the diesel-powered locomotives at the railway station (Figure 4.9 and Table 4.8, ID = 5), which is about 4.4 km away. Very little knowledge is available in the literature on the emissions of railway operations and their consequences on the environment, compared to road traffic.[259] Studies in the literature identified that railway ballast constitutes the main source of Cr in the railway industry [259,260]. Chromium is among the alloying metals that increase the strength and corrosion resistance of steel, which finds its application as steel rails.[259,260] Hence friction processes in passenger trains are known to be another source of Cr emission since it leads to the abrasion of steel rails and wheels when the trains slow down or stop [259,260]. The two industrial Cr facilities (Aktobe Ferroalloy Plant and Aktobe Chromium Compounds Plant, ~700m apart, Figure 4.9) are nearby, and their potential contribution to Cr(VI) concentrations was investigated in this study. However, these Cr facilities would become important sources if the prevailing wind is NW. The wind rose (Figure 4.14) shows that the chance to get NW wind is low since the prevailing wind direction is SW and W during our study period. Fractional contributions (Table 4.11) of the Cr species showed that only soluble Cr(VI) had a contribution of 55.9% from the E direction, while the others had their maximum contributions in the S wind direction; total Cr(VI) with 44.9%, insoluble Cr(VI) with 45.5%, total Cr with 36.2%, and total Cr(III)

with 52.7%. Assuming that the chromium plants contributed significantly to the Cr concentrations, one would have expected significant contributions from the N winds. However, only 2.7% of fractional contributions were obtained for total Cr(VI) in the N wind direction with a single sampler. Notwithstanding, the low sample frequency is also a very low frequency of wind during the entire sampling period. Unfortunately, on this particular day when the wind direction was from the north, we only collected one total Cr(VI) sample and we lost the corresponding soluble Cr(VI) sample due to contamination. In this regard, we could not report on the contributions of soluble Cr(VI) and insoluble Cr (VI) for north winds (Table 4.11).
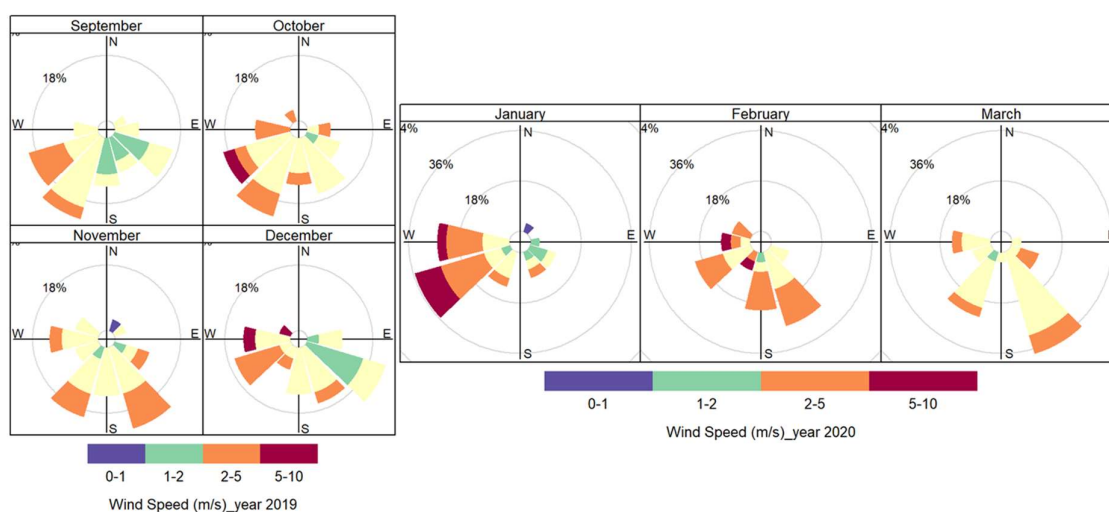
Figure 4.14 The wind rose during the study period

4.2.6.4   Comparison of Cr(VI) Levels in This Study to Other Studies

The concentrations of Cr(VI) were compared to already reported Cr(VI) concentrations in the literature (**Table 4.6**). Soluble Cr(VI) concentrations measured in winter in our study (0.1 ng/m^3) showed significantly higher values compared to the concentrations of 0.019 ng/m^3 as reported by Amouei Torkmahalleh, et al. [62]. The winter soluble Cr(VI) concentrations were again higher than the winter concentrations of 0.02 ng/m^3 and 0.03 ng/m^3 at the MERI and William sites, respectively, as reported by Yu, et al. [234]. In general, **Table 4.6** indicates that the concentrations in this present study were comparable to soluble Cr(VI) concentrations reported in the literature across the world. The total Cr(VI) concentrations in this study are higher than previously reported values in the literature as presented in **Table 4.6**. For example, Huang, et al. [70]

reported total Cr(VI) concentrations in PM$_{10}$ on average as 1.05-1.41 ng/m^3 and 0.99-1.56 ng/m^3, respectively, for winter and summer. The main source of Cr(VI) according to the authors was due to the highway close to their sampling station, whereas in our study the potential sources were the Cr compound and processing plants, railway station, airport, and autoclaved aerated concrete production industries situated in few kilometers to the sampling station.

In this study. the calculated mean total Cr(VI) concentration of 3.73 (2.45) ng/m^3 did not exceed the chronic Inhalation Reference Concentration (RfC) of 8 ng/m^3 as established by USEPA [235] This RfC for upper respiratory effects is based on nasal mucosal irritation, atrophy, and perforation associated with occupational exposures to chromic acid mists and dissolved hexavalent chromium aerosols [235]. It is uncertain whether RfC is based on soluble or total Cr(VI) however if it is based on the soluble Cr(VI), then its calculation must be revisited using the total or insoluble Cr(VI) concentrations. With the knowledge that the toxicity of the insoluble Cr(VI) could be more than soluble Cr(VI), then lower concentrations of RfC would be expected, which would indicate the exact toxic level of the observed average Cr(VI) concentrations in Aktobe. Considerating the individual values for the PM$_{10}$ in this study, the total Cr(VI) concentrations exceeded the RfC on two occasions in the fall with values of 9.44 and 8.31 ng/m^3. Under the Hygienic Norms for Atmospheric Air in Urban and Rural Residential Areas adopted on February 28, 2015, adopted by Kazakhstan[261], the maximum permissible average daily concentration of chromium (in terms of chromium (VI) oxide) in the ambient air is 0.0015 mg/m^3 (1500 ng/m^3), and the approximate safe level of exposure to chromium (III) compounds in ambient air is given as 0.01 mg/m^3. The results of our investigation did not exceed these two permissible levels anyway. However, toxicologists or epidemiologists who quantified the highest Cr(VI) concentration that can influence the health of animals or humans, respectively, possibly made use of only the soluble chromium species since in the past, methods for the quantification of insoluble Cr(VI) were limited. The availability of modern methods to quantify ambient insoluble Cr(VI) now gives an opportunity to revise existing standards and thresholds based on insoluble Cr(VI) species.

4.2.6.5   Potential Source Contributions of Trace Metals (Cr, Pb, Mn, Fe)

Figure 4.15 (a) identifies a source contribution in the NW wind direction for total Cr. The source appears to be a distant source with a wind speed of 4-6 m/s and contrib-

utes approximately 14% probability from this direction. The fractional contribution of total Cr (Table 4.12) indicates that the highest contribution of 36.2% was associated with the S wind direction. The CBPF plots (Figure 4.15(a)-5.14(d)) also recognized local sources at low wind speed (<2 m/s), which could be due to probable diffuse emissions from the Aktobe urban area. Such emissions are generally dominated by ground-level road traffic and domestic heating, especially in winter.

(a) CPF at the 75th percentile (=18)   (b) CPF at the 75th percentile (=33)

(c) CPF at the 75th percentile (=1215)   (d) CPF at the 75th percentile (=5.6)
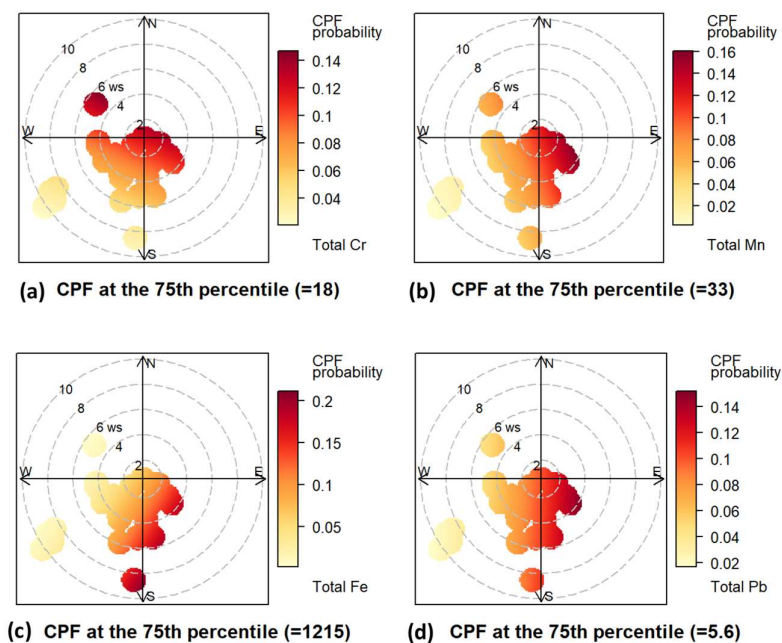
Figure 4.15 CBPF plots showing the potential source(s) of (a) Total Cr, (b) total Mn, (c) total Fe, and (d) total Pb.

Table 4.12 Fractional contributions of trace metal species per wind direction.

Direction	Total Cr	Total Mn	Total Fe	Total Pb
North	22.0%	4.0%	2.0%	3.0%
East	16.4%	34.8%	36.7%	43.0%
South	36.2%	40.0%	40.1%	27.1%
West	25.4%	21.3%	21.2%	26.9%

Figures 4.14(b) to 6.14(d) showed potential sources associated with SSE winds having probabilities of about 10%, 15%, and 12%, respectively, for Mn, Fe, and Pb, at a wind speed of 4-6 m/s. One of the possible sources in the SSE direction is the Ak-

tobe International Airport (Figure 4.9 and Table 4.8, ID = 4), at a distance of ~6 km from the sampling station. A far distant source with a speed of 8-10 m/s in the S wind direction was visible for Fe & Pb with probabilities of about 20% and 12% respectively. The fractional contributions of species per wind direction (Table 4.12) recognized that the highest contributions of Cr; 36.2%, Mn; 40.0%, and Fe; 40.1% came from the S wind direction. Hence, the influence of S winds on trace metals highlights that this source could be an essential contributor to the surrounding air quality in the city. Another source emanating from the SE direction with a speed of 2-5 m/s was obvious for all trace metals: Cr (12%), Mn (16%), Fe (15%), and Pb (15%). One of the likely sources in the SE direction could be due to emissions from the diesel-powered locomotives available at the railway station (Figure 4.9 and Table 4.8, ID = 5); about 4.4 km from the sampling station.

4.2.6.6 Impact of the Selected Trace Metals in PM_{10} on Cr(VI)

Studies conducted by Nico, et al. [110] on simulated atmospheric aging on redox dynamics of mixed metal (Mn, Cr, and Fe) in PM particles, identified that two reaction pathways - reductive and oxidative- normally operate together. The oxidative pathway is usually favored by the presence of Mn, which leads to higher net Cr oxidation.[110] A summary of some selected trace metal and their influence on Cr speciation is illustrated in xxxx. The reduction of Cr(VI) to Cr(III) is however favored by Fe present in the ambient particles via the reactions in Equation 4.5:

$$Cr(VI) + 3Fe(II) \rightarrow Cr(III) + 3Fe(III) \text{ [247]} \quad\quad (4.5)$$
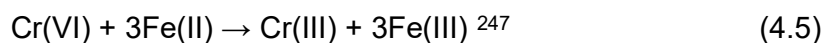
In this study, Fe in the PM_{10} samples had an average concentration of 747.58 ng/m^3 in the range of 7.07-3409.93 ng/m^3. Trace levels of Fe were detected in all the field samples (n = 31). In the fall, the ambient Fe concentration was 1204.37 (799.12) 7.19-3409.93 ng/m^3, while in winter we recorded mean concentrations of 192.90 (129.66) in the range of 7.07-475.10 ng/m^3 in winter (Table 4.10). The Fe value was about 4.9 times statistically significantly (p < 0.001) higher in the fall than in the winter.

Manganese also plays an essential role in ambient Cr chemistry by oxidizing Cr(III) to Cr(VI).[32,83] Lead (Pb) also acts as one of the intermediate elements that lead

to the oxidation of Cr(III) to Cr(VI).[32] Figure 4.12 illustrates the statistical distributions of Mn, Fe, and Pb present in the ambient PM_{10} samples. The Mn was detected in all samples (n=31) with an average concentration of 22.66 ng/m^3 within the range of 0.13- 98.40 ng/m^3. In the fall season (Table 4.10), the ambient Mn concentrations were 36.16 (24.77) [0.13-98.40] (n=17) ng/m^3, while a reduction in winter was found with a mean of 6.26 (6.95) [0.13-28.32] (n=14) ng/m^3. In fall, the concentrations were about 5.8 times statistically significantly higher compared to the winter concentrations (p < 0.001).

The mean concentration of Pb was 5.0 ng/m^3, in the range of 0.26-31.02 ng/m^3. The distribution of trace levels of the ambient Pb in the fall and winter (Table 4.10, Figure 4.12(c)) were 6.99 (7.40) [0.26-31.02] (n=17) ng/m^3, and 2.58 (1.95) [0.27-6.67] (n=14) ng/m^3, respectively. Although the seasonal variation was not statistically significant (p = 0.045), we observed that Pb concentrations were about 2.7 times higher in the fall than in the winter. Hence, the calculated higher concentration of Pb and Mn obtained in the fall could support the observed increase in total and insoluble Cr(VI) in this study since the Pb and Mn in ambient PM usually favor the oxidative pathway, leading to higher net Cr oxidation.[32]
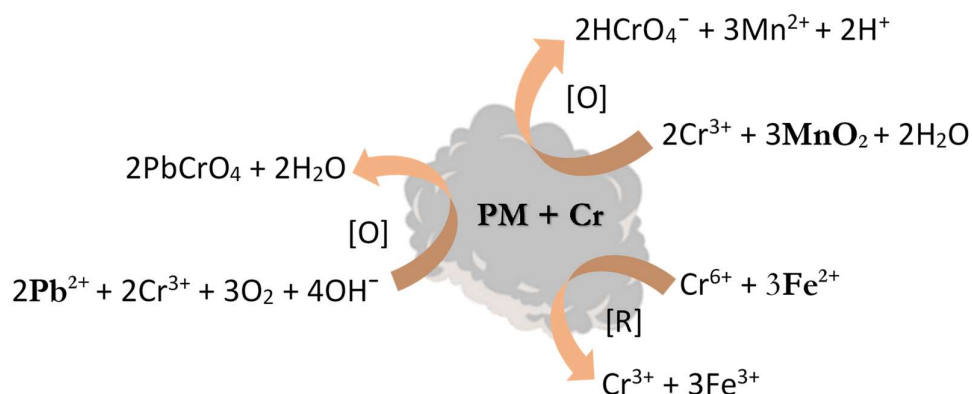
Figure 4.16 Schematic diagram to show metal-induced Cr interconversion.

4.2.6.7 Atmospheric Chemistry Of Cr(VI)

Aqueous reactions and gas-solid reactions are the two main types of reactions that can facilitate the interconversion of Cr in ambient PM. Cr(VI) and Cr(III) interconversion can occur in the solution upon the deliquescence[93] as well as via the gas-solid reactions amid ozone, reactive oxygen species (ROS), and available volatile organic

carbons (VOCs).[112] The measured total Cr concentrations in fall and winter in this study (Figure 4.12(d)) did not show any statistically significant differences, and we identified Cr(III) as the major fraction of Cr. Additionally, this study identified that insoluble Cr(VI) concentrations could be up to an order of magnitude higher than soluble Cr(VI). The modeling studies conducted by our team indicated that the dominant forms of Cr(VI) and Cr(III) in ambient PM are insoluble Cr(VI) and insoluble Cr(III), respectively.[95,96] Hence, reactions such as the gas-solid reactions of the insoluble Cr(III) with ozone and insoluble Cr(VI) with VOCs could be an essential phenomenon to be investigated given atmospheric Cr chemistry.

Table 4.13 The coefficient of determination of insoluble and soluble Cr(VI) with temperature (Temp), Relative Humidity (RH), wind speed (WS), and Wind direction (WD)

Variables	Insoluble Cr(VI)	Soluble Cr(VI)	Temp	RH	WS
Soluble Cr(VI)	0.067				
Temp	0.210	0.010			
RH	0.480	0.0092	0.410		
WS	0.027	0.0038	0.110	0.00007	
WD	0.072	0.0350	0.037	0.0036	0.324

Table 4.14 The coefficient of determination of trace metals (Cr, Mn, Pb, Fe), total and soluble Cr(VI)

Direction	Cr	Mn	Fe	Pb	Insoluble Cr(VI)
Mn	0.0338				
Fe	0.0057	0.9562			
Pb	0.1215	0.4521	0.501		
Insoluble Cr(VI)	0.0035	0.1438	0.1648	0.059	
Soluble Cr(VI)	0.1373	0.1753	0.1383	0.2596	0.0672

The changes in temperature during the study period were also conducted to ascertain any seasonal variability and correlation with Cr(VI). Statistically, significant changes were observed in the ambient temperature during the fall and winter seasons ($p < 0.001$). Initially, a temperature range of -2.31 to 17.08 °C, with a mean of 7.39 °C was obtained during the fall sampling period. Furthermore, lower mean temperatures of -6.60 °C in the range of -17.92 to (-0.35) °C were recorded in the winter season (Table 4.8). The coefficient of determination (r^2) in Table 4.13 showed that insoluble Cr(VI) concentrations in PM_{10} correlated positively with temperature ($r^2 = 0.21$), indicating a faster chemical reaction could occur at relatively higher tempera-

tures in fall to enhance photochemical reactions in the atmosphere and a resultant impact on Cr chemistry.[112]

Table 4.10 shows a statistically significant increase in the average total Cr(VI) and soluble Cr(VI) concentrations in fall compared to winter ($p < 0.001$), respectively. The increased temperature and the concentrations of atmospheric oxidants and reductants such as ozone, ROS, and VOCs in the fall compared to the winter could promote the gas-solid reaction rates. In the gas-solid reactions, a steady state is reached within a few hours via the conversion of Cr(VI) to Cr(III) when VOC is present and the re-conversion of Cr(III) to Cr(VI) by oxidants such as O_3 and ROS.[112] It is worth noting that the overall direction and conversion of these reactions at a steady state could change with the different reactant concentrations and temperature variations, however, no known kinetics information has been developed for such reactions. The results of our study identified that Cr(III) concentrations were higher than Cr(VI) concentrations (Table 4.10). As such, the overall direction of the gas-solid reactions could favor Cr(III) to Cr(VI) conversion leading to the formation of both insoluble and soluble Cr(VI) species. In the fall season with increasing temperature and reactant concentrations (VOCs and oxidants), the steady-state could be reached faster[112] with a resultant increase in the reaction rates in both directions. The increased Cr(VI) concentrations in the fall than in the winter implies the net reaction rate for Cr(III) $\leftrightharpoons$ Cr(VI) (Cr(III)-oxidants minus Cr(VI)-VOCs) could be greater in the fall than in winter. Results in Table 4.10 show that the conversion did not statistically significantly change with respect to Cr(III) concentration, and Cr(III) was found to be the dominant species of Cr in the atmosphere, which is in agreement with other researchers.[236,244]

An alternative pathway for the observed higher concentrations of soluble Cr(VI) in fall than in winter could be due to the higher Mn concentration in fall than in winter (Table 4.10), where the reaction rate of Mn with Cr(III) in the solution occurs. Meanwhile, the concentrations of Fe and Pb increase in the fall than in winter (Table 4.10) which could promote the conversion of Cr(VI) to Cr(III) and Cr(III) to Cr(VI), respectively. The results in Table 4.14 indicated that soluble Cr(VI) correlated positively with Pb ($r^2 = 0.26$), Mn ($r^2 = 0.17$), and Fe ($r^2 = 0.14$). Hence, the higher temperature in fall could enhance the reactions of Cr(VI)-Cr(III) in both directions. With the high

amount of Cr(III) concentration measured in the PM_{10} samples, the overall aqueous reaction direction could be favored by the oxidation of Cr(III).

4.2.6.8   Environmental Factors Influencing Total Cr(VI) Concentrations

In the fall season, a mean relative humidity (RH) was 60.32% within the range of 34.51- 84.87 %, while a higher mean RH of 83.15% in the range of 70.30 - 92.80% was recorded in winter. The RH was about 1.38 times higher in winter than in fall. Results of the coefficient of determination (Table 4.13) show that insoluble Cr(VI) concentrations correlated with changes in RH (r^2 = 0.48) and again with temperature (r^2 = 0.21). The higher RH and lower soluble Cr(VI) concentrations in winter com-pared to fall predicts the influence of deliquescence on the aqueous chemistry of Cr(VI) [93]. At the DRH (76%), Amouei Torkmahalleh, et al. [93] reported that PM ab-sorbs enough amount of H_2O which dissolves soluble compounds like Cr and Fe salts, etc. in a newly formed aqueous layer, followed by oxidation-reduction reactions in the solution matrix.[93] The authors[93] also found a significant conversion of Cr(VI) to Cr(III) (33%) when the RH was ~96%. Their finding was similar to the work of Huang, et al. [111] which reported a reduction of Cr(VI) within the RH 40-70%. Hence intercon-version between Cr(III) and Cr(VI) could occur under higher RH, as recorded in our study, due to the deliquescence.[93]

In summary, the mean total Cr(VI) concentration of 3.73 (2.45) ng/m^3 during this study was below the RfC of 8 ng/m^3, although two daily exceedances were ob-served for individual samples. These exceedances in an urban area such as Aktobe city calls for future monitoring at different locations within the city to fully establish the concentrations of Cr(VI) in ambient PM. Although we considered the importance of gas-solid chemistry of Cr, criteria gases were not measured in this study and thus future studies would be tailored to investigating the influence of gases on ambient Cr chemistry. The concentrations of Cr(VI) were statistically significantly different over the fall and winter seasons. Results showed that total Cr and total Cr(VI) was domi-nated by Cr(III) and insoluble Cr(VI), respectively. Finally, this study suggests that there is a need to upgrade the sampling and analysis of Cr(VI) to fully quantify the total and insoluble Cr(VI). Additionally, the threshold values that were initially estab-lished with the soluble Cr(VI) concentration could be revised based on the insoluble Cr(VI).

4.3   A pilot study to characterize PM$_{10}$ samples collected in Aktobe City

Airborne PM comprises a complex mixture of chemical species from varying sources.[262] PM$_{10}$ particles, having an aerodynamic diameter of less than 10 µm, are classified as inhalable particles with the ability to enter the bronchi of the lungs. Possible origins are from anthropogenic activities including construction activities, combustion, road traffic emissions, and processing industries. The aforementioned sources and natural sources are the major issues affecting major megacities in the world,[263] since they can affect the air quality, ecosystem, and human health.[264] Health consequences such as increased respiratory issues, lung dysfunction, asthma, cough, sore throat, and cardiac arrhythmias have been associated with exposure to airborne PM.[265,266]

Apart from particle characterization being a useful way to assess health effects in populated areas and the impact on regional climate change[267,268], it also helps to identify the shape of particles that can influence their radiative and chemical characteristics. A wide range of techniques are available to measure the size, shape, and elemental compositions of PM[269] and the advancement of technology has further introduced novel techniques such as scanning electron microscopy (SEM) combined with energy dispersive spectrometry (EDS)[270,271] to measure the size and shape of airborne PM. The use of SEM has proven to be an efficient method for characterizing the mixed sources of particles in ambient air.[272,273] Identifying the elemental composition of PM is also helpful to know the origin and potential effects that PM can have on humans. For instance, Xue, et al. [274] conducted work in an industrial area and reported the morphology PM as circular and columnar, signifying the presence of sources such as fuel combustion, biomass burning, and vehicle emissions. The work of Pipal, et al. [275] and Wang, et al. [276] also used SEM-EDS to identify elemental compositions, shapes, and morphology of PM$_{10}$ as well as the potential sources and transport.

There are limited studies on the characterization of ambient PM in Kazakhstan, and no comprehensive study has been reported in Kazakhstan on the use of SEM-EDS for analyses. Aktobe city, an industrial hub of western Kazakhstan, lacks this type of study which otherwise could complement the characterization of aerosols and identify potential source contributions. The very few ambient PM monitoring conducted in Kazakhstan reported that common cancers, such as of the lungs and

esophagus, were associated with air pollution.[212,219,277-279] Typical environmental pollution in Aktobe City was determined as a consequence of emissions of various chemicals into ambient air, which results in dust particles containing varying compounds. The work of Sarsembin, et al. [280] assessed the air pollution in Aktobe city by measuring only a few priority pollutants, however, PM was included in their study. Limited information is available in the literature to fully ascertain the constituents of pollutants ambient PM in Aktobe city.

This pilot study, therefore, aims at the characterization of trace elements, and morphology, and identifying probable sources of these elements in Aktobe city, Kazakhstan, via analytical methods including XRD, FT-IR, FeSEM-EDS, IC, and ICP-MS.

4.3.1 Experimental Details

4.3.1.1 Aerosol sampling

Sampling was conducted at the same station and period as described previously in section 4.2.1

4.3.1.2 Statistical Analyses

The linear coefficient of determination (r^2) was calculated among the water-soluble ions, trace elements, and meteorological variables. The Shapiro-Wilk normality test [228] showed that the data were not normally distributed, and hence the non-parametric two-sample Wilcoxon rank sum test [227,229] was used for comparisons between groups of samples.

4.3.1.3 Cluster Analysis (CA)

CA is a multivariate method used to classify systems of objects or clusters based on their similarities, intending to determine an optimal grouping for clusters that have similar observations and those with dissimilar into another cluster(s). This type of organization of the variables into clusters helps to predict common properties of overall group membership.[281] In this study, CA was performed on the selected elements in the PM_{10} and the results were illustrated as a dendrogram.

4.3.1.4 Ion balance and Acidity

The ion balance and acidity of the PM_{10} samples were calculated by converting the ion mass concentrations ($\mu g/m^3$) into micro equivalents ($\mu mol/m^3$) by:

$$\text{Anion Equivalent} = \frac{NO_3^-}{62} + \frac{Cl^-}{35.5} + \frac{SO_4^{2-}}{96} \times 2 \tag{4.7}$$

$$\text{Cation Equivalent} = \frac{K^+}{39} + \frac{Na^+}{23} + \frac{NH_4^+}{18} + \frac{Mg^{2+}}{24} \times 2 + \frac{Ca^{2+}}{40} \times 2 \tag{4.8}$$

4.3.1.5 Conditional Probability Bivariate Function (CBPF)

CBPF[230] and the Fractional Contributions (%) of elements in the PM_{10} were determined as previously described in section 4.1.7

4.3.2 Results and Discussions

4.3.2.1 Seasonal trend of PM_{10}

The PM_{10} concentrations from the sampling station are shown in Table 4.15 and the statistical distribution is displayed i. The overall mean PM_{10} concentration was 29.7 $\mu g/m^3$ in the range of 0.4-179.6 $\mu g/m^3$. In the fall (September-November) the PM_{10} concentrations had a mean (SD) of 50.2 (38.9) $\mu g/m^3$ in the range of 21.1-179.6 $\mu g/m^3$, while in winter (December-February) it had a mean value of 13.2 (11.9) $\mu g/m^3$ in the range of 0.4-45.6 $\mu g/m^3$. The concentration in the fall was 4 times statistically significantly higher compared to the winter concentrations ($p < 0.05$). There were 5 days (55.0, 64.8, 71.6, 94.4, 179.6 $\mu g/m^3$) when the average daily concentration of PM_{10} exceeded the average daily WHO standards for PM_{10} (50 $\mu g/m^3$). Concerning the average daily maximum allowable PM_{10} concentration (MAC) standard of 60 $\mu g/m^3$ established in Kazakhstan [221,261], four samples exceeded that limit (64.8, 71.6, 94.4, 179.6 $\mu g/m^3$). Even though only a few studies on the seasonal trends of PM_{10} exist in Kazakhstan, those available in the literature reported mainly the annual mean of cities in Kazakhstan such as Astana city with an average annual PM_{10} in 2014 as 20 $\mu g/m^3$ and in 2016 as 100 $\mu g/m^3$ [282]. In another study [283], the authors reported the annual mean concentration (2008-2010) of estimated-PM_{10} for some major cities; Almaty (142.3 mg/m^3), Astana (264.6 mg/m^3), Shymkent (101.65 mg/m^3), Zhezkazgan (172.75 mg/m^3), Taraz (66.8 mg/m^3), Pavlodar (70.95 mg/m^3), Ust-Kamenogorsk (80.4 mg/m^3), Semey (76.3 mg/m^3), Atyrau (216.35 mg/m^3), Temirtau (108.65 mg/m^3), and Aktau (118.75 mg/m^3).[283] During the study period, according to

the authors[283], no nationwide PM_{10} or $PM_{2.5}$ measurements were available in Ka-zakhstan, as such monitoring and reporting on the PM were only based on TSP. As such these reported annual average concentrations were based on the conversion of TSP concentrations to PM_{10} with a coefficient of 0.5 [283], which could over-/underestimate the actual concentrations of PM_{10}. This gap could be filled by using the gravimetric method of analyses, as used in our study, to directly measure the ambient PM_{10} concentrations which will yield fewer probable biases in the dataset.
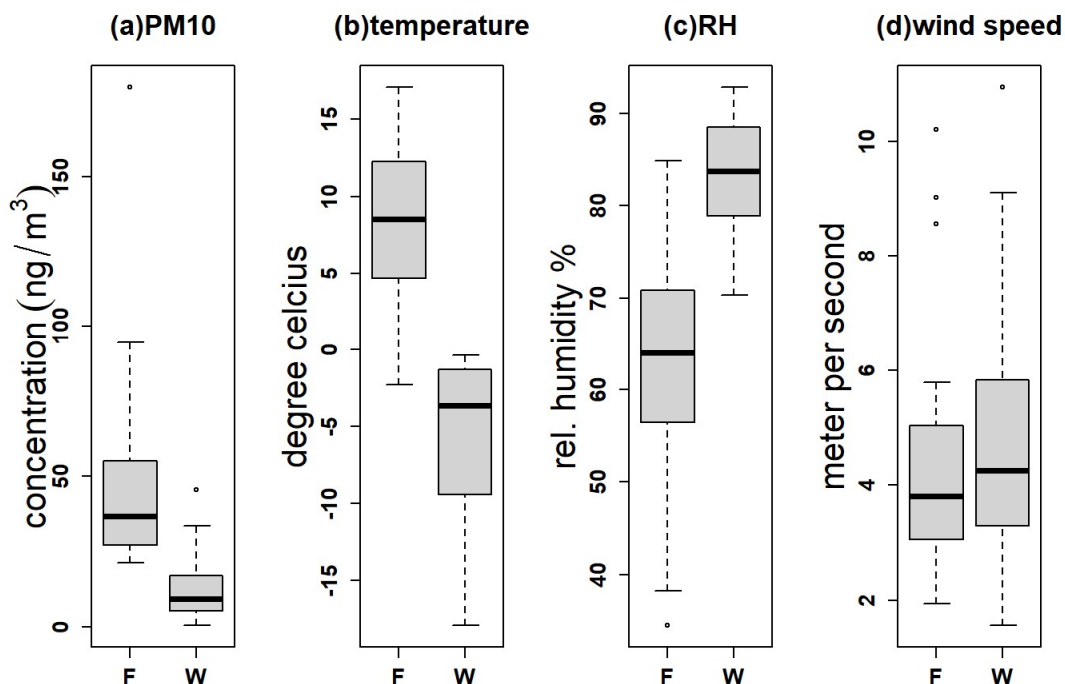
Figure 4.17 Seasonal distribution of daily PM_{10} concentration, temperature, wind speed, and relative humidity (RH) over the sampling period

Probable reasons for the lower concentrations of PM_{10} in the winter than in fall could be because of the increased precipitation and snow scavenging, as well as reduced dust resuspension. Aktobe city is familiar with its extreme meteorological parameters (Table 4.15) such as high wind speed (mean of 5 m/s and a maximum of 10.9 m/s) in the winter season. These meteorological parameters could strongly influence the samples collected in winter, which could increase the rate of removal of ambient PM via the scavenging effect. The relatively high wind speed observed in our study, however, is in contrast to earlier studies where researchers reported high PM_{10} con-centration in winter due to possible increased anthropogenic activities including bio-mass and fossil fuel burning, and meteorological conditions such as low wind speed,

low planetary boundary layer, and high relative humidity.[284] At high wind speeds in Aktobe, the effect of local sources and metrological conditions might be insignificant in seasonal variations of the PM_{10}.

Table 4.15 Concentrations of PM_{10} (µg/m³), soluble ions (µg/m³) in the samples and meteorological conditions

Parameters		Overall (N=38)	Fall (N=17)	Winter (N=21)	Significant?
PM_{10}, µg/m³		29.7(32.8) [0.4-179.6] (n=38)	50.2(38.9) [21.1-179.6] (n=17)	13.2(11.9) [0.4-45.6] (n=21)	Yes $p < 0.05$
Temperature, °C		0.2(9.0) [-17.9-17.1] (n=38)	7.8(5.6) [-2.3-17.1] (n=17)	-6.0(5.9) [-18-(-0.4)] (n=21)	Yes $p < 0.05$
Relative Humidity, %		73.6(14.9) [34.5-92.8] (n=38)	62.0(14.3) [34.5-84.9] (n=17)	82.9(6.6) [70.3-92.8] (n=21)	Yes $p < 0.05$
Wind Speed, m/s		4.7(2.5) [1.6-10.9] (n=38)	4.5(2.5) [1.9-10.2] (n=17)	4.9(2.6) [1.6-10.9] (n=21)	Yes $p < 0.05$
Cation µg/m³	Na^+	0.22(0.37) [0-1.63] (n=37)	0.21(0.30) [0.04-1.30] (n=17)	0.24(0.45) [0-1.63] (n=20)	No $p = 0.23$
	Ca^{2+}	1.72 (1.53) [0.02-5.93] (n=37)	2.94(1.26) [0.82-5.93] (n=17)	0.68(0.78) [0.02-3.15] (n=20)	Yes $p < 0.0001$
	NH_4^+	0.54(0.53) [0.01-1.98] (n=37)	0.55(0.45) [0.10-1.80] (n=17)	0.53(0.60) [0-1.98] (n=20)	No $p = 0.33$
	K^+	0.11(0.11) [0-0.52] (n=37)	0.18(0.13) [0.04-0.52] (n=17)	0.05(0.04) [0-0.16] (n=20)	Yes $p < 0.001$
	Mg^{2+}	0.11(0.16) [0-0.92] (n=37)	0.20(0.21) 0.04-0.92] (n=17)	0.04(0.05) [0-0.19] (n=20)	Yes $p < 0.001$
Anion µg/m³	Cl^-	0.21(0.23) [0-0.92] (n=37)	0.26(0.27) [0.04-0.92] (n=17)	0.15(0.18) [0-0.73] (n=20)	No $p = 0.11$
	NO_3^-	0.95(0.90) [0-3.18] (n=37)	0.94(0.65) [0.22-2.38] (n=17)	0.96(1.08) [0-3.18] (n=20)	No $p = 0.46$
	SO_4^{2-}	1.74(1.89) [0-10.41] (n=37)	2.32(2.26) [0.63-10.41] (n=17)	1.25(1.38) [0-3.18] (n=20)	Yes $p < 0.05$

.

4.3.2.2 Water soluble ions

Analyses of the ion chromatography identified that cations (Na^+, Ca^{2+}, NH_4^+, K^+, Mg^{2+}) and anions (Cl^-, NO_3^-, and SO_4^{2-}) were present in the PM samples (Table 4.15, Figure 4.18). Results of the soluble water cations showed that the average concentrations of Na^+ (p =0.23) and NH_4^+ (p =0.33) were not statistically significantly different in the fall and winter seasons. However, the mean concentrations of Ca^{2+} (p < 0.0001), K^+ (p < 0.001), and Mg^{2+} (p < 0.001) were statistically significantly higher in fall than in winter. For the anions, the mean concentrations of Cl^- (p =0.11) and NO_3^- (p =0.46) did not statistically significantly change when over the two seasons. The mean concentration of SO_4^{2-} ions was however statistically significantly higher in fall compared to winter (p < 0.05). Furthermore, SO_4^{2-} was identified as the most abundant water-soluble ion present in the PM with an overall mean concentration of 1.74 $\mu g/m^3$. The mean concentrations of the remaining water-soluble ions are in the order of Ca^{2+} > NO_3^- > NH_4^+ > Na^+ > Cl^- > Mg^{2+} > K^+ (Table 4.15). The seasonal trend of the water-soluble ions can be influenced by local and regional changes in seasons and meteorological factors that would influence their formation, transportation, and transformation.[285] Typically, sulfate concentrations are higher in winter, however, this study found lower concentrations in winter compared to fall. In Aktobe city, the relatively high wind speed recorded in winter as compared to fall possibly aided good dispersion of the particles in the winter season.[285] The seasonal trend of NO_3^- revealed a slightly higher concentration in winter compared to fall although the change was statistically insignificant. The RH and temperature are the major parameters that could affect the thermodynamic features of nitrate, wherein the high temperature and low RH lead to nitrate volatilization.[285] Hence the low temperature and high RH recorded in winter rather enhanced nitrate stabilization and its subsequent loadings of PM_{10} provided a suitable surface area for the heterogeneous formation of nitrate.
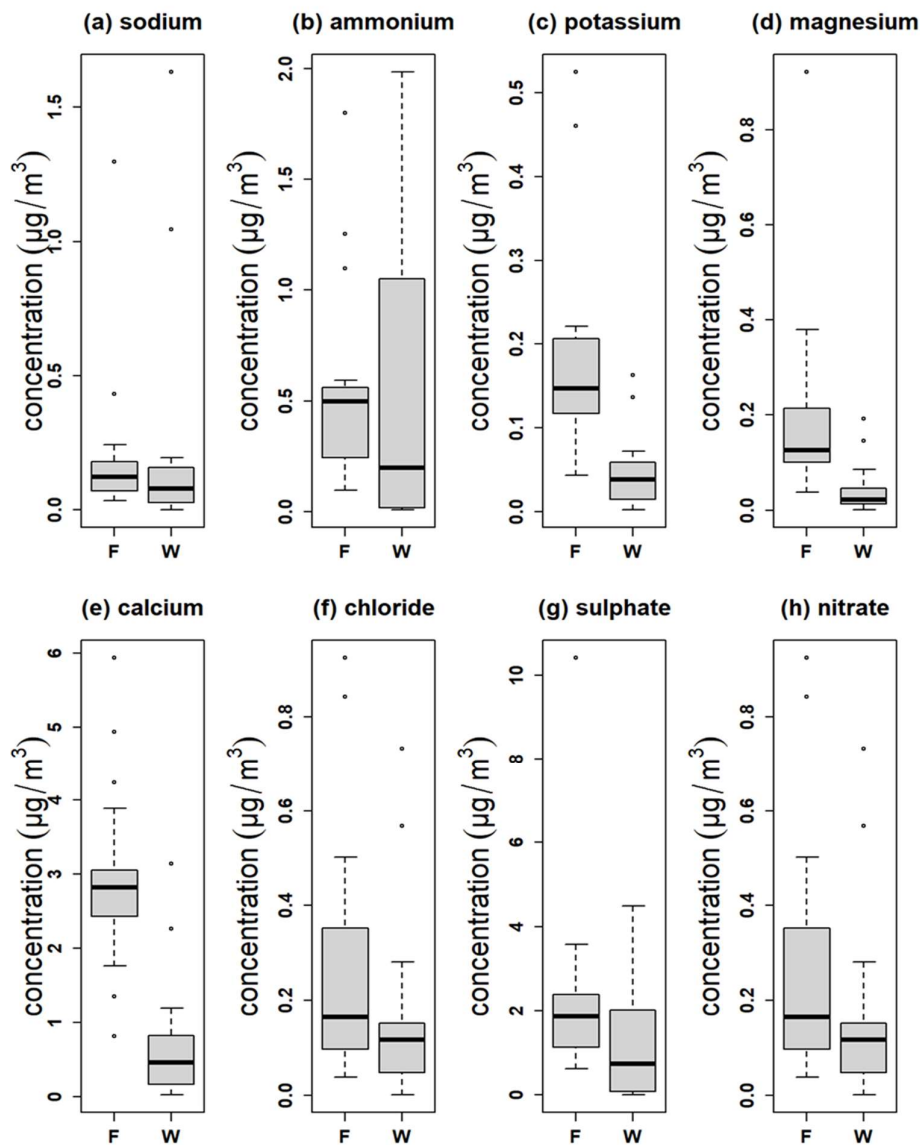
Figure 4.18 Seasonal distribution of water-soluble ions in the PM_{10} samples

4.3.2.3 Stoichiometric analyses of ions and the chemical forms of sulfate and nitrates

Figure 4.19(a) shows the scatter plots of anion equivalent (AE) versus cation equivalent (CE), and the weak correlations (all points not falling on the 1:1 line) between the AE and CE indicate that although we measure 8 ions in the PM sample, other ionic components could be present as well. Again in Figure 4.19(a), most of the fall samples were above the 1:1 line (AE/CE) which suggests the acidic nature of the samples collected in the fall. The acidic nature was probably due to the enhanced for-

mation of sulfate and a subsequent loss of cations from the volatilization of nitrate and ammonium in the fall season.[285] As exemplified in the linear regression analyses (Table 4.16), SO_4^{2-} ions show strong correlations with other ionic species in fall (r^2 of 0.91, 0.69, 0.67, and 0.83, respectively for Na^+, NH_4^+, K^+, and Mg^{2+}). Except for one point, all winter samples in Figure 4.19(a) were below the 1:1(AE/CE) line indicating a deficiency of anions, which is typical of dust particles with alkaline forms [285]. Species such as CO_3^{2-} and HCO_3^- are the main contributors to anion deficiency; however, these species were not measured in this study.

The scatter plots of NH_4^+ versus SO_4^{2-}, $SO_4^{2-} + NO_3^-$, and $SO_4^{2-} + NO_3^- + Cl^-$ that represent electron equivalent concentrations are displayed in Figures 4.17(b)-5.17(d). Since the salt of $(NH_4)_2SO_4$ is less volatile and easily formed compared to NH_4NO_3 and NH_4Cl, we explored the association between NH_4^+ and SO_4^2 to identify the chemical forms of nitrates and sulfates (Figure 4.19b). Figure 4.19(b) shows that in winter, NH_4^+ was associated with SO_4^{2-}, since most data points fell above the 1:1 (NH_4^+/SO_4^{2-}) line, indicating a nearly complete neutralization of SO_4^{2-} by NH_4^+, and so $(NH_4)_2SO_4$ might be the major specie available in winter. More data points in the fall samples (Figure 4.17(b)) were however below the 1:1 (NH_4^+/SO_4^{2-}) line. The higher temperature in fall than in winter usually enhances the formation of the secondary ion SO_4^{2-} while NH_4^+ is easily removed by decomposition.[285] Hence there were insufficient NH_4^+ ions in the fall to fully neutralize SO_4^{2-}, so other species such as NH_4HSO_4 could also be present.[285] In terms of available nitrates in the PM, the majority of the winter samples (Figure 4.17c) contained enough NH_4^+ to neutralize both SO_4^{2-} and NO_3^- (data falls on or above the 1:1 line) and possible salts that may be present would be $(NH_4)_2SO_4$ and NH_4NO_3. Except for one data point of the fall samples, Figure 4.19(c) all others were below the 1:1 line indicating that there were an insufficient amount of NH_4^+ ions to fully neutralize SO_4^{2-} and NO_3^-. Figure 4.19(d) suggests the abundance of NH_4^+, mostly in winter, which neutralized the SO_4^{2-}, NO_3^-, and Cl^- ions. This further suggests that dominant species including $(NH_4)_2SO_4$, NH_4NO_3, and NH_4Cl could be present in the winter season. The relatively high NO_3^- concentrations reported in this study (Table 4.15) with moderate levels of NH_4^+, similar to previous studies[285], suggest that the rate of nitrate formation was probably higher than other available ions.
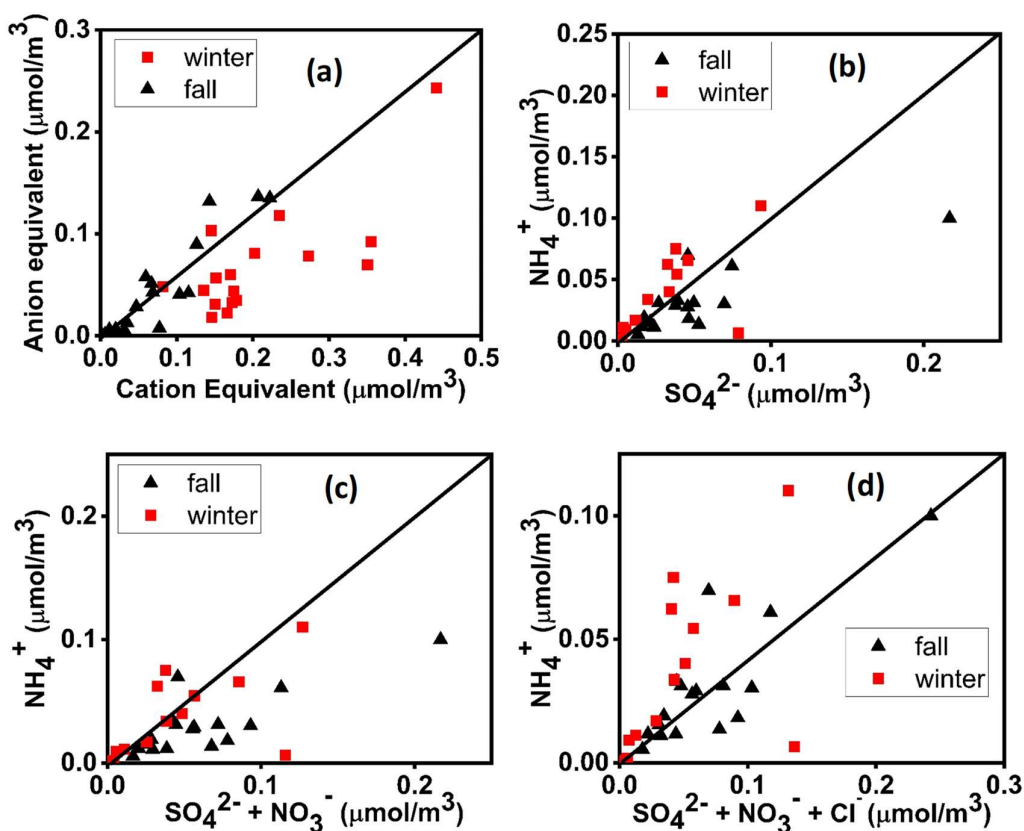
Figure 4.19 Scatter plots of (a) total cation vs. total anions, (b)-(d) ammonium, and the major acidic anions in PM_{10}

The possible chemical forms of nitrate were investigated by calculating the coefficient of determination (r^2) between NO_3^- and other cations (Table 4.16). In fall (Table 2) NO_3^- showed a moderate correlation with NH_4^+ ($r^2 = 0.44$), and a weak correlation with the remaining cations, suggesting that NH_4NO_3 is probably the dominant specie of nitrate available in fall. The higher NO_3^- concentrations in winter (Table 4.15) showed strong correlations with most cations, except Na^+ ($r^2 = 0.38$) implying that salts including NH_4NO_3, KNO_3, $Mg(NO_3)_2$, and $Ca(NO_3)_2$ accounted for the larger chemical species in the PM_{10} in winter. This study noticed a high correlation between the concentrations of Na^+ and Cl^- winter. Winter periods in Aktobe are generally filled with thick layers of snow, as a popular practice salt/salt brine is spread on the road to melt down the thick snow. As such after the road salt aerosolizes, more Na gets injected into the PM in the atmosphere.[286] This phenomenon can increase the amount of Na and Cl ions present in the winter compared to fall.[286] This is noticeable in the observed high correlation coefficient for Na^+ with Cl^- ($r^2 = 0.99$), and for Cl^- with K^+ (r^2

= 0.89), Mg^{2+} (r^2 = 0.73), and Ca^{2+} (r^2 = 0.77) in winter compared to their respective correlation in fall.

Table 4.16 Linear coefficient of determination (r^2) between cations and anions in fall and winter.

	SO_4^{2-}	NO_3^-	Cl^-	Na^+	NH_4^+	K^+	Mg^{2+}
FALL							
NO_3^-	0.57						
Cl^-	0.50	0.42					
Na^+	0.91	0.11	0.55				
NH_4^+	0.69	0.44	0.54	0.55			
K^+	0.67	0.14	0.37	0.74	0.34		
Mg^{2+}	0.83	0.24	0.66	0.83	0.46	0.51	
Ca^{2+}	0.06	0.11	0.42	0.09	0.05	0.10	0.15
WINTER							
NO_3^-	0.78						
Cl^-	0.45	0.45					
Na^+	0.60	0.38	0.94				
NH_4^+	0.58	0.59	0.01	0.01			
K^+	0.65	0.67	0.86	0.84	0.11		
Mg^{2+}	0.41	0.49	0.73	0.70	0.01	0.65	
Ca^{2+}	0.38	0.55	0.72	0.67	0.02	0.64	0.96

4.3.2.4 Spectral analyses with FTIR and XRD

The FTIR spectra identified many defined peaks as well as others with no well-defined forms due to the overlap since other molecules can absorb IR radiation within the same range.[287] Figure 4.20(a) thus reveals that PM_{10} samples contained some inorganic components. Due to vibrational frequencies, the functional groups in the PM sample were identified as SO_4^{2-} (601, 671 cm^{-1}), NO_3^- (835 cm^{-1}), SiO_4^{4-} (777, 794 and 1027 cm^{-1}), CO_3^{2-} (712, 874 cm^{-1}), NH_4^+ (1408 cm^{-1}), carbonyl group, C=O (1636 cm^{-1}), aliphatic carbon, C-H (2920, 2849, 2957 cm^{-1}) and alcohols, -OH, (3406, 3537 cm^{-1}).[287,288] The presence of the absorption frequencies in the range of 3241–3406 cm^{-1} was attributed to O-H stretching, due to the presence of crystalline water in gypsum. Coarse particulate matter is known to contain more $CaSO_4.2H_2O$ due to the sulfation process evident in urban environments.[287] Montana, et al. [289] indicated

that the majority of the sulfur emanated from fossil fuel combustion. Thus, the SO_4^{2-} content found in the PM_{10} can be associated with probable industrial activities in Aktobe city, including fossil fuel combustion. The absorption peak at 712, and 874 cm^{-1} are typical of CO_3^{2-} functional groups were present, and the FTIR analysis of pure crystalline calcite and dolomite[290] identified that such peaks were related to $CaCO_3$. This suggests the presence of calcite and dolomite in the PM samples. Halites, also known as rock salts, occur in the range of 1000-1200 cm^{-1} and 1620 cm^{-1}, and the peaks present at 1003, 1027, and 1617 cm^{-1} suggest the presence of halites in the PM_{10} samples.
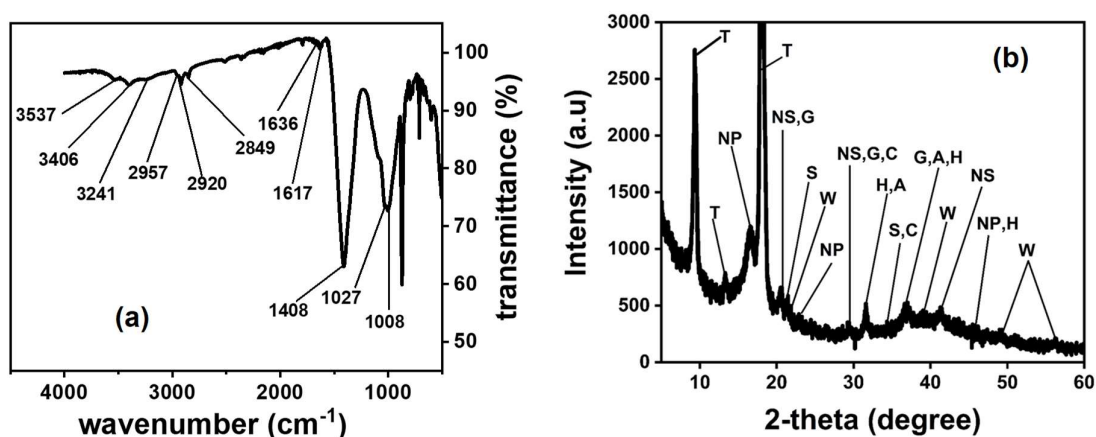
Figure 4.20 (a) FT-IR and (b) XRD pattern of PM10 sample with different mineral contents; Teflon filter (T), NH_4HPO_4 (NP), $(NH_4)_2SO_4$ (NS), Gypsum (G), Silica (S), Calcite (C), Halite (H), Alumina (A), $CaSiO_3.H_2O$ (W).

XRD mineralogy investigated the mineral contents of the PM_{10} sample (Figure 4.18(b)). Well-defined peaks were visible to indicate that silica, calcite, and gypsum among other mineral phases were available in the samples. The result from the XRD thus confirms the earlier FTIR spectra that suggested the presence of clay and quartz mineral as the dominant phase of the mineral. This is exemplified by the fact that soil gets suspended in the air by the action of wind.

4.3.2.5   SEM/EDS Analyses

The micrographs (**Figure 4.21**) show that the particles had irregular, smooth rounded, porous, columnar, and chain-branched structures, which is indicative of various types of particles such as tar balls, soot, biological particles, etc. These structures in

the PM samples are similar to detected SEM images in the literature.[274,284,291-293] The presence of tar balls in the PM samples, having spherical and amorphous structures, did not form aggregates with other particles. Typically, sources including. The impact of tar balls includes the scattering and absorption of light which contributes to radiative forcing and the formation of regional haze.[284,291] Porous particles, known to emanate from agricultural/forest burning and waste incineration, were also identified in the PM samples. Panda and Nagendra [293] indicated that porous particles contain significant amounts of carbon and thus facilitate the deposition of other guest particles to form complex structures. The presence of biological particles in the PM is linked to fragments of leaves, algae, bacteria, protozoa, pollens, and excrements of insects collected from the atmosphere.[294] Irregular particles found in the PM samples are known to come from varying sources such as quartz, alumino-silicate, iron, chloride, and calcium-rich particles.[284] The chain/branched particles are linked to soot particles with unique structures from linear to complex branched aggregates of particles. The soot particles in the SEM micrograph appear as a small aggregate of spherulites with chain-like structures, which can be associated with diesel exhaust sources.[295] Coal-burning industries and power stations that utilize very high-temperature processes are also sources that generate soot particles.[292] These sources, therefore, suggest the complex sources that could impact the air quality of the city under study.

The micrograph of EDS (Appendix Figure 1) identified particles to be rich in Ca, K, Al, Fe, Na, Mg, and Si which are constituents of soil and mineralogical sources that are associated with mining activities.[295,296] The Fe-rich particles in the PM samples are indicative of nearby vehicular traffic as a potential source of emission.[295] Additionally, Cr elements were identified in the samples with different compositions. Aktobe region is the industrial hub for many chemical, metallurgical, oil, and gas processing plants, among which are lots of enterprises that are involved in the mining and processing of chromium ore. Probable anthropogenic emissions from these facilities could be some of the sources linked to the presence of Cr in the PM. The substantial amount of sulfur that was detected in all samples tested with EDS can be traced to sources including fossil fuel burning, and the wear and tear of rubber tires. Briefly, the FESEM and EDS results on the PM_{10} particles can be grouped into anthropogenic (soot) and natural (soil, minerals) sources.
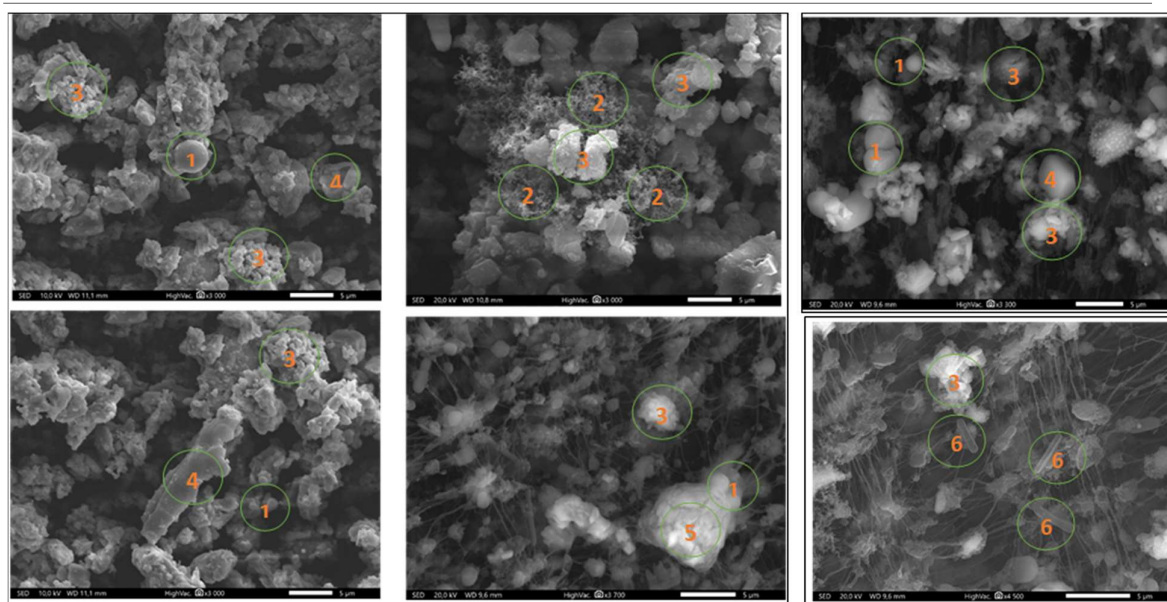
Figure 4.21 Morphological results of PM10 particles; (1) Circular particles, (2) Soot particles, (3) Chain and branched particles, (4) Irregular particles, (5) Porous particles, (6) Biological particles

4.3.2.6   Trace elements analyses

Some selected inorganic elements were determined in the PM_{10} samples using ICP-MS (Table 4.17). Generally, elements found in the earth's crust include Al, Si, P, K, Ca, Mn, and Fe, while anthropogenic activities contribute to so-called "pollution elements" such as Ni, S, Cu, and Pb.[274] Studies indicated that trace levels of elements can help identify possible pollution sources, for example, windblown re-suspended dust is known to contribute to Al, Ca, Ti, and Si in PM. Industrial activities are known to contribute to Cr, Mn, and Cu emissions, and S emanating mainly from fossil fuel combustion and rubber tire wear and tear. Zinc is mostly available from soil dust, garbage waste, and motor vehicular emissions, while K is released from biomass burning. Lead (Pb) is linked to industrial emissions and motor vehicles that use leaded gasoline.[274,297,298] Since significant pollution elements from industrial productions such as Cr, Cu, Pb, and Ni were detected in the samples, there is an indication that industrial emissions are contributory sources of PM_{10} in Aktobe city.

Table 4.17 Selected elemental composition of PM_{10} samples (ng/m^3) using ICP-MS

Elements	Fall (N=17)	Winter (N=21)	Statistical Significant
B	3.78(2.80)[0.003-8.88]	0.60(1.01)[0.003-3.05]	(p<0.01)
Na	118.37(234.60)[0.496-874.71]	77.25(107.44)[0.49-326.71]	(p=0.38)
Mg	741.46(734.27) [2.03-3131.65]	185.24(255.29)[0.59-1029.02]	(p<0.01)
Al	1166.87(756.86)[3.60-3181.39]	207.61(348.70)[4.22-1393.24]	(p<0.001)
P	59.66(43.17)[11.52-173.35]	11.92(2.50)[10.36-20.54]	(p<0.001)
K	472.72(277.07)[5.72-1007.56]	89.14(72.69)[1.01-292.52]	(p<0.001)
Ca	380.39(276.72)[2.66-1061.25]	92.36(102.82)[3.81-403.86]	(p<0.01)
Ti	23.06(15.15)[0.56-53.57]	6.96(8.21)[0.29-30.95]	(p<0.01)
V	3.60(2.34)[0.24-9.50]	0.62(0.34)[0.22-1.41]	(p<0.001)
Cr	99.97(248.90)[0.77-1018.43]	26.27(68.55)[0.60-261.60]	(p=0.35)
Mn	37.91(25.41)[0.28-98.40]	6.28(6.93)[0.26-28.32]	(p<0.001)
Fe	1287.93(827.06)[15.22-3409.93]	193.92(128.10)[14.13-475.10]	(p<0.001)
Co	0.59(0.44)[0.05-1.58]	0.10(0.10)[0.02-0.43]	(p<0.001)
Ni	5.20(4.80)[0.11-19.69]	1.65(1.68)[0.10-4.97]	(p<0.01)
Cu	9.10(9.79)[0.04-36.48]	2.28(1.68)[0.22-5.70]	(p<0.01)
Zn	40.44(67.38)[4.71-295.70]	19.67(35.66)[2.04-141.62]	(p<0.01)
As	12.05(36.88)[0.08-154.93]	1.40(1.78)[0.08-5.034]	(p<0.05)
Cd	0.74(2.21)[0.05-9.29]	0.07(0.05)[0.01-0.15]	(p<0.001)
Sn	0.56(1.19)[0.013-4.65]	0.10(0.18)[0.01-0.71]	(p<0.05)
Ba	29.07(20.11)[0.21-87.20]	5.08(2.65)[0.20-8.91]	(p<0.001)
Pb	19.85(50.81)[0.35-214.96]	2.62(1.90)[0.45-6.67]	(p<0.05)

The seasonal variations of the trace elements presented in Table 4.17 showed statistically significant differences in their concentrations over the two sampling seasons except for Na (p=0.38) and Cr (p=0.35). Fe exhibited the highest average concentrations of 1287.93 ng/m^3 with a standard deviation of 287.06 ng/m^3 in the range of 15.22-3409.93 ng/m^3 in the fall. The ten-highest concentrations in fall are in the order of Fe>Al>Mg>K>Ca>Na>Cr>P>Zn>Mn. In winter, Al had the highest average concentration of 207.61 ng/m^3 in the range of 4.22-1393.24 ng/m^3. The ten-highest average concentrations of elements in winter were in the order of Al>Fe>Mg>Ca>K>Na>Cr>Zn>P>Ti.

This study also calculated the fractional distribution of elements in each daily PM and tabulated it in **Appendix Table 2**. Three trends were visible in the distribution of elements in the daily PM samples. First, the average fractional percentages of Co and Cd in winter did not show any difference in values when compared to fall, and both elements were statistically insignificant over the seasons. The reason could be

that the elements were from the same emission source that did not change over the two seasons. Second, the fractional percentages for Al, K, Mn, Fe, and Pb were 1.16, 1.11, 1.27, 1.22, and 1.05 times, respectively, higher in fall compared to winter. However, only Al (p=0.05) and Pb (p<0.05) showed statistically significant higher percentage contributions in fall than in winter. This category shows the probable impact of re-suspended dust/industrial activities (Al, Fe, Mn), vehicular emissions (Fe, Pb), and biomass burning (K) on the fate of PM samples collected in the fall season. Third, the remaining elements B, Na, Mg, Ca, Ti, V, Cr, Ni, Cu, Zn, As, Sn, and Ba had lower percentages of composition in fall when compared to winter, but only fractional values of Na ($p<0.05$) and Zn ($p< 0.01$) were statistically significantly lower in fall than in winter. This trend shows the consequences of potential vehicular traffic emissions and industrial activities on collected PM samples, especially in winter. During the extreme winter seasons in Aktobe, salt/salt brine application on the road is a conventional practice. Thus, we would expect the road salt to be aerosolized, and more Na to be injected into the PM in the atmosphere.[286] This tends to increase the amount of Na and Cl available in the winter compared to fall,[286] a similar trend observed in our study. More in-depth potential source contributions for each element are discussed in the next sections.

4.3.2.7   Cluster analysis (CA)

CA for the fall showed a dendrogram (Figure 4.22a), grouping the variables into four different clusters: (cluster 1) Fe, Al; (cluster 2) Mg, K, Ca; (cluster 3) P, Cd, Co, Sn, B, Cu, V, Ni, Mn, Ti, Ba, Zn, As, Pb, Na, Cr, Temperature, WS; and (cluster 4) PM_{10}, WD, and RH. The various clusters show that some variables behave differently in different seasons. Fe and Al show the same behavior in both fall and winter by being in same the cluster, which signifies that their sources are different from the remaining trace elements. These two elements are known to predominantly originate from crustal emissions.[299] The group Ca–K appears in similar groups in both fall and winter, and is known to originate from re-suspended dust, and K could also be due to biomass burning.[300] The aforementioned cluster 3 contains the remaining trace elements (except Na) in both fall and winter, which are typically emitted from anthropogenic sources, underlining the importance of industrial or vehicular emissions.[299,300] During winter (Figure 4.22b) however, Na is grouped with Ca-K-RH. Cluster 4 com-

prises PM₁₀-RH-WD in the fall, which could be interpreted as due to predominant geographical sources in Aktobe city on ambient PM. This phenomenon is however different in the winter when WD existed alone as a group (Figure 4.22b).
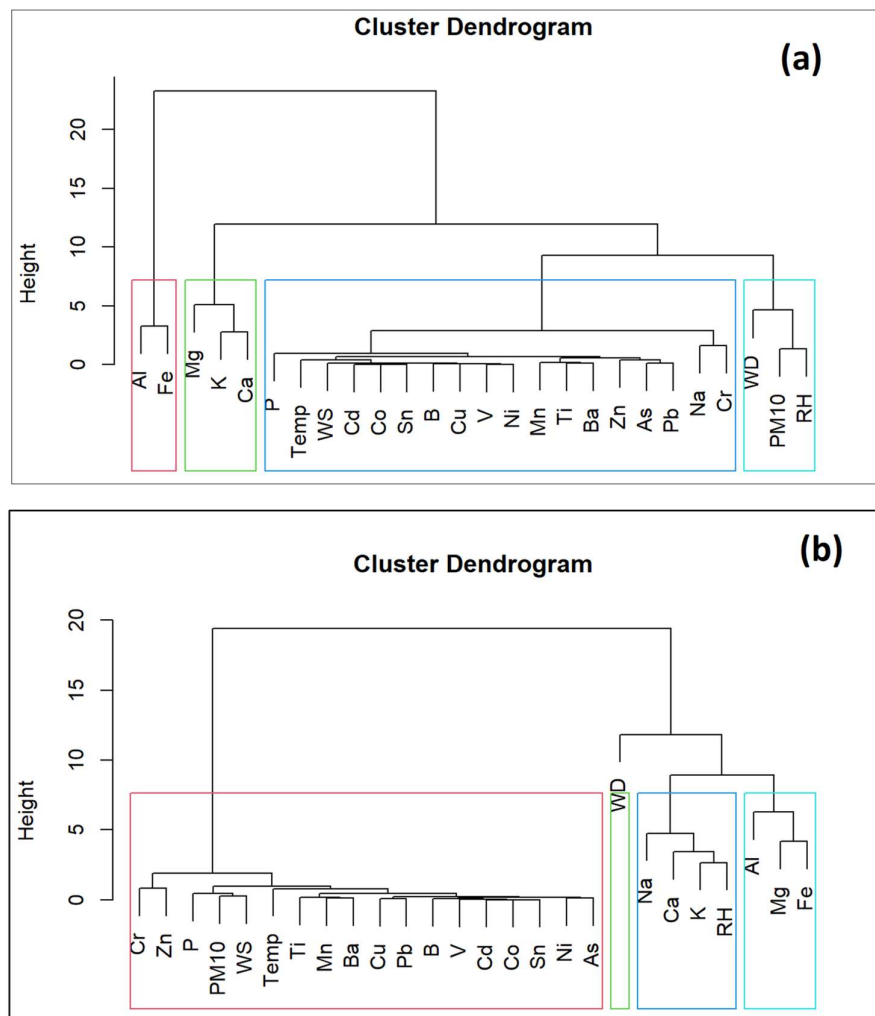
Figure 4.22 Dendrogram from the cluster analysis of the elements in PM₁₀ and meteorological factors in (a) fall and (b) winter seasons.

4.3.2.8   Potential sources contribution of selected metals

The CBPF plots for PM₁₀ (Figure 4.23) show that the main source contribution is located in the SE direction with a 6 m/s wind speed. The probability of producing PM₁₀ more than 45 µg/m³ (75 percentile) when the wind direction was SE at 6 m/s was approximately 50% indicating the significant contribution of this source in producing PM₁₀. The fractional contribution (Appendix Table 2) shows 43.54% of this source

influencing the concentration of PM_{10} in the SE-S direction. Potential sources in this direction are the railway station and the airport, which are about 4.4 km and 6 km, respectively, away from the sampling station. The CBPF plots further identified source(s) in the E-SE direction when the wind speed is approximately 5-6 m/s (Appendix Figure 2) for many metals. Apart from K and Ni, which had 15% and 30% probabilities respectively, the remaining metals (P, Ti, V, Mn, Fe, Co, Cu, and Ba) predicted about 20% probability of emission for each in the E-SE direction.
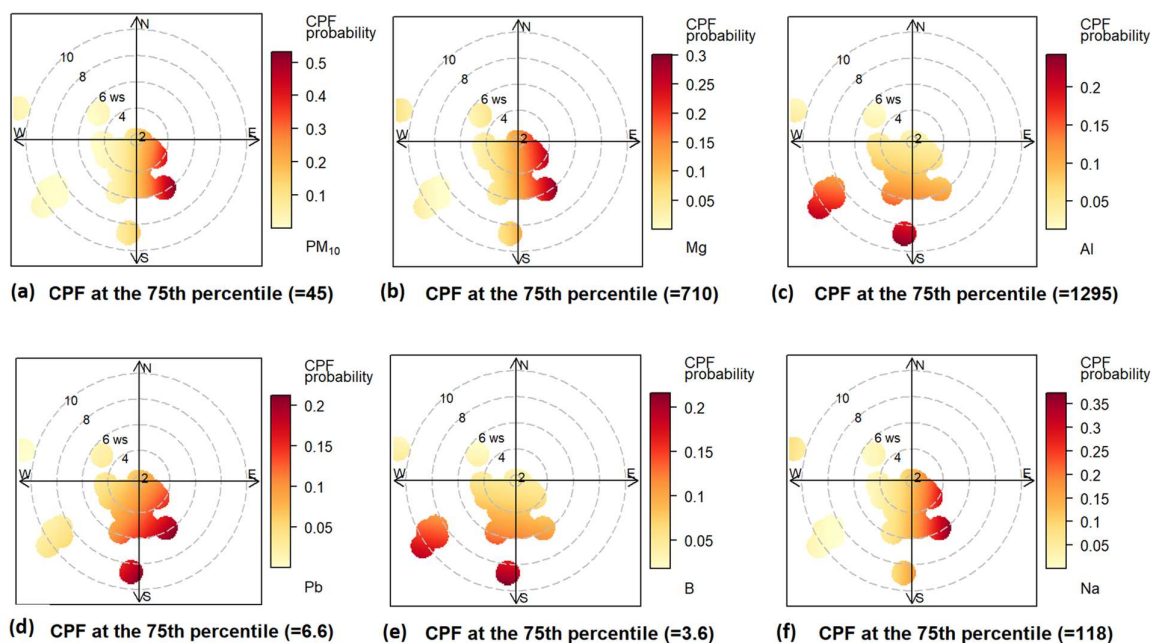
Figure 4.23 CBPF plots highlighting potential source(s) of (a) PM_{10} µg/m³, and trace elements available in the PM as (b) Mg ng/m³, (c) Al ng/m³, (d) Pb ng/m³, (e) B ng/m³, and (f) Na ng/m³

Quantitatively, the fractional contributions of these metals listed in **Appendix Table 2** showed the contributions as P (33.31%), K (33.01%) Ti (30.49%), V (28.59%), Mn 31.45%), Fe (30.76%), Co (30.21%), Ni (33.01%), Cu (38.35%), and Ba (33.71%) in the E-SE direction. The potential source could be due to emissions from the railway station that uses diesel-powered locomotives for transportation and is situated about 4.4 km away from our sampling station. This is exemplified in the few studies on the emissions of railway operations and their fate on environmental consequences where researchers identified that railway ballast contained a signifi-cant amount of trace metals (Fe, Mn, Cu, Cr, and Ni) and quite appreciable contami-

nations of Cd, Co, Cr, Cu, Fe, Mn, Ni, Pb, and Zn also originated from the herbicides in use.[260,301]

The SE-S winds from the CBPF (Figure 4.23) also indicated significant source contributions to the trace metal contents in PM_{10}. The railway station and airport are nearby (~3 km apart) and as such could be potential contributors to trace metal concentrations in this study. These potential sources are important since from the wind rose the prevailing wind directions are the SSE/SE/S. The probability of the source contributions coming from the SE/S (Figure 4.23) was identified for Na (35%), Mg (25%), Cr (45%), Zn (40%), As (10%), and 20% each for Cd, Sn, and Pb. Fractional contributions of these metals in the SE-S direction revealed relatively higher percentages (Appendix Table 2) especially for Cr (60.27%), As (74.52%), Cd (73.37%), and Pb (62.21%). Studies conducted by Szmagliński, et al. [301] detected trace metals such as Zn, Pb, Cd, Ni, Cr, Cu, and Fe in soils sampled near railway tracks, and similar to the constituents reported by Samarska, et al. [260]. Another indication of potential source contributions from SW-W was visible with a 20% probability each for B, Al, and Ca. Although the source in the SW-W is unknown, it was quite important with substantial fractional contributions as seen for B, Al, and Ca (Appendix Table 2). It is also important to mention that the SW-W source(s) appears to be a far distant source that appears at high-speed > 10 m/s. Two chromium industrial plants are located in the NW and one would have expected their impact on the trace element concentrations however, from the CBPF plots, less than a 10% probability of their impacts was realized (from NW/N). However, the frequency of the NW/N wind is insignificant. In this study, PM_{10} concentrations collected in Aktobe city were characterized by different modern technologies, and potential sources were identified for the first time. This study was limited to only a few numbers of samples collected during the pilot sampling period and this could not be a true representation of the entire city. Thus, a longer sampling duration of ambient PM monitoring is required, and more sampling sites must be included to cover the entire seasons in Kazakhstan. Additionally, particle size-fractioned measurements would be essential to confirm the studies in this industrial region. Atmospheric reactions and physicochemical factors could influence airborne PM as such future studies should incorporate criteria gases to understand better the atmospheric chemistry behavior of elements in the city of Aktobe.

In conclusion, the overall mean ambient PM_{10} concentration during this pilot study was below the 60 µg/m^3 average daily maximum allowable PM_{10} concentration (MAC) standard set in Kazakhstan.[221,261] However, the daily concentration of PM_{10} in this study exceeded the average daily for PM_{10} established by WHO standards (50 µg/m^3) by 1.10 to 3.59 times, and about 1.08 to 2.99 times above the 60 µg/m^3 average daily PM_{10} concentration (MAC) standard set by Kazakhstan. One would have expected the major industrial Cr facilities situated in the NW to be potential contributors to the PM concentrations. This study, however, identified the prevailing wind predominantly from NE-NW. Hence, the Cr facilities did not influence the PM levels significantly, since the wind rose shows that the sampling station was upwind from the Cr facilities during the period of this study. Morphological analyses of the PM identified the presence of constituents originating from anthropogenic and natural sources, with the former source highlighting the importance of industrial activities on the air quality within Aktobe city. The ionic constituents indicated that Ca^{2+}, K^+, Mg^{2+}, and SO_4^{2-} were statistically significantly higher in fall than in winter, due to low humidity and wet deposition. The PM samples were mostly acidic in the fall and alkaline during winter. The chemical forms of sulfate in winter suggested a complete neutralization of SO_4^{2-} by NH_4^+, and thus, $(NH_4)_2SO_4$ is the major species present, while higher temperatures in fall resulted in the formation of SO_4^{2-} which promoted the easy removal of NH_4^+ by decomposition. In the fall, NO_3^- ions showed a moderate association with NH_4^+ suggesting that NH_4NO_3 might be the dominant species. Relative humidity and temperature affect the thermodynamic features of nitrate, where nitrate volatilization is associated with high temperature and low RH.[285] The low temperature and high RH in winter, therefore, enhanced nitrate stabilization, and its subsequent loadings of PM_{10} increased the aerosol surface area for the heterogeneous formation of nitrate.

This pilot study seeks to highlight the need to plan a more intensive and long-term sampling campaign in Aktobe city to fully investigate the morphology, trace metal constituents, and potential source contributions to pollution of Aktobe city. This will go a long way to understanding the air quality of the city over a broader spectrum geared towards environmental pollution control.

4.4 Investigation into the disparity of total Cr(VI) concentrations using the Clarkson Sampler (Aktobe Study)

Researchers have reported that the interconversion of Cr(VI) during sampling could be due to the deliquescence of the ambient PM which provides an aqueous reaction route, as well as reactions with organic matter, SO_2, and reductants.[93,94,111] Amouei Torkmahalleh, et al. [62] indicated that the RH changes during a typical 24-hr sampling period due to the variations in the atmospheric conditions. That is the ambient RH exceeds the deliquescence relative humidity (DRH) at least twice during the 24-hr period; early mornings and after sunset. As the RH exceeds the DRH (76%) of the ambient PM, [94] there is still the possible conversion of Cr(VI) to Cr(III) even after the RH drops below the DRH. Previous studies suggested that the conversion of Cr(III) to Cr(VI) could be due to the reaction of Cr(III) with Mn[32,83] and with water-soluble organic carbons (WSOC) containing secondary organic aerosol (SOA).[111] The reduction of Cr(VI) to Cr(III) was reported as due to reactions with gaseous oxidants e.g. O_3 and particle-bound reactive oxygen species (ROS).[62,109] Amouei Torkmahalleh, et al. [62] later indicated that Cr(VI) concentrations in the aforementioned studies may have been biased by the Cr(VI) reduction and Cr(III) oxidation during sampling, filter storage, filter extraction, and analysis. Hence, Amouei Torkmahalleh, et al. [62] designed, constructed, and used the Clarkson sampler (sections 4.2.4 and 4.2.5) to preserve Cr(VI) concentration by reducing the RH of the ambient air during sampling to prevent deliquescence in cooler days, and cooling the ambient air in warmer days. In their work[62], the Clarkson sampler was tested for the recovery of soluble Cr(VI) spikes after 24-hr sampling intervals in summer and winter, as well as field sampling of soluble Cr(VI) in ambient air. To improve the quantification of Cr(VI) in ambient air, the aerosol collected on filters must be prevented from deliquescing. For this reason, our current study seeks to investigate the role of incorporating the Clarkson sampler in quantifying total Cr(VI) from the ambient PM.

4.4.1 Experimental Details

4.4.1.1 Aerosol sampling/data

Sampling was conducted at the same station as described previously in section 4.2.1. A full season cycle of sampling in Aktobe was covered in this study; fall (Sep-

tember 2021-November 2021), winter (December 2021-February 2022), spring (March 2022-May 2022), and summer (June 2022-August 2022) seasons.

4.4.1.2   Materials and Reagents

Total Cr(VI) in the PM samples was collected on Teflon filters as previously described in section 4.2.3. No pretreatments were needed for the Teflon filters before sampling. However, the filters collected after sampling are stored in a freezer (-20 °C) until analyses.

4.4.1.3   Determination of total Cr(VI) in Ambient Air

The method discussed earlier in section 4.1.4.2 for the determination of total Cr(VI) was used in this study. A total of 162 Teflon filter samples were collected over the seasonal cycles. The Clarkson sampler connected to the drying unit collected 23 filter samples in fall, 24 samples in the winter, 17 samples in the spring, and 18 samples in the summer seasons. The control study (without the drying unit) sampled 21, 24, 17, and 18 filter samples, respectively in fall, winter, spring, and summer. Cr(VI) was detected in all the filed samples (N=162).

4.4.1.4   Clarkson Cr(VI) Sampler

Two Clarkson Cr(VI) samplers (section 4.2.4, Figure 4.10) designed and constructed by Amouei Torkmahalleh, et al. [62] were used in this study; where one sampler was connected to a drying unit (as described in section 4.2.5) and the other sampler was used as the control study (without the drying unit).

4.4.1.5   Statistical Analyses:

The Shapiro-Wilk normality test[228] showed that the data were not normally distributed, and hence the non-parametric two-sample Wilcoxon rank sum test[227,229] was used for comparisons between the total Cr(VI) samples.

4.4.1.6   Conditional Probability Bivariate Function (CBPF)

CBPF[230] and the Fractional Contributions (%) of elements in the PM_{10} were determined as previously described in section 4.1.7

4.4.2 Results and Discussions

4.4.2.1   The influence of the Drying Unit during Cr(VI) sampling

The use of the Clarkson Cr(VI) sampler, designed and constructed by Amouei Torkmahalleh, et al. [62], helped to keep the sampling filters dry (RH < 76%) during the sampling and post-sampling periods. This principle enables the RH of the air passing over the filter to be maintained below 76% (i.e. the deliquescence relative humidity of the ambient particles) to keep the filter dry.[62,93] Thus, the dry filter slows down the reduction reactions of Cr(VI) with ambient particles by inhibiting the aqueous Cr(VI) chemistry.[112] Sampling over the full seasonal cycles enabled the investigation to include conditions that would be suitable for deliquescence to occur as seen in the low temperature (-7 °C)/high RH (81 %) values recorded in the winter, which were all statistically significant over the rest of the seasons (Table 4.18). Although the wind direction (Table 4.18, Figure 4.25) was not significant, the speed of the prevailing wind was statistically significant with the summer season having the lowest wind speed (3.9 m/s) and the highest of 5.3 m/s recorded in spring. The lowest temperature was recorded in winter with an mean value of -7.5 °C, followed by fall (3.3 °C), spring (11.0 °C), and the highest in summer (21.0 °C).

Results in Table 4.18 shows that the total Cr(VI) concentration determined from the sampler with drying unit (T2) was relatively higher than those obtained from the sampler without the drying unit (T1= control study), except for the values obtained in fall (T1=10.08 ng/m^3; T2= 7.57 ng/m^3). Concentrations of total Cr(VI) in summer for example show that T2 is higher than T1 since the particles were dry so less deliquescence occurred (prevents aqueous interconversion), and thus conversion of Cr(III) to Cr(VI) is more dominant. Statistically significant differences were observed for both T1 and T2 when the entire seasonal cycles were considered. This implies that the sources of Cr(VI) in the ambient environment near the sampling site changed per season. As expected, the same seasonal pattern for the potential source distribution was observed for T1 and T2 since the samplers were collocated. The CBPF plots for T1 during fall (Figure 4.24a) show a source contribution located in the NE direction with ~4 m/s wind speed, showing about a 30% probability of the source in this direction. Another source in the SE wind (6 m/s) shows ~35% probability of source contribution to the concentrations of Cr(VI) measured in this study. The SE winds indicate the influence of distant sources and from Figure 4.9 the potential sources in this di-

rection are the railway station and the airport. In the winter season (Figure 4.24b and 4.23f), the CBPF plots show about a 50% probability of sources in the SW direction when the wind speed is approximately 2-4 m/s. This low wind speeds suggest that the source contributions are mostly local sources such as the diffusion from vehicular traffics since the sampling station is close to two highways (Zhubanov Brothers 263 and Aliya Moldagulova Avenue 34).

Another source contribution with a ~50% probability is seen in the WNW winds during winter. This source with a speed of 4 m/s appears as a distant source, and the potential sources identified in this direction are the mixed concrete production plants. The trend during the spring season (Figure 4.24c and 4.23g) shows potential sources (60-100% probabilities) with the ENE winds (6-7 m/s), indicating distant sources in this direction could impact the air quality of the city in spring. The CBPF of Figure 4.24(g) further shows potential sources with the easterly wind (5 m/s, ~90% probability), and also a far distant source (~90% probability) in the southerly wind direction having a wind speed of 7 m/s. This unidentified source in the southerly wind could also greatly impact the quality of air in the city during the spring season. The potential source contribution in summer (Figure 4.24d and 4.23h) is seen with the WNW direction with winds speeds in the range of 3-5 m/s. About 60-80% probabilities of the source's contribution are seen in this direction and pointed out that, in summer distant sources in the WNW direct could play significant roles in the quality of air in the city.

To ascertain if the overall concentrations obtained without/with the drying system were significant, the Wilcoxon rank sum test per season for T1 and T2 was conducted (Table 4.19). The results showed no significant differences (winter, p=0.57; spring, p=0.37; summer, p=0.32) in the concentrations except in fall (p<0.05). Amouei Torkmahalleh, et al. [62] reported average recovery values of 57% and 72%, respectively, in summer and winter, for Cr(VI) spikes after 24-hour sampling with the Clarkson sampler. Their study however investigated only soluble Cr(VI). Results from our seasonal study however did not show any statistically significant differences in the total Cr(VI) concentrations, suggesting that employing the drying unit would be more appropriate when investigating soluble Cr(VI) concentrations in ambient PM. That is the impact of deliquescence is more susceptible to quantifying the soluble form of Cr(VI) in the ambient, and does not significantly impact the total Cr(VI) con-

centrations when under investigation. Nonetheless, no drying could convert Cr(VI) to Cr(III) and thus it is still important to use a drying system during the sampling campaigns of ambient Cr(VI).

Table 4.18 Summary of the descriptive statistics of parameters over the seasonal cycles

Parameter	Winter	Spring	Fall	Summer	Significance
T1 (ng/m^3)	5.08 (6.46)	3.77 (3.58)	10.08 (16.26)	12.71(18.97)	$p < 0.05$
T2 (ng/m^3)	7.68 (13.47)	4.43 (3.96)	7.57 (22.04)	23.54 (40.64)	$p < 0.001$
Temp (°C)	-7.48 (11.45)	11.02 (8.69)	3.29 (13.29)	20.97 (8.02)	$p < 0.001$
RH (%)	81.63 (5.84)	62.83(17.54)	65.24(19.33)	58.22 (8.74)	$p < 0.001$
WD (°)	167.57(68.42)	168.92(62.94)	200.58(66.76)	200.17(69.99)	$p = 0.15$
WS (m/s)	4.1 (1.90)	5.33 (1.67)	5.06 (2.24)	3.88 (1.15)	$p < 0.05$

NB: T1= total Cr(VI) concentration obtained from the sampler without a drying unit, T2= total Cr(VI) concentration obtained with a drying unit connected to the sampler. Values reported as mean (S.D)

Table 4.19 Seasonal comparisons of T1 versus T2

Seasons	p-values	T1 vs T2 significant?
Fall	$p < 0.05$	yes
Winter	$p = 0.57$	no
Spring	$p = 0.37$	no
Summer	$p = 0.32$	no

NB: T1= total Cr(VI) concentration obtained from the sampler without a drying unit, T2= total Cr(VI) concentration obtained with a drying unit connected to the sampler. Values reported as mean (S.D)
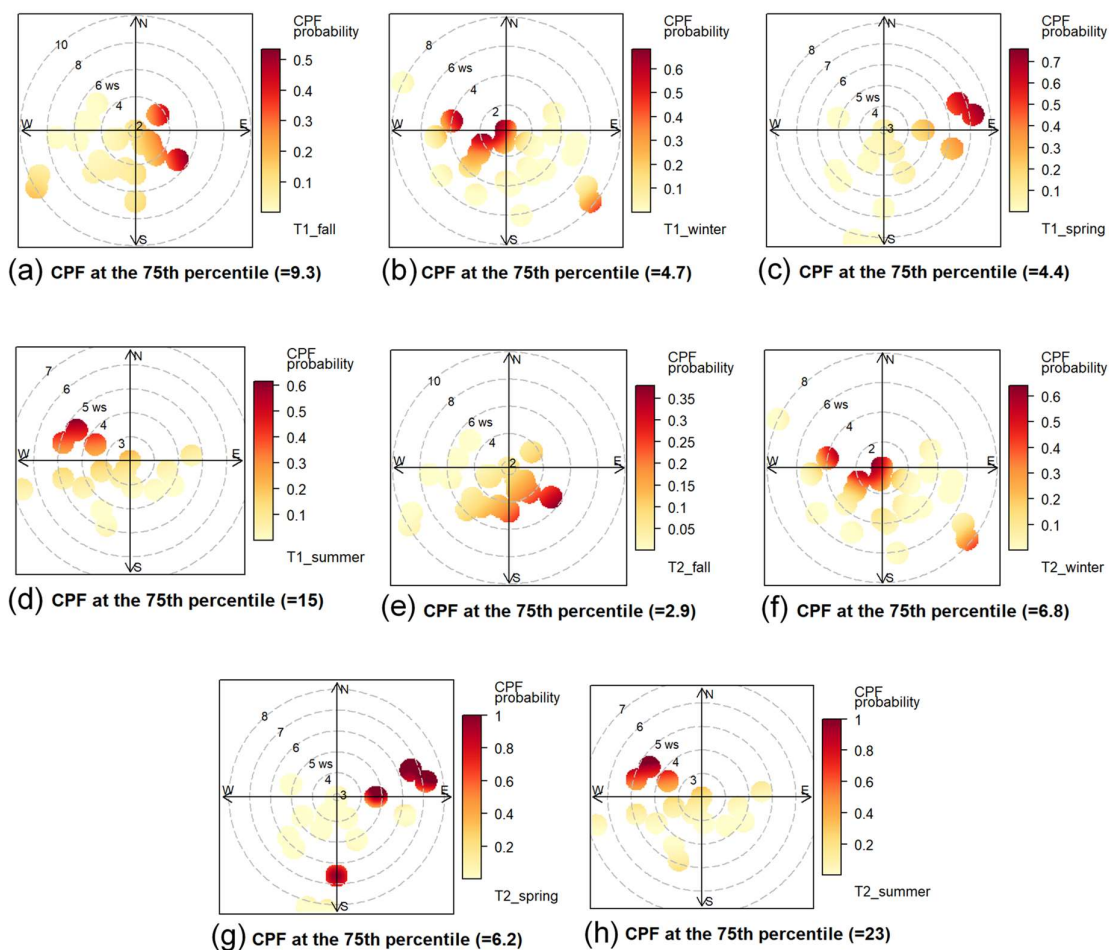
Figure 4.24 CBPF plots showing the seasonal variation in the potential sources for total Cr(VI) concentrations
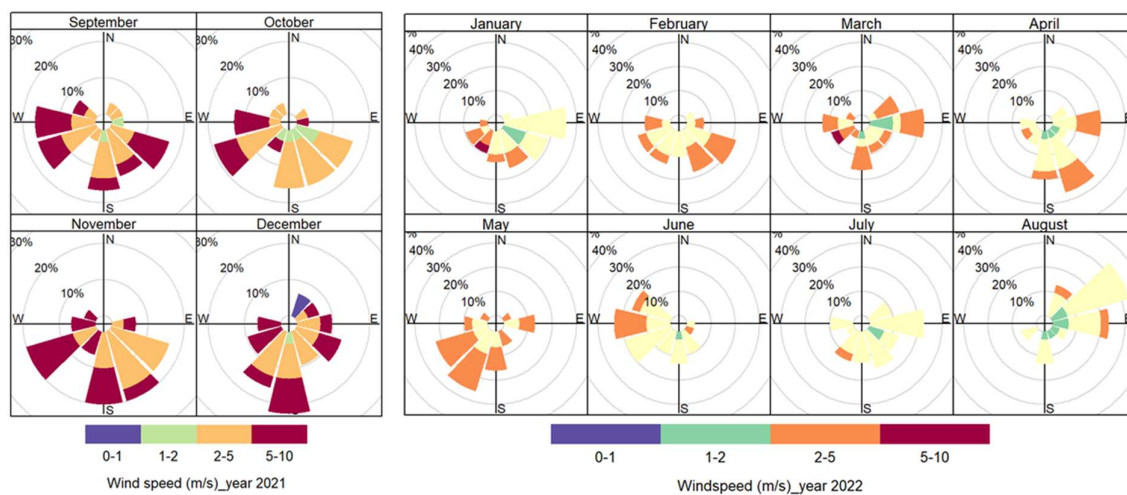
Figure 4.25 Windrose showing the prevailing wind directions during the study period

CHAPTER 5.   CONCLUSIONS AND RECOMMENDATIONS

5.1   Conclusions

The need to alleviate environmental pollution has prompted the development of functional materials that can act as sensors for the detection of toxic substances in the environment. This doctoral dissertation provides new findings into the use of functional carbon materials as a sensor for the detection of hexavalent Cr in water and ambient PM. Earlier modeling study[96] identified that at pH=4, Cr(III) precipitated as insoluble $Cr_2(SO_4)_3$(s) at equilibrium over 35 hours. Interconversions between Cr(VI) and Cr(III) occurred and the overall direction was from Cr(VI) to Cr(III). Other species including $Cr(OH)_3$, K_2CrO_4, and Na_2CrO_4 were soluble at pH 4. Their simulation subsequently identified that insoluble compounds such as $(NH_4)_2CrO_4$, $CaCrO_4$, $PbCrO_4$, and $BaCrO_4$ precipitated in the solution after the system attained equilibrium. The results of the modeling prompted the need to develop a novel analytical method to quantify the insoluble Cr(VI) in ambient PM.

A functional carbon material containing nitrogen and sulfur co-doped onto carbon-based materials (N,S-CDs) was successfully synthesized in a single-stage microwave method. The successful material was attained after manipulating parameters including the types of precursors, amount of precursors incorporated, temperature variations, and synthesis durations. The optimal synthesis involved reacting 420 mg of citric monohydrate, 1mL of 4-pyridinecarboxaldehyde, and 50 mg of thiourea in 5 mL of double distilled water using microwave conditions: 5 min ramp to 190 °C, 30 min hold at a pressure less than 200 psi with constant stirring. Characterization of the particles revealed that the fluorescent N,S-CDs had a hydrodynamic diameter of ~20 nm using the DLS principle. The morphology of the particles was irregularly shaped with some agglomeration in the bulk material. The quantitative analyses with EDS confirmed the presence of nitrogen, sulfur, and carbon in the structure of the fluorescent material. The TEM images identified that the carbon dots in the solution were polydispersed and nearly spherical shaped with a mean particle diameter of about 10 nm.

The chemical bond information was investigated using the XPS technique by deconvolution and fitting of C1s, N1s, S2p, and O1s spectra. Not only do these functional groups improve upon the hydrophilicity of the functional material but they also

introduced chromophoric/auxochromic characteristics to the fluorescence spectra. XPS analyses investigated the mechanism of Cr(VI)'s attachment to the fluorescent material in the presence of protonated pyridyl, aldehyde, and hydroxyl groups in the composite. The good water-solubility of the particles enabled the possibility to study the variability in the successful uptake of Cr(VI) to determine the elemental attachment that could occur in the aqueous system. The deconvolution of the Cr2p3/2 peak showed at 572.7 eV and 575.2 eV, assigned to elemental Cr and Cr-O/Cr-N, respectively. The Cr(VI) standard added was in the form of $NH_4(CrO_4)$, and the reversible reaction with chromate (CrO_4^{2-}) ions and H^+ will ionize to form dichromate ($Cr_2O_7^{2-}$) ions. Thus, the Cr(VI) ions in the solution interacted with the N,S-CDs through the pyridyl nitrogen (-NH), and so we theorize that pyridyl nitrogen is responsible for the coordination of Cr(VI) species through an electron transfer with the Cr(VI) ions, that resulted in the quenching of the fluorescent spectra of the carbon material in solution.

The fluorescence intensity of the functional carbon material decreased proportionally with an increase in the concentration of Cr(VI) anions. The weak binding between pyridyl nitrogen and the aldehyde in the ligand contributed to the reduction in the intra-ligand fluorescence efficiency upon an increase in Cr(VI) concentrations. Overall, the calculated detection limit of total Cr(VI) was 5.32 ng/L (0.1 nM) Cr(VI) ions. The outstanding feature of this work is its application to total/insoluble Cr(VI) species and ambient PM samples. The results of the fluorescent analyses showed average (%RSD) recoveries of 106.0% (5.3%), 102.3% (3.6%), 96.4% (1.9%), and 101.7% (2.2%), respectively, for $PbCrO_4$, $BaCrO_4$, $CaCrO_4$, and $(NH_4)_2CrO_4$, Generally, the relative standard deviation (RSD) was about 5% for all the insoluble chromates which signifies its ability to be used as a sensor for total/insoluble Cr(VI) detection. The application of the proposed fluorescent method on field PM samples resulted in a MDL of 0.32 ng/m^3 for total Cr(VI) quantification. This MDL is much lower than the NIOSH 7605 (50 ng/m^3), OSHA ID-215 (3 ng/m^3), and ASTM D 5281-92(0.2-1.0 ng/m^3) methods, but comparable to the 0.33 ng/m^3 value reported by Huang, et al. [70].

Insoluble Cr(VI) in this study referred to the difference between the total and soluble Cr(VI) components. After subjecting the PM extracts to the newly developed fluorescent spectrophotometric method, comparable results for total and soluble Cr(VI) concentrations using IC-UV were obtained. The calculated insoluble Cr(VI)

concentrations in the ambient PM using the proposed fluorescent method were in the range of 7.5-58.0 ng/m^3 with a mean of 14.3 ng/m^3. The practical application of the fluorescent carbon materials to quantify insoluble Cr(VI) with acceptable recoveries, and consistency with the IC-UV results indicates that the fluorescent probe has a promising tendency to be used as a sensor to monitor the concentration of Cr(VI) in ambient PM.

Field studies in Astana and Aktobe demonstrated that total Cr(VI) including soluble and insoluble Cr(VI) dominated the ambient PM and higher temperature promoted the conversion of Cr(VI) to Cr(III)[210], where temperature and total Cr(VI) were positively correlated. The discrepancy in understanding the chemistry of atmospheric Cr existed in the literature since previous researchers implemented analytical methods that quantified only soluble forms of Cr(VI) rather than insoluble forms. However, current analytical methods that measure total Cr(VI) (insoluble + soluble) enabled the investigation into the influence of gas-solid chemistry than the aqueous chemistry on atmospheric Cr. Our field studies[210] demonstrated that insoluble Cr(III) and insoluble Cr(VI) dominated atmospheric Cr(III) and Cr(VI). The seasonal variabilities in the gas concentrations, total Cr(VI) concentrations, temperatures as well as the correlations between the gas concentrations and total Cr(VI) concentrations enabled us to reach the condensed gas-solid reaction of Cr as given in equation 4.4.

5.2 Recommendations

Although this research improved upon the recovery of insoluble Cr(VI) by developing a new analytical method, additional material engineering improvements should be considered to scale up the production of functional materials for commercial purposes. The current study was only limited to laboratory-scale production.

- This study utilized functional materials in the form of carbon dots as a sensor for Cr(VI) detection in solution. Environmental management necessitates the use of reusable materials that will be eco-friendly when used as a sensor or adsorbent during environmental monitoring. The carbon dots are known to have low toxicity, however, they were not reusable, and thus the development of other materials such as reusable catalysts (MOFs or ZIFs) could be explored in the future to achieve the same application of detecting Cr(VI) in ambient PM.

- The proposed fluorescent method using the functional N,S-CDs was only applicable to detect Cr(VI) without any means to measure the potential conversions from Cr(VI) to Cr(III) or vice versa. Thus, there could be some biases in the data presented. Hence further studies should be conducted to possibly incorporate the dual sensing ability of Cr(VI) and Cr(III) with doped CDs to avert this situation in the statistical analyses.

- In this method development, very few field samples were collected to test the applicability of the N,S-CDs to detect Cr(VI). To ascertain the robustness of the N,S-CDs to function as a good sensor towards Cr(VI) detection, samples should be collected over all seasonal cycles and tested with the proposed fluorescent method.

- The field studies conducted in Astana only centralized on size-segregated Cr(VI) concentrations and its associated Cr-chemistry with some gases. Future investigations could explore the kinetics of such reactions at varying RH, temperature, and concentrations in the laboratory.

- It is uncertain whether the chronic Inhalation Reference Concentration (RfC) of 8 ng/m^3 as established by USEPA [235] is based on soluble or total Cr(VI). However if it is based on only soluble Cr(VI), its calculation must be revisited using the total or insoluble Cr(VI) concentrations. Since the toxicity of insoluble Cr(VI) could be more than soluble Cr(VI), then lower concentrations of RfC would better indicate the exact toxic level of Cr(VI) concentrations in ambient environments.

- In Kazakhstan, the Hygienic Norms for Atmospheric Air in Urban and Rural Residential Areas adopted on February 28, 2015,[261] established the maximum permissible average daily concentration of chromium (in terms of chromium (VI) oxide) in the ambient air as 0.0015 mg/m^3, and the approximate safe level of exposure to chromium (III) compounds in ambient air is given as 0.01 mg/m^3. Since in the past, methods for the quantification of insoluble Cr(VI) were limited, such standards were based on the soluble Cr(VI) species. However, the availability of modern methods to measure ambient insoluble Cr(VI) now allows for revising existing standards and thresholds based on insoluble Cr(VI) species.

- The Clarkson sampler should be improved upon in terms of possibly being automated in order to adjust the temperature of the drying unit as the seasons change. This will reduce the tasks of readjusting the temperature manually as the seasons change.

APPENDICES I

Pilot study on the characterization of PM_{10} samples from Aktobe City
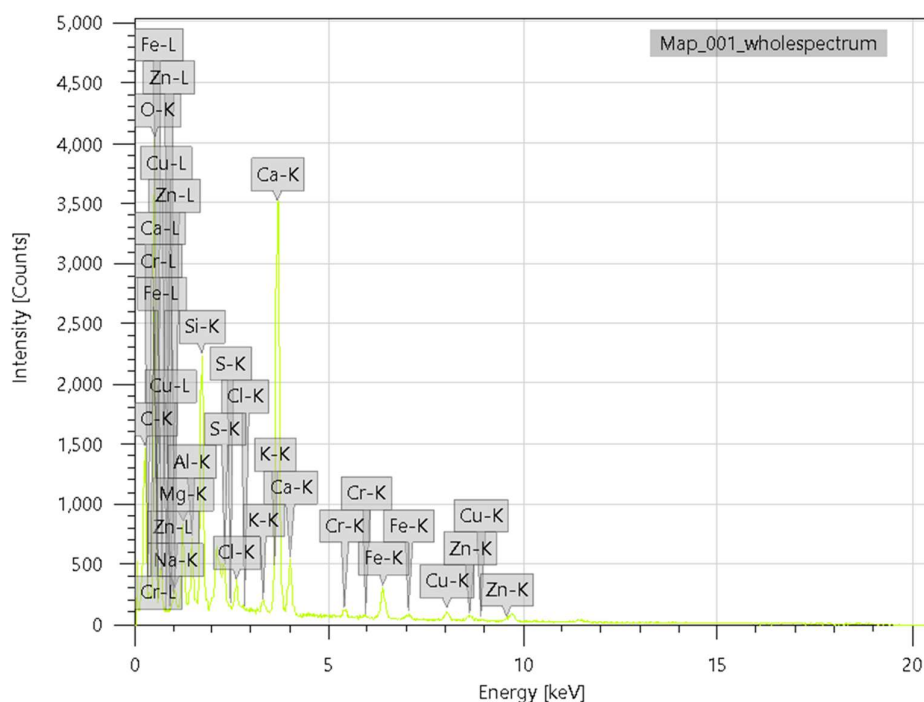
Appendix Figure 1. A typical EDS of PM_{10} sample collected from the sampling site

Appendix Table 1. Elemental composition of some PM_{10} samples via EDS (mass %)

Element	Sample1	Sample2	Sample3	Sample4	Sample5	Sample6
C	19.36±0.12	23.40±0.04	20.20±0.04	21.37±0.05	22.63±0.05	28.78±0.06
F	-	59.95±0.09	39.15±0.09	39.86±0.09	27.46±0.08	24.25±0.08
O	46.40±0.28	8.87±0.04	23.52±0.06	20.07±0.06	23.61±0.09	26.94±0.10
Na	0.71±0.04	-	-	2.12±0.02	0.75±0.01	0.73±0.02
Mg	2.32±0.05	-	0.69±0.01	1.92±0.02	1.48±0.01	1.13±0.01
Al	1.64±0.04	-	1.82±0.01	1.25±0.01	1.18±0.01	0.72±0.01
Si	5.42±0.06	0.60±0.01	5.31±0.02	2.19±0.02	3.19±0.02	2.11±0.02
S	0.73±0.03	1.33±0.01	0.58±0.01	2.32±0.02	1.80±0.01	1.58±0.01
Cl	0.81±0.03	-	0.11±0.00	0.69±0.01	0.66±0.01	0.50±0.01
K	0.43±0.02	-	0.44±0.01	0.29±0.01	0.32±0.01	0.26±0.01
Ca	16.36±0.11	1.09±0.01	3.91±0.02	1.32±0.01	9.51±0.03	6.11±0.03
Cr	0.60±0.03	-	-	0.82±0.01	0.58±0.01	0.80±0.02
Fe	2.86±0.07	0.28±0.01	1.35±0.02	1.32±0.02	1.92±0.02	1.18±0.02
Cu	1.43±0.07	0.29±0.01	-	0.30±0.01	-	-
Zn	0.95±0.07	-	-	-	-	-
Ti	-	-	0.10±0.01	-	-	-

Appendix Table 2. Fractional contribution for inorganic element per a given wind direction.

Elements	N-NE	NE-E	E-SE	SE-S	S-SW	SW-W	W-NW	NW-N
B	0%	0%	27.84%	10.42%	20.55%	38.73%	2.45%	0%
Na	0%	0%	30.64%	44.02%	11.76%	13.55%	0.03%	0%
Mg	0%	0%	28.92%	30.64%	16.83%	23.59%	0.02%	0%
Al	0%	0%	29.69%	12.38%	25.35%	32.55%	0.04%	0%
P	0%	0%	33.31%	15.50%	22.29%	26.98%	1.93%	0%
K	0%	0%	33.01%	13.76%	24.55%	28.63%	0.05%	0%
Ca	0%	0%	30.99%	17.39%	20.24%	31.22%	0.17%	0%
Ti	0%	0%	30.49%	15.73%	23.37%	30.29%	0.12%	0%
V	0%	0%	28.59%	20.76%	22.54%	27.47%	0.64%	0%
Cr	0%	0%	20.69%	60.27%	1.87%	17.09%	0.07%	0%
Mn	0%	0%	31.45%	20.87%	21.46%	26.15%	0.07%	0%
Fe	0%	0%	30.76%	19.92%	23.84%	25.36%	0.12%	0%
Co	0%	0%	30.21%	24.17%	20.60%	24.22%	0.80%	0%
Ni	0%	0%	33.01%	25.54%	15.22%	24.72%	1.51%	0%
Cu	0%	0%	38.35%	25.35%	16.37%	19.63%	0.29%	0%
Zn	0%	0%	32.05%	37.25%	10.76%	19.34%	0.59%	0%
As	0%	0%	7.01%	74.52%	4.24%	12.31%	1.92%	0%
Cd	0%	0%	9.38%	73.37%	7.10%	9.50%	0.65%	0%
Sn	0%	0%	27.31%	56.79%	8.27%	7.05%	0.57%	0%
Ba	0%	0%	33.71%	15.55%	25.63%	25.04%	0.07%	0%
Pb	0%	0%	16.94%	62.21%	6.34%	14.23%	0.29%	0%
PM_{10}	0%	0%	19.08%	43.54%	14.31%	21.32%	1.75%	0%
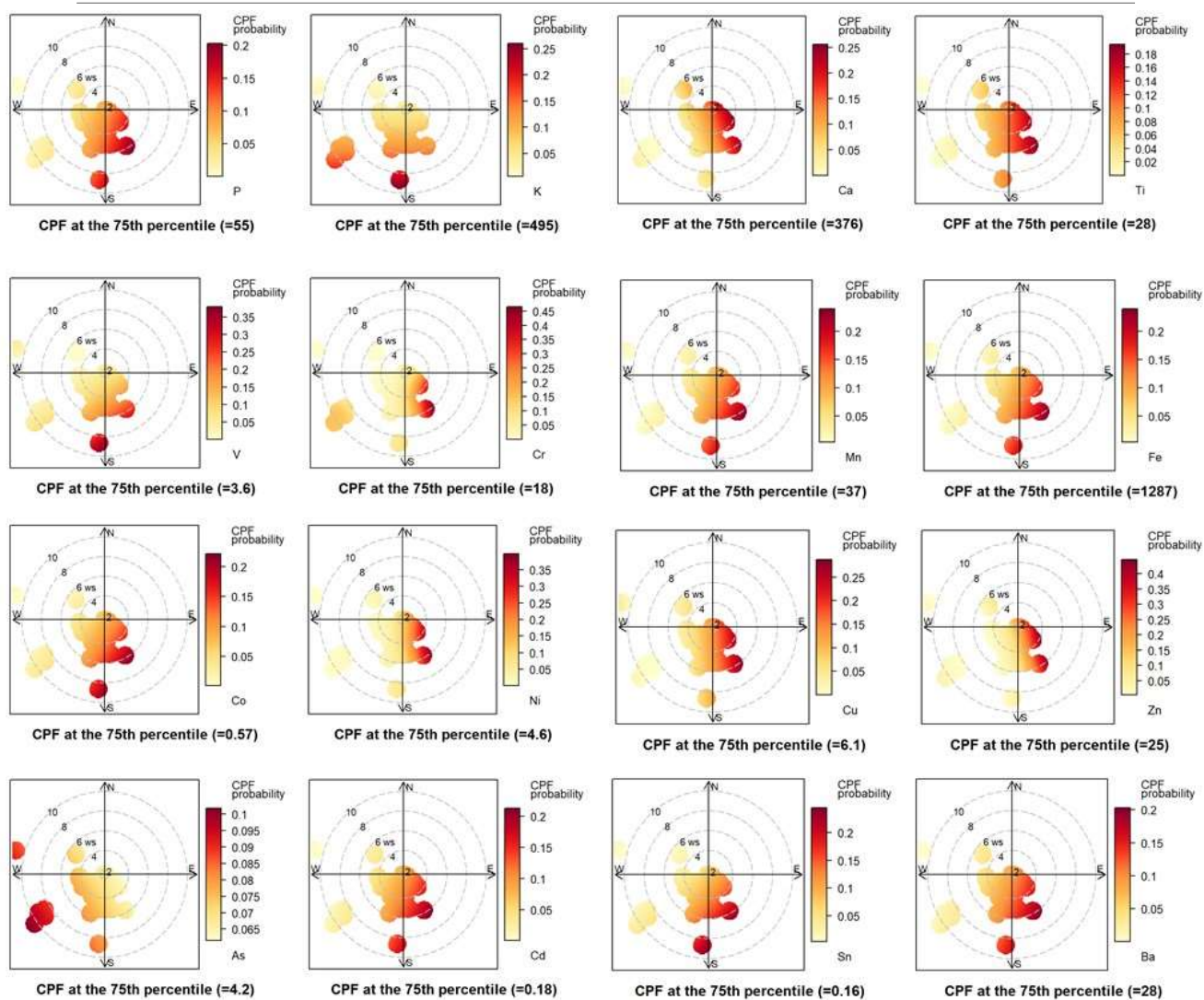
Appendix Figure 2 Figure S6. CBPF plots highlighting the potential sources of the trace elements in PM$_{10}$

REFERENCES

1   Evans, J. D. *et al.* Metal-organic frameworks in Germany: From synthesis to function. *Coordination Chemistry Reviews* **380**, 378-418, doi:10.1016/j.ccr.2018.10.002 (2019).

2   Vaseashta, A. *et al.* Nanostructures in environmental pollution detection, monitoring, and remediation. *Science and technology of advanced materials* **8**, 47-59, doi:10.1016/j.stam.2006.11.003 (2007).

3   Ravichandiran, P. *et al.* Naphthoquinone-Based Colorimetric and Fluorometric Dual-Channel Chemosensor for the Detection of Fe^{2+} Ion and Its Application in Bio-Imaging of Live Cells and Zebrafish. *Acs Sustainable Chemistry & Engineering* **7**, 17210-17219, doi:10.1021/acssuschemeng.9b03822 (2019).

4   Ravichandiran, P. *et al.* Simple Fluorescence Turn-On Chemosensor for Selective Detection of Ba(2+) Ion and Its Live Cell Imaging. *Analytical chemistry* **91**, 10095-10101, doi:10.1021/acs.analchem.9b02057 (2019).

5   Ravichandiran, P. *et al.* A phenoxazine-based fluorescent chemosensor for dual channel detection of Cd^{2+} and CN^- ions and its application to bio-imaging in live cells and zebrafish. *Dyes and Pigments* **172**, 107828, doi:10.1016/j.dyepig.2019.107828 (2020).

6   Leonard, A. & Lauwerys, R. R. Carcinogenicity and mutagenicity of chromium. *Mutation Research* **76**, 227-239, doi:10.1016/0165-1110(80)90018-4 (1980).

7   Huvinen, M., Uitti, J., Oksa, P., Palmroos, P. & Laippala, P. Respiratory health effects of long-term exposure to different chromium species in stainless steel production. *Occupational Medicine* **52**, 203-212, doi:10.1093/occmed/52.4.203 (2002).

8   Norseth, T. The carcinogenicity of chromium. *Environmental Health Perspect* **40**, 121-130, doi:10.1289/ehp.8140121 (1981).

9   Fournier-Salaün, M.-C. & Salaün, P. Quantitative determination of hexavalent chromium in aqueous solutions by UV-Vis spectrophotometer. *Central European Journal of Chemistry* **5**, 1084-1093, doi:10.2478/s11532-007-0038-4 (2007).

10   Wojasińska, E. & Trojanowicz, M. Ion chromatographic speciation of chromium with diphenylcarbazide-based spectrophotometric detection. *Journal of Chromatography A* **736**, 141-150, doi:10.1016/0021-9673(95)01373-3 (1996).

11   Inoue, Y., Sakai, T. & Kumagai, H. Simultaneous Determination of Chromium(Iii) and Chromium(Vi) by Ion Chromatography with Inductively-Coupled Plasma-Mass Spectrometry. *Journal of Chromatography A* **706**, 127-136, doi:10.1016/0021-9673(95)00125-7 (1995).

12   Sacher, F., Raue, B., Klinger, J. & Brauch, H. J. Simultaneous determination of Cr(III) and Cr(VI) in ground and drinking waters by IC-ICP-MS. *International Journal of Environmental Analytical Chemistry* **74**, 191-201, doi:10.1080/03067319908031425 (1999).

13   Moghadam, M. R., Dadfarnia, S. & Shabani, A. M. H. Speciation and determination of ultra trace amounts of chromium by solidified floating organic drop micro-extraction (SFODME) and graphite furnace atomic absorption spectrometry. *Journal of Hazardous Materials* **186**, 169-174, doi:10.1016/j.jhazmat.2010.10.101 (2011).

14   Sari, T. K., Takahashi, F., Jin, J., Zein, R. & Munaf, E. Electrochemical Determination of Chromium(VI) in River Water with Gold Nanoparticles-Graphene Nanocomposites Modified Electrodes. *Analytical Sciences* **34**, 155-160, doi:10.2116/analsci.34.155 (2018).

15   Jin, H. G., Zong, W. B., Yuan, L. & Zhang, X. B. Nanoscale zeolitic imidazole framework-90: selective, sensitive and dual-excitation ratiometric fluorescent detection of hazardous Cr(VI) anions in aqueous media. *New Journal of Chemistry* **42**, 12549-12556, doi:10.1039/c8nj02047g (2018).

16   Liu, C. & Yan, B. Luminescent zinc metal-organic framework (ZIF-90) for sensing metal ions, anions and small molecules. *Photochemical & Photobiological Sciences* **14**, 1644-1650, doi:10.1039/c5pp00107b (2015).

17   Sun, X. *et al.* An ultrastable Zr-MOF for fast capture and highly luminescence detection of $Cr_2O_7^{2-}$ simultaneously in an aqueous phase. *Journal of Materials Chemistry A* **6**, 6363-6369, doi:10.1039/C8TA01060A (2018).

18   Batool, M. *et al.* Metal Ion Detection by Carbon Dots-A Review. *Critical Reviews in Analytical Chemistry* **52**, 756-767, doi:10.1080/10408347.2020.1824117 (2022).

19   Bleibtreu, A., Bertine, M., Bertin, C., Houhou-Fidouh, N. & Visseaux, B. Focus on Middle East respiratory syndrome coronavirus (MERS-CoV). *Med Mal Infect* **50**, 243-251, doi:10.1016/j.medmal.2019.10.004 (2020).

20   Chen, W. F. *et al.* Synthesis of graphene quantum dots from natural polymer starch for cell imaging. *Green Chemistry* **20**, 4438-4442, doi:10.1039/c8gc02106f (2018).

21   Zhang, Y., Fang, X., Zhao, H. & Li, Z. A highly sensitive and selective detection of Cr(VI) and ascorbic acid based on nitrogen-doped carbon dots. *Talanta* **181**, 318-325, doi:10.1016/j.talanta.2018.01.027 (2018).

22   Atabaev, T. S. Doped Carbon Dots for Sensing and Bioimaging Applications: A Minireview. *Nanomaterials (Basel)* **8**, 342, doi:10.3390/nano8050342 (2018).

23   Atchudan, R. *et al.* Facile synthesis of a novel nitrogen-doped carbon dot adorned zinc oxide composite for photodegradation of methylene blue. *Dalton Transactions* **49**, 17725-17736, doi:10.1039/d0dt02756a (2020).

24   Zhou, J. *et al.* Carbon dots doped with heteroatoms for fluorescent bioimaging: a review. *Microchimica Acta* **184**, 343-368, doi:10.1007/s00604-016-2043-9 (2017).

25   Li, Y. *et al.* Nitrogen-doped graphene quantum dots with oxygen-rich functional groups. *Journal of the American Chemical Society* **134**, 15-18, doi:10.1021/ja206030c (2012).

26   Xue, G. B. *et al.* Boosting the electron mobility of solution-grown organic single crystals via reducing the amount of polar solvent residues. *Materials Horizons* **3**, 119-123, doi:10.1039/c5mh00190k (2016).

27   Dong, Y. *et al.* Carbon-based dots co-doped with nitrogen and sulfur for high quantum yield and excitation-independent emission. *Angewandte Chemie International Edition* **52**, 7800-7804, doi:10.1002/anie.201301114 (2013).

28   Li, F., Yang, D. & Xu, H. Non-Metal-Heteroatom-Doped Carbon Dots: Synthesis and Properties. *Chemistry* **25**, 1165-1176, doi:10.1002/chem.201802793 (2019).

29   Barnhart, J. Occurrences, uses, and properties of chromium. *Regulatory Toxicology and Pharmacology* **26**, S3-7, doi:10.1006/rtph.1997.1132 (1997).

30   Guertin, J., Avakian, C. P. & Jacobs, J. A. *Chromium (VI) handbook*. (CRC press, 2016).

31   Kotaś, J. & Stasicka, Z. Chromium occurrence in the environment and methods of its speciation. *Environ Pollut* **107**, 263-283 (2000).

32   Seigneur, C. & Constantinou, E. Chemical kinetic mechanism for atmospheric chromium. *Environmental Science & Technology* **29**, 222-231, doi:10.1021/es00001a029 (1995).

33   Phelan, J. M. *et al.* Airborne Aerosol Measurements in the Quiescent Plume of Mount St-Helens - September, 1980. *Geophysical Research Letters* **9**, 1093-1096, doi:10.1029/GL009i009p01093 (1982).

34   Pacyna, J. & Nriagu, J. *Atmospheric emissions of chromium from natural and anthropogenic sources*. Vol. 20 (Wiley and Sons: New York, 1988).

35   Richard, F. C. & Bourg, A. C. M. Aqueous Geochemistry of Chromium - a Review. *Water Research* **25**, 807-816, doi:10.1016/0043-1354(91)90160-R (1991).

36   Papp, J. F. Chromium life cycle study. (US Bureau of Mines, 1994).

37   USGS. Mineral commodity summaries 2022. Report No. 2022, 202 (Reston, VA, 2022).

38   USGS. Mineral Commodity Summaries 2019. (Reston, VA, 2019).

39   Beukes, J. P., Dawson, N. F. & van Zyl, P. G. Theoretical and practical aspects of Cr(VI) in the South African ferrochrome industry. *Journal of the Southern African Institute of Mining and Metallurgy* **110**, 743-750 (2010).

40   Howat, D. D. Chromium in South-Africa. *Journal of the South African Institute of Mining and Metallurgy* **86**, 37-50 (1986).

41   Kleynhans, E. L. J., Beukes, J. P., Van Zyl, P. G., Kestens, P. H. I. & Langa, J. M. Unique challenges of clay binders in a pelletised chromite pre-reduction process. *Minerals Engineering* **34**, 55-62, doi:10.1016/j.mineng.2012.03.021 (2012).

42   Beukes, J. P., van Zyl, P. G. & Ras, M. Treatment of Cr(VI)-containing wastes in the South African ferrochrome industry-a review of currently applied methods. *Journal of the Southern African Institute of Mining and Metallurgy* **112**, 347-352 (2012).

43   Kudekov, T. *et al.* Report on Air Emissions Inventory and Atmospheric Air Pollution Monitoring and Modelling in Kazakhstan. 1-88 (UN ECE Working Group on Environmental Monitoring, 2003).

44   Nugumanova, L., Frey, M., Yemelina, N. & Yugay, S. Environmental problems and policies in Kazakhstan: Air pollution, waste and water. (IOS Working Papers, 2017).

45   Kibatayev, K. M. *et al.* The content of heavy metals in the soil in Aktobe city. *International Journal of Science Education* **11**, 11405-11414 (2016).

46   AktobeNefteKhim. *AktobeNefteKhim*, <http://www.kazexpo.kz/eng/neftekhim/about_city_eng.htm> (2018).

47   UK07444, S. C. U. L. A competent persons report on the mineral assets of JSC Kazchrome, Kazakhstan 1-156 (2017).

48   Katya Koryakovtseva, L. N. Kazakhstan's mining industry. *Engineering and Mining Journal* **211**, 74-92 (2015).

49   Kazchrome. Kazchrome Annual Report_2020. (2020).

50   Kazchrome. Kazchrome Annual Report 2020. (2019).

51   Ott, W. R., Steinemann, A. C. & Wallace, L. A. *Exposure analysis*. (CRC Press, 2006).

52   Ishikawa, Y. *et al.* Hot-Spots of Chromium Accumulation at Bifurcations of Chromate Workers Bronchi. *Cancer Research* **54**, 2342-2346 (1994).

53   ATSDR. Toxicological profile for chromium. US Department of Health and Human Services. 1-419 (2012).

54   IARC., L.   (Who Geneva, 1987).

55   NationalToxicityProgram. Chromium hexavalent compounds CAS No. 18540-29-9 report on carcinogens. (Department of Health and Human Services, 2016).

56   USEPA. Toxicological review of hexavalent chromium: national center for environmental assessment, office of research and development. (1998).

57   WHO.   139-142 (WHO Regional Publications, European Series, No. 91, 2000).

58   ACGIH.   20 (American Conference of Governmental Industrial Hygienists).

59   NIOSH. NIOSH pocket guide to chemical hazards. (Atlanta, GA: National Institute for Occupational Safety and Health, Centers for Disease Control and Prevention, 2005).

60   OSHA. Air contaminants, occupational safety and health administration (OSHA). Code of Federal Regulations, 29 CFR 1910.1000, Table Z 1. (2007b).

61   OSHA. Chromium (VI); occupational safety and health administration, code of federal regulations. 29 CFR 1910.26. (2007a).

62   Amouei Torkmahalleh, M. *et al.* Improved atmospheric sampling of hexavalent chromium. *Journal of the Air & Waste Management Association* **63**, 1313-1323, doi:10.1080/10962247.2013.823894 (2013).

63   Vitale, R. J., Mussoline, G. R. & Rinehimer, K. A. Environmental monitoring of chromium in air, soil, and water. *Regul Toxicol Pharmacol* **26**, S80-85, doi:10.1006/rtph.1997.1144 (1997).

64   Sheehan, P., Ricks, R., Ripple, S. & Paustenbach, D. Field evaluation of a sampling and analytical method for environmental levels of airborne hexavalent chromium. *American Industrial Hygiene Association journal* **53**, 57-68, doi:10.1080/15298669291359302 (1992).

65   Vairavamurthy, A., Roberts, J. M. & Newman, L. Methods for determination of low molecular weight carbonyl compounds in the atmosphere: A review. *Atmospheric Environment. Part A. General Topics* **26**, 1965-1993, doi:https://doi.org/10.1016/0960-1686(92)90083-W (1992).

66   Beasley, R. K., Hoffmann, C. E., Rueppel, M. L. & Worley, J. W. Sampling of formaldehyde in air with coated solid sorbent and determination by high performance liquid chromatography. *Analytical chemistry* **52**, 1110-1114, doi:10.1021/ac50057a026 (1980).

67   Andersson, G., Andersson, K., Nilsson, C.-A. & Levin, J.-O. Chemosorption of formaldehyde on Amberlite XAD-2 coated with 2,4-dinitrophenylhydrazine. *Chemosphere* **8**, 823-827, doi:https://doi.org/10.1016/0045-6535(79)90044-4 (1979).

68   ERG. Collection and Analysis of Hexavalent Chromium in Ambient Air. Eastern Research Group. (2007).

69   Meng, Q. Y. *et al.* Development and evaluation of a method for hexavalent chromium in ambient air using IC-ICP-MS. *Atmospheric Environment* **45**, 2021-2027, doi:10.1016/j.atmosenv.2011.02.009 (2011).

70   Huang, L. *et al.* Measurement of Soluble and Total Hexavalent Chromium in the Ambient Airborne Particles in New Jersey. *Aerosol and Air Quality Research* **14**, 1939-1949, doi:10.4209/aaqr.2013.10.0312 (2014).

71   Hazelwood, K. J., Drake, P. L., Ashley, K. & Marcy, D. Field Method for the Determination of Insoluble or Total Hexavalent Chromium in Workplace Air. *Journal of Occupational and Environmental Hygiene* **1**, 613-619, doi:10.1080/15459620490493810 (2004).

72   (OSHA), O. S. a. H. A.   (Salt Lake City: OSHA, 1998).

73   Barceloux, D. G. Chromium. *J Toxicol Clin Toxicol* **37**, 173-194, doi:10.1081/clt-100102418 (1999).

74   Boiano, J. M. *et al.* Comparison of three sampling and analytical methods for the determination of airborne hexavalent chromium. *Journal of environmental monitoring : JEM* **2**, 329-333, doi:10.1039/b002456m (2000).

75   Boiano, J. M. *et al.* Comparison of three sampling and analytical methods for the determination of airborne hexavalent chromium. *Journal of Environmental Monitoring* **2**, 329-333 (2000).

76   Rai, D., Sass, B. M. & Moore, D. A. Chromium(III) Hydrolysis Constants and Solubility of Chromium(Iii) Hydroxide. *Inorganic chemistry* **26**, 345-349, doi:10.1021/ic00250a002 (1987).

77   Palmer, C. D. & Puls, R. W. in *EPA Environmental Assessment Sourcebook*   57-72 (Ann Arbor Press, INC. Chelsea, Michigan, 1994).

78   Davis, A. & Olsen, R. L. The Geochemistry of Chromium Migration and Remediation in the Subsurface. *Ground Water* **33**, 759-768, doi:10.1111/j.1745-6584.1995.tb00022.x (1995).

79   Rai, D., Eary, L. E. & Zachara, J. M. Environmental chemistry of chromium. *Science of the Total Environment* **86**, 15-23, doi:10.1016/0048-9697(89)90189-7 (1989).

80   Huang, L., Yu, C. H., Hopke, P. K., Shin, J. Y. & Fan, Z. Trivalent chromium solubility and its influence on quantification of hexavalent chromium in ambient particulate matter using EPA method 6800. *Journal of the Air & Waste Management Association* **64**, 1439-1445, doi:10.1080/10962247.2014.951745 (2014).

81   Schroeder, D. C. & Lee, G. F. Potential Transformations of Chromium in Natural-Waters. *Water Air Soil Poll* **4**, 355-365, doi:10.1007/Bf00280721 (1975).

82   Guertin, J., Jacobs, J. A. & Avakian, C. P. *Chromium (VI) handbook*. (Taylor & Francis, 2005).

83   Nico, P. & Zasoski, R. Importance of Mn (II) availability of Cr (III) oxidation on birnessite. *Environmental Science & Technology* **38**, 5253-5260, doi:10.1021/es991462j (2000).

84   Eckert, J., Stewart, J., Waite, T., Szymczak, R. & Williams, K. J. A. C. A. Reduction of chromium (VI) at sub-μg l− 1 levels by fulvic acid. **236**, 357-362, doi:10.1016/S0003-2670(00)83334-6 (1990).

85   Pettine, M., Barra, I., Campanella, L. & Millero, F. J. Effect of metals on the reduction of chromium (VI) with hydrogen sulfide. *Water Research* **32**, 2807-2813, doi:10.1016/S0043-1354(98)00011-6 (1998).

86   Eary, L. E. & Rai, D. Chromate removal from aqueous wastes by reduction with ferrous ion. *Environmental Science & Technology* **22**, 972-977, doi:10.1021/es00173a018 (1988).

87   Pettine, M., Millero, F. J. & Passino, R. Reduction of Chromium(VI) with Hydrogen-Sulfide in Nacl Media. *Marine Chemistry* **46**, 335-344, doi:10.1016/0304-4203(94)90030-2 (1994).

88   Pettine, M., Tonnina, D. & Millero, F. J. Chromium (VI) reduction by sulphur (IV) in squeous solutions. *Marine chemistry* **99**, 31-41, doi:10.1016/j.marchem.2005.02.003 (2006).

89   Khan, Z., Hashmi, A. A. & Kabir-ud-Din. Reduction of chromium(VI) by phosphonic acid. *Transition Metal Chemistry* **23**, 147-150, doi:10.1023/A:1006995026227 (1998).

90   Abu-Saba, K. E., Sedlak, D. L. & Flegal, A. R. Indirect reduction of hexavalent chromium by copper in the presence of superoxide. *Marine Chemistry* **69**, 33-41, doi:10.1016/S0304-4203(99)00090-0 (2000).

91   Lee, R. E., Crist, H. L., Riley, A. E. & Macleod, K. E. Concentration and Size of Trace-Metal Emissions from a Power-Plant, a Steel Plant, and a Cotton Gin. *Environmental Science & Technology* **9**, 643-647, doi:10.1021/es60105a012 (1975).

92   Goshu, I. V., Tsarev, Y. V. & Kostrov, V. V. Study of chromium(VI) reduction in the presence of metal salt additives. *Russian Journal of Applied Chemistry* **80**, 2024-2027, doi:10.1134/S1070427207120030 (2007).

93   Amouei Torkmahalleh, M., Lin, L., Holsen, T. M., Rasmussen, D. H. & Hopke, P. K. The impact of deliquescence and pH on Cr speciation in ambient PM samples. *Aerosol Science and Technology* **46**, 690-696, doi:10.1016/j.atmosenv.2013.02.005 (2012).

94   Grohse, P. *The fate of hexavalent chromium in the atmosphere*. (Research Triangle Institute, 1988).

95   Amouei Torkmahalleh, M., Karibayev, M., Konakbayeva, D., Fyrillas, M. & Rule, A. M. Aqueous chemistry of airborne hexavalent chromium during sampling. *Air Quality, Atmosphere, and Health* **11**, 1059-1068, doi:10.1007/s11869-018-0607-z (2018).

96   Konakbayeva, D. *et al.* A conceptual model to understand the soluble and insoluble Cr species in deliquesced particles. *Air Quality Atmosphere and Health* **12**, 1091-1102, doi:10.1007/s11869-019-00725-5 (2019).

97   Shah, D., Karibayev, M., Adotey, E. K. & Amouei Torkmahalleh, M. Impact of volatile organic compounds on chromium containing atmospheric particulate: insights from molecular dynamics simulations. *Scientific Reports* **10**, 17387, doi:10.1038/s41598-020-74522-x (2020).

98   Ashley, K., Howe, A. M., Demange, M. & Nygren, O. Sampling and analysis considerations for the determination of hexavalent chromium in workplace air. *J. Environ. Monit.* **5**, 707-716 (2003).

99   Pettine, M. & Capri, S. Digestion treatments and risks of Cr(III)-Cr(VI) interconversions during Cr(VI) determination in soils and sediments-a review. *Analytica Chimica Acta* **540**, 231-238 (2005).

100   USEPA.   (1996).

101   Vitale, R. J., CPC, Mussoline, G. R. & Rinehimer, K. A. Environmental monitoring of chromium in air, soil and water. *Regulatory Toxicology and Pharmacology* **26**, S80-S85 (1997).

102   Morales-Munoz, S., Luque-Garcia, J. L. & Castro, M. D. L. d. A continuous approach for the determination of Cr(VI) in sediment and soil based on the coupling of microwave-assisted water extraction, preconcentration, derivatization and photometric detection. *Analytica Chimica Acta* **515**, 343-348 (2004).

103   Falerios, M., Schild, K., Sheehan, P. & Paustenbach, D. J. Airborne Concentrations of Trivalent and Hexavalent Chromium from Contaminated Soils at Unpaved and Partially Paved Commercial/Industrial Sites. *J. Air Waste Manage. Assoc.* **42**, 40-48 (1992).

104   Li, Y., Pradhan, N. K., Foley, R. & Low, G. K. C. Selective determination of airborne hexavalent chromium using inductively coupled plasma mass spectrometry. *Talanta* **57**, 1143-1153 (2002).

105   Talebi, S. M. Determination of total and hexavalent chromium concentrations in the atmosphere of the city of Isfahan. *Environmental Research* **92**, 54-56 (2003).

106   Milacic, R., Scancar, J. & Tusek, J. Determination of Cr(VI) in welding fumes by anion-exchange fast protein liquid chromatography with electrothermal atomic absorption spectrometric detection. *Anal Bioanal Chem* **372**, 549-553 (2002).

107   Wang, J., Ashley, K. & Marlow, D. Field Method for the Determination of Hexavalent Chromium by Ultrasonication and Strong Anion-Exchange Solid-Phase Extraction. *Anal. Chem.* **71**, 1027-1032 (1999).

108   Sheehan, P., Ricks, R., Ripple, S. & Paustenbach, D. Field evaluation of a sampling and analytical method for environmental levels of airborne hexavalent chromium. *American Industrial Hygiene Association Journal* **53**, 57-68 (1992).

109   Werner, M., Nico, P., Guo, B., Kennedy, I. & Anastasio, C. Laboratory study of simulated atmospheric transformations of chromium in ultrafine combustion aerosol particles. *Aerosol Science and Technology* **40**, 545-556, doi:10.1080/02786820600714353 (2006).

110   Nico, P. S., Kumfer, B. M., Kennedy, I. M. & Anastasio, C. Redox Dynamics of Mixed Metal (Mn, Cr, and Fe) Ultrafine Particles. *Aerosol Science and Technology* **43**, 60-70, doi:10.1080/02786820802482528 (2009).

111   Huang, L. *et al.* Interconversion of chromium species during air sampling: effects of O₃, NO₂, SO₂, particle matrices, temperature, and humidity. *Environmental Science & Technology* **47**, 4408-4415, doi:10.1021/es3046247 (2013).

112   Amouei Torkmahalleh, M., Lin, L., Holsen, T. M., Rasmussen, D. H. & Hopke, P. K. Cr speciation changes in the presence of ozone and reactive oxygen species at low relative humidity. *Atmospheric Environment* **71**, 92-94, doi:10.1016/j.atmosenv.2013.02.005 (2013).

113   De Volder, M. F., Tawfick, S. H., Baughman, R. H. & Hart, A. J. Carbon nanotubes: present and future commercial applications. *Science* **339**, 535-539, doi:10.1126/science.1222453 (2013).

114   Hammel, E. *et al.* Carbon nanofibers for composite applications. *Carbon* **42**, 1153-1158, doi:10.1016/j.carbon.2003.12.043 (2004).

115   Krishnamoorthy, K., Kim, G. S. & Kim, S. J. Graphene nanosheets: Ultrasound assisted synthesis and characterization. *Ultrasonics Sonochemistry* **20**, 644-649, doi:10.1016/j.ultsonch.2012.09.007 (2013).

116   Benítez-Martínez, S. & Valcárcel, M. Graphene quantum dots in analytical science. *TrAC Trends in Analytical Chemistry* **72**, 93-113, doi:10.1016/j.trac.2015.03.020 (2015).

117   Terrones, M. *et al.* Graphene and graphite nanoribbons: Morphology, properties, synthesis, defects and applications. *Nano Today* **5**, 351-372, doi:10.1016/j.nantod.2010.06.010 (2010).

118   Li, Q., Mahmood, N., Zhu, J. H., Hou, Y. L. & Sun, S. H. Graphene and its composites with nanoparticles for electrochemical energy applications. *Nano Today* **9**, 668-683, doi:10.1016/j.nantod.2014.09.002 (2014).

119   Tajik, S. *et al.* Carbon and graphene quantum dots: a review on syntheses, characterization, biological and sensing applications for neurotransmitter determination. *RSC Advances* **10**, 15406-15429, doi:10.1039/d0ra00799d (2020).

120   Lin, H.-Y., Nurunnabi, M., Chen, W.-H. & Huang, C.-H. in *Biomedical Applications of Graphene and 2D Nanomaterials*   337-351 (Elsevier, 2019).

121   Liu, J., Li, R. & Yang, B. Carbon Dots: A New Type of Carbon-Based Nanomaterial with Wide Applications. *ACS Central Science* **6**, 2179-2195, doi:10.1021/acscentsci.0c01306 (2020).

122   Xu, X. *et al.* Electrophoretic analysis and purification of fluorescent single-walled carbon nanotube fragments. *Journal of the American Chemical Society* **126**, 12736-12737, doi:10.1021/ja040082h (2004).

123   Sun, Y. P. *et al.* Quantum-sized carbon dots for bright and colorful photoluminescence. *Journal of the American Chemical Society* **128**, 7756-7757, doi:10.1021/ja062677d (2006).

124   Zhu, S. *et al.* Highly photoluminescent carbon dots for multicolor patterning, sensors, and bioimaging. *Angewandte Chemie International Edition* **52**, 3953-3957, doi:10.1002/anie.201300519 (2013).

125   Liu, J. *et al.* Deep Red Emissive Carbonized Polymer Dots with Unprecedented Narrow Full Width at Half Maximum. *Advanced Materials* **32**, e1906641, doi:10.1002/adma.201906641 (2020).

126   Ding, H., Yu, S. B., Wei, J. S. & Xiong, H. M. Full-Color Light-Emitting Carbon Dots with a Surface-State-Controlled Luminescence Mechanism. *ACS Nano* **10**, 484-491, doi:10.1021/acsnano.5b05406 (2016).

127   Li, D. *et al.* Near-Infrared Excitation/Emission and Multiphoton-Induced Fluorescence of Carbon Dots. *Advanced materials* **30**, e1705913, doi:10.1002/adma.201705913 (2018).

128   Yuan, F. *et al.* Engineering triangular carbon quantum dots with unprecedented narrow bandwidth emission for multicolored LEDs. *Nature Communications* **9**, 2249, doi:10.1038/s41467-018-04635-5 (2018).

129   Zhang, M. *et al.* Maltase Decorated by Chiral Carbon Dots with Inhibited Enzyme Activity for Glucose Level Control. *Small* **15**, e1901512, doi:10.1002/smll.201901512 (2019).

130   Li, F. *et al.* Highly Fluorescent Chiral N-S-Doped Carbon Dots from Cysteine: Affecting Cellular Energy Metabolism. *Angewandte Chemie International Edition* **57**, 2377-2382, doi:10.1002/anie.201712453 (2018).

131   Jiang, K., Wang, Y., Gao, X., Cai, C. & Lin, H. Facile, Quick, and Gram-Scale Synthesis of Ultralong-Lifetime Room-Temperature-Phosphorescent Carbon Dots by Microwave Irradiation. *Angewandte Chemie International Edition* **57**, 6216-6220, doi:10.1002/anie.201802441 (2018).

132   Tao, S. *et al.* Design of Metal-Free Polymer Carbon Dots: A New Class of Room-Temperature Phosphorescent Materials. *Angewandte Chemie International Edition* **57**, 2393-2398, doi:10.1002/anie.201712662 (2018).

133   Zhu, S. J. *et al.* The photoluminescence mechanism in carbon dots (graphene quantum dots, carbon nanodots, and polymer dots): current state and future perspective. *Nano Research* **8**, 355-381, doi:10.1007/s12274-014-0644-3 (2015).

134   Peng, J. *et al.* Graphene quantum dots derived from carbon fibers. *Nano Letters* **12**, 844-849, doi:10.1021/nl2038979 (2012).

135   Fang, J. *et al.* Graphene quantum dots-gated hollow mesoporous carbon nanoplatform for targeting drug delivery and synergistic chemo-photothermal therapy. *Int J Nanomedicine* **13**, 5991-6007, doi:10.2147/IJN.S175934 (2018).

136   Xia, C. *et al.* Hydrothermal Addition Polymerization for Ultrahigh-Yield Carbonized Polymer Dots with Room Temperature Phosphorescence via Nanocomposite. *Chemistry* **24**, 11303-11308, doi:10.1002/chem.201802712 (2018).

137   Zhu, S., Song, Y., Shao, J., Zhao, X. & Yang, B. Non-Conjugated Polymer Dots with Crosslink-Enhanced Emission in the Absence of Fluorophore Units. *Angewandte Chemie International Edition* **54**, 14626-14637, doi:10.1002/anie.201504951 (2015).

138   Li, X. *et al.* Preparation of carbon quantum dots with tunable photoluminescence by rapid laser passivation in ordinary organic solvents. *Chemical Communications* **47**, 932-934, doi:10.1039/c0cc03552a (2011).

139   Qiao, Z. A. *et al.* Commercially activated carbon as the source for producing multicolor photoluminescent carbon dots by chemical oxidation. *Chemical Communications* **46**, 8812-8814, doi:10.1039/c0cc02724c (2010).

140   Zhang, Q. H., Sun, X. F., Ruan, H., Yin, K. Y. & Li, H. G. Production of yellow-emitting carbon quantum dots from fullerene carbon soot. *Science China-Materials* **60**, 141-150, doi:10.1007/s40843-016-5160-9 (2017).

141   Tang, L., Ji, R., Li, X., Teng, K. S. & Lau, S. P. Size-dependent structural and optical characteristics of glucose-derived graphene quantum dots. *Particle & Particle Systems Characterization* **30**, 523-531, doi:10.1002/ppsc.201200131 (2013).

142   Guo, Y. M., Wang, Z., Shao, H. W. & Jiang, X. Y. Hydrothermal synthesis of highly fluorescent carbon nanoparticles from sodium citrate and their use for the detection of mercury ions. *Carbon* **52**, 583-589, doi:10.1016/j.carbon.2012.10.028 (2013).

143   Song, Y. B. *et al.* Investigation from chemical structure to photoluminescent mechanism: a type of carbon dots from the pyrolysis of citric acid and an amine. *Journal of Materials Chemistry C* **3**, 5976-5984, doi:10.1039/c5tc00813a (2015).

144   Wang, Q. L. *et al.* Microwave-hydrothermal synthesis of fluorescent carbon dots from graphite oxide. *Carbon* **49**, 3134-3140, doi:10.1016/j.carbon.2011.03.041 (2011).

145   Chen, B. *et al.* Large scale synthesis of photoluminescent carbon nanodots and their application for bioimaging. *Nanoscale* **5**, 1967-1971, doi:10.1039/c2nr32675b (2013).

146   Titirici, M. M. & Antonietti, M. Chemistry and materials options of sustainable carbon materials made by hydrothermal carbonization. *Chemical Society Reviews* **39**, 103-116, doi:10.1039/b819318p (2010).

147   Zhu, H. *et al.* Microwave synthesis of fluorescent carbon nanoparticles with electrochemiluminescence properties. *Chemical Communications* 5118-5120, doi:10.1039/b907612c (2009).

148   Umrao, S. *et al.* Microwave bottom-up route for size-tunable and switchable photoluminescent graphene quantum dots using acetylacetone: New platform for enzyme-free detection of hydrogen peroxide. *Carbon* **81**, 514-524, doi:10.1016/j.carbon.2014.09.084 (2015).

149   Ke, X., Bittencourt, C. & Van Tendeloo, G. Possibilities and limitations of advanced transmission electron microscopy for carbon-based nanomaterials. *Beilstein Journal of Nanotechnology* **6**, 1541-1557, doi:10.3762/bjnano.6.158 (2015).

150   Pan, D., Zhang, J., Li, Z. & Wu, M. Hydrothermal route for cutting graphene sheets into blue-luminescent graphene quantum dots. *Advanced materials* **22**, 734-738, doi:10.1002/adma.200902825 (2010).

151   Ţucureanu, V., Matei, A. & Avram, A. M. FTIR spectroscopy for carbon family study. *Critical reviews in analytical chemistry* **46**, 502-520, doi:10.1080/10408347.2016.1157013 (2016).

152   Zuo, P. L., Lu, X. H., Sun, Z. G., Guo, Y. H. & He, H. A review on syntheses, properties, characterization and bioanalytical applications of fluorescent carbon dots. *Microchimica Acta* **183**, 519-542, doi:10.1007/s00604-015-1705-3 (2016).

153   Zheng, X. T., Ananthanarayanan, A., Luo, K. Q. & Chen, P. Glowing graphene quantum dots and carbon dots: properties, syntheses, and biological applications. *Small* **11**, 1620-1636, doi:10.1002/smll.201402648 (2015).

154   Cao, M. *et al.* A novel method for the preparation of solvent-free, microwave-assisted and nitrogen-doped carbon dots as fluorescent probes for chromium(vi) detection and bioimaging. *RSC Advances* **9**, 8230-8238, doi:10.1039/c9ra00290a (2019).

155   Jiang, K. *et al.* Red, green, and blue luminescence by carbon dots: full-color emission tuning and multicolor cellular imaging. *Angewandte Chemie International Edition* **54**, 5360-5363, doi:10.1002/anie.201501193 (2015).

156   Zhao, K. X. *et al.* Multi-color fluorescent carbon dots with single wavelength excitation for white light-emitting diodes. *Journal of Alloys and Compounds* **793**, 613-619, doi:10.1016/j.jallcom.2019.04.146 (2019).

157   Ming, F. *et al.* One-step synthesized fluorescent nitrogen doped carbon dots from thymidine for Cr (VI) detection in water. *Spectrochimica Acta, Part A: Molecular and Biomolecular Spectroscopy* **222**, 117165, doi:10.1016/j.saa.2019.117165 (2019).

158   Wu, J. B., Lin, M. L., Cong, X., Liu, H. N. & Tan, P. H. Raman spectroscopy of graphene-based materials and its applications in related devices. *Chemical Society Reviews* **47**, 1822-1873, doi:10.1039/c6cs00915h (2018).

159   Dervishi, E., Ji, Z., Htoon, H., Sykora, M. & Doorn, S. K. Raman spectroscopy of bottom-up synthesized graphene quantum dots: size and structure dependence. *Nanoscale* **11**, 16571-16581, doi:10.1039/c9nr05345j (2019).

160   Junaid, H. M., Batool, M., Harun, F. W., Akhter, M. S. & Shabbir, N. Naked Eye Chemosensing of Anions by Schiff Bases. *Critical Reviews in Analytical Chemistry* **52**, 463-480, doi:10.1080/10408347.2020.1806703 (2022).

161   Babazadeh, S. *et al.* Colorimetric Detection of Chromium(VI) Ions in Water Using Unfolded-Fullerene Carbon Nanoparticles. *Sensors (Basel)* **21**, doi:10.3390/s21196353 (2021).

162   Daniel, S. Carbon dot-based molecular receptor for the colorimetric sensing of Cr(VI) from aqueous solutions. *Materials Science and Technology* **38**, 742-752, doi:10.1080/02670836.2022.2063500 (2022).

163   Goswami, J., Saikia, L. & Hazarika, P. Carbon Dots-Decorated g-C3N4 as Peroxidase Nanozyme for Colorimetric Detection of Cr (VI) in Aqueous Medium. *ChemistrySelect* **7**, e202201963, doi:10.1002/slct.202201963 (2022).

164   Xu, Z. *et al.* Microwave-Assisted Rapid Synthesis of Amphibious Yellow Fluorescent Carbon Dots as a Colorimetric Nanosensor for Cr (VI). *Particle & Particle Systems Characterization* **32**, 1058-1062, doi:10.1002/ppsc.201500172 (2015).

165   Shen, J., Shang, S. M., Chen, X. Y., Wang, D. & Cai, Y. Highly fluorescent N, S-co-doped carbon dots and their potential applications as antioxidants and sensitive probes for Cr (VI) detection. *Sensors and Actuators B-Chemical* **248**, 92-100, doi:10.1016/j.snb.2017.03.123 (2017).

166   Ma, Y. *et al.* Ratiometric fluorescent detection of chromium(VI) in real samples based on dual emissive carbon dots. *Talanta* **185**, 249-257, doi:10.1016/j.talanta.2018.03.081 (2018).

167   Zheng, M. *et al.* On-off-on fluorescent carbon dot nanosensor for recognition of chromium(VI) and ascorbic acid based on the inner filter effect. *ACS applied materials & interfaces* **5**, 13242-13247, doi:10.1021/am4042355 (2013).

168   Laddha, H. *et al.* One-pot microwave-assisted synthesis of blue emissive multifunctional N-S-P co-doped carbon dots as a nanoprobe for sequential detection of Cr(VI) and ascorbic acid in real samples, fluorescent ink and logic gate operation. *Journal of Molecular Liquids* **346**, 117088, doi:10.1016/j.molliq.2021.117088 (2022).

169   Zhang, H. Y. *et al.* Rapid detection of Cr(VI) ions based on cobalt(II)-doped carbon dots. *Biosensors and Bioelectronics* **87**, 46-52, doi:10.1016/j.bios.2016.08.010 (2017).

170   Qing, W. X., Chen, K., Yang, Y. Y., Wang, Y. & Liu, X. H. Cu2+-doped carbon dots as fluorescence probe for specific recognition of Cr (VI) and its antimicrobial activity. *Microchemical Journal* **152**, 104262, doi:10.1016/j.microc.2019.104262 (2020).

171   Adotey, E. K., Amouei Torkmahalleh, M., Hopke, P. K. & Balanay, M. P. N,Zn-Doped Fluorescent Sensor Based on Carbon Dots for the Subnanomolar Detection of Soluble Cr(VI) Ions. *Sensors* **23** (2023).

172   Liu, S. *et al.* Hydrothermal treatment of grass: a low-cost, green route to nitrogen-doped, carbon-rich, photoluminescent polymer nanodots as an effective fluorescent sensing platform for label-free detection of Cu (II) ions. *Advanced materials* **24**, 2037-2041, doi:10.1002/adma.201200164 (2012).

173   Bu, L. L. *et al.* Fluorescent carbon dots for the sensitive detection of Cr(VI) in aqueous media and their application in test papers. *RSC Advances* **6**, 95469-95475, doi:10.1039/c6ra19977a (2016).

174   Li, C., Liu, W. J., Sun, X. B., Pan, W. & Wang, J. P. Multi sensing functions integrated into one carbon-dot based platform via different types of mechanisms. *Sensors and Actuators B-Chemical* **252**, 544-553, doi:10.1016/j.snb.2017.06.036 (2017).

175   Wang, D. X., Zhang, L., Li, P. X., Li, J. F. & Dong, C. Convenient synthesis of carbon nanodots for detecting Cr(vi) and ascorbic acid by fluorimetry. *New Journal of Chemistry* **44**, 20806-20811, doi:10.1039/d0nj04495d (2020).

176   Wang, J. L., Wu, Z. L., Chen, S. H., Yuan, R. & Dong, L. A novel multifunctional fluorescent sensor based on N/S co-doped carbon dots for detecting Cr (VI) and

toluene. *Microchemical Journal* **151**, 104246, doi:10.1016/j.microc.2019.104246 (2019).

177   Song, S. *et al.* A label-free nano-probe for sequential and quantitative determination of Cr(VI) and ascorbic acid in real samples based on S and N dual-doped carbon dots. *Spectrochim Acta A Mol Biomol Spectrosc* **215**, 58-68, doi:10.1016/j.saa.2019.02.065 (2019).

178   Yang, H. *et al.* Fluorescent carbon dots synthesized by microwave-assisted pyrolysis for chromium(VI) and ascorbic acid sensing and logic gate operation. *Spectrochimica Acta Part A: Molecular and Biomolecular Spectroscopy* **205**, 12-20, doi:10.1016/j.saa.2018.07.015 (2018).

179   Liu, Y. *et al.* Carbon-based dots co-doped with nitrogen and sulfur for Cr(VI) sensing and bioimaging. *RSC Advances* **6**, 28477-28483, doi:10.1039/c6ra02653b (2016).

180   Furukawa, H., Cordova, K. E., O'Keeffe, M. & Yaghi, O. M. The chemistry and applications of metal-organic frameworks. *Science* **341**, 1230444, doi:10.1126/science.1230444 (2013).

181   Jones, C. G. *et al.* Versatile Synthesis and Fluorescent Labeling of ZIF-90 Nanoparticles for Biomedical Applications. *ACS applied materials & interfaces* **8**, 7623-7630, doi:10.1021/acsami.5b11760 (2016).

182   Saber-Samandari, S. & Saber-Samandari, S. Biocompatible nanocomposite scaffolds based on copolymer-grafted chitosan for bone tissue engineering with drug delivery capability. *Mater Sci Eng C Mater Biol Appl* **75**, 721-732, doi:10.1016/j.msec.2017.02.112 (2017).

183   Khan, W. U. *et al.* High Quantum Yield Green-Emitting Carbon Dots for Fe(capital I, Ukrainiancapital I, Ukrainiancapital I, Ukrainian) Detection, Biocompatible Fluorescent Ink and Cellular Imaging. *Scientific Reports* **7**, 14866, doi:10.1038/s41598-017-15054-9 (2017).

184   Amjadi, M., Abolghasemi-Fakhri, Z. & Hallaj, T. Carbon dots-silver nanoparticles fluorescence resonance energy transfer system as a novel turn-on fluorescent probe for selective determination of cysteine. *Journal of Photochemistry and Photobiology a-Chemistry* **309**, 8-14, doi:10.1016/j.jphotochem.2015.04.016 (2015).

185   Wang, C. I., Wu, W. C., Periasamy, A. P. & Chang, H. T. Electrochemical synthesis of photoluminescent carbon nanodots from glycine for highly sensitive detection of hemoglobin. *Green Chemistry* **16**, 2509-2514, doi:10.1039/c3gc42325e (2014).

186   Abdi, H. & Williams, L. J. Principal component analysis. *Wiley interdisciplinary reviews: computational statistics* **2**, 433-459 (2010).

187   Tang, L. *et al.* Deep ultraviolet photoluminescence of water-soluble self-passivated graphene quantum dots. *ACS Nano* **6**, 5102-5110, doi:10.1021/nn300760g (2012).

188   Manioudakis, J. *et al.* Effects of nitrogen-doping on the photophysical properties of carbon dots. *Journal of Materials Chemistry C* **7**, 853-862, doi:10.1039/c8tc04821e (2019).

189   Adotey, E. K., Amouei Torkmahalleh, M. & Balanay, M. P. Zinc metal-organic framework with 3-pyridinecarboxaldehyde and trimesic acid as co-ligands for selective detection of Cr (VI) ions in aqueous solution. *Methods and Applications in Fluorescence* **8**, 045007, doi:10.1088/2050-6120/abb364 (2020).

190   Chen, B. *et al.* A luminescent metal-organic framework with Lewis basic pyridyl sites for the sensing of metal ions. *Angewandte Chemie International Edition* **48**, 500-503, doi:10.1002/anie.200805101 (2009).

191   Basumallick, L. & Rohrer, J. Sensitive determination of hexavalent chromium in drinking water. **179** (2012). <https://assets.thermofisher.com/TFS-

Assets/CMD/Application-Notes/AU-179-IC-Hexavalent-Chromium-Drinking-Water-AU70415-EN.pdf>.

192   Bai, J. L. *et al.* Solvent-controlled and solvent-dependent strategies for the synthesis of multicolor carbon dots for pH sensing and cell imaging. *Journal of Materials Chemistry C* **7**, 9709-9718, doi:10.1039/c9tc02422k (2019).

193   Amanulla, B., Subbu, H. K. R. & Ramaraj, S. K. A sonochemical synthesis of cyclodextrin functionalized Au-FeNPs for colorimetric detection of Cr(6+) in different industrial waste water. *Ultrason Sonochem* **42**, 747-753, doi:10.1016/j.ultsonch.2017.12.041 (2018).

194   Jose, S. P. & Mohan, S. FT-IR and FT-RAMAN investigations of nicotinaldehyde. *Spectrochim Acta A Mol Biomol Spectrosc* **64**, 205-209, doi:10.1016/j.saa.2005.06.040 (2006).

195   Mahalakshmi, G. & Balachandran, V. FT-IR and FT-Raman spectra, normal coordinate analysis and ab initio computations of Trimesic acid. *Spectrochim Acta A* **124**, 535-547, doi:10.1016/j.saa.2014.01.061 (2014).

196   Thendral, M., Selvarajan, G. & Mariappan, M. Thermal, UV, XRD and FTIR studies of Thiourea Urea Potassium Iodide single crystal.

197   Popova, A. N. Crystallographic Analysis of Graphite by X-Ray Diffraction. *Coke and Chemistry* **60**, 361-365, doi:10.3103/S1068364x17090058 (2017).

198   Gupta, B. *et al.* Role of oxygen functional groups in reduced graphene oxide for lubrication. *Scientific Reports* **7**, 45030, doi:10.1038/srep45030 (2017).

199   Suleiman, M. *et al.* Synthesis of nano-sized sulfur nanoparticles and their antibacterial activities. *J Mater Environ Sci* **6**, 513-518 (2015).

200   Awwad, A. M., Salem, N. M. & Abdeen, A. O. Noval approach for synthesis sulfur (S-NPs) nanoparticles using Albizia julibrissin fruits extract. *Advanced Materials Letters* **6**, 432-435, doi:10.5185/amlett.2015.5792 (2015).

201   Siburian, R., Sihotang, H., Raja, S. L., Supeno, M. & Simanjuntak, C. New Route to Synthesize of Graphene Nano Sheets. *Oriental Journal of Chemistry* **34**, 182-187, doi:10.13005/ojc/340120 (2018).

202   Sahiner, N., Suner, S. S., Sahiner, M. & Silan, C. Nitrogen and sulfur doped carbon dots from amino acids for potential biomedical applications. *Journal of fluorescence* **29**, 1191-1200, doi:10.1007/s10895-019-02431-y (2019).

203   Biesinger, M. C., Brown, C., Mycroft, J. R., Davidson, R. D. & McIntyre, N. S. X-ray photoelectron spectroscopy studies of chromium compounds. *Surface and Interface Analysis* **36**, 1550-1563, doi:10.1002/sia.1983 (2004).

204   Huang, X. F. *et al.* Thermal Stability of CrWN Glass Molding Coatings after Vacuum Annealing. *Coatings* **10**, 198, doi:10.3390/coatings10030198 (2020).

205   Bandara, P. C., Pena-Bahamonde, J. & Rodrigues, D. F. Redox mechanisms of conversion of Cr(VI) to Cr(III) by graphene oxide-polymer composite. *Scientific Reports* **10**, 9237, doi:10.1038/s41598-020-65534-8 (2020).

206   Kaur, H., Sinha, S., Krishnan, V. & Koner, R. R. Photocatalytic Reduction and Recognition of Cr(VI): New Zn(II)-Based Metal-Organic Framework as Catalytic Surface. *Industrial & Engineering Chemistry Research* **59**, 8538-8550, doi:10.1021/acs.iecr.9b06417 (2020).

207   Bakhtiari, N. & Azizian, S. Adsorption of copper ion from aqueous solution by nanoporous MOF-5: A kinetic and equilibrium study. *Journal of Molecular Liquids* **206**, 114-118, doi:10.1016/j.molliq.2015.02.009 (2015).

208   Maleki, A., Hayati, B., Naghizadeh, M. & Joo, S. W. Adsorption of hexavalent chromium by metal organic frameworks from aqueous solution. *Journal of Industrial and Engineering Chemistry* **28**, 211-216, doi:10.1016/j.jiec.2015.02.016 (2015).

209   EPA. Definition and Procedure for the Determination of the Method Detection Limit, Revision 2. (2016).

210   Adotey, E. K. *et al.* Quantification and the sources identification of total and insoluble hexavalent chromium in ambient PM: A case study of Aktobe, Kazakhstan. *Chemosphere* **307**, 136057, doi:10.1016/j.chemosphere.2022.136057 (2022).

211   Lin, L. *et al.* A facile synthesis of highly luminescent nitrogen-doped graphene quantum dots for the detection of 2,4,6-trinitrophenol in aqueous solution. *Nanoscale* **7**, 1872-1878, doi:10.1039/c4nr06365a (2015).

212   Bekmukhambetov, Y., Mamyrbayev, A., Jarkenov, T., Makenova, A. & Imangazina, Z. Malignant Neoplasm Prevalence in the Aktobe Region of Kazakhstan. *Asian Pacific Journal of Cancer Prevention* **16**, 8149-8153, doi:10.7314/apjcp.2015.16.18.8149 (2015).

213   Nyssanbayeva, A. S., Cherednichenko, A. V., Cherednichenko, A. V., Cherednichenko, V. S. & Pablo, F. A. Temporal dynamics of ground-level ozone and its impact on morbidity in Almaty city in comparison with Astana city, Kazakhstan. *International Journal of Biometeorology* **63**, 1381-1392, doi:10.1007/s00484-019-01754-6 (2019).

214   Kerimray, A. *et al.* Assessing air quality changes in large cities during COVID-19 lockdowns: The impacts of traffic-free urban conditions in Almaty, Kazakhstan. *Science of the Total Environment* **730**, 139179, doi:10.1016/j.scitotenv.2020.139179 (2020).

215   Barthelemy, M. *The structure and dynamics of cities*. (Cambridge University Press, 2016).

216   Akimat. *Akimat of Nur-Sultant (Official website of the Nur-Sultant city Akimat)*, <http://astana.gov.kz/en> (2020).

217   Muratova, N. T. & Madibekov, A. S. Assessment of the level of air pollution in Astana. *Young Scientist* **20**, 64–69 (2019).

218   Akimat. *Cause of smog over Astana explained to environmentalists*, <http://astana.gov.kz/en/news/news/17089#:~:text=At%20the%20same%20time%2C%20the,total%20gross%20emissions%20of%20pollutants.> (2018).

219   Bekmukhambetov, Y., Imangazina, Z., Jarkenov, T. & Mamyrbayev, A. Cancer incidence and mortality data in Aktobe, west Kazakhstan, 2000-2010. *Asian Pacific Journal of Cancer Prevention* **16**, 2379-2383, doi:10.7314/apjcp.2015.16.6.2379 (2015).

220   Kutikhin, A. G. *et al.* Analysis of cancer incidence and mortality in the industrial region of South-East Siberia from 1991 through 2010. *Asian Pacific Journal of Cancer Prevention* **13**, 5189-5193, doi:10.7314/apjcp.2012.13.10.5189 (2012).

221   Assanov, D., Zapasnyi, V. & Kerimray, A. Air Quality and Industrial Emissions in the Cities of Kazakhstan. *Atmosphere* **12**, 314, doi:10.3390/atmos12030314 (2021).

222   AEROQUAL. *Aeroqual AQM65-Compact Air Quality Monitoring Station*, <https://www.aeroqual.com/wp-content/uploads/AQM-65-Long-Brochure.pdf> (2020).

223   Aeroqual. *Ozone Analyzer Module*, <https://www.aeroqual.com/product/ozone-analyzer-module> (2020).

224   Masiol, M., Squizzato, S., Chalupa, D., Rich, D. Q. & Hopke, P. K. Evaluation and Field Calibration of a Low-Cost Ozone Monitor at a Regulatory Urban Monitoring Station. *Aerosol and Air Quality Research* **18**, 2029-2037, doi:10.4209/aaqr.2018.02.0056 (2018).

225   SOP. Procedure for the determination of trace elements in particulate matter emitted from motor vehicle exhaust using inductively coupled plasma mass spectrometry (ICP-MS). (2018).

226   Jenner, G. A., Longerich, H. P., Jackson, S. E. & Fryer, B. J. ICP-MS a Powerful Tool for High-Precision Trace-Element Analysis in Earth Sciences - Evidence from Analysis of Selected Usgs Reference Samples. *Chemical Geology* **83**, 133-148, doi:Doi 10.1016/0009-2541(90)90145-W (1990).

227   Wilcoxon, F. in *Breakthroughs in statistics*   196-202 (Springer, 1992).

228   Royston, P. Approximating the Shapiro-Wilk W-test for non-normality. *Statistics and computing* **2**, 117-119 (1992).

229   Bauer, D. F. Constructing Confidence Sets Using Rank Statistics. *Journal of the American Statistical Association* **67**, 687-690, doi:10.1080/01621459.1972.10481279 (1972).

230   Uria-Tellaetxe, I. & Carslaw, D. C. Conditional bivariate probability function for source identification. *Environmental Modelling & Software* **59**, 1-9, doi:10.1016/j.envsoft.2014.05.002 (2014).

231   Ashbaugh, L. L., Malm, W. C. & Sadeh, W. Z. A Residence Time Probability Analysis of Sulfur Concentrations at Grand-Canyon-National-Park. *Atmospheric Environment* **19**, 1263-1270, doi:Doi 10.1016/0004-6981(85)90256-2 (1985).

232   Pipal, A. S., Rohra, H., Tiwari, R. & Taneja, A. Particle size distribution, morphometric study and mixing structure of accumulation and ultrafine aerosols emitted from indoor activities in different socioeconomic micro-environment. *Atmospheric Pollution Research* **12**, 101-111, doi:10.1016/j.apr.2021.02.015 (2021).

233   Churg, A., Brauer, M., del Carmen Avila-Casado, M., Fortoul, T. I. & Wright, J. L. Chronic exposure to high levels of particulate air pollution and small airway remodeling. *Environmental Health Perspectives* **111**, 714-718, doi:10.1289/ehp.6042 (2003).

234   Yu, C. H., Huang, L., Shin, J. Y., Artigas, F. & Fan, Z. H. Characterization of concentration, particle size distribution, and contributing factors to ambient hexavalent chromium in an area with multiple emission sources. *Atmospheric Environment* **94**, 701-708, doi:10.1016/j.atmosenv.2014.06.004 (2014).

235   USEPA. *Chromium(VI) CASRN 18540-29-9, DTXSID7023982-Reference Concentration for Inhalation Exposure (RfC)*, <https://cfpub.epa.gov/ncea/iris2/chemicalLanding.cfm?substance_nmbr=144> (2017).

236   Bell, R. W. & Hipfner, J. C. Airborne hexavalent chromium in southwestern Ontario. *Journal of the Air & Waste Management Association* **47**, 905-910, doi:10.1080/10473289.1997.10464454 (1997).

237   Hagendorfer, H. & Uhl, M. Speciation of chromium in particulate matter (PM10): development of a routine procedure, impact of transport and toxicological relevance. *Umweltbundesamt, Vienna*, 29 (2007).

238   Nusko, R. & Heumann, K. G. Cr(III)/Cr(VI) speciation in aerosol particles by extractive separation and thermal ionization isotope dilution mass spectrometry. *Fresenius Journal of Analytical Chemistry* **357**, 1050-1055, doi:10.1007/s002160050303 (1997).

239   Kang, B.-W. *et al.* Distribution of airborne hexavalent chromium concentrations in large industrial complexes in Korea. *Asian Journal of Atmospheric Environment* **10**, 208-216, doi:10.5572/ajae.2016.10.4.208 (2016).

240   Li, Y. R., Pradhan, N. K., Foley, R. & Low, G. K. C. Selective determination of airborne hexavalent chromium using inductively coupled plasma mass spectrometry. *Talanta* **57**, 1143-1153, doi:10.1016/S0039-9140(02)00196-0 (2002).

241   Zereini, F. *et al.* Concentration and distribution of heavy metals in urban airborne particulate matter in Frankfurt am Main, Germany. *Environmental Science & Technology* **39**, 2983-2989, doi:10.1021/es040040t (2005).

242   Talebi, S. M. Determination of total and hexavalent chromium concentrations in the atmosphere of the city of Isfahan. *Environmental Research* **92**, 54-56, doi:10.1016/s0013-9351(02)00036-1 (2003).

243   Khlystov, A. & Ma, Y. L. An on-line instrument for mobile measurements of the spatial variability of hexavalent and trivalent chromium in urban air. *Atmospheric Environment* **40**, 8088-8093, doi:10.1016/j.atmosenv.2006.09.030 (2006).

244   Świetlik, R., Molik, A., Molenda, M., Trojanowska, M. & Siwiec, J. Chromium (III/VI) speciation in urban aerosol. *Atmospheric Environment* **45**, 1364-1368, doi:10.1016/j.atmosenv.2010.12.001 (2011).

245   Venter, A. D. *et al.* Regional atmospheric Cr(VI) pollution from the Bushveld Complex, South Africa. *Atmospheric Pollution Research* **7**, 762-767, doi:10.1016/j.apr.2016.03.009 (2016).

246   Richter, P., Grino, P., Ahumada, I. & Giordano, A. Total element concentration and chemical fractionation in airborne particulate matter from Santiago, Chile. *Atmospheric Environment* **41**, 6729-6738, doi:10.1016/j.atmosenv.2007.04.053 (2007).

247   Tirez, K. *et al.* Determination of hexavalent chromium in ambient air: A story of method induced Cr(III) oxidation. *Atmospheric Environment* **45**, 5332-5341, doi:10.1016/j.atmosenv.2011.06.043 (2011).

248   Alves, C. *et al.* Speciation of organic compounds in aerosols from urban background sites in the winter season. *Atmospheric Research* **150**, 57-68, doi:10.1016/j.atmosres.2014.07.012 (2014).

249   Choi, N. R., Lee, S. P., Lee, J. Y., Jung, C. H. & Kim, Y. P. Speciation and source identification of organic compounds in PM(1)(0) over Seoul, South Korea. *Chemosphere* **144**, 1589-1596, doi:10.1016/j.chemosphere.2015.10.041 (2016).

250   Liu, J. *et al.* Atmospheric levels and health risk of polycyclic aromatic hydrocarbons (PAHs) bound to PM2.5 in Guangzhou, China. *Marine Pollution Bulletin* **100**, 134-143, doi:10.1016/j.marpolbul.2015.09.014 (2015).

251   Pipal, A. S. & Satsangi, P. G. Study of carbonaceous species, morphology and sources of fine (PM2.5) and coarse (PM10) particles along with their climatic nature in India. *Atmospheric Research* **154**, 103-115, doi:10.1016/j.atmosres.2014.11.007 (2015).

252   I.S.U. *Iowa Environmental Mesonet*, <https://mesonet.agron.iastate.edu/request/download.phtml?network=KZ__ASOS> (2020).

253   SOP. Measurement of $PM_{2.5}$ and PM_{10} in outdoor air with the Harvard Impactor-ESCAPE Project. 1-13 (ESCAPE: European Study of Cohor ts for Air Pollution Effects, 2008).

254   Sigma-Aldrich. Certificate of Analysis Chromium (VI) in Soil-SQC012. (2020).

255   Sigma-Aldrich. Chromium (VI) standard for ICP (2020).

256   Masiol, M., Squizzato, S., Cheng, M. D., Rich, D. Q. & Hopke, P. K. Differential Probability Functions for Investigating Long-term Changes in Local and Regional Air Pollution Sources. *Aerosol and Air Quality Research* **19**, 724-736, doi:10.4209/aaqr.2018.09.0327 (2019).

257   Abegglen, M. *et al.* Chemical characterization of freshly emitted particulate matter from aircraft exhaust using single particle mass spectrometry. *Atmospheric Environment* **134**, 181-197, doi:10.1016/j.atmosenv.2016.03.051 (2016).

258   Turgut, E. T. *et al.* Elemental characterization of general aviation aircraft emissions using moss bags. *Environmental Science and Pollution Research* **26**, 26925-26938, doi:10.1007/s11356-019-05910-8 (2019).

259   Burkhardt, M., Rossi, L. & Boller, M. Diffuse release of environmental hazards by railways. *Desalination* **226**, 106-113, doi:10.1016/j.desal.2007.02.102 (2008).

260   Samarska, A., Zelenko, Y. & Kovrov, O. Investigation of Heavy Metal Sources on Railways: Ballast Layer and Herbicides. *Journal of Ecological Engineering* **21**, 32-46, doi:10.12911/22998993/127393 (2020).

261   Kazakhstan, R. o. *Order of the Minister of National Economy of the Republic of Kazakhstan, Hygienic Standards for Atmospheric Air in Urban and Rural Settlements*, <https://adilet.zan.kz/rus/docs/V1500011036> (2015).

262   Colbeck, I. & Lazaridis, M. Aerosols and Environmental Pollution. *Naturwissenschaften* **97**, 117-131, doi:10.1007/s00114-009-0594-x (2010).

263   Cheng, Z., Jiang, J. K., Fajardo, O., Wang, S. X. & Hao, J. M. Characteristics and health impacts of particulate matter pollution in China (2001-2011). *Atmospheric Environment* **65**, 186-194, doi:10.1016/j.atmosenv.2012.10.022 (2013).

264   Schmale, J., Shindell, D., von Schneidemesser, E., Chabay, I. & Lawrence, M. J. N. N. Air pollution: clean up our skies. **515**, 335 (2014).

265   Künzli, N. *et al.* Public-health impact of outdoor and traffic-related air pollution: a European assessment. **356**, 795-801 (2000).

266   Massey, D., Masih, J., Kulshrestha, A., Habil, M. & Taneja, A. Indoor/outdoor relationship of fine particles less than 2.5 μm (PM2. 5) in residential homes locations in central Indian region. *Building and Environment* **44**, 2037-2045, doi:10.1016/j.buildenv.2009.02.010 (2009).

267   Chen, Y. Z., Shah, N., Huggins, F. E. & Huffman, G. P. Microanalysis of ambient particles from Lexington, KY, by electron microscopy. *Atmospheric Environment* **40**, 651-663, doi:10.1016/j.atmosenv.2005.09.036 (2006).

268   Lammel, G. *et al.* Transformation of aerosol chemical properties due to transport over a city. *Journal of Atmospheric Chemistry* **51**, 95-117, doi:10.1007/s10874-005-7646-1 (2005).

269   Wilson, W. E. *et al.* Monitoring of particulate matter outdoors. *Chemosphere* **49**, 1009-1043, doi:10.1016/s0045-6535(02)00270-9 (2002).

270   Paoletti, L., De Berardis, B. & Diociaiuti, M. Physico-chemical characterisation of the inhalable particulate matter (PM10) in an urban area: an analysis of the seasonal trend. *The Science of the total environment* **292**, 265-275, doi:10.1016/s0048-9697(01)01134-2 (2002).

271   Xie, R. K., Seip, H. M., Leinum, J. R., Winje, T. & Xiao, J. S. Chemical characterization of individual particles (PM10) from ambient air in Guiyang City, China. *Science of The Total Environment* **343**, 261-272, doi:10.1016/j.scitotenv.2004.10.012 (2005).

272   Liu, X. D. *et al.* Single particle characterization of spring and summer aerosols in Beijing: Formation of composite sulfate of calcium and potassium. *Atmospheric Environment* **39**, 6909-6918, doi:10.1016/j.atmosenv.2005.08.007 (2005).

273   Shi, Z., Zhang, D., Ji, H., Hasegawa, S. & Hayashi, M. Modification of soot by volatile species in an urban atmosphere. *The Science of the total environment* **389**, 195-201, doi:10.1016/j.scitotenv.2007.08.016 (2008).

274   Xue, H. Q., Liu, G. J., Zhang, H., Hu, R. Y. & Wang, X. Elemental Composition, Morphology and Sources of Fine Particulates (PM2.5) in Hefei City, China. *Aerosol and Air Quality Research* **19**, 1688-1696, doi:10.4209/aaqr.2018.09.0341 (2019).

275   Pipal, A. S., Kulshrestha, A. & Taneja, A. Characterization and morphological analysis of airborne PM2.5 and PM10 in Agra located in north central India. *Atmospheric Environment* **45**, 3621-3630, doi:10.1016/j.atmosenv.2011.03.062 (2011).

276   Wang, J., Hu, Z. M., Chen, Y. Y., Chen, Z. L. & Xu, S. Y. Contamination characteristics and possible sources of PM10 and PM2.5 in different functional areas of Shanghai, China. *Atmospheric Environment* **68**, 221-229, doi:10.1016/j.atmosenv.2012.10.070 (2013).

277   Bilyalova, Z. *et al.* Epidemiological evaluation of breast cancer in ecological areas of Kazakhstan--association with pollution emissions. *Asian Pacific Journal of Cancer Prevention* **13**, 2341-2344, doi:10.7314/apjcp.2012.13.5.2341 (2012).

278   Mamyrbayev, A. *et al.* The Incidence of Malignant Tumors in Environmentally Disadvantaged Regions of Kazakhstan. *Asian Pacific Journal of Cancer Prevention* **17**, 5203-5209, doi:10.22034/APJCP.2016.17.12.5203 (2016).

279   Beysebayev, E., Bilyalova, Z., Kozhakeeva, L., Baissalbayeva, A. & Abiltayeva, A. Spatial and Temporal Epidemiological Assessment of Breast Cancer Incidence and Mortality in Kazakhstan, 1999-2013. *Asian Pacific Journal of Cancer Prevention* **16**, 6795-6798, doi:10.7314/apjcp.2015.16.15.6795 (2015).

280   Sarsembin, U. *et al.* Chemical pollution of the air around the oil and gas refining complex. *International journal of chemical sciences. London: Elsevier BV, 2014, Vol. 12, iss. 4* (2014).

281   Elhadi, R. E. *et al.* Source Identification of Heavy Metals in Particulate Matter (PM 10) in a Malaysian Traffic Area Using Multivariate Techniques. *Polish Journal of Environmental Studies* **26**, doi:10.15244/pjoes/69941 (2017).

282   Kerimray, A., Bakdolotov, A., Sarbassov, Y., Inglezakis, V. & Poulopoulos, S. Air pollution in Astana: analysis of recent trends and air quality monitoring system. *Materials Today-Proceedings* **5**, 22749-22758, doi:DOI 10.1016/j.matpr.2018.07.086 (2018).

283   Kenessariyev, U. *et al.* Human health cost of air pollution in Kazakhstan. *Journal of Environmental Protection* **4**, 869, doi: 10.4236/jep.2013.48101 (2013).

284   Prabhu, V., Shridhar, V. & Choudhary, A. Investigation of the source, morphology, and trace elements associated with atmospheric PM 10 and human health risks due to inhalation of carcinogenic elements at Dehradun, an Indo-Himalayan city. *SN Applied Sciences* **1**, 429, doi:10.1007/s42452-019-0460-1 (2019).

285   Chen, Y., Xie, S. D., Luo, B. & Zhai, C. Z. Characteristics and Sources of Water-Soluble Ions in PM2.5 in the Sichuan Basin, China. *Atmosphere* **10**, 78, doi:10.3390/atmos10020078 (2019).

286   Kolesar, K. R. *et al.* Increases in wintertime PM2.5 sodium and chloride linked to snowfall and road salt application. *Atmospheric Environment* **177**, 195-202, doi:10.1016/j.atmosenv.2018.01.008 (2018).

287   Varrica, D., Tamburo, E., Vultaggio, M. & Di Carlo, I. ATR-FTIR Spectral Analysis and Soluble Components of PM10 And PM2.5 Particulate Matter over the Urban Area of Palermo (Italy) during Normal Days and Saharan Events. *International journal of environmental research and public health* **16**, 2507, doi:10.3390/ijerph16142507 (2019).

288 Radulescu, C., Stihi, C., Iordache, S., Dunea, D. & Dulama, I. D. Characterization of Urban Atmospheric PM2.5 by ATR-FTIR, ICP-MS and SEM-EDS Techniques. *Revista De Chimie* **68**, 805-810 (2017).

289 Montana, G., Randazzo, L., Oddo, I. A. & Valenza, M. The growth of "black crusts" on calcareous building stones in Palermo (Sicily): a first appraisal of anthropogenic and natural sulphur sources. *Environmental Geology* **56**, 367-380, doi:10.1007/s00254-007-1175-y (2008).

290 Ji, J. F., Ge, Y., Balsam, W., Damuth, J. E. & Chen, J. Rapid identification of dolomite using a Fourier Transform Infrared Spectrophotometer (FTIR): A fast method for identifying Heinrich events in IODP Site U1308. *Marine Geology* **258**, 60-68, doi:10.1016/j.margeo.2008.11.007 (2009).

291 Hand, J. L. *et al.* Optical, physical, and chemical properties of tar balls observed during the Yosemite Aerosol Characterization Study. *Journal of Geophysical Research-Atmospheres* **110**, doi:10.1029/2004jd005728 (2005).

292 Gao, Y. & Ji, H. B. Microscopic morphology and seasonal variation of health effect arising from heavy metals in PM2.5 and PM10: One-year measurement in a densely populated area of urban Beijing. *Atmospheric Research* **212**, 213-226, doi:10.1016/j.atmosres.2018.04.027 (2018).

293 Panda, S. & Nagendra, S. M. S. Chemical and morphological characterization of respirable suspended particulate matter (PM10) and associated heath risk at a critically polluted industrial cluster. *Atmospheric Pollution Research* **9**, 791-803, doi:10.1016/j.apr.2018.01.011 (2018).

294 Després, V. *et al.* Primary biological aerosol particles in the atmosphere: a review. *Tellus B: Chemical and Physical Meteorology* **64**, 15598, doi:10.3402/tellusb.v64i0.15598 (2012).

295 Islam, N., Rabha, S., Silva, L. F. O. & Saikia, B. K. Air quality and PM10-associated poly-aromatic hydrocarbons around the railway traffic area: statistical and air mass trajectory approaches. *Environmental Geochemistry and Health* **41**, 2039-2053, doi:10.1007/s10653-019-00256-z (2019).

296 Jiang, N. *et al.* Characterization of PM10 and PM2.5 Source Profiles of Fugitive Dust in Zhengzhou, China. *Aerosol and Air Quality Research* **18**, 314-329, doi:10.4209/aaqr.2017.04.0132 (2018).

297 Schroeder, W. H., Dobson, M., Kane, D. M. & Johnson, N. D. Toxic trace elements associated with airborne particulate matter: a review. *JAPCA* **37**, 1267-1285, doi:10.1080/08940630.1987.10466321 (1987).

298 Vallius, M. *et al.* Source apportionment of urban ambient PM2.5 in two successive measurement campaigns in Helsinki, Finland. *Atmospheric Environment* **37**, 615-623, doi:10.1016/S1352-2310(02)00925-1 (2003).

299 Pongpiachan, S. & Iijima, A. Assessment of selected metals in the ambient air PM10 in urban sites of Bangkok (Thailand). *Environmental Science and Pollution Research* **23**, 2948-2961, doi:10.1007/s11356-015-5877-5 (2016).

300 Yusup, Y. & Alkarkhi, A. F. M. Cluster analysis of inorganic elements in particulate matter in the air environment of an equatorial urban coastal location. *Chemistry and Ecology* **27**, 273-286, doi:10.1080/02757540.2010.547491 (2011).

301 Szmagliński, J., Nawrot, N., Pazdro, K., Walkusz-Miotk, J. & Wojciechowska, E. The fate and contamination of trace metals in soils exposed to a railroad used by Diesel Multiple Units: Assessment of the railroad contribution with multi-tool source tracking. *Science of the Total Environment* **798**, 149300, doi:10.1016/j.scitotenv.2021.149300 (2021).